



**SURFACE CHARACTERISTICS AND
IN VITRO BIO-ACCEPTABILITY OF
MACHINED AND CAST
PURE TITANIUM
AND TITANIUM ALLOY**

BY

LORNA CELIA CARNEIRO

Thesis submitted in fulfillment for the requirements
of the degree

Philosophiae Doctor

In the School of Dentistry
Faculty of Health Sciences
University of Pretoria

Promotor

Prof Dr SJ Botha
Centre of Stomatological Research
School of Dentistry, University of Pretoria.

Co-Promotor

Prof Dr PL Kemp
Department of Prosthetics
School of Dentistry, University of Pretoria

January~2003

DECLARATION

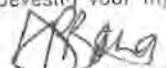
I, Lorna Celia Carneiro, declare that this thesis entitled:

**“Surface Characteristics and *In Vitro* Bio-acceptability
of Machined and Cast Pure Titanium and Titanium Alloy”**

which I herewith submit to the University of Pretoria for the Degree of Philosophiae Doctor in Dentistry, is my own original work, and has never been submitted for any academic award to any other tertiary institution for any degree.

2003
Date


Lorna Celia Carneiro

<p>Die verklaarder erken dat hy/sy ten volle op hoogte is van die inhoud van hierdie verklaring en dit begryp. Hierdie verklaring was beëdig/bevestig voor my.</p> <p></p> <p>Landdrostdistrik/Magisterial District Kom. van Ede/Com. of Oaths PRETORIA</p>	<p>The deponent has acknowledged that he/she knows and understands the contents of this affidavit which was sworn to/affirmed before me.</p> <p>DANIEL PIETER BOTHA Asst. Registrateur/Registrar Univ. van/of Pretoria</p> <p>Datum <u>28/01/03</u> Date</p>
--	--

DEDICATION

My late brother-in-law

Agnelo

My parents

My husband

Primo

Our children

Ryan, Elton and Michael

*Commit to the LORD whatever you do, and your plans
will succeed*

Proverbs 16:3

ACKNOWLEDGEMENTS

The Training Fund for Tanzanian Women for the partial scholarship grant.

The Muhimbili National Hospital/Muhimbili University College of Health Sciences for study leave and partial scholarship grant.

Prof SJ Botha for his untimely effort in planning, constant encouragement and many other aspects for which there are no words just gratitude.

Prof PL Kemp for his profound contribution to unlimited knowledge, constant assistance and guidance.

Colleagues in the Centre of Stomatological Research and Department of Prosthetic Dentistry.

Southern Implants - Graham Blackbeard and Hein van Heerden for all machined samples and the enhancement of cast samples.

J & D Chrome, Deon Botha and Johan Voss for the fabrication of Cast Titanium samples.

Department of Materials Science and Metallurgical Engineering, University of Pretoria for the different microscopic utilities especially Prof Von Moltke, Robert Ehlers and Prem Premachandra.

Gerrit Myburg for doing the Radio Frequency Glow Discharge Treatment of samples.

Wynand Louw - from the Council for Scientific & Industrial Research for the Depth profile analysis of samples.

Department of Electron Microscopy, University of Pretoria and especially Ian Hall and Chris van de Merwe for samples preparation, training and assistance in using the Scanning Electron Microscope.

Dr PJ Becker from the Medical Research Council, for guidance assistance and processing of the statistics.

Gerald Grossberg - L N administrator, School of Dentistry for help with the network, digital camera and computer technicalities.

Library staff (Susan Marsh, Maria Skosana, Antionette Kemp, Patrick Maibelo and Marinda Maritz) of the Pre Clinical Library of the University of Pretoria for their tireless effort in retrieving of publications.

Colleagues from the Assistant Dental Officer's Training School/Faculty of Dentistry, Muhimbili University College of Health Sciences, Tanzania.

Primo, my husband, for his love, support, prompting, advice and encouragement to persevere.

My children, Ryan, Elton and Michael who besides many sacrifices were deprived of my presence.

My parents for their continued love and support.

Ivan, my brother for his spiritual support besides the many other times he has been there for me.

Riantes Residence - The Rossi's -you provided not only boarding and meals during the many times I was busy working but love, care and consideration.

My friends Monica, Hulda, Marna, Carol, Cecilia and lice -both near and far, for their prayers, friendship and words of encouragement.

Lastly not forgetting the families of Dr Hennie and Annelie van Jaarsveld, Monica and Guillermo Hamity, Fanie and Francien Botha, Rina and Hennie de Wet, Ina and Jan de Wet and Hulda and Fidelis Swai - you all provided me a family to be part of. Thank-you.

SUMMARY

Properties making Ti and its alloys popular implant materials are determined by manufacturing conditions. With introduction of cast Ti into the dental fraternity, alternative methods of implant fabrication are possible. This study determined and compared differences in bio-acceptability between surface characteristics of machined and cast Ti and Ti-alloy in relation to materials used, fabrication procedure employed, surface enhancements and Radio Frequency Glow Discharge Treatment (RFGDT). Discs of 6.35mm diameter, 2mm thick, were prepared using cpTi and Ti6Al4V by machining and casting, and specific topographies were introduced. The first group of surfaces was from machining and casting procedures (controls). The second group was surfaces enhanced according to proprietary specifications of Southern Implants (SI). The third group was experimentally enhanced surfaces (ES). Enhancement included grit blasting and acid etching. From each group 21 of 24 samples were RFGDT. Electron Spectroscopy and Profilometric analysis of the Ti surfaces determined chemical composition, oxide thickness and surface roughness. Growth of human gingival fibroblasts and osteoblast-like cells, and scanning electron microscopy (SEM) determined *in vitro* bio-acceptability of different samples. Surface chemical composition was the same for cpTi and Ti6Al4V samples. Cast and enhanced samples were different from machined samples with higher % concentration of Sodium and Aluminium ($p < 0.05$). RFGDT reduced Carbon and other surface contaminants and enhanced the Oxygen and Titanium atomic % concentration ($p < 0.05$). The Sodium and Aluminium atomic % concentration was not affected. The major surface peak was TiO_2 for Ti and oxygen peaks varied considerably between machined and cast samples. Surface topography of cast samples had higher surface analysis values compared to machined samples ($p < 0.05$). RFGDT increased surface area and R_p values ($p < 0.05$). No significant differences in

oxide thickness were observed between materials employed, but it was significantly higher for cast and enhanced samples. RFGDT significantly increased oxide thickness of samples. Fibroblasts showed significant increases in % attachment efficiency and proliferation (%AEP) with time while osteoblast-like cells showed a significant decrease with time. The %AEP of fibroblasts and osteoblast-like cells on different samples was not significantly different. Cast Ti6Al4V control and machined Ti6Al4V SI samples had relatively higher %AEP for osteoblast-like cells than the control or other samples. SEM revealed that fibroblasts and osteoblast-like cells displayed similar attachment behaviour. On machined surfaces cells spread, displaying the underlying topography while on cast and enhanced surfaces cells attached to the available peaks and used these attachments to suspend themselves over the surface. Filopodia were responsible for the attachment of cells. Significant differences in chemical composition were introduced by casting and surface enhancement procedures. RFGDT significantly reduced the concentration of Carbon and other contaminants on the surface exposing the surface Titanium oxide. Cast samples had rougher surface topography than machined samples. RFGDT significantly increased surface area and peak height. Casting, surface enhancement and RFGDT significantly increased oxide thickness. With time fibroblasts showed significant increases in %AEP while osteoblast-like cells significant decreases. Fibroblasts tended to proliferate on relatively smooth surfaces whereas osteoblast-like cells favored rougher surface topography produced by casting and surface enhancement.

CONTENTS

	PAGE
Declaration	ii
Dedication	iii
Words of Wisdom	iv
Acknowledgements	v
Summary	vii
List of Figures	xvi
List of Tables	xxiv
Chapter 1 Introduction	1
Chapter 2 Review of Literature	4
2.1 Overview on Titanium	4
2.1.1 Titanium Development	4
2.1.2 Pure/Unalloyed Titanium	4
2.1.3 Titanium Alloy	5
2.1.4 Properties of Titanium	6
2.1.5 Titanium Oxides	8
2.1.6 Corrosion of Titanium	10
2.2 Fabrication of Titanium	12
2.2.1 Machining of Titanium	12
2.2.2 Casting of Titanium	12
2.2.2.1 Casting Machines	13

2.2.2.2	Cyclarc Titanium Casting Machine	13
2.2.2.3	Investment Material	14
2.3	Osseointegration	15
2.4	Titanium and its Alloys as Dental Implants	18
2.5	Classification of Dental Implants	19
2.5.1	The Implant Surface	20
2.5.1.1	Machined Surfaces	20
2.5.1.2	Osseotite Surface	21
2.5.1.3	Grit Blasted Surfaces	22
2.5.1.4	Bioactive Coated Surfaces	23
2.6	Surface Characterization	24
2.6.1	Compositional-Considerations	26
2.6.1.1	X-ray Photoelectron Spectroscopy (XPS)	27
2.6.2	Surface Topography	29
2.6.2.1	Atomic Force Microscope (AFM)	31
2.6.3	Depth Profiling	34
2.6.4	Cleaning and Sterilization of Implants	37
2.6.4.1	Radio Frequency Glow Discharge Treatment (RFGDT)	39
2.7	Cell Culturing	41
2.7.1	Types of Cells used in Culture	42

2.7.2	Cell Attachment	46
2.7.3	Cell Detachment	47
2.7.4	Inoculation/Seeding of Cells	48
2.7.5	Estimation of Cell Number	48
2.7.6	Cell Proliferation	49
2.8	Bio-acceptibility	50
2.8.1	Scanning Electron Microscopy (SEM)	51
Chapter 3	Aim of the Study	52
Chapter 4	Materials and Methods	54
4.1	Fabrication of Specimen Discs	54
4.1.1	Preparation of Machined Discs	54
4.1.2	Fabrication of Cast Discs	55
4.1.2.1	Preparation of Resin Disc Patterns	55
4.1.2.2	Casting Procedures	57
4.2	Preparation of Different Surfaces	59
4.2.1	Non-enhanced Surfaces	60
4.2.2	Enhanced Surfaces	60
4.2.2.1	Surface Enhancement of Samples according to Southern Implants (SI)	60
4.2.2.2	Experimental Enhancement of Samples (ES)	61

4.3	Sterilization by Radio Frequency Glow Discharge Treatment	61
4.4	Analysis of Surface Characterization	62
4.4.1	X-ray Photoelectron Spectroscopy (XPS)	62
4.4.2	Atomic Force Microscope (AFM)	63
4.4.3	The Quantum 2000 Scanning ESCA Microprobe	65
4.5	Cell Culturing	66
4.5.1	Cell Cultures	66
4.5.1.1	Fibroblasts	66
4.5.1.2	Osteoblast-like cells	66
4.5.2	Cultivation of Cell cultures	66
4.5.3	Cell Concentration	67
4.5.4	Inoculation of Cells onto Sample Discs	67
4.5.5	Incubation	68
4.5.6	Counting Procedures	68
4.5.6.1	Preparation of Trypan Blue	68
4.5.6.2	Cell Detachment for Osteoblast-like cells	69
4.5.6.3	Cell Detachment for Fibroblasts	69
4.5.6.4	Neubauer Haemocytometer	70

4.5.6.5	Estimation of Cell Number and Proliferation	71
4.5.7	Fixation Procedures	71
4.6	Scanning Electron Microscopy (SEM)	72
4.7	Statistical Analysis	72
Chapter 5	Results	74
5.1	Surface Characterization	74
5.1.1	Chemical Composition	74
5.1.1.1	Atomic Percent Concentration	74
	XPS Survey Spetra	76
	Carbon	78
	Oxygen	79
	Titanium	80
	Aluminium	81
	Sodium	82
5.1.1.2	Curve Fitting	83
	Carbon sub peaks	83
	Oxygen sub peaks	85
	Titanium sub peaks	86
	Aluminium sub peaks	88
	Sodium sub peaks	88
5.1.2	Surface Roughness	89
5.1.2.1	Area Analysis	89

	Area Ra and RMS	92
	Average height and Maximum range	94
	Surface Area	96
5.1.2.2	Line Analysis	99
	Ra	104
	Rt	105
	Rtm	105
	Rp	105
	Rpm	105
5.1.3	Depth Profile	106
5.2	Cell Culturing	109
5.2.1	Cell Attachment	109
5.2.1.1	Fibroblasts	109
5.2.1.2	Osteoblast-like Cells	116
5.2.2	Scanning Electron Microscope Analysis	123
5.2.2.1	Fibroblasts	123
	Two days	123
	Twenty-eight days	126
5.2.2.2	Osteoblast-like Cells	129
	Two days	129
	Twenty-eight days	133

Chapter 6	Discussion	137
6.1	Chemical Composition	139
6.2	Surface Roughness	143
6.2.1	Area Analysis	144
6.2.2	Line Analysis	146
6.3	Depth Profile	147
6.4	Cell Culturing	150
6.5	Scanning Electron Microscopy	154
6.6	Bio-acceptability	157
Chapter 7	Conclusion and Recommendations	159
7.1	Conclusions	159
7.2	Recommendations	162
Chapter 8	References	164
Addendum A		178
Addendum B		179
Addendum C		180
Addendum D		183
Addendum E		188
Addendum F		193
Addendum G		196
Addendum H		200

LIST OF FIGURES

	PAGE	
Fig 2-1:	Three separate phenomena of osseointegration taken from The Colgate Oral Care Report (2000)	17
Fig 2-2:	a) Cast surface (An isotropic surface) and b) Machined surface (An anisotropic surface) taken from Mummery (1992)	30
Fig 4-1:	Sample discs of cpTi (Grade 3) and Ti6Al4V (Grade 5) as received from Southern Implants	55
Fig 4-2:	DuraLay resin rods as fabricated from the duplicating mould	56
Fig 4-3:	Slow speed cutting saw sectioning resin rods into discs	57
Fig 4-4:	The Morita Cyclarc Casting Machine taken from (J.Morita, Europe, GMBA)	58
Fig 4-5:	Coded sample discs	60
Fig 4-6:	Placing of sample discs into tissue culture wells	68
Fig 4-7:	Neubauer haemocytometer being filled by capillary action prior to cell counting	70
Fig 5-1:	XPS survey spectra for cpTi cast control sample surfaces before RFGDT	76

Fig 5-2:	XPS survey spectra for cpTi cast control sample surface after RFGDT	77
Fig 5-3:	XPS survey spectra of cpTi machined RFGDT sample (AG=green) and cpTi cast RFGDT sample (FG=blue) of control surfaces	77
Fig 5-4:	XPS survey spectra of Ti6Al4V machined RFGDT sample (CG=green) and Ti6Al4V cast RFGDT sample (HG=blue) of control surfaces	78
Fig 5-5:	Atomic percent concentration of Carbon before and after RFGDT of sample surfaces	78
Fig 5-6:	Atomic percent concentration of Oxygen before and after RFGDT of sample surfaces	80
Fig 5-7:	Atomic percent concentration of Titanium before and after RFGDT of sample surfaces	81
Fig 5-8:	Atomic percent concentration of Aluminium before and after RFGDT of sample surfaces	82
Fig 5-9:	Atomic percent concentration of Sodium before and after RFGDT of sample surfaces	83
Fig 5-10:	Deconvolution of XPS Carbon envelope of Ti6Al4V cast control RFGDT sample surfaces	84

Fig 5-11:	Deconvolution of XPS Oxygen envelope of Ti6Al4V cast control RFGDT sample surface	86
Fig 5-12:	Deconvolution of XPS Titanium envelope of Ti6Al4V cast control RFGDT sample surface	87
Fig 5-13:	Deconvolution of Aluminium envelope for Ti6Al4V cast control sample surface	88
Fig 5-14:	AFM 3D images of 20µm scans of cpTi machined control sample surface	89
Fig 5-15:	AFM 3D images of 20µm scans of Ti6Al4V machined control sample surface	89
Fig 5-16:	AFM 3D images of 20µm scans of cpTi cast control sample surface	90
Fig 5-17:	AFM 3D images of 20µm scans of Ti6Al4V cast control sample	90
Fig 5-18:	Average roughness (Ra and RMS) of the different sample surfaces by material employed and RFGDT for 20µm scans	93
Fig 5-19:	Average roughness (Ra and RMS) of the different samples by material employed and RFGDT for 5µm scans	94
Fig 5-20:	Average height and Maximum range for 20µm scans of sample surfaces	95
Fig 5-21:	Average height and Maximum range for 5µm scans of sample surfaces	95

Fig 5-22:	Average Projected surface area of the 20µm scans for sample surfaces	96
Fig 5-23:	Average Projected surface area of the 5µm scans for sample surfaces	97
Fig 5-24:	Percent increase of Projected surface areas of samples for the 20µm scans	98
Fig 5-25:	Line analysis of the 20µm scans of cpTi machined control sample surfaces	99
Fig 5-26:	Line analysis of the 20µm scans of cpTi cast control sample surfaces	100
Fig 5-27:	Line analysis of the 20µm scans of Ti6Al4V machined control sample surfaces	100
Fig 5-28:	Line analysis of the 20µm scans of Ti6Al4V cast control sample surface	101
Fig 5-29:	Line analysis of the 5µm scans of cpTi machined control sample surfaces	102
Fig 5-30:	Line analysis of the 5µm scans of cpTi cast control sample surfaces	102
Fig 5-31:	Line analysis of the 5µm scans of Ti6Al4V machined control sample surfaces	103
Fig 5-32:	Line analysis of the 5µm scans of Ti6Al4V cast control sample surfaces	103
Fig 5-33:	Different values of line analysis of sample surfaces as related to fabrication procedures for the 20µm scan	106

Fig 5-34:	Tracing of the depth profile of Ti6Al4V cast control RFGDT sample	107
Fig 5-35:	Oxide thickness of samples	109
Fig 5-36:	Percent attachment efficiency and proliferation of fibroblasts on machined cpTi samples	110
Fig 5-37:	Percent attachment efficiency and proliferation of fibroblasts on machined Ti6Al4V samples	111
Fig 5-38:	Percent attachment efficiency and proliferation of fibroblasts exposed to cast cpTi samples	112
Fig 5-39:	Percent attachment efficiency and proliferation of fibroblasts exposed to cast Ti6Al4V samples	112
Fig 5-40:	Percent attachment efficiency and proliferation of fibroblasts exposed to machined samples	113
Fig 5-41:	Percent attachment efficiency and proliferation of fibroblasts exposed to cast samples	114
Fig 5-42:	Percent attachment efficiency and proliferation of fibroblasts exposed to different control samples	114
Fig 5-43:	Percent attachment efficiency and proliferation of fibroblasts exposed to SI enhanced samples	115
Fig 5-44:	Percent attachment efficiency and proliferation of fibroblasts exposed to ES samples	116

Fig 5-45:	Percent attachment efficiency and proliferation of osteoblast-like cells exposed to machined cpTi samples	117
Fig 5-46:	Percent attachment efficiency and proliferation of osteoblast-like cells exposed to machined Ti6Al4V samples	118
Fig 5-47:	Percent attachment efficiency and proliferation of osteoblast-like cells exposed to cast cpTi samples	118
Fig 5-48:	Percent attachment efficiency and proliferation of osteoblast-like cells exposed to cast Ti6Al4V samples	119
Fig 5-49:	Percent attachment efficiency and proliferation of osteoblast-like cells exposed to machined samples	120
Fig 5-50:	Percent attachment efficiency and proliferation of osteoblast-like cells exposed to cast samples	121
Fig 5-51:	Percent attachment efficiency and proliferation of osteoblast-like cells exposed to control surfaces	121
Fig 5-52:	Percent attachment efficiency and proliferation of osteoblast-like cells exposed to SI samples	122
Fig 5-53:	Percent attachment efficiency and proliferation of osteoblast-like cells exposed to ES samples	122
Fig 5-54:	Growth of fibroblasts on surfaces of machined cpTi samples after 2 days incubation	124

Fig 5-55:	Growth of fibroblasts on surfaces of machined Ti6Al4V samples after 2 days incubation	124
Fig 5-56:	Fibroblasts aligned according to the grooves created by machining on surfaces of machined Ti6Al4V control sample	125
Fig 5-57:	Growth of fibroblasts on surfaces of cast cpTi samples after 2 days incubation	125
Fig 5-58:	Growth of fibroblasts on cast Ti6Al4V samples after 2 days incubation	126
Fig 5-59:	Growth of fibroblasts on surfaces of control samples after 28 days incubation	127
Fig 5-60:	Growth of fibroblasts on surfaces of enhanced samples after 28 days incubation	128
Fig 5-61:	Growth of fibroblasts on surfaces of SI enhanced samples after 28 days incubation	129
Fig 5-62:	Osteoblast-like cells have completely covered the surface of the machined cpTi and Ti6Al4V control sample after 2 days incubation	130
Fig 5-63:	Growth of osteoblast-like cells on surfaces of machined enhanced samples after 2 days incubation	131

Fig 5-64:	Growth of osteoblast-like cells on surfaces of cast control samples after 2 days incubation	131
Fig 5-65:	Growth of osteoblast-like cells on cast enhanced samples after 2 days incubation	132
Fig 5-66:	Attached osteoblast-like cell seen on the different Titanium surfaces	133
Fig 5-67:	Growth of osteoblast-like cells on surfaces of machined samples after 28 days incubation	134
Fig 5-68:	Growth of osteoblasts on surfaces of cast samples after 28 days incubation	135
Fig 5-69:	Network of osteoblast-like cells formed on surfaces of cast Ti6Al4V control samples after 28 days incubation	136

LIST OF TABLES

		PAGE
Table 2-1	Maximum impurity limits of pure Titanium taken from Donachie (1984)	5
Table 2-2	Normal values of Titanium, Aluminium and Vanadium in Humans taken from Vargas <i>et al</i> (1992)	11
Table 2-3	Surface analytic techniques used to study material interaction with host fluids and tissues taken from Baier & Meyer (1988)	25
Table 4-1	Description of materials used in this study for sample fabrication	54
Table 4-2	Summary of the designation of sample material, fabrication procedure adopted and introduced surface enhancement	59
Table 5-1	A summary of the elemental composition of sample surfaces (At %)	75
Table 5-2	Deconvoluted Carbon 1s envelope with respective sub peak positions (Bold figures indicate highest percent)	84
Table 5-3	Deconvoluted Oxygen 1s envelope with respective sub peak positions (Bold figures indicate highest percent)	85
Table 5-4	Deconvoluted Titanium 2p envelope with respective sub peak positions (Bold figures indicate highest percent)	87

Table 5-5	Average tabulated values of the surface topography of samples for 20 μ m scans (N=5)	91
Table 5-6	Average tabulated values of the surface topography of samples for 5 μ m scans (N=5)	92
Table 5-7	Projected surface area of samples with their relative percent increase	98
Table 5-8	Averages of the line analysis done for the different sample surfaces for the 20 μ m scan	101
Table 5-9	Averages of the line analysis done for the different sample surfaces for the 5 μ m scan	104
Table 5-10	Sputter time and Oxide thickness of samples	108

CHAPTER 1 INTRODUCTION

To most people, tooth-loss is a matter of great concern and the replacement of teeth with artificial substitutes to preserve and reinstate a comparable functional and aesthetic result, is essential to the continuance of a normal life. This attitude is by no means novel, since both archeological and histological records provide adequate evidence of such endeavors. The recent discovery of a cranium approximately 2000 years old featuring a metallic oral implant, serves to demonstrate that dental implantology is one of the oldest forms of artificial tooth replacement (Glantz, 1998).

Regarding metals, Titanium has been found to be an unusually suitable material for dental implants (Kasemo, 1983). The desire for restorative materials with superior mechanical properties, has motivated the use of Titanium-Aluminium-Vanadium alloys for the manufacture of implants.

Titanium and its alloy forms were limited to wrought appliances until the beginning of the 1980's (Miyakawa *et al*, 1996; Papadopoulos *et al*, 1999; Renner, 2001). Casting of Titanium was difficult due to the high melting point of the metal and its remarkable chemical reactivity at high temperatures (Al Mesmar *et al*, 1999). Employing the lost-wax casting technique and commercially available Titanium ingots (Darvell *et al*, 1995), casting of Titanium has been made possible by the advent of specifically designed casting machines (Ida *et al*, 1984; Hamanaka, 1989) and investment materials that are more stable than the conventional investments (Mori *et al*, 1994).

In the modern era, successful clinical employment of implants requires clear evidence of osseointegration. While the term has found considerable use in the clinical community as a means of describing the anchorage of an implant in bone able

to withstand functional loading, it has eluded satisfactory scientific definition. Thus, the use of the term osseointegration has provided virtually no insight into the mechanisms by which bone becomes juxtapositioned to an endosseous implant surface.

Fortunately, although there is still a paucity of such information, we now realize that the mechanisms by which endosseous implants become integrated with bone, can be subdivided into three distinct bone healing phases, each of which can be evaluated experimentally: The phenomenon of osteoconduction relies on the migration of differentiating cells to the implant surface. Implant design such as surface roughness and the chemistry of the surface have a profound influence on osteoconduction. The second phenomenon, de nova bone formation and bonding onto the implant surface, is generally accepted to be a function of chemical surface reactivity. The existence of micro-topographically complex implant surface, which allows micro-mechanical interdigitations, is essential for bone bonding to the implant surface. De nova bone formation results in a mineralized interfacial matrix. The third leading healing phase is that of bone remodeling (Davies, 1998).

The physiochemical and biological properties of the interface zone between the inorganic implant surface and most tissues constitute a largely unexplored focus of research. When criteria for selecting implant materials are reviewed, it becomes apparent that the entire groups of possible alloplastic implant material fall into one of three categories: metal and metal alloys; ceramics and carbons; and synthetic polymers. Although each of these categories has its own virtue, the choice for a particular purpose is always a compromise between different requirements (Glantz, 1998).

Over a period of approximately 20 years various experimental methods have evolved to predict and evaluate the long-term

success of implant materials. However further criteria for selection of specific dental implant materials remain to be identified or have only been partially delineated.

One group of significant factors that have been identified concerns the chemical characteristics of the implant surface. These factors, which determine the tendency to absorb foreign atoms or molecules onto the surface, are therefore inherently associated with the chemical aspects of biocompatibility (Glantz, 1998).

At a molecular and cellular level, the complex phenomenon of bio-adhesion of dental implants may be enhanced by mechanisms such as wetting and spreading (Baier *et al*, 1984; Kasemo & Lausmaa, 1986). Surface topography has been shown to have a definitive influence on both wetting and cell attachment (Buser *et al*, 1991; Brunski *et al*, 2000). In considering cell attachment and adhesion, it is of utmost importance to note that cells do not attach directly to the implant surface but through an intermediate conditioning film (Glantz, 1998).

Since treatment outcomes in dental implantology are critically dependent on these characteristics, the analytical consideration of the present study will be directed towards that level.

2.1 Overview on Titanium

Wilhelm Gregor was the first to discover the element we know as Titanium. Martin Klaproth named Titanium after the mythological Titans (the children of heaven and earth) after having discovered what he thought was "a new earth in rutile". He also found that ilmenite contained Titanium and that this element was identical to Gregor's discovery (William, 1981).

2.1.1 Titanium Development

Titanium is widely distributed in the earth's crust (ninth most abundant element) (Parr *et al*, 1985) but it took over 150 years for Titanium to become a commercially available metal due to its high reactivity. Presently the industrial process used for Titanium extraction is based on a reduction process developed by Dr Wilhelm Kroll in the 1930's. The reduction is carried out in an atmosphere of Argon, and the metal is obtained in the form of a sponge (Briquettes). This sponge is then fused into ingots. The conversion of the Titanium ingots into mill products is accomplished by conventional metalworking equipment. Although there have been modifications in the industrial process, essentially the same process is used today (William, 1981).

At present the metal is obtainable in rod, bar or sheet form of various dimensions and must be hand worked or machined into the forms desired - a time consuming and relatively expensive procedure (Beder & Ploger, 1959).

2.1.2 Pure/Unalloyed Titanium

Pure Titanium is a relatively soft non-magnetic material. The physical and mechanical properties of chemically pure Titanium can be greatly varied by the addition of small traces of other

elements such as Oxygen, Iron and Nitrogen. Based on the incorporation of small amounts of Oxygen, Nitrogen, Hydrogen, Iron and Carbon during the purification procedures unalloyed Titanium is available in four different grades I-IV (see Table 2-1) (Donachie, 1984).

Table 2-1: Maximum impurity limits of pure Titanium taken from Donachie (1984).

Impurity Limits (WT%)					
Type	N (Max)	Fe (Max)	O (Max)	C (Max)	H (Max)
ASTM grade I	0.03	0.20	0.18	0.10	0.015
ASTM grade II	0.03	0.30	0.25	0.10	0.015
ASTM grade III	0.05	0.30	0.35	0.10	0.015
ASTM grade IV	0.05	0.50	0.40	0.10	0.015

ASTM = American Society for Testing and Materials

2.1.3 Titanium Alloy

Although pure Titanium is a very useful material, additions of alloying elements is known to improve the physical properties (William, 1981). Extensive research in the early 1950's resulted in several types of alloys, the most important being Titanium-6%Aluminium-4%Vanadium Alloy (Ti6Al4V) because of its desirable proportion and predictable producibility (William, 1981; Wang & Fenton, 1996).

Titanium alloys of interest in dentistry exist in three crystalline forms: alpha, beta and alpha-beta. These types originate when pure Titanium is heated, mixed with elements such as Aluminium and Vanadium in certain concentrations and then cooled. This treatment produces true solid solutions and the added elements are said to act as phase condition stabilizers (Guy, 1976). Elements that occupy the interstitial sites between the parent Titanium atoms in the lattice tend to stabilize the alpha phase. Oxygen, Nitrogen and Carbon come into this category while Aluminium is a further important

alpha stabilizer. Any of the transition elements is able to stabilize the beta phase i.e. Vanadium, Molybdenum, Niobium and Tantalum (William, 1981).

As Aluminium or Vanadium is added to Titanium the temperature at which the alpha to beta transformation occurs changes to a range of temperatures. In this range, both the alpha and beta form may exist. The alloy form desired is maintained at room temperature by quenching the alloy from the temperature at which the desired form exists. While Aluminium serves to increase the strength and decrease the weight of the alloy, Vanadium is called the beta phase stabilizer and once incorporated into the alloy, is said to inhibit corrosion (Renner 2001). Being an alloy it is 400% stronger and less susceptible to fracture under occlusal forces and stresses (Meffert, 1997).

The stability of the alpha and beta phases may be controlled by alloying additions, leading to a variation in the metallographic appearances of Titanium alloys (William, 1981). There are a number of thermal treatments that may give rise to varying microstructures. If the alloy is heavily worked above 900°C, a structure consisting entirely of transformed beta will be produced. The material will have low ductility and would normally be annealed. If the alloy is directly cast from the liquid phase, the beta phase is stable immediately upon solidification but has to partly transform to the alpha on cooling, leading again to an alpha and beta structure. However, in this case the acicular alpha phase is nucleated within the preexisting beta areas, which on cooling tend to give a much coarser structure. Annealing the cast alloy at 700 to 750°C will homogenize the structure (Williams, 1981).

2.1.4 Properties of Titanium

Titanium exists as a pre metal element listed in the periodic table with an atomic number of 22 and an atomic weight of

47.9. It is a silver gray, very light metal, having a density of 4.505gm/cm^3 at 25°C . It has a melting point of 1665°C though slightly variable data are reported due to the effect of impurities (William, 1981).

Titanium burns in air and it's the only metal that will burn in the presence of Nitrogen. Pure Titanium undergoes a crystallographic change on heating above 882.5°C , and can dissolve several other elements like Silver, Aluminium, Arsenic, Copper, Iron, Gallium, Uranium, Vanadium and Zinc to form alloys (Parr et al, 1985).

Titanium exists in two allotropic forms: the low temperature form, known as α (alpha) Titanium that has a close-packed hexagonal crystal structure and the body centered cubic structure called β (beta) Titanium that is stable above 882.5°C (William, 1981).

Environmental resistance of Titanium is dependant primarily on a thin, tenacious, and highly protective surface oxide film. Titanium develops stable surface oxides with high integrity, tenacity and good adherence. The surface oxide of Titanium will, if scratched or damaged, immediately reheal and restore itself regardless of its environment (Wang & Fenton, 1996). The protective passive oxide film on Titanium (TiO_2) is stable over a wide range of pH, potential difference and temperatures and is specially favored as the oxidizing character of the environment increases. For this reason Titanium generally resists mild reducing, neutral and highly oxidizing environments up to reasonably high temperatures. The major exceptions are strong solutions of some acids, particularly Sulphuric acid, Hydrochloric acid, Phosphoric acid, Oxalic and Formic acid and also solutions containing the Fluoride ion (William, 1981; Wang & Fenton, 1996).

2.1.5 Titanium Oxides

Titanium is a reactive metal (Parr et al, 1985) and within a millisecond of exposure to air, a 1nm oxide layer will be formed on the exposed surface of pure Titanium (Kasemo, 1983). Within a minute this layer can become 10nm thick. Within a few seconds the oxidation is often virtually completed, since the surface oxide growth is stopped as a result of the slow transport of Oxygen and unreacted metal atoms (Glantz, 1998). Passivity of Titanium is normally due to a few nanometers ($1\text{nm}=10^{-9}\text{m}$) thick film of amorphous Titanium dioxide (Schutz & Thomas, 1987).

A metal that is passive does not mean that it will not corrode but that the rate of corrosion is significantly reduced by the presence of the protective surface oxide film. Under physiological conditions in which implants function, even this slow rate may produce adverse tissue reactions (Parr et al, 1985).

The passivated oxide layer at the surface of Titanium has the physical properties of a ceramic and most metal oxides share this property (Albrektsson et al, 1983). The manufacturing procedure (air composition, impurities, temperature, coolant) influences the composition of the oxide layer and eventually the biocompatibility of the material. Therefore a strict standardization of the procedure and bulk metal is mandatory (Van Steenberghe, 1988; Young, 1988; Keller et al, 1989). Many of the Titanium alloys, in which Titanium is present in concentrations of 85% to 95%, maintain the passivity of pure Titanium. Although there is no universally accepted definition of the term "passivity" for our purposes, if an implant metal is oxidized and the oxide does not breakdown under physiologic conditions, the metal is said to be passive or passivated. The oxide layer will repair itself instantaneously on damage such as might occur during insertion of an implant (Parr et al, 1985).

Common Titanium oxides appear in three different crystalline forms (anatase, rutile and brookite), each with different physical properties. Rutile (TiO_2) is the most stable and widely used. Of special interest is the dielectrical constant - for anatase it is 48, for brookite 78 and for rutile it is between about 110-117 depending on orientation. No other metal oxides have such high dielectric constants (Albrektsson *et al*, 1983).

There are 7 different possible types of oxides that can form on Titanium materials and they include: (1) amorphous oxide, (2) cubic Titanium oxide (TiO), (3) hexagonal Titanium sesquioxide (Ti_2O_3), (4) tetragonal Titanium dioxide (TiO_2) (anatase), (5) orthorhombic TiO_2 (brookite), (6) tetragonal TiO_2 (rutile), and (7) nonstoichiometric oxides (Ti_xO_y). Normally, anodic oxidation with chromic acid forms amorphous Titanium oxide (Lim *et al*, 2001). The stoichiometric composition of cpTi allows its classification into four grades that vary mainly in the Oxygen content, with grade 4 having the most (0.4%) and grade 1 the least (0.18%) (Albrektsson, 1985).

The oxide layer on alloyed Titanium has a thickness approximately corresponding to pure Titanium. The major differences between pure and alloyed Titanium are (Kasemo & Lausmaa, 1991):-

1. The oxide on the alloy is enriched with the alloying elements Al and V,
2. The surface texture and microstructure are more complex and heterogeneous on the alloy,
3. Even thick anodic oxide films do not crystallize as those on pure Titanium.

The growth of the oxide film obeys the high field theory i.e. the thickness of the oxide film depends on the potential

difference across the film (Young, 1972). Accordingly the natural oxide growth under open circuit conditions has been suggested to be a weak function of time with a very low expected oxide growth rate (Mattsson, 1990).

Normally Titanium forms a passive surface oxide layer that is relatively stable and acts as a barrier against diffusion of elements from within the metal itself to the surface and from the outside onto the metal. In the passive state the rate of dissolution of the oxide layer is relatively low but occurs especially when the environment contains aggressive ions. The presence of contaminants modifies the oxide layer and influences its corrosion resistance. The oxide layers on Ti6Al4V have been found to be more amorphous and Ti6Al4V is generally less corrosion resistant than Titanium itself, which is normally covered by a stoichiometric oxide layer (Low, 1997).

2.1.6 Corrosion of Titanium

Titanium is well tolerated by tissues; indeed it readily lends itself to the descriptive title of a physiologically indifferent metal (William, 1981) and in tissue Titanium is no chemical burden because of its inert reaction in solution (Steinemann, 1998). When Titanium is coupled with metals with greater corrosion potentials, the other metal may corrode by mechanism of galvanic corrosion (Parr *et al*, 1985) and release metallic species into tissues (Williams, 1982).

In the presence of chlorides, localized breakdown has been found to occur despite the highly passive oxide layer on cpTi and Ti6Al4V. Breakdown events are enhanced by increased acidity, while an alkaline environment may enhance a reaction by being negatively charged in physiological solutions, attracting the positively charged ions with in the body fluids and facilitating bonding leading to bio-acceptability (Shirkhanzadeh, 1996).

The precise amount of Titanium, Aluminium and Vanadium that is released by the implants has not yet been determined. Table 2-2 summarizes average normal values of these elements in humans (Vargas *et al*, 1992).

Table 2-2: Normal values of Titanium, Aluminium and Vanadium in Humans taken from Vargas *et al* (1992).

Element	Total body burden	Normal daily intake	Normal daily excretion rate
Titanium	15 mg	0.3-1 mg	0.3 mg
Aluminium	300 mg	5 mg (mean)	N/A
Vanadium	0.1-0.2 mg	12-28 µg	9.3 µg

N/A – not determined

The normal value of Titanium in serum is still doubtful, but is probably less than 10ng.ml^{-1} , that for Aluminium is below 10ng.ml^{-1} ; for Vanadium less than 1ng.ml^{-1} . (Versiek, 1984; Lugowski *et al*, 1987). The concentration of Titanium in the contact tissue around implants is about 100 times higher than that of muscle tissue, but to date no case of local or systemic reaction for Titanium has been documented (Steinemann, 1998).

Based on its biological activity, release of Aluminium ions has the potential to be associated with neurological disorders such as Dialysis Dementia, Alzheimer's disease (Smith, 1988; Bruneel & Helsen, 1988; Pilliar, 1991) and Encephalopathy (Winship, 1992). Aluminium has also been implicated in Osteomalacia, Microcytic Anemia and bone diseases, which include Vitamin D Refractory Osteodystrophy, and Hypercalcaemia (Smith, 1988; Bruneel & Helsen, 1988).

Toxicity of Vanadium ions is much less understood than the toxicity of Aluminium but is not considered to be very high. Aluminium is mainly associated with irreversible enzymatic

disturbance (Bruneel & Helsen, 1988) as well as inhibition of the mineralization process of bone (Albrektsson, 1989; Pilliar, 1991). Most Vanadium effects are associated with phosphate biochemistry by affecting the mechanism of Na^+ , K^+ , Ca^{2+} and H^+ ATPases, since Vanadium acts as a Phosphorus analog (Boyd & Kustin, 1984).

2.2 Fabrication of Titanium

Titanium in its pure and alloy form was limited to wrought appliances until the beginning of the 1980's, when it was introduced into Prosthodontics as a cast material (Miyakawa *et al*, 1996; Papadopoulos *et al*, 1999; Renner, 2001).

2.2.1 Machining of Titanium

Titanium is available in bar or rod form of different diameters (ASTM, 1999). Fabrication of Titanium into different forms is achieved by use of lathe machines. The desired shape is cut and hand ground through 600- grit Silicon Carbide metallographic papers followed by a final polish with 1 μm diamond paste. After polishing, the specimen is cleaned using a solvent (Methylethyl ketone), washed in double distilled water and acid passivated in 30% Nitric acid. Autoclaving is then done. Different companies have their own way of fabricating implants from Titanium but basically follow the above-mentioned process.

2.2.2 Casting of Titanium

Titanium casting is difficult because of its high melting point and remarkable chemical reactivity at high temperatures. To overcome these difficulties special equipment and systems have been developed for casting this metal (Al-Mesmar *et al*, 1999).

There are two ways to cast pure Titanium or Titanium based alloys for use in dentistry. One is to utilize the conventional dental casting technique by alloying and thus lowering the melting temperature of Titanium, and the other is to use a super high temperature resistant mould material and a casting machine suitable for casting of Titanium. To avoid contamination the casting procedure must be carried out in a vacuum or in an atmosphere of inert gas, hence modification of the established melting and casting techniques used for most metals (Beder & Ploger, 1959).

2.2.2.1 Casting Machines

Titanium is cast in specially designed casting machines using different technology compared with that used for conventional noble and base metal dental alloys. Available casting machines are classified into three types (Zinelis, 2000):

- a) Inert gas arc-melting/gas pressure casting machines that consist of 2 chamber: an upper chamber (melting chamber) for arc melting under an inert atmosphere (Ar gas) and a lower chamber (mold Chamber) with a muffle in which the molten metal is forced into, under gravitational acceleration and inert gas pressure; (e.g. Castmatic system, Titaniumer machine, Tycast machine, Cyclarc system)
- b) Inert gas arc-melting/centrifugal casting machines with vertical or horizontal centrifugal casting;
- c) High-frequency induction-melting/gas pressure casting machines.

2.2.2.2 Cyclarc Titanium Casting Machine

Bessing & Bergman (1992) evaluated the castability of unalloyed Titanium in three casting machines and reported that

the Cyclarc machine produced the best results. The Cyclarc Titanium-Casting Machine¹ was produced especially to cast pure Titanium for the field of dentistry (it casts Titanium preserving its original properties). It is an Arc-type casting machine and the Cyclarc equipment contains the melting/casting unit, transformer, and protection gas. It has an extraordinary casting ability by using the pressure-differential method. The casting chamber consists of an upper melting chamber and a lower casting chamber, both of which are connected by a central hole with each other (see 4.1.2.2, p58). The casting ring is set at the bottom of the hole, and a crucible made of copper lies on top of it. An ingot or billet is placed in the centre of the copper crucible. First both the upper and lower chambers are evacuated by a built-in vacuum pump. The high degree of vacuum exhaust eliminates the reaction of molten Titanium with Oxygen, Nitrogen and moisture. After the air is exhausted, compressed Argon is fed into the upper chamber and an arc is generated between a Tungsten electrode (-) and the ingot/billet (+). Since the lower chamber is kept under vacuum (12Pa), a flow of Argon is maintained in the casting ring due to the pressure differences between the upper and lower chambers. Immediately after the billet has melted in the Argon environment, the molten metal falls down through the central hole and runs into the mould in the ring (Anony, 1991; J Morita Corp., Kyoto, Japan).

2.2.2.3 Investment Material

Two methods of casting have been developed which seem satisfactory. The first is shell molding and the second is investment casting with which the dental profession is familiar (Beder & Ploger, 1959). The properties required for an investment material for use in casting include controlled thermal expansion, hot strength to resist cracking and

¹ J Morita Corp., Kyoto, Japan

fracture, low hot deformation and minimal interaction with the metal to be formed (Curtis, 1998).

It is difficult to cast Titanium into a mould that is made of conventional investment materials. Therefore, more stable oxides than Titanium have been experimentally applied as refractory agents for its casting; such oxides include Calcia, Magnesia and Zirconia. In many dental laboratories, on the other hand, a Phosphate Bonded Alumina/Silica investment has been used for the same purpose (Miyakawa *et al*, 1989).

Phosphate bonded investment materials are extensively used in the lost wax casting technique because of their heat resistance at applicable casting temperatures. The thermal expansion of the refractory mould is used in the casting process to compensate for the solidification shrinkage of the cast alloy. Chemical interactions are known to occur between Phosphate bonded investment materials and cast metal surfaces during casting hence the necessity to grit blast cast metal surfaces to remove refractory material that adheres to the casting after devesting (Curtis, 1998).

2.3 Osseointegration

The process of "osseointegration" is considered of pivotal importance for establishing an intimate and stable connection between bone and implant surface (Branemark, 1983). Branemark *et al* (1985) describes "osseointegration" as a direct structural and functional connection between ordered, living bone and the surface of a load-carrying implant without soft tissue intervention.

According to Meffert (1997), osseointegration needs to be redefined into "adaptive osseointegration" in which the osseous tissue approximate the surface of the implant without any apparent soft tissue interface and "biointegration" is a direct biochemical bone interface.

How well an implant is fixated to the surrounding bone tissue is dependant on different implant and host related factors. The exact biological, biomechanical, and operative conditions which promote optimal osseointegration of implants are not known though six factors listed by Albrektsson *et al* (1981) and Matsuda *et al* (1998) have gained a general acceptance as being specially important: biocompatibility, design, surface quality, status of host tissue, surgical technique and loading conditions. The first three factors are implant related.

The mechanisms by which implants become integrated in bone can be subdivided into three separate phenomena, each of which can be tested experimentally (Davies, 1998). Bone may be formed on an implant surface either by distant or contact osteogenesis (Osborn & Newesley, 1980). In distant osteogenesis, new bone is formed on the surfaces of bone in the peri-implant site, similar to normal appositional bone growth. The existing bone surfaces provide a population of osteogenic cells that lay down new matrix, which as osteogenesis continues, encroaches on the implant itself - surrounding it. One can deduce that the implant surface is obscured from bone by intervening cells and connective tissue. In the second phenomena of contact osteogenesis, new bone forms first on the implant surface - *de nova* bone, which requires the recruitment of potentially osteogenic cells to the site of future matrix formation (see Fig 2-1, p17) (The Colgate Oral Care Report, 2000).

Puleo & Nanci (1999), suggest that bone is deposited directly on the surface of the implant, extending outwards from the biomaterial. Thus bone formation in the peri-prosthetic region occurs in two directions; not only does the healing bone approach the biomaterial, but bone also extends from the implant towards the healing bone. Interestingly the bone that forms away from the implant forms at a rate of about 30% faster than that moving towards the biomaterial.

Osseointegration of dental implants

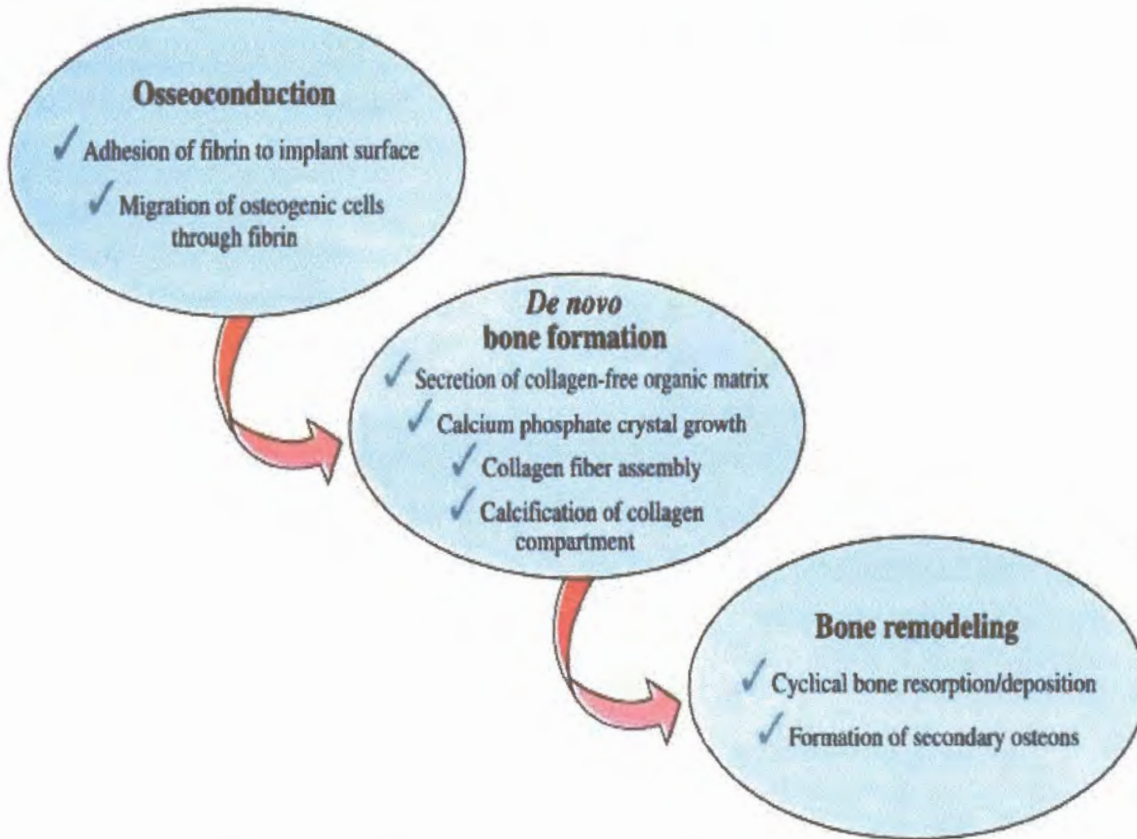


Fig 2-1: Three separate phenomena of osseointegration taken from The Colgate Oral Care Report, 2000)

In reality, one can assume that any implant healing compartment will display both the distance and contact osteogenesis phenomena. Subsequently, a third tissue response, that of bone remodeling will also, at discrete sites, create de nova bone formation at an implant surface (Davies, 1998).

If osseointegration is not successfully achieved, fibrous tissue is generated instead, leading ultimately to loosening and loss of the implant (Groessner-Schreiber & Tuan, 1992). A properly osseointegrated implant at the cortical passage should have a minimal direct bone contact of 90% to 95% of the implant surface (Albrektsson & Jacobsson, 1987).

Osseointegration is associated with intimate and long lasting contact between bone and the alloplastic tooth root

replacement material. There is as yet no generally accepted device or method for the objective clinical assessment of osseointegration (Zarb & Albrektsson, 1993).

2.4 Titanium and its Alloys as Dental Implants

Implant materials used by early practitioners of implant dentistry included Gold, Precious stones, Ivory, Iridium, Iridio-platinum, Vanadium and others (Balkin, 1988).

Even at very early stages of implantology it was acknowledged that it makes sense not to use materials that are frankly toxic, either to the tissues immediately surrounding the implant or systematically. Likewise, materials that are quite brittle or relatively soft were understood early on not to be adequate (Glantz, 1998).

Beder & Ploger in 1959 described the use of Titanium as intra-oral implants. Presently Titanium in various forms appears to be the most popular metallic implant material in use due to its high corrosion resistance against chemical attacks, desirable physical and mechanical properties and its excellent bio-acceptability (Buser *et al*, 1991; Glantz, 1998).

The dental implant differs from the typical orthopedic fixture, which heals and remains in a buried environment, in that the dental implant is intimately connected with the oral cavity, as it is semi-buried (Dmytryk *et al*, 1990).

According to the ASTM (1995) XI Rationale of the Standard Specifications for Unalloyed Titanium for Surgical Implant Applications, the choice of composition and mechanical properties is dependent upon the design and application of the medical device. Alloys possess many favorable mechanical and physical properties that make them excellent implant materials. The finer microstructure and two-phase alloy indicate a higher material strength. This condition improves

certain properties, such as fatigue strength, which is critical for some implant designs (Lemons, 1986).

The Titanium oxide or oxides never allow for any molecular contacts to be established between the true implant metal and the host tissue, but rather between the tissue and the surface oxide(s) of the implant. Even if surface oxides of metals and metal alloys contain both defects and impurities they still form stable oxides - TiO_2 (Glantz, 1998).

2.5 Classification of Dental Implants

Dental implants may be classified according to their constituent material, their position, and their design or physical form.

a) By constituent material: Most implants are made of metal. The metals include commercially pure Titanium, Stainless Steel and other alloys like $Ti6Al4V$ (Worthington, 1988).

b) By position, they may vary in that they may be placed (Worthington, 1988):

- Beneath the periosteum (subperiosteal implants)
- Through the full vertical thickness of the lower jaw (transosteal implants).
- They may be inserted into the bone of either jaw (endosteal implants)

c) By design: Titanium can be easily prepared into many different shapes and textures without affecting its biocompatibility (Schwartz *et al*, 1996). There are two types of retention for the endosseous implant: mechanical and direct bonding. Mechanical retention would consist of some type of macro-retention that is visible such as threads, pores, grooves, steps, holes, slots, dimples, etc. into which the bone would grow during the healing phase. Direct bonding

implies a chemical bonding of the bone to the implant material, such as would occur in ankylosis (Meffert, 1986).

The design of implants must suit the desired application, and in implant dentistry, screw and cylindrical implants are the preferred shape because they are relatively easy to place and remove (Gotfredsen *et al*, 1988; Gotfredsen *et al*, 1992; Albrektsson, 1993). Introduction of threads to the cylindrical implant improves the implant stability significantly (Frandsen *et al*, 1984).

2.5.1 The Implant Surface

The surfaces of currently available dental implants range from relatively smooth machined surfaces to those roughened by coatings, abrasions or blastings, acid etching, or combinations of these techniques (Buser, 1999).

Rough surfaces can be made using an addition or a subtraction technique. For instance, the addition of a hydroxyapatite (HA) surface coating on implants is popular because it is a highly biocompatible material. Subtraction techniques are simpler and provide a more uniform roughness and grit blasting is most commonly used (Mugnolo & Filliponi, 2001). The term "roughened" is erroneously used today to describe many different implant surface modifications, even though these modifications do not make the modified implant surface rougher than machined surfaces (Klokkevold, 2002).

2.5.1.1 Machined Surfaces

Threaded implants represent the most common design of dental implants, and although their primary form of fixation is macroscopic mechanical interlock with bone, much finer microscopic surface features exist that may influence the osseointegration potential of these designs (Branemark *et al*, 1977).

The primary mode of fixation of threaded implants relies on the macroscopic thread geometry. By appropriate selection of thread geometry, stresses dissipated in bone can be lowered and this presumably will reduce the possibility of localized crestal bone loss (Pilliar, 1998).

The microscopic features are related to the machining operation used for forming the threaded shapes and include fine machining lines, pits and gouges as well as some zones where metallic debris has been "cold welded" to the surface (Pilliar, 1998).

Differences in appearance due to variation in machining techniques do exist. It is however recognized that different implant companies have surfaces that are similar but not identical (Cochran, 1999).

The relatively smooth machined implant surface gained early popularity in the United States after its introduction in Canada in the early 1980's. Presently virtually every dental implant manufacturer markets implants that feature some form of roughened surface (Cochran, 1999).

2.5.1.2 Osseotite Surface

Chemical etching has also been used to develop textured bone-interfacing implant surfaces for enhanced implant fixation. This technique has been used for modifying surfaces of blade-type implants as well as threaded and cylindrical root-form implants subsequent to machining or other forming operations. As a result of controlled surface chemical attack that results from exposure to acid solutions, small pits form more or less regular arrays over the implant surface. Typically these are micron- to sub-micron sized and results in increasing the surface area of the implant (Pilliar, 1998). This implant is characterized by a hybrid design, a short, approximately 2- to 3-mm long machined surface in the crestal area, and an acid-

etched (Sulphuric-acid/Hydrochloric-acid) surface overall². The Osseotite surface features micro-pits produced by the etching procedure, but its profile is flatter since no grit blasting procedure is used prior to the etching resulting in a Ra value of 1.3µm (Buser *et al*, 1998).

Lazzara *et al* (1999) assessed the Osseotite surface and concluded that the surface develops a statistically higher bone to implant contact and had an enhanced osteoconductive potential in poor quality bone when compared to the machined surface. Even if similar techniques are utilized to obtain a roughened surface, the conditions of the treatment could have an effect. For example, if an acid is used, the concentration of the acid, the time of exposure and the temperature of the acid bath can all influence the resulting surface characteristics.

2.5.1.3 Grit Blasted Surfaces

One approach for producing surfaces with irregularities is to grit-blast using an appropriate blasting medium. Typically SiC, Al₂O₃, glass or TiO₂ shot (particles) is used to erode a substrate to form irregular surfaces with pits and depressions that vary in size and shape depending on the blasting conditions (blasting medium, pressure, distance from blasting nozzle to implant surface, blasting time). Blasting also enlarges the surface area of an implant. Wennerberg *et al* (1996), demonstrated that the size of the blasting particles have a great effect on the amount of bone-implant contact, while the type of particle has no effect.

The Sand blasted, Large grit, Acid etched (SLA) surface was launched in mid June 1998 at the ITI world symposium in Boston and it is said to have a macro/micro double roughness (Scacchi, 2000). Pioneering work by Buser *et al* (1991), using

² Osseotite, Implant Innovations, Palm Beach Gardens, Florida, USA.

Scanning Electron Microscopy described the SLA surface as being characterized by a primary roughness produced by the sandblasting process that creates "valleys" whereas the acid-etching procedure removes remnants of grits and attacks the Titanium surface producing a secondary roughness that is apparent in the scanning electron micrographs. According to Buser (1998), the rough-blasted surface had superimposed micro-pits of 1- to 2- μm -diameter and a Ra value of 2.0 μm .

The SLA is a solid screw implant (4.05mm diameter), characterized by a sandblasted (Large grit of 250 to 500 μm and acid etched (sulphuric-acid/hydrochloric-acid) surface³ and has consistently showed the best results both in histomorphometric and biomechanical testing. Aaboe *et al*, (2000) also showed that osseointegration of subperiosteal implants could be obtained when the surface was sandblasted and acid etched. However, long-term clinical studies on the survival of these implants have not been published.

2.5.1.4 Bioactive Coated Surfaces

The term bioactive or surface-active material is commonly used to describe those materials that generate direct biological or chemical bonding to their surfaces (Davies, 1989).

Plasma spray coating of implants to create a porous surface was first reported by Hann & Palich (1970). The Titanium sprayed surface is obtained by thermal spraying of Titanium on to the Titanium implant giving it a semi-porous structure. Plasma spray technique has also been used to coat Titanium implants with HA - hydroxyapatite (Buser *et al*, 1991).

Dental implants formed by sintering Ti6Al4V alloy powders to a machined Ti alloy substrate represents still another approach for achieving fixation by bone in-growth and micro-mechanical

³Institut Straumann, Waldenburg, Switzerland

interlock (Pilliar *et al*, 1991). Following sintering, an integral implant structure is formed with a solid inner region providing overall mechanical strength and a porous surface region within which bone can form, thereby resulting in secure implant-to-bone fixation.

The uniqueness of this sintered porous structure compared with the other surface structures described previously, is the interconnectivity of the pores of appropriate size to allow rapid bone ingrowth during healing. The Ti6Al4V alloy powders used to form the porous surface zone are nearly spherical in shape by virtue of the atomization process used for their formation. Clinical experiences with sintered porous-surface dental implants indicate cumulative success rates over 8-year periods similar to those reported for other designs despite the fact that porous-surfaced implants of significantly shorter lengths were used (Pilliar, 1998).

In contrast to calcium phosphate coatings, biochemical surface modifications utilizes critical organic components of bone to affect tissue response. Coatings incorporating biomolecules are also being explored for delivering biomolecules to the tissue-implant interface (Brunski *et al*, 2000).

According to Rieger *et al* (1989), neither clinicians nor manufacturers should assume that bioactive coatings or bone bonding in general improve the biomechanical prognosis of implants.

2.6 Surface Characterization

Surface characterization is critical to biomaterials science because it provides the following information: unknown identification, reproducibility assurance, quality assurance, contamination detection and correlation between measured surface properties and biological responses (Baier & Meyer,

1988). The different techniques used for characterization are summarized with regard to their utility in Table 2-3.

Table 2-3: Surface analytic techniques used to study material interactions with host fluids and tissues taken from Baier & Meyer (1988).

Technique	Utility
Profilometry	Surface texture roughness
Electron Microscopy	Ultrastructure, surface morphology
Electron Spectroscopy for chemical analysis	Elemental and chemical bonding data for outermost 0.001 to 0.01 μm of surface
Scanning auger microprobe analysis	Elemental and Chemical state data for outermost 0.001 to 0.005 μm ; depth profiling

Biomaterials research requires specific information about the quality of a surface utilized for experimentation or application. The most important contribution that surface characterization could make to the field of biomaterials science would be the direct correlation of surface structure or chemistry with the *in vivo* performance of materials in humans. This desirable goal, unfortunately, is still far from being realized. An intermediate goal might be to use physical surface characterization tools to perform preliminary screening on materials in order to eliminate unlikely samples from expensive biological evaluation (Ratner, 1983).

There are several ways to modify surface chemistry, topography and microstructure, although controlling all the parameters simultaneously is very difficult (Larsson, 2000). Various preparative procedures are known to introduce differences in surface topography and surface energy (Smith *et al*, 1991). Comprehensive surface characterization is therefore necessary to interpret cellular and, ultimately, tissue response to such surfaces (Smith *et al*, 1991).

2.6.1 Compositional-Considerations

The properties of an implant are determined, in part, by its chemical composition (Schwartz *et al*, 1996). The important fact that the implant surface consists of a relatively thick Titanium oxide must be remembered when the chemistry of the implant-tissue interface is considered. The chemical properties, and therefore the interface chemistry, are determined by the oxide layer and not by the metal itself (Mesaros, 1989). A dense oxide film with a thickness of approximately 10nm covers the bulk Titanium metal. Because surface oxides grow by inward transport of oxygen atoms (from O₂ molecules or H₂O in the atmosphere) and/or outward metal atom transport from the oxide-metal interface, there will be some concentration gradients for Oxygen and Titanium (Kasemo, 1983).

The chemical properties of the biomaterial surface play an important role for the tissue responses elicited by the material. This is at least one main reason why the tissues respond differently to different materials. A material with a surface that is accepted by the tissue seems to exhibit improved integration with bone, either due to passive growth, leading to a tight connection between implants and bone, or by stimulation that probably leads to bone implant bonding (Ellingsen, 1998).

It is now well understood that the surface composition of most implant materials is substantially different from the bulk, and a variety of techniques have been used to characterize such surfaces (Ratner, 1988; Smith, 1991). Klauber *et al* (1990) found considerable variation in surface contamination on as supplied dental implants with some showing high levels of Silicate in the oxide layer. Lausmaa *et al* (1990) found a dominance of Titanium and Oxygen peaks with relatively strong Carbon signal that they assigned as a normal observation for exposed surfaces. The Titanium and Oxygen signals show that

the surface consists mainly of Titanium oxide layer. Taborelli *et al* (1997), found negligible chemical compositional differences between samples they analysed and related it to the stability of the oxide layer formed upon exposure to air. Variable chemical composition from preparative procedures may also be accompanied by changes in surface topography and surface energy (Smith, 1991). Surface composition can be assessed at different depths - 1nm or greater than 5nm.

2.6.1.1 X-ray Photoelectron Spectroscopy (XPS)

XPS is used to elicit surface elemental and chemical information. The sample is exposed to a flux of X-ray photons, which excite electrons within the sample. The energy of the electrons is quantitized, and therefore discrete and the energy position of these (discrete) electronic energy levels is different for every atom (or solid) in the periodic table. Thus, the number of excited electrons with the energy close to each particular energy level will be higher than the number of electrons excited at other energies (Kittel, 1996). Moving through the solid towards the surface the electrons undergo (inelastic) collisions with ions and other electrons (Dowben, 1994). Therefore, only those electrons that were excited close to the surface (typically few electronic mean free paths away from the surface) have a reasonably high probability to reach the detector and be detected. Thus the information in XPS comes from a region close to the surface, at most 25nm below the outermost atomic layer (Krozer *et al*, 1999).

Surface analysis by XPS involves irradiating a solid *in vacuo* with monoenergetic soft X-rays and analyzing the emitted electrons by energy. The spectrum is obtained as a plot of the number of detected electrons per energy interval versus their kinetic energy. Each element has a unique spectrum. The spectrum from a mixture of elements is approximately the sum of the peaks of the individual constituents. Quantitative data

can be obtained from peak heights or peak areas and identification of chemical states often can be made from exact measurements of peak position and separation as well as from certain spectral features. Each element has a unique set of binding energies and XPS can be used to identify and determine the concentration of the elements in the surface. The electrons leaving the sample are detected by an electron spectrometer according to their kinetic energy. The analyzer is usually operated as an energy window referred to as the pass energy, accepting only electrons that are within the range of its window. A broad survey spectrum is obtained to identify the elements present, after which higher resolution scans can be performed around an elemental peak to identify chemical states. Curve fitting is normally applied to the high resolution peaks (Moulder *et al*, 1992).

A spectrum is used as a "fingerprint" of the surface (Kasemo and Lausmaa, 1988b). The atomic percent of each element on the surface can be calculated from the photo peak by marking and measuring the area by use of the XPS computer software. The detection limit of the machine for elements is ~ 0.1%. Identification of the different spectra can be done by use of the Handbook of X-ray Photoelectron Spectroscopy (Moulder *et al*, 1992).

Various photoelectron peak constituents can be obtained from peak separation measurements and full widths half maximum values (FWHM) using the Gaussian-Lorentzian curve fitting for elements with atomic percentage greater than 3% (Kilpadi *et al*, 1998a; Kilpadi *et al*, 2000).

As mentioned the sample is irradiated with X-rays, most commonly XPS can be performed at angles of $\sim 5^\circ$ to 90° with the sample normal, depending on what depth one wants to extract data from. If the sample surface is not totally flat, screening of the irradiating source by surface features can occur and "dead spots" are created on the surface.

2.6.2 Surface Topography

A surface is the boundary between two media and can be divided into two categories: functional and non functional. A non-functional area can be either mirror smooth or sandpaper rough without influencing the quality of the part while a functional surface is required to perform a function that is related to the users perception of the part's quality. Regardless of the function, the surface texture has a direct influence on the quality of the part. When the correlation between surface topography and part function is known, quality can be optimized. A surface is made by a combination of one or more formative processes. There are three broad categories of production processes that can influence surface topography:

1. Material removing processes
2. Material adding processes
3. Forming processes

Processes can also be classified as either random or periodic. A random process is one where there is no discernable pattern on the surface. This is called an isotropic surface (investment casting)(see Fig 2-2a, p30). A periodic process creates a surface that has evenly spaced irregularities on it (turning). This is called an anisotropic surface (see Fig 2-2b, p30). A particular manufacturing process is capable of producing a limited range of surface roughness values (Mummery, 1992).

Surface geometric features are categorized as either macroscopic or microscopic. Macroscopic surface features can be readily characterized by unaided visual observation (magnification instruments are not needed). Typically, macroscopic features have dimensions measured in millimeters or greater. Microscopic variables describe features that can only be characterized fully with the assistance of optical or

electron microscopy. The dimensions of these features range from hundreds of microns (but less than a millimeter) to submicrons (Pilliar, 1998).

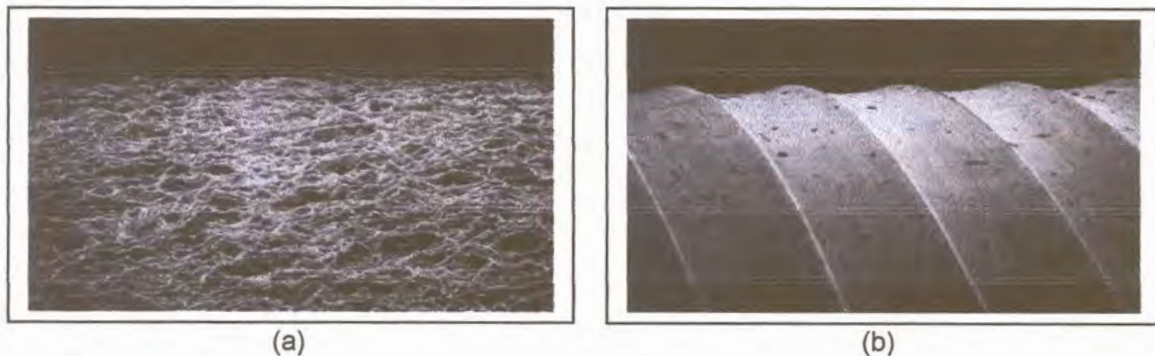


Fig 2-2: a) Cast surface (An isotropic surface) and b) Machined surface (An anisotropic surface) taken from Mummery (1992)

Another important factor of the surface configuration is the microstructure of the implant surface probably in conjunction with macro-irregularities. This can vary considerably depending on the surface treatment of the implant. Variation of the surface microstructure has been reported to influence the stress distribution, retention of the implant in bone and cell responses to the implant surface. Surface roughness on a smaller scale was, however, found to be important for integration of the bone with the implant surface (Ellingsen, 1998).

Surface roughness on the atomic scale can, on the contrary, also influence the (local) chemical bonding through the particular geometric arrangements that can be established. When van der Waals interaction is prevailing, surface roughness will in principle also modify the interaction since it influences the local electromagnetic fields at the surface (Kasemo, 1983). The optimal surface topography for cell attachment to implants may differ for different cell types (Chehroudi et al, 1989). Abron et al (2001) in their study confirmed that alterations in cpTi implant topography alter the degree of bone formed at the implant surface. They associated a "rougher" implant surface with increased bone-to-

implant contact. Two surfaces with very different (R_a and R_p - v) parameters (non-ideal vs machined) did not show differing abilities to support bone formation. These results indicate the gross inadequacy of defining an implant in general terms of "rough or "smooth".

If two surfaces with different roughness characteristics are measured, the results for each surface should yield different values; this difference should be reflected by the roughness parameters. If the values do not show the difference, the measured data is meaningless and another parameter should be chosen. A roughness parameter should be used only if it is sensitive to the important surface characteristics. The selection of roughness parameters should be carried out with this criterion in mind (Mummery, 1992). The characterization of the surface topography was previously performed with stylus profilometry, a method frequently used to characterize Titanium surfaces with different roughness values (Wennerberg *et al*, 1992). The Atomic Force Microscope is another type of instrument that has been employed to access surface roughness.

2.6.2.1 Atomic Force Microscope (AFM)

The Atomic Force Microscope is a recent innovation that relies on a mechanical probe for generation of magnified images. The essential component in the AFM is a sensor with very high spatial resolution. The sensors can routinely measure distances with an accuracy of 0.01nm. The force sensor measures the deflection of a cantilever such that when the cantilever moves the light beam from a small laser moves across the face of a four-section photo detector. Imaging modes sometimes referred to, as "scan modes" or "operating modes" are the methods that are used to move the AFM probe over the sample surface and sense the surface in order to create an image. Imaging modes can be classified as "contact" or "non contact" depending on the net forces between the probe

and sample. In non-contact imaging mode the cantilever is pulled towards the sample by attractive forces while in the non contact imaging mode the cantilever is curved away from the sample due to repulsive forces. The force most commonly associated with atomic force microscopy is an inter-atomic force called the van der Waals force. The cantilever is held on the order of tens to hundreds of angstroms from the surface sample. The tip of the cantilevers for the AFM microscope are fabricated from Silicon Nitride and is located at the free end of a cantilever that is usually 100 to 200 μm long (Anony, 1996).

There are several scanners available and the choice of scanner depends on the dynamic scan range required. Scanning Probe Microscopes were used solely for measuring surface topography and though they can be used to measure many other surface properties it is still their primary application (Anony, 1996).

The AFM microscope with its software is normally used for interpreting images created as a result of the AFM scanning probe. Depending on the required investigations either a 3D or 2D image is displayed after the removal of any scan line anomalies. Using the 3D image, values of area analysis can be measured namely R_a , RMS, maximum range, average height and projected surface area (see Area analysis, p33). For line analysis, required lines are drawn either on the horizontal, vertical or transverse axis on the 2D scanned image also after leveling and shading. Software is then used to define the values of the drawn lines namely R_a , R_p , R_{pm} , R_t , R_{tm} (see Line analysis, p33-34) (Anony, 1996).

The scanners come in different sizes ranging from 130 μm to 7 μm . Normally depending on the image required a corresponding scanner is used but smaller scan images can be zoomed from selected areas and analyzed (Anony, 1996).

Each of the values of area analysis and line analysis can be defined as follows (Mummery, 1992):

a) Area analysis

- i) Area Ra - Ra is the average roughness of the scanned area.
- ii) Area RMS - RMS is the root mean square of Ra. It is more sensitive than the numerical average of Ra.
- iii) Average height - The highest point from the zero value on the whole surface is regarded as the Average height.
- iv) Maximum range - Maximum range is the range between the highest to lowest point along the surface area, even below the zero value.
- v) Projected surface area - calculated area increase due to surface topography.

b) Line analysis

- i) Ra -Average roughness -The mostly used roughness parameters is Ra. In the past, Ra was known as the CLA - Center Line Average in England or AA - Arithmetic Average in the U.S.A. It is expressed in microinches or micrometers and does not differentiate between peaks and valleys. Since it is the average deviation of the profile from the mean line, defects in the surface do not influence the measured results greatly.
- ii) Rt -Is a true indication of the Maximum peak height to the Maximum valley depth of the roughness profile over the total assessment length. The values of Ra (see (i)) and Rtm (see (iii), p34) are more useful than Rt.

- iii) R_{tm} -Is the Mean peak-to-valley height within an assessed profile. It is the average of the Peak-to-valley heights. Since maximum profile heights and not averages are being examined, it is generally more sensitive to changes in surface finish than R_a (see (i), p33). R_{tm} values that are similar indicate a consistent surface finish while a significant difference indicates a surface defect in an otherwise consistent surface.
- iv) R_p -Is the Maximum peak height (the highest single peak) within the line profile.
- v) R_{pm} -Mean peak height is the distance from the highest peak to the profile mean line that is determined within each cut-off length. The mean of the peak heights is the parameter R_{pm} . It is a valuable tool in monitoring the variation of surface finish in a production process. Values that are similar indicate a consistent surface finish while a significant difference indicates a surface defect in an otherwise consistent surface.

R_{pm} is useful in predicting the bearing characteristics of a surface. A low R_{pm} and a large R_{tm} (see (iii)) indicates a plateau surface. The ratio R_{pm}/R_{tm} quantifies the asymmetry on a surface bearing area. Therefore a low ratio of R_{pm}/R_{tm} is preferred for bearing surfaces.

2.6.3 Depth Profiling

As already mentioned (see 2.1.5, p8) Titanium is a reactive metal. This means that in air, water or any other electrolyte, an oxide is spontaneously formed on the surface of the metal (Steinemann, 1998). The native oxide film has a thickness of about 4nm or 20 times the inter-atomic distance. Its mode of

growth is specific in that the Oxygen ions migrate towards the metal and react with the counter-ion Titanium at the base of the oxide. The specific mode of oxide growth on Titanium has the positive effect that no metal ion will reach the surface and be released into the electrolyte (Steinemann, 1998). An important consequence is that a biological molecule approaching the implant from the bone side sees a metal oxide and not the metal surface (Albrektsson *et al*, 1983). Larsson *et al* (1997) found that the oxide thickness of machined samples was about 3-5nm and increasing the oxide thickness of rough machined implants had no significant effect on bone response.

There is no absolute means of measuring Titanium oxide thickness, but oxide thickness can be estimated from depth profiles (Binon *et al*, 1992). Depth concentration profiles are maps of the concentration of various elements as a function of the distance from the outermost surface into the material. This is achieved by ion bombardment (sputtering) of the surface to remove layer by layer of surface atoms, thus exposing deeper lying atomic layers for analysis (Kasemo & Lausmaa, 1988a). In a depth profile the relative concentrations of the elements are displayed as a function of sputtering time (depth from the surface). Sputtering is often continuous and as the depth profiles pass through the oxide, over the oxide metal interface and into the bulk metal, the Titanium signal increases and the Oxygen signal decreases, as expected. The oxide thickness can be estimated from depth profiles as the depth at which the oxygen signal had decreased to half of its maximum intensity (Lausmaa *et al*, 1990; Larsson *et al*, 1997; Louw, 1997). Other researchers (Keller *et al*, 1990; Ong & Lucas, 1998) approximated the oxide thickness by multiplying the sputter rate by the crossover time obtained from the auger depth profile during continuous sputtering. Crossover time is the time corresponding to equal intensities of the Titanium and Oxygen auger signals.

The sputter yield or sputter rate is dependent on a number of factors, such as material being sputtered, crystallinity of the material and orientation to the ion beam. It is well known that metallic oxides sputter at different rates and many sputter more slowly than the pure metal. Although referenced literature assumes constant ion sputtering rates, the rate actually increases, as the oxide is sputter removed. Absolute sputter rates are unknown because of the continuously changing composition of the specimen with depth. In most instances where reliable and reproducible thickness measurements are required, the sputter rate is measured by sputtering a layer of standard material of known thickness for a known period of time (Ong & Lucas, 1998; Louw, 1997).

During 1993/1994, the first scanning X-ray photoelectron microprobe was introduced into the surface analytical market. It utilizes a scanned focused electron beam from a LaB₆ electron filament that generates X-rays on an Aluminium anode. The X-rays are focused using an ellipsoidal monochromator and produces a scanned, focused X-ray beam on a sample surface. The X-ray beam diameter is variable and X-rays can be rapidly scanned across a surface, generating secondary electrons that form an X-ray induced secondary electron image (SXI). An important advantage of the Quantum 2000 is that only the active areas defined on the image are irradiated, minimizing X-ray induced sample damage. Sputter depth profiles can be performed with computerized Zalar rotation, where the sample is rotated around a center point defined by the selected analysis point. With Zalar rotation, buried interfaces can be examined with no loss of depth resolution, as surface roughening and cone formation are minimized (Louw, 1997).

Depth profiling is normally conducted with the photoelectron analyzer set at the same resolution as for the high-resolution spectra. The sputter depth profiling is usually conducted with a preferentially pumped focused ion gun in the "alternating"

mode, where the sample is sputtered; then the ion gun is turned off and the photoelectron spectra is recorded (Louw, 1997).

2.6.4 Cleaning and Sterilization of Implants

A surface that looks perfectly clean to the eye may still be extremely dirty (contaminated) in a chemical sense, since it may be covered by hundreds of molecular layers of foreign, contaminating elements, invisible to the naked eye. In the strictest sense a clean surface means that the bulk material extends all the way to the surface, without change of chemical composition, and with no foreign elements attached to the surface (Kasemo & Lausmaa, 1988b).

Unsaturated chemical bonds will attract air impurities and it will take a few seconds at most before the surface is contaminated by several percent of a molecular monolayer. After about one minute most of the unsaturated chemical bonds are saturated. The nature of the contamination layer is also determined by the composition of the environment to which the implant is exposed (Kasemo & Lausmaa, 1988b).

Surface contamination must not be regarded a "*priori*" as having a negative effect on biological responses. The effects could actually be beneficial in some cases, but the significance is unknown (Aronsson *et al*, 1997).

Probably the most common source of both inorganic and organic superficial contaminating deposits on implant devices is from sterilization procedures. It has been noted previously that conventional processes of steam autoclaving, ethylene oxide gas sterilization, glass bead immersion, and cold solution exposure all leave disabling residues on the implant surface (Baier *et al*, 1982; Doundoulakis, 1987).

National and international standards on the properties of metallic biomaterials for surgical implants are fairly broad,

allowing for several possible procedures prior to implantation - cleaning, passivation and sterilization that may include exposure to elevated temperatures (Albrektsson *et al*, 1981).

ASTM (1997)- The Standard Guide for Descaling and Cleaning Titanium and Titanium Alloy Surfaces states that it is not intended that these procedures be mandatory for removal of any of the indicated contaminants but rather serves as a guide when Titanium and Titanium alloys are being processed in the wrought, cast, or fabricated form.

Several techniques have been suggested to produce a clean and sterile Titanium implant surface with minimal contaminants. A common procedure used in the past for the Branemark implant was to clean the Titanium fixture with residue free detergent, rinse with distilled water and clean ultrasonically with a series of butanol and ethanol (Hobo *et al*, 1989) followed by autoclave sterilization at 2psi and 120⁰C for 20 min (Hobo *et al*, 1989; Hartman *et al*, 1989; Keller *et al*, 1990;). Another method of cleaning was ultrasonic cleaning for 20 min in 99% ethanol and air dried in a laminar flow hood (Kononen *et al*, 1992). Baier *et al* (1982) found that steam sterilization compromised the properties of carefully prepared biomedical implants by depositing hydrophobic organic and hygroscopic salt contaminants over the implant surfaces.

In addition to contaminated surfaces by adsorption of organic molecules from ambient air (Kasemo & Lausmaa, 1988b; Mittal, 1979) impurities due to specific preparation methods on biomaterials are residues from grit blasting media (e.g. Silicon and Aluminium) residues or reaction layers from the processing fluids (electrolytes, etchants, and cleaning solvents), and residues from sterilization procedures (e.g. autoclaving or ethylene oxide) (Kasemo & Lausmaa, 1988b).

The ultimate goal of a cleaning procedure should be to remove the contaminants and restore the elemental composition of the

surface oxide without changing the surface topography (Mouhyi *et al*, 2000). Bone tissue response seems to be disturbed by contaminated implants as compared to clean controls (Ivanoff *et al*, 1996).

2.6.4.1 Radio Frequency Glow Discharge Treatment (RFGDT)

Plasma treatments have for some time been a relative common method for increasing the surface energy and for surface cleaning of biomaterials before using them in biological evaluation studies (Kasemo & Lausmaa, 1988b; Baier & De Palma, 1970). Baier *et al* (1984) found RFGDT to be an effective method for cleaning and sterilizing inorganic surfaces and elevating them to a high energy state correlated with greater cellular - adhesion potential.

The criterion for efficient plasma cleaning is that the process removes chemical impurities without adding new ones (Aronson *et al*, 1997). RFGDT technique basically utilizes a vacuum chamber and a radio frequency generator to take a gas into a "plasma" state. A characteristic of a plasma is a visible glow discharge caused by the electrically excited elements returning to lower energy levels (Fassel, 1978). After a vacuum has been obtained, Argon gas is allowed into the chamber and the radio-frequency generator activates the gas into a plasma state. Impaction of the plasma's ion and electrons on objects within the chamber acts to sputter away and then microash any surface contaminants from inorganic objects (e.g. implants) leaving them in sterile, high surface energy states that improve their wettability, thereby facilitating adhesion by organic materials (Baier & De Palma, 1970).

Vargas *et al* (1992) hypothesized that the specific glow discharge treatment applied, modified the superficial oxide layers of the implants in a two-step process. First by removing the contaminated over-layers rich in hydrocarbons and

other elements, and then "leveling" the subjacent, irregular oxide layer remaining from prior manufacturing and sterilizing procedures. This removal of both superficial contaminants and oxide protrusions (e.g. oxide needles, as proposed by Solar *et al*, 1979) resulted in a clean, more uniform oxide layer that reacts with Oxygen present in the environment to create a new, more coherent and corrosion resistant "passive" surface. Sterilization by RFGDT for 3 to 5 minutes was found to produce an extremely high surface energy with minimal contaminants for samples with flat surfaces (Doundoulakis, 1987; Baier & Meyer, 1988).

A drawback of RFGDT is that the very clean surface is also very reactive and will react with even minute impurities in the process gas, or with impurities that are desorbed from the walls of the process chamber. As the energetic ions hit surfaces other than the sample under treatment, material from these other surfaces may thus be deposited on, and contaminate the sample. After RFGDT is terminated the clean, reactive, high-energy surface will then be exposed to the remaining atmosphere in the vacuum chamber depending on how fast the atmosphere is evacuated. Finally the removal of the sample from the RFGDT apparatus will definitely cause exposure to a new environment (Kasemo & Lausmaa, 1988b).

Redeposition of sputtered material is frequently reported for different plasma systems. It becomes a serious problem if the sputter rate is too low, sputtered material is not pumped away fast enough, or if the initial surface contamination is large. Upon readsorption on the surface, the particles react with the surface atoms, and then reaction layers such as carbides and/or nitrides are formed. These layers can be difficult to sputter away and therefore often remain after the plasma treatment (Baier & Meyer, 1988).

Carlsson *et al* (1989) and Hartman *et al* (1989) found glow discharge to be a suitable preoperative cleaning and sterilization method for Titanium implants.

2.7 Cell Culturing

Irrespective of their use and destination, all materials (metallic or non metallic) designed for biomedical application in humans must be submitted to bio-acceptability *in vitro* and *in vivo* tests (Davies, 1989) aimed at verifying the response and the behavior of the cells interacting with them, according to the rules of the ISO 10993.

A general *in vitro* approach applicable to all types of medical devices is represented by the cytotoxicity method performed by incubating nearly confluent monolayers of mammalian cells in the presence of extractables from the device material (indirect method). In the case of devices projected and destined to be colonized by tissue in which they are implanted, the *in vitro* biocompatibility test can be accomplished more usefully by a direct contact method. In this approach the cells are cultured directly onto the material under investigation and observed over a period of days or weeks relative to their morphologic and functional features. In the direct contact method, biomaterials should be tested with cell populations typical of the implant site (Calandrelli *et al*, 2002).

In vitro assays are relevant to *in vivo* behavior but the choice of *in vitro* assay must critically depend upon both the type of information sought and the geometry of the testing system (Davies *et al*, 1989). When designing either an *in vivo* or an *in vitro* cell culture experiment it is essential to define the aims of the experiment and which aspects of the tissue reaction to the implant are to be investigated (Davies, 1989). Investigation of continuous cellular and tissue reactions to a material using *in vivo* studies is impossible

because of the wide deviation due to the existence of a number of unknown factors. *In vitro* methods using the techniques of tissue culture allow a more easily controlled test situation and higher statistical accuracy than when an *in vivo* system is used and has become one of the important methods for the biological standardization of dental materials (Kawahara *et al*, 1968).

In vitro methods can potentially be specifically designed to investigate the reactions of single cell types to implant surfaces. *In vitro* assays are usually more rapidly carried out than *in vivo* assays and almost inevitably cheaper (Davies, 1989). Assessing the attachment and growth of various cell types to a biomaterial *in vitro* offers a well controlled, quantitative, and cost effective model of interactions at the tissue-implant-interface. Not only can the biocompatibility of the implant be determined, but also the physical and chemical characteristics of the implant surface can be modified to maximize the attachment and growth of selected cell populations (Kamen, 1989).

Since materials which are destined for human implantation should, ideally be tested with human cells rather than animal cells, it is only by developing methods *in vitro* that there is a chance that these methods may be adapted for use with human cells (Davies, 1988).

2.7.1 Types of Cells used in Culture

Of particular importance is the use of cultured cells that are as close as possible in origin and phenotype to the cells of interest (Kamen, 1989). Connective cell and bone cell models are increasingly employed to study bone-biomaterial interactions. Primary and passaged cells from several species and anatomical locations have been used, as well as several cancerous, transformed, clonal and immortalized cell lines (Puleo & Nanci, 1999).

According to Mustafa *et al* (1998) and Mustafa *et al* (2000) the importance of using the relevant cell systems when evaluating dental implant materials has been clearly established and they recommend the use of human oral fibroblast and osteoblast-like cells derived from human mandibular bone.

i) Osteoblast cells

Bone is the only tissue of higher vertebrates that differentiate continuously, remodel internally, and regenerate completely after injury (Urist *et al*, 1983). The mechanical stimuli are the main mode for controlling bone turnover since osteoblast differentiation is a stress/strain responsive process (Mesaros, 1989).

Bone tissue comprises three cell types. Osteoblasts arise from undifferentiated mesenchymal cells and are responsible for the formation and mineralization of bone matrix. Osteocytes, osteoblasts that have become surrounded by the matrix they have elaborated, are responsible for maintaining the matrix. Osteoclasts resorb bone matrix and are thus essential for the process of bone remodeling (Davies *et al*, 1989).

Osteoblasts, osteoid, and mineralized matrix have been observed adjacent to the lamina limitans, (Linder 1985; Davies *et al*, 1990; Murai *et al*, 1996) suggesting that bone can be deposited directly on the surface of the implant, extending outward from the biomaterial. Thus bone formation in the peri-implant region occurs in two directions: not only does the healing bone approach the biomaterial, but bone also extends from the implant towards the healing bone (Puleo & Nanci, 1999) (see 2.3, p16).

Osteoblasts are ideally positioned to function as cellular mediators of hormonally regulated skeletal metabolism and evidence suggests that the effects of osteotropic hormones, cytokines and prostaglandins on the skeleton including

osteoclast activation are mediated through the osteoblast (Rodan & Martin, 1981). Osteoblast-like cells demonstrate a cell morphology with a central spherical body with filopodial-like processes extending away from the central area in all directions (Bowers *et al*, 1992).

A variety of methods have been developed to grow osteoblast-like cells. Many studies employ the method of using enzymatically-digested cells from bone fragments (Matsuda *et al*, 1987; Ishaug *et al*, 1997) consequently bone-forming cells have been obtained from newborn calvaria of different animals. Bellows *et al* (1986); Keller *et al* (1994); Ishaug *et al* (1997), used stromal osteoblastic cells isolated from calvariae of Sprague-Dawley rats by collagenase digestion. Bowers *et al* (1992) and Lumbikanonda & Sammons (2001) used parietal plates from 3 day old Wistar rats calvarial explants as osteoblast while Sudo *et al* (1983) and Cooper *et al* (1993) established the clonal MC3T3-E1 cell line from new born calvaria that resembles osteogenic cells *in vitro* in many ways (Ham, 1969) and a number of studies employed the culture system using this MC3T3-E1 cell line (Itakura *et al*, 1988; Ito *et al*, 1995; Kurachi *et al*, 1997). Transformed osteoblast-like cells (Schwartz *et al*, 1996), chick embryonic calvaria (Groessner-Schreiber & Tuan, 1992) and immature New Zealand rabbits (Cheung & Haak, 1989) have been used as a source of most cell types and have also been a favorite model for studying the interaction of an implant with "bone" cells.

Human osteoblast-like cells from human osteosarcoma have also been used (Martin *et al*, 1995; Kieswetter *et al*, 1996). Schmidt *et al* (2002) used collagenase treated human explants from bone tissue of femur or femoral head while Anselme *et al* (2000) used trabecular bone from the iliac crest. Mustafa *et al* (2001) used human mandibular bone to harvest osteoblasts.

ii) Fibroblasts

In human gingiva, the fibroblasts lay down and maintain the dense fibrous connective tissue enmeshing the vascular plexus and sensory nerve fibres of the lamina propria (Takarada *et al*, 1975).

Considerable progress in the field of connective-tissue research has brought about detailed information on the behavior of fibroblastic cells under culture conditions and *in vivo* situations. Well-characterized biological functions of fibroblasts include cell migration, cell attachment, cell proliferation and biosynthesis as well as degradation of multiple connective tissue components. An exact control of these functions is essential in physiological processes of tissue development and repair, while on the other hand, fibrotic disease or poor wound healing are associated with functional deviances of fibroblasts (Heckmann & Krieg, 1989).

An acceptable bone to implant interface is equally dependent on the development and maintenance of a suitable soft connective tissue implant interface in the coronal implant region (Pilliar, 1998).

Fibroblasts cells from procine periodontal ligament were isolated and sub-cultured by Brunette *et al* (1976). Since then most studies have employed the use of human gingival fibroblasts (Inoue *et al*, 1987; Kononen *et al*, 1992; Oakley & Brunette, 1993; Botha, 1995).

Another source of human fibroblasts was that obtained from fore skin explants - this cell model has been used to study the effect of implant surface modifications on cellular responses and there is no evidence to indicate that these cells are phenotypically different from fibroblasts derived gingival connective tissue (Keller *et al*, (1989).

Few studies have used Mouse fibroblastic L929 cells (Morra & Cassinelli, 1997; Orsini *et al*, 2000) or 3T3 mouse fibroblasts (Saltzman *et al*, 1991).

2.7.2 Cell Attachment

Rate of cell attachment characterizes cells and indicates their viability. Cellular attachment and regeneration are influenced by the method of disaggregation (Weiss & Kapes, 1966). Therefore passage of cells by enzymatic digestion or any other method influence subsequent cellular attachment, spreading and proliferation for an extended period of time after the actual process has been inactivated (Weiss & Kapes, 1966; Davies, 1989; Clavin *et al*, 1990)

In order for normal embryonic or adult cells from avian or mammalian organisms to survive and divide *in vitro*, they stringently require adherence to a specific type of tissue culture substrate. Malignant cells, however, frequently loose this stringent anchorage dependence and can be adapted to grow as single cells in suspension (Culp, 1978). Cells transformed with oncogenic viruses or derived from tumors have been shown to move more aggressively across the substrate (Gail & Boone, 1972).

It is apparent from the literature that osteoblast-like cells and other anchorage-dependent cells, such as fibroblasts, show similar morphologic behavior in attachment studies (Brunette, 1988; Zreiqat *et al*, 1996). The cell membrane is the first contact a cell has with its surrounding environment and as such must play an important role in determining cellular activity and function (Shelton *et al*, 1987). The strength of adhesion of a cell settling on the substratum would increase progressively as the area of its contact with the substratum increases (Grinnell *et al*, 1973).

The process of cell adhesion and spreading consists of four events (Rajaraman *et al*, 1974)

- Attachment of cells at point of contact with the substratum - this was effected by microvilli-like cell processes.
- Centrifugal growth of filopodia - the microvilli like processes elongate into processes called filopodia
- Cytoplasmic webbing - filopodia growth always precedes cytoplasmic webbing during cell spreading
- Flattening of the central mass.

Cell spreading starts immediately after adhesion of cells to the surface has taken place. The process of cell attachment and spreading cannot be divided by specific time intervals but is an inter-twining process (Chen, 1981; Grinnel & Bennett, 1981; Brunette, 1986a). Most studies have used tissue treated polystyrene as a standard against which to measure cell attachment to the surface of biomaterials (Kamen, 1988).

2.7.3 Cell Detachment

The usual approach to studying the process of cell attachment is to detach cells from their growth surface by trypsinization and to place them on the test surface. The number of cells attached to the surface is then measured as a function of time (Brunette, 1988).

Weiss & Kapes (1966) indicated that crystalline Trypsin gave the best results as a cell detachment agent and a study by Clavin *et al* (1990) suggested that a mixture of Trypsin and EDTA (Ethylene-Diamine-Tetraacetic-Acid) yielded the most desirable single cell suspensions. Thom *et al* (1979) used Tetracaine (local anaesthetic) as a cell detachment agent and results of Botha (1995) support Tetracaine as an alternative cell detachment agent. Tetracaine causes paralysis of the

cells thereby lifting them off the surface. It requires a much longer time interval for action compared to Trypsin-EDTA.

2.7.4 Inoculation/Seeding of Cells

According to Ishaug *et al* (1997) cell-seeding density affected initial cell attachment and proliferation rate, but differences became less significant over time. Different studies have used different cell concentration or densities for inoculation or seeding. Morra & Cassinelli (1997) and Brunette *et al* (1976) used a seeding concentration of 1×10^5 cells. ml^{-1} while Botha (1995) seeded cells at a concentration of $3-5 \times 10^5$ cells. ml^{-1} and Kononen *et al* (1992) seeded cells at a density of 2×10^4 cells. cm^{-2} .

2.7.5 Estimation of Cell Number

Several methods exist for the quantification of cell numbers in a specific culture, namely, surface measurement, counting chambers, electronic particle counter and many others. Groessner-Schreiber & Tuan (1992) used the method of measuring cellular protein content and level of cytosolic enzyme to compare cell numbers between cultures while Guy *et al* (1993); Cooper *et al* (1993) used tritiated thymidine to determine cell attachment.

Electronic particle counters⁴ have been used for decades. It has obvious advantages of simplicity, accuracy and rapid operation but has the disadvantage that it counts all cells in suspension regardless if they are viable or not (Harris, 1959).

The method of using counting chambers such as the Neubauer haemocytometer has also been used in haematology for several decades with great success. Hemocytometer counts do not distinguish between living and dead cells but a number of

⁴ Coulter Cell Counters

stains are useful to make this distinction. Trypan blue among others⁵ is excluded by the membrane of the viable cells whereas the nuclei of damaged or dead cells take up the stain. Although this distinction has been questioned, it has the virtue of being simple and giving a good approximation (Hakkinen *et al*, 1988; Saltzman *et al*, 1991; Botha, 1995).

In previous investigations, the numbers of attached cells have usually been determined indirectly from counts of detached cells (Bowers *et al*, 1992; Keller *et al*, 1994). Botha (1995) determined the number of attached cells by counting an aliquot of the cell suspension using a haemocytometer.

The viable cell concentration in the cell suspension can be calculated per ml by the following formula:

$$\text{Viable cells per ml} = \text{average viable cell count per square} \times \text{dilution factor} \times 10^4$$

The non-attached cells can also be counted to confirm the accuracy of the method (Marmary *et al*, 1976).

2.7.6 Cell Proliferation

Proliferation of cells represents the final stage of the cellular processes involved in the viability and survival properties of cells and can be summarized in sequential stages of contact, attachment, spreading and proliferation (Kamen, 1988). The efficiency of cell attachment and cell proliferation can be calculated into a percentage by the following method (Botha, 1995):

$$\% \text{ Attachment efficiency and proliferation} = \frac{VT}{VI} \times 100$$

VT = Number of viable cells per ml at a given time

VI = Number of viable cells per ml in initial suspension

⁵ Erythrosin B, Nigrosin

2.8 Bio-acceptability

The cycle of events when a cell is placed on a biomaterial surface indicate that the whole process of attachment, spreading and proliferation are important criteria for the evaluation of surface bio-acceptability (Davies, 1988).

Many surfaces of biomaterials, including metals and polymers, could provide adequate mechanical support for the attachment of cells. The differences in cell behavior following attachment to different surfaces must be related to physico-chemical properties of the surface (Saltzman *et al*, 1991).

Titanium has an excellent bio-acceptability due to the fact that it is highly insoluble in body fluids and forms a protective oxide layer on the surface (see 2.1.4, p7; 2.1.5, p8; 2.1.6, p10). In addition to its chemistry, however surface topography of the bulk material is important (see 2.6.2, p29). An analysis of cell behaviour carried out under well-controlled conditions allows conclusions about the bio-acceptability of a material (see 2.7, p41) and cellular morphology is an accepted parameter of bio-acceptability tests (Schmidt *et al*, 2002). *In vitro* studies with cells from target tissues are useful tools for the investigation of implant behaviour, because these cells react differently on various surface structures and chemical properties (Schmidt *et al*, 2002). Several *in vitro* experiments and animal studies have demonstrated the importance of the implant surface to host response during healing and the quality of implant anchorage in bone (Buser *et al*, 1991; Bowers *et al*, 1992; Gotfredsen *et al*, 1992; Buser *et al*, 1998). From the animal studies, results showed that the interaction between implant material and the surrounding tissues was affected by the surface structure and that better bone contact was achieved to implants with rougher surfaces than with polished surfaces (Buser *et al*, 1991; Gotfredsen *et al*, 1992; Wennerberg *et al*, 1996). In most studies the type of surface preparation and/or

characterization methods used prevent any firm conclusions being drawn as to which surface properties were the determining factors for the observed differences in biological response (Larsson *et al*, 1997).

2.8.1 Scanning Electron Microscopy (SEM)

Scanning Electron Microscopy can be used to quantitate cell adhesion to implant surfaces hence enabling the evaluation of cell attachment to different surfaces (Kasten *et al*, 1990). Keller *et al* (1994) using the scanning electron microscope found that in general cells appeared spherical in shape with early signs of filopodial extensions extending to adjacent areas of the prepared surfaces. Over time considerable spreading had occurred on rough surfaces, however it was not clear how intimately the cells had adapted to the irregularities on the respective surfaces. There were no significant differences in cell morphology between cpTi and Titanium alloy surfaces. Mustafa *et al* (2000) used the SEM to quantify the percentages of attached cells on each of their specimens and they confirmed that in accordance to other previous studies that the type of roughness on a Titanium surface affects cell attachment and spreading. Brunette (1986b) found that fibroblast cells had adopted an elliptical shape and increasingly aligned with the direction of the grooves and cells on smooth Titanium surfaces were circular in shape. Kononen *et al* (1992) found that fibroblast attachment and spreading was not so good on sandblasted Titanium surfaces as on electropolished Titanium surfaces and the fibroblasts on sandblasted surfaces grew in clusters, suggesting that their ability to migrate was impaired. Lumbikanonda & Sammons (2001) found that on smooth Titanium implants, cells were polygonal or circular in shape with complete cytoplasmic extensions of the cell body on the substrate surface forming intimate contact with the implant surface such that the underlying topography of the surface was visible beneath the cell. On rougher surfaces cells spanned across pits, grooves and pores, mostly contacting prominent features of the surface.

CHAPTER 3

AIM OF THE STUDY

A great interest in the use of cast Titanium for dental prosthesis has evolved in the dental community. Because of its high melting point and strong tendency to oxidize, Titanium is cast in specially designed dental casting machines. The use of cast Titanium restorations in dentistry are still very low and probably related to the lack of knowledge among dentists or long term clinical follow-up.

Rehabilitation treatment utilizing dental implants is not a readily available service to most in the southern hemisphere due to its high cost. The relatively high cost of implants could be related to its fabrication and the different methods employed for surface enhancement that is regarded as a "priori" for bio-acceptability. Depending on its bio-acceptability an alternative to the high priced available implants in the market could be cast Titanium and Titanium alloy implants, which could then be manufactured into custom made implants and implant superstructures.

The Aim of this study was:

1. To determine and compare the elemental and chemical composition of Machined and Cast Titanium and Titanium alloy before and after surface enhancement by using
 - Atomic Percent Concentration of elements on the surface of samples
 - Chemical composition by curve fitting
2. To determine and compare the surface topography of the differently fabricated samples by using
 - Area Analysis
 - Line analysis

3. To determine and compare the oxide thickness formed on samples as a result of the different fabrication procedures by using
 - Depth Profiles
4. To evaluate the effects of RFGDT on the different fabrication procedures by
 - Analyzing samples before and after RFGDT
5. To assess the degree of bio-acceptability of the above mentioned variables with *in vitro* fibroblasts and osteoblast-like cell cultures by determining
 - Count of viable cells and
 - Cell % attachment efficiency and proliferation

CHAPTER 4

MATERIALS AND METHODS

4.1 Fabrication of Specimen Discs

4.1.1 Preparation of Machined Discs

Custom-manufactured experimental discs measuring 6.35mm in diameter and 2mm in thickness were manufactured from rods of both commercially pure Titanium (cpTi) Grade 3 and Titanium alloy (Ti6Al4V) Grade 5 (see Table 4-1).

Table 4-1: Description of materials used in this study for sample fabrication

Material	Batch No.	Source
cpTi	BN 3720	T. Wire, Weissenstrasse 8, CH 8034 Zurich, Switzerland
Ti6Al4V	000XY07	L. Klein SA, Lanfeldweg 110, 614 Bienne/biel, Switzerland
President Putty	KJ390	Coltene® A G Feldwiesenstrasse 20, 9450 Altstätten, Switzerland
DuraLay Resin	022900	Dental Mfg.Co. 5805 W, 117 th Pl. Worth, Illinois, U.S.A.
Rematitan Plus	029527	75104 Pforzheim, Federal Republic of Germany

The discs were manufactured using machining procedures that were identical to those used for manufacturing commercially available machined-surface, threaded Titanium implants. Southern Implants⁶, carried out these commercial production procedures according to proprietary specifications.

The prepared discs were cleaned using alternating ultrasonic cycles of ethanol and N-hexane and were sterilized using gamma radiation with a dose level of 30kGy as used for dental implants. Packing was done under a laminar flow hood with air filtered through a 2µm Hepa filter to remove dust and microorganisms. Fig 4-1 (see p55) shows the packaged samples as received from Southern Implants.

⁶ Southern Implant, P.O. Box 605 Irene 0062, South Africa



Fig 4-1: Sample discs of cpTi (Grade 3) and Ti6Al4V (Grade 5) as received from Southern Implants

4.1.2 Fabrication of Cast Discs

Ingots with identical chemical compositions as those used for the machined discs were used to cast discs of similar dimension.

4.1.2.1 Preparation of Resin Disc Patterns

A duplicating mould using a glass pipette measuring 6.35mm in diameter and 100mm in length was made from President impression putty (see Table 4-1, p54). After removal of the pipette, standardized acrylic resin rods were fabricated using DuraLay, a Chemical polymerizing Inlay Pattern Resin (see Table 4-1, p54). The resin was prepared by mixing a ratio of 1ml monomer with 0.95gm polymer in a mixing bowl. The mixed resin was then poured into the duplicating mould and allowed to polymerize at room temperature. After curing, the resin

rods were removed from the mould and inspected for processing defects. Fig 4-2 shows the duplicating mould used and the obtained cured resin disc.



Fig 4-2: DuraLay resin rods as fabricated from the duplicating mould

These rods were then sectioned into discs of 2mm thickness using a Slow Speed Cutting Saw (Isomet^{FM})⁷ (see Fig 4-3, p57).

Dimensional accuracy of all discs was checked by a digital caliper⁸ and corrected using Silicon Carbide 600 grit sandpaper⁹ with water.

⁷ Buehler Lake Bluff, Illinois, USA

⁸ Laboratory & Scientific Equipment Company (Gauteng) (Pty) Ltd. P. O. Box 1296, North Riding 2162, South Africa

⁹ IMP Scientific and Precision Equipment, P. O. Box 1110, Boksburg 1460, South Africa.

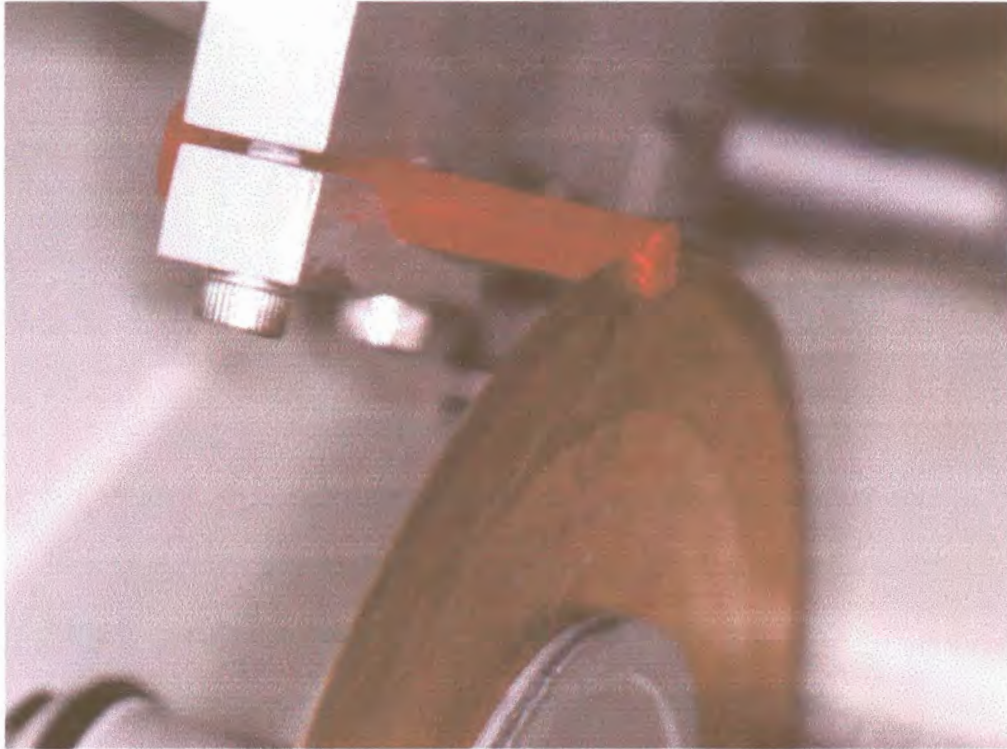


Fig 4-3: Slow speed cutting saw sectioning resin rods into discs

4.1.2.2 Casting Procedures

Twelve groups of 12 resin disc patterns were sprued and invested with a Phosphate bonded investment material, Rematitan Plus (see Table 4-1, p54). The powder and liquid were mixed at prescribed ratios in vacuum for 30 seconds prior to pouring into 60mm in diameter and 50mm high cylindrical moulds. After bench drying for 24 hours, the mould with the resin patterns underwent a three-stage thermo-cycle: 250°C for 20 minutes, 500°C for 20 minutes and finally 920°C for 60 minutes. The heating rate between the hold times at the respective temperatures was 5°C per minute. The invested discs were made from DuraLay resin because it volatilizes in 40 minutes at approximately 300°C leaving, no residue. Prior to casting, the mould was cooled down to 500°C at a rate of 5°C per minute.

A Centrifugal Titanium Casting System¹⁰ (see Fig 4-4, p58) was used to cast cpTi and Ti6Al4V into the moulds. The casting

¹⁰ Morita Cyclarc Casting Machine, Kyoto, Japan

chamber was evacuated to a pressure of 13.33Pa three times and back filled with 99.99% pure Argon gas.

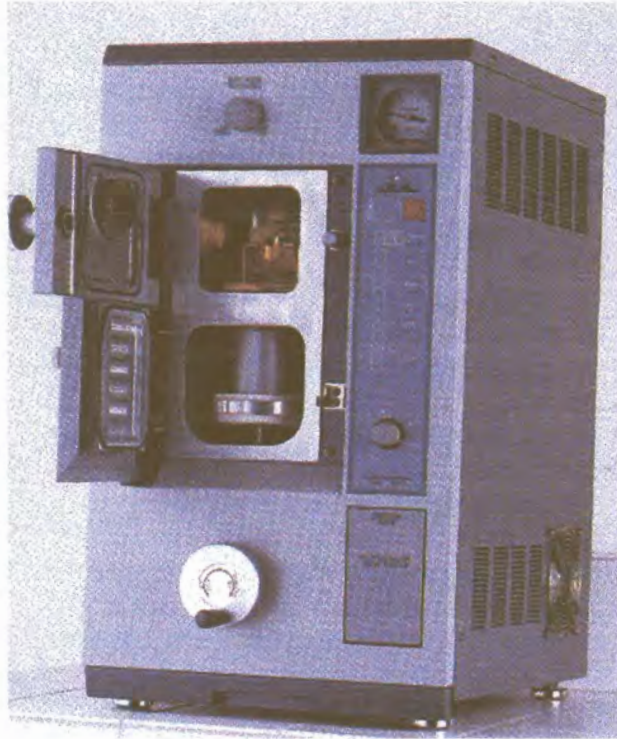


Fig 4-4: The Morita Cyclarc Casting Machine (J.Morita, Europe, GMBA)

Surgical ingots, each of 25mm diameter and 11mm in height of cpTi and Ti6Al4V were arc-melted in the copper crucible in an Argon atmosphere under gas pressure of 0.69MPa. Heating was facilitated by Tungsten electric arc melting with an electric arc current of 250A until the major portion of the ingot was liquidified. The liquid Titanium was then cast using a vertical centrifical system. The Argon supply continued for about 2 minutes after the molten metal was cast into the mould. Hereafter the machine stopped automatically and air was allowed to enter the casting chamber (Anony, 1991).

After the casting had solidified in the moulds, the partially cooled moulds were immersed in water at room temperature. The cast patterns were sectioned and divested using a small hammer. The remaining closely adhered investment material was removed by grit blasting the casting with 100µm Aluminum particles at 5-6bar for about 3 minutes at a nozzle distance

of approximately 60mm. The cast patterns were detached from the sprue with separating disc, specifically grouped for the envisaged experimental procedures and stored in labeled Argon filled sterile plastic containers (Anony, 1991).

4.2 Preparation of Different Surfaces

Specific predetermined topographies were introduced on selected surfaces of the machined and cast fabricated disc groups of cpTi and Ti6Al4V (see Table 4-2).

Table 4-2: Summary of the designation of sample material, fabrication procedures adopted and introduced surface enhancement.

Material Employed (N=144)	Method of Fabrication (N=72)	Types of Surface Characterization (N=24)
Commercially Pure Titanium (cpTi)	Machined Grade 3	As is (Control surface)
		110 sandblasted and etched (SI)
		250 sandblasted and etched (ES)
	Cast Grade 3	As is (Control surface)
		110 sandblasted and etched (SI)
		250 sandblasted and etched (ES)
Titanium Alloy (Ti6Al4V)	Machined Grade 5	As is (Control surface)
		110 sandblasted and etched (SI)
		250 sandblasted and etched (ES)
	Cast Grade 5	As is (Control surface)
		110 sandblasted and etched (SI)
		250 sandblasted and etched (ES)

SI – surface enhancement according to Southern Implants, Irene, South Africa
ES- experimental surface enhancement

Depending on the specific type of surface enhancement, the non selected surface or opposite base of the disc was coded by engraving (see Fig 4-5).



Fig 4-5: Coded sample discs

4.2.1 Non-enhanced Surfaces

The first group features samples of cpTi and Ti6Al4V as obtained from both machined and cast procedures - These samples were used as controls (see Table 4-2, p59).

4.2.2 Enhanced Surfaces

The second and third test groups also featured samples of cpTi and Ti6Al4V from both machined and cast procedures that were further enhanced.

4.2.2.1 Surface Enhancement of Samples according to Southern Implants (SI)

The second group featured samples of cpTi and Ti6Al4V as obtained from both machined and cast procedures that were surface enhanced according to production procedures of Southern Implants. Enhancement entailed grit blasting using

110 μ m Aluminum particles and acid etching at room temperature (see Table 4-2, p59).

4.2.2.2 Experimental Enhancement of Samples (ES)

The third group featured samples of cpTi and Ti6Al4V as obtained from both machined and cast procedures that were enhanced by grit blasting with 250 μ m Aluminum particles and acid etched using a 20% concentration of Hydrochloric-acid/Sulphuric-acid for five minutes at room temperature (see Table 4-2, p59).

4.3 Sterilization by Radio Frequency Glow Discharge Treatment

RFGDT was used as a method of cleaning and sterilizing samples. Twenty-one of the 24 samples from each of the specified groups underwent RFGDT¹¹. The remaining three samples from each group were the controls to treatment rendered.

After the different samples were placed into the vacuum chamber - the chamber was backfilled with Argon gas (99.9% pure) to a partial pressure of 1×10^{-2} mbar and the radio - frequency generator activated the gas into a plasma state using a current of 200W for 10 minutes. Impaction of the plasma's ion and electrons on objects within the chamber acts to sputter away and then subsequently microash all the surface contaminants. The flow of pure Argon gas through the chamber sweeps the contaminants off the sample surface and out of the chamber. Controlled oxidization of the clean surfaces was then obtained using the same 200W current and an Oxygen pressure of 5×10^{-3} mbar for one minute. The background pressure was maintained at $\leq 5 \times 10^{-4}$ mbar. After RFGDT sample discs were stored in sterile plastic containers filled with pure Argon

¹¹ Department of Physics, University of Pretoria, Pretoria 0001, South Africa

gas. A pair of sterile pure Titanium tweezers was used to handle the sample discs.

4.4 Analysis of Surface Characterization

4.4.1 X-ray Photoelectron Spectroscopy (XPS)

X-ray Photoelectron Spectroscopy, also known as Electron Spectroscopy for Chemical Analysis (ESCA) was used to elicit surface elemental and chemical information associated with the different preparative procedures adopted for the twelve different sample groups (see Table 4-2, p59). The XPS analysis using the Perkin-Elmer - PHI 5400 X-ray Photoelectron Spectrometer SYSTEM¹² was conducted using an Aluminum anode as an X-ray source and an X-ray monochromator (produces X-rays with narrow frequency range).

After samples were placed onto the stage using a pair of sterile pure Titanium tweezers they were secured and immediately placed in the pre-vacuum chamber of the XPS machine to avoid contamination of the surface. The samples were then located in the main chamber with the stage adjusted to an analyzing angle of 65° and a large round aperture of 1.1mm was employed. X-rays generated with a primary acceleration voltage of 14kV, yielding 300W Al-X-rays was used. Attempts were made to maintain the chamber vacuum at approximately 10⁻⁷Pa.

The binding energies for all photopeaks were corrected by using the Carbon (1s) photopeak at 284.6eV for referencing. This is a common procedure for correcting the binding energies of XPS spectra.

A spectrum of all identified elements was obtained as a plot of the number of detected electrons per energy interval versus their kinetic energy. Survey scans for each sample were run

¹² Perkin-Elmer Corporation, Norwalk, CT

for 10 minutes using a pass energy of 44.75 with an eV/step of 0.5 and a range of 0 to 1100 eV. Atomic concentrations of identified elements on the sample surface were determined from a subsequent multiplex spectral scan with a pass energy of 17.9 with an eV/step of 0.1 and run for 15 minutes. The atomic percent of each element on the surface was calculated from the photopeak by selecting the peak area of elements from beginning to end of spike and atomic percent was calculated by use of the XPS computer software. The detection limit of the technique for elements is said to be ~0.1 atomic percent. Each element has its own sensitivity factor (see Addendum H, p200-209) for quantification.

Peak separation measurements and full width half maximum (FWHM) values were standard fitting parameters determined using the Gaussian-Lorentzian curve fitting for the elements with atomic percentage greater than 3% (Moulder et al, 1992).

Identification of the different spectra was performed using the Handbook of X-ray Photoelectron Spectroscopy (Moulder et al, 1992).

4.4.2 Atomic Force Microscope (AFM)

Surface roughness of samples was determined using the TopoMetrix TMX 2010 Discovery Atomic Force Microscope¹³ from the Department of Materials Science and Metallurgical Engineering¹⁴. Samples that had been used for chemical and elemental composition analysis were re-used for surface roughness evaluation.

Samples were fixed with glue (cyanoacrylate) to tin foil squares of 5mm X 5mm using a sterile Titanium tweezers. Each glued sample was probed to ensure that it was firmly attached

¹³ Santa Clara, USA.

¹⁴ Industrial Metals and Minerals Research Institute, Department of Materials Science and Metallurgical Engineering, University of Pretoria, Pretoria 0001, South Africa

to the tin foil before mounting them on the magnetic stage of the microscope.

A 130 μ Z AFM Scanner was used to quantify surface roughness of the different samples. Five scans were randomly performed for each sample to achieve a more accurate determination of surface roughness. The scan range was set at 20 μ m. A 5 μ m scan was then magnified from a randomly selected area of the 20 μ m scan. As the size of a cell is approximately 20 microns the scan area of 20 X 20 μ m was chosen specifically as a representation of cell size. The smaller scan of 5 X 5 μ m was specifically chosen for the evaluation of the primary topography.

The scan rate was set to be three times higher than the scan range. The AFM probe was a V shaped cantilever with a 0.032N/m force constant and an arm length of 200 μ m. The tip of the cantilever was fabricated from Silicon Nitride (Si_3N_4).

Images were shaded and flattened with a zero-order line fit to remove scan line anomalies prior to being placed into a quadratic plane in the x and y directions.

The TopoMetrix software¹⁵ was used to interpret each corrected image. Surface roughness values were determined in terms of area analysis and line analysis.

For area analysis scanned images were depicted as 3D images and analyzed values were reported as Projected surface area, Area Ra, Area RMS, Maximum range and Average height (see 2.6.2.1, p33).

For line analysis scanned images were depicted as 2D images on which three pre-determined lines (*ca.* line 50, 100 and 150) were drawn. Standard roughness values for each of the three pre-determined lines were determined as Ra (Average roughness), Rp (Maximum peak height), Rpm (Mean peak height), Rt (Maximum

¹⁵ Microsoft Windows SPM LAB V3.06.06 software, Santa Clara, USA.

peak valley for assessment length) and R_{tm} (Mean peak to valley height) (see 2.6.2.1, p33-34) (Anonymous, 1996).

4.4.3 The Quantum 2000 Scanning ESCA Microprobe

The same samples used for the above characterization procedures were employed to determine the oxide thickness on the surface. Since depth profiling is a destructive technique, it was done last.

Measurements of oxide thickness were done by depth profiling using the Quantum 2000 Scanning ESCA Microprobe with a hemispherical analyzer (HMA) at a base pressure of $<5 \times 10^{-7}$ Pa. Depth profiles were recorded with a monochromated, 100 μ m beam diameter, 450W Al-K α -X-ray beam. The sputter depth profiling was conducted with a preferentially pumped focused ion gun in the "alternating" mode, where the sample was sputtered, the gun was turned off and the signal measured. The chamber pressure rose to $<2 \times 10^{-6}$ Pa during sputtering. Primary beam energy of 1 KeV was used with a sputter rate of 3.5nm.min⁻¹ for all samples. The sputter rate was calibrated by performing depth profiles through (200 \pm 20) nm Ti layer on Si substrate (Louw, 1997).

The oxide thickness for samples was estimated according to the method described by Lausmaa et al, (1990), Larsson et al (1997) and Louw (1997). On the depth profile two lines were drawn, one at the maximum Oxygen concentration and one at the Oxygen background level. A line was then drawn to intersect the Oxygen profile at half the value of the height between maximum and background. The point of intersection of this line with the sputter time was then used to calculate the oxide depth using the calibrated sputter rate of 3.5nm.min⁻¹.

4.5 Cell Culturing

4.5.1 Cell Cultures

Two different cell lines namely Fibroblasts and Osteoblast-like cells were used for *in vitro* culture of cells onto the differently fabricated and enhanced samples. The different cell lines were maintained to confluence in 75cm² Tissue Culture Flasks¹⁶ (Botha, 1995).

4.5.1.1 Fibroblasts

Healthy gingival tissue that was acquired from patients during periodontal surgery was used as a primary source of Human Gingival Fibroblasts cell line¹⁷. The medium used to maintain the cells was EMEM (Eagles Minimum Essential Medium) with NEAA (Non-Essential Amino Acids)¹⁸ and 10% Fetal Calf Serum and 100U/ml Penicillin and 100 MCG/ML Streptomycin Sulphate¹⁹.

4.5.1.2 Osteoblast-like Cells

A cell line of Human Osteosarcoma ACC 439, CAL-72 was obtained from DSMZ²⁰. Medium used to maintain the cells was 90% Dulbecco's MEM²¹ + 2mM L-glutamine²¹ + 1X insulin-transferrin-sodium selenite²¹ + 10% Fetal Bovine Serum¹⁹.

4.5.2 Cultivation of Cell cultures

Confluent cultures were used for plating after cultivation. The culture media was removed from the confluent cultures and cells were washed twice with Phosphate Buffer Saline (PBS). Detachment of cells from the tissue culture plastic was by

¹⁶ AEC-Amersham (PTY) LTD, P. O. Box 1596, Kelvin 2054, South Africa.

¹⁷ Center for Stomatological Research, School of Dentistry, University of Pretoria, P. O. Box 1266, Pretoria 0001, South Africa

¹⁸ National Institute of Virology, Private Bag X4, 2131 Sandringham, South Africa

¹⁹ Highveld Biological (PTY) LTD, P. O. Box 1456, Lyndhurst 2106, South Africa

²⁰ German Collection of Microorganisms and Cell Cultures. Department of Human and Animal Cell Cultures, Mascheroder Weg 1b, D-38124 Braunschweig, Germany

²¹ Sigma-Aldrich (Pty) Ltd, 1630, Aston Manor, South Africa)

trypsinization with 3ml of 0.5% Trypsin and 0.2% ethylene-tetra-acetic-acid (EDTA). Detachment of the cells was confirmed using an inverted microscope and the trypsinization process was stopped by adding 3ml of media + 10% fetal calf serum¹⁹. Cells were then harvested by centrifugation²² at a speed of 1600rpm for 5 minutes (67.1 xg). The cells that were obtained after centrifugation were seeded into measured tissue culture media (Botha, 1995).

4.5.3 Cell Concentration

The concentration of the cell suspension was determined by Trypan blue²³ exclusion counts using a Neubauer haemocytometer²⁴. The cell concentration was determined by mixing 0.5mls of the cell suspension into 0.5mls of Trypan blue. The inoculating cell concentration used was standardized to 3-5 X 10⁵ cells per ml of media (Botha, 1995).

4.5.4 Inoculation of Cells onto Sample Discs

Using a sterile Titanium forceps, the differently prepared Titanium disc samples were placed into the 6.4mm diameter 96 tissue culture wells²⁵ with utmost care to avoid contamination of the surface by unwanted molecules or elements (see Fig 4-6, p68).

Fibroblasts and Osteoblast-like single cell suspensions of cells were then seeded by placing 0.25ml of the cell suspension onto the Titanium discs. Wells without any material were considered as controls and consisted of Tissue Culture Plastic (TTC) that was also inoculated with the same concentration of viable cells.

²² Sorvall, Newtown, Connecticut, 06470, USA

²³ Sigma Chemical Company, U.S.A. Batch 68F-50355

²⁴ American Optical Corporation, Buffalo, New York, 14215, USA

²⁵ Corning, Adcock Ingram Scientific, P. O. Box 6888, Johannesburg 2000, South Africa

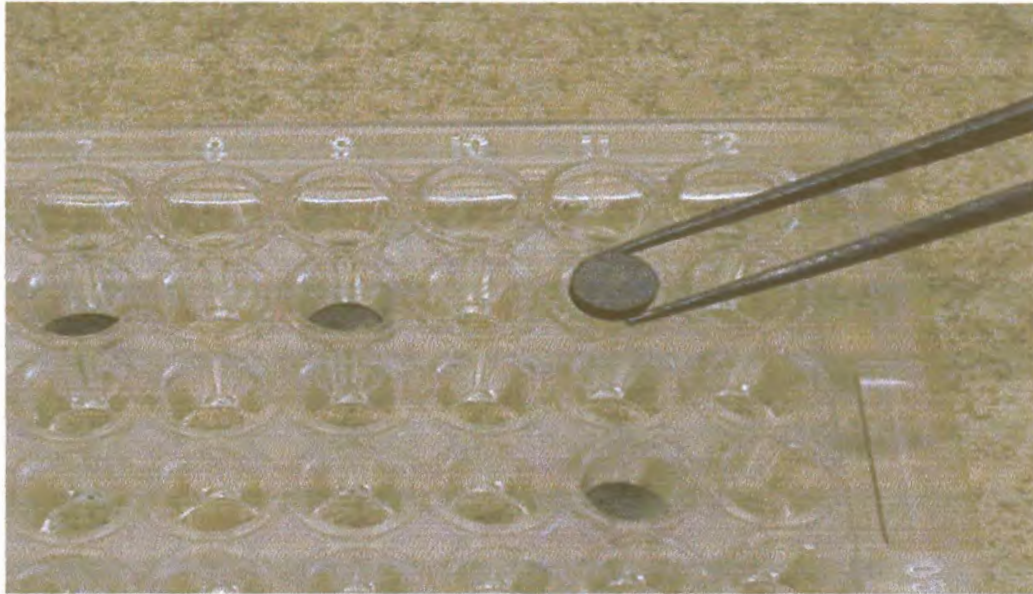


Fig 4-6: Placing of sample discs into tissue culture wells

4.5.5 Incubation

Inoculated tissue culture wells with the Titanium discs and controls were incubated at 37°C in a 95% relative humidity and an atmosphere of 5% CO₂ and 95% air in a CO₂ incubator²⁶. Feeding using cultivating media was done twice weekly. The old media was removed and new media was introduced.

At time intervals ranging from 1day, 2days, 14days and 28days the cells on the different surfaces were counted.

4.5.6 Counting Procedures

4.5.6.1 Preparation of Trypan Blue

In all instances the Trypan blue exclusion method²⁷ was used for the determination of viable cell count. Viable cells remain unstained while non-viable cells stain blue. The Trypan blue was prepared by mixing of 0.5mls of Trypan blue stock solution in 4.5mls of PBS. It is essential to have a 1:1 ratio of Trypan blue to cell suspension. Required volumes of Typan

²⁶ ShellLab, CO₂ Incubator, Model TC2323, ELMULAB (Pty) LTD, P. O. Box 124, Roodepoort 1725, South Africa

²⁷ Sigma Cell Culture Reagents, 1992

blue were placed in blue-topped tubes. Once the equivalent amount of cell suspension was present in the Trypan blue the Cell-Trypan blue mixture was placed on Hemocytometer and cell counting was done within five minutes. This is due to the fact that the dye penetrates into non-viable cells and viable cells can absorb the dye on long exposure to Trypan blue resulting in inability to distinguish between viable and non-viable cells (Botha, 1995).

4.5.6.2 Cell Detachment for Osteoblast-like Cells

All media with unattached cells was withdrawn using a pipette. Attached cells were washed twice with PBS prior to detachment. Detachment was facilitated by adding 0.125ml of 4mM Tetracaine free-base²⁸. The Tetracaine and cells were then placed in the incubator for 30min. Detachment of cells from control surfaces (Tissue Culture Wells) was confirmed with a Nikon Stereo Microscope²⁹. When cells had rounded on the tissue culture wells indicating detachment it was assumed that they had also detached from the Titanium discs. Cells were then carefully pipetted to ensure a single cell suspension. The detached cells were then collected using a pipette and placed into the test-tube containing 0.125ml of Trypan blue.

4.5.6.3 Cell detachment for Fibroblasts

All media was withdrawn using a pipette and to get rid of unattached cells, the cells were rinsed twice with PBS. Attached cells were detached by placing 0.125ml of 0.25% Trypsin and 0.1 % EDTA. Detachment of cells from control surfaces (Tissue Culture Wells) was confirmed with a Nikon Stereo Microscope²⁹. When cells had lifted from the tissue culture wells it was assumed that they had also lifted from the Titanium discs. To stop the trypsinization reaction

²⁸ No. T-7383, Sigma®, Chemical Company, St Louis, USA

²⁹ Research Instruments cc, P. O. Box 1148, Gallo Manor 2052, South Africa

0.125ml of respective media was added and cells carefully and pipetted to ensure a single cell suspension. The detached cells and media were then collected using a pipette and placed in to the test-tube containing 0.25ml of Trypan blue (Botha, 1995).

4.5.6.4 Neubauer Haemocytometer

Using a pipette, a small volume of the Trypan blue-Cell suspension was transferred to both chambers of the Neubauer haemocytometer by carefully touching the edge of the cover slip with the pipette tip and allowing each chamber to fill by capillary action (see Fig 4-7).

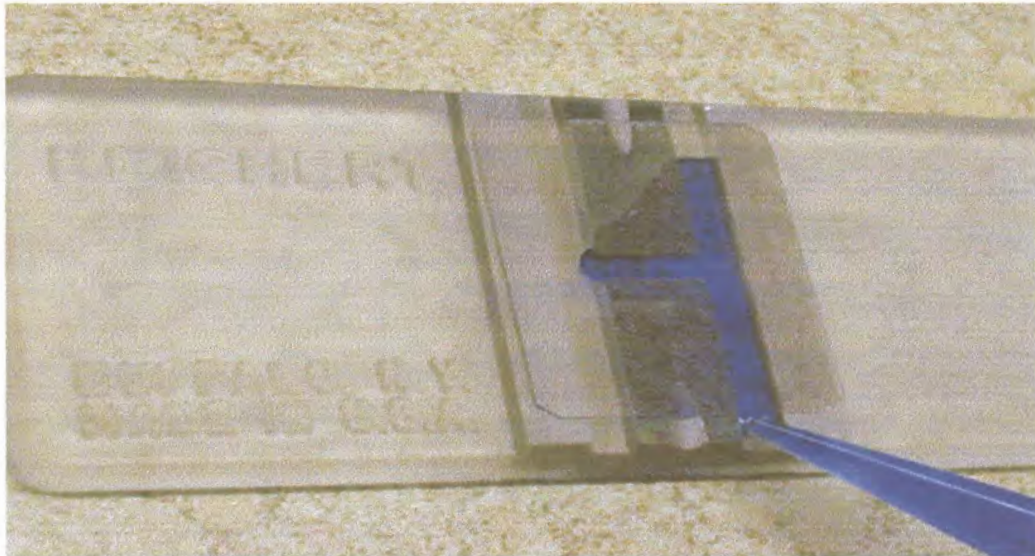


Fig 4-7: Neubauer haemocytometer being filled by capillary action prior to cell counting.

Counting was done using an ordinary light microscope (100X) with a 10X ocular and 10X objective lens. Starting with one chamber, all the viable cells in the center 1mm^2 and the four corner 1mm^2 of the Haemocytometer were counted. This procedure was repeated for the other chamber. Counts were in duplicate and results were tabulated (see Addendum A and B, p178, 179).

4.5.6.5 Estimation of Cell Number and Proliferation

At time intervals of 1 day, 2 days, 14 days and 28 days viable cell counts were determined. The viable cell concentration was then calculated per ml by the following formula (Botha, 1995):

$$\text{Viable cells per ml} = \text{average viable cell count per square} \times \text{dilution factor} \times 10^4$$

The efficiency of cell attachment and proliferation was calculated in percent by the following formula:

$$\% \text{ Attachment efficiency and proliferation} = \frac{VT}{VI} \times 100$$

VT = viable cells per ml at a given time interval

VI = viable cells per ml in initial suspension

4.5.7 Fixation Procedures

At 2 days and 28 days samples and controls with attached cells were washed twice with PBS to remove the culture medium and unattached cells. Fixation of cells was done using 0.25ml of 2.5% Glutaraldehyde in 0.075M Phosphate buffer at a pH of 7.4-7.6 for one hour. The wells were then rinsed three times each for 5min with 0.25ml of 0.075M phosphate buffer. Post-fixation using 0.25ml of 0.25% Aqueous Osmium Tetroxide³⁰ was also done for half an hour under a fume hood. All samples were then rinsed three times each for 5min with distilled water whilst in the fume hood. Dehydration of the cells was then undertaken on a bench by exposing each of the samples to varying concentrations of ethanol, 30%, 50%, 70% and 96% three times for a period of 5min respectively. Cells were transported to the Scanning Electron Microscopy Department immersed in 96% ethanol for further processing (Bullock & Petrusz, 1985).

³⁰ Merck Chemicals (Pty) LTD, Halfway house 1685, South Africa

4.6 Scanning Electron Microscopy (SEM)

Scanning electron microscopy was used to study cellular morphology as a function of time exposed to the differently treated Titanium surfaces. Samples were removed from ethanol and placed in a critical point dryer using liquid CO₂. The dried specimens were mounted on viewing stubs. Carbon was placed on sample sides to ensure conductivity before sputtering with gold. The sputtered samples were viewed and analyzed using the JEOL JSM-840 Scanning Electron Microscope³¹ with an accelerated voltage of 5.0KV, probe current of 6×10^{-11} , and the working distance of 10mm. Representative photomicrographs of cell morphology on the different sample surfaces were taken at X500, X2000 and X5000 magnification. Other magnifications taken were specifically for viewing certain morphological characteristics.

4.7 Statistical Analysis

The data obtained were coded, tabulated and analyzed using a linear model doing a General Analysis of Variance (ANOVA)³². The factors were Material (cpTi = 1; Ti6Al4V = 2), Method of Fabrication (Machined = 1; Cast = 2), Surface enhancement (Control = 1; SI enhanced = 2 and ES enhanced = 3) and Treatment rendered (not RFGD Treated = 1; RFGD Treated = 2).

The response variables for oxide thickness and chemical were analysed as follows: OXI_DEP, M2C, M2O, M2Ti, M2Zn, M2Pb, M2Na, M2Ca, M2N, M2V, M2Zr, M2Al (see Addendum F, p193).

The response variables for surface topography were analyzed as follows: M3Ra, M3RMS, M3HEIG, M3RAN, M3SUR, M3Ra_1, M3RMS_1, M3HEI_1, M3RAN_1, M3SUR_1, LARA, LARTM, LART, LARPM, LARP, LARA_1, LARTM_1, LAART_1, LARPM_1, and LARP_1 (see Addendum F, p194).

³¹ JEOL Ltd, Tokyo, Japan

³² The statistical package employed was Statistix for Windows Version 7

The growth of osteoblasts (OSTEO) and fibroblasts (FIBRO) were analyzed in a two factor ANOVA with Surface at 13 and 12 levels and Time at 3 (2, 14 and 28 days) and 4 (1, 2, 14, 28 days) levels respectively (see Addendum F, p195).

Testing was done at the 0.05 level of significance.

CHAPTER 5 RESULTS

5.1 Surface Characterization

5.1.1 Chemical Composition

The chemical composition of the surfaces of samples was determined using XPS. The quantitative measurements of detected elements were presented as Atomic Percent Concentration while the qualitative measurements were determined by high-resolution scans in terms of peak fittings of detected elements.

5.1.1.1 Atomic Percent Concentration

Table 5-1 (see, p75) shows the different samples with their atomic percent composition. The dominant signals are Carbon, Oxygen and Titanium with weaker contributions from Aluminium and Sodium. Other occasional smaller signals from Calcium, Zinc, Lead, Nitrogen, Zirconium and Vanadium were observed.

Carbon, Oxygen and Titanium were found in varying amounts on samples. Oxygen was observed to have the highest atomic percent concentration for most samples. Aluminium was found on all except the cpTi machined control samples. Sodium was detected on all cast, but only Ti6Al4V machined (SI) samples. Though in small amounts, Calcium was detected on all samples, with the exception of RFGDT machined cpTi and Ti6Al4V control samples. Lead was present only on machined cpTi and Ti6Al4V control surfaces and disappeared with RFGDT. Zinc and Nitrogen were present mostly on untreated samples and disappeared with RFGDT. Vanadium was detected on Ti6Al4V (machined and cast) control samples before RFGDT. Enhanced samples had no Vanadium detected. Zirconium showed up after the RFGDT of all cast samples and some machined samples.

Table 5-1: A summary of the elemental composition of sample surfaces (At %)

Element	C	O	Ti	Al	Na	Zn	Pb	Ca	N	V	Zr
cpTi machined control surface	37.7	45.8	11.2	0.0	0.0	2.7	0.5	0.6	1.4	0.0	0.0
cpTi machined control surface RFGDT	20.8	56.4	21.6	0.0	0.0	0.0	0.0	0.0	0.8	0.0	0.4
cpTi machined SI Enhanced	41.5	43.6	7.2	5.2	0.0	0.5	0.0	0.4	0.0	0.0	0.0
cpTi machined SI Enhanced RFGDT	19.9	52.7	12.9	9.7	0.0	0.0	0.0	0.3	0.0	0.0	0.0
cpTi machined ES Enhanced	29.5	51.4	8.8	5.8	0.0	1.4	0.0	0.9	0.0	0.0	0.0
cpTi machined ES Enhanced RFGDT	15.1	55.9	14.7	7.5	0.0	0.0	0.0	0.4	0.0	0.0	0.0
Ti6Al4V machined control surface	36.8	48.7	10.3	1.1	0.0	2.1	0.3	0.3	0.5	0.9	0.0
Ti6Al4V machined control surface RFGDT	21.8	56.7	18.8	1.1	0.0	0.0	0.0	0.0	0.0	0.0	0.7
Ti6Al4V machined SI Enhanced	36.7	43.8	4.2	8.7	5.9	0.0	0.0	0.2	0.5	0.0	0.0
Ti6Al4V machined SI Enhanced RFGDT	14.9	55.3	12.9	9.8	6.2	0.2	0.0	0.3	0.0	0.0	0.4
Ti6Al4V machined ES Enhanced	29.2	52.2	5.5	9.5	0.0	0.7	0.0	0.8	0.0	0.0	0.0
Ti6Al4V machined ES Enhanced RFGDT	16.1	55.5	13.7	9.2	0.0	0.0	0.0	0.3	0.0	0.0	0.0
cpTi cast control surface	23.6	53.6	5.3	12.7	4.6	0.0	0.0	0.2	0.0	0.0	0.0
cpTi cast control surface RFGDT	15.1	57.9	9.2	12.9	4.7	0.0	0.0	0.4	0.0	0.0	0.2
cpTi cast SI Enhanced	37.3	43.9	4.3	10.5	2.2	0.2	0.0	0.5	1.1	0.0	0.0
cpTi cast SI Enhanced RFGDT	15.5	56.3	14.6	8.2	4.5	0.0	0.0	0.4	0.0	0.0	0.5
cpTi cast ES Enhanced	25.6	52.9	7.1	9.8	3.3	0.7	0.0	0.5	0.0	0.0	0.0
cpTi cast ES Enhanced RFGDT	23.1	51.3	12.9	7.9	3.0	0.0	0.0	0.5	0.9	0.0	0.3
Ti6Al4V cast control surface	28.7	51.4	5.6	9.6	3.3	0.0	0.0	0.4	0.8	0.2	0.0
Ti6Al4V cast control surface RFGDT	25.3	55.4	6.2	10.5	1.5	0.0	0.0	1.0	0.0	0.0	0.1
Ti6Al4V cast SI Enhanced	32.7	47.7	8.4	8.0	2.2	0.1	0.0	0.2	0.7	0.0	0.0
Ti6Al4V cast SI Enhanced RFGDT	14.9	55.5	9.9	15.1	3.5	0.0	0.0	0.1	0.0	0.0	0.4
Ti6Al4V cast ES Enhanced	28.9	52.3	4.8	10.1	2.4	0.5	0.0	0.6	0.4	0.0	0.0
Ti6Al4V cast ES Enhanced RFGDT	15.9	56.6	12.6	10.9	3.2	0.0	0.0	0.4	0.0	0.0	0.4

XPS survey spectra

A typical XPS survey spectrum of a cpTi cast sample before RFGDT is shown in Fig 5-1 and after RFGDT in Fig 5-2 (see p77). XPS spectra for all other samples are given in Addendum H (see p200-209). The spectrum depicts elements with binding energies from 0 to 1100eV that are detected from the surface layer of samples. Every element has its own binding energy value and detected peaks were identified by the computer database in most instances and counterchecked (Moulder et al, 1992). Major lines identified were Carbon (1s), Titanium (2p) and Oxygen (1s). Associated weaker lines were also identified but not further monitored.

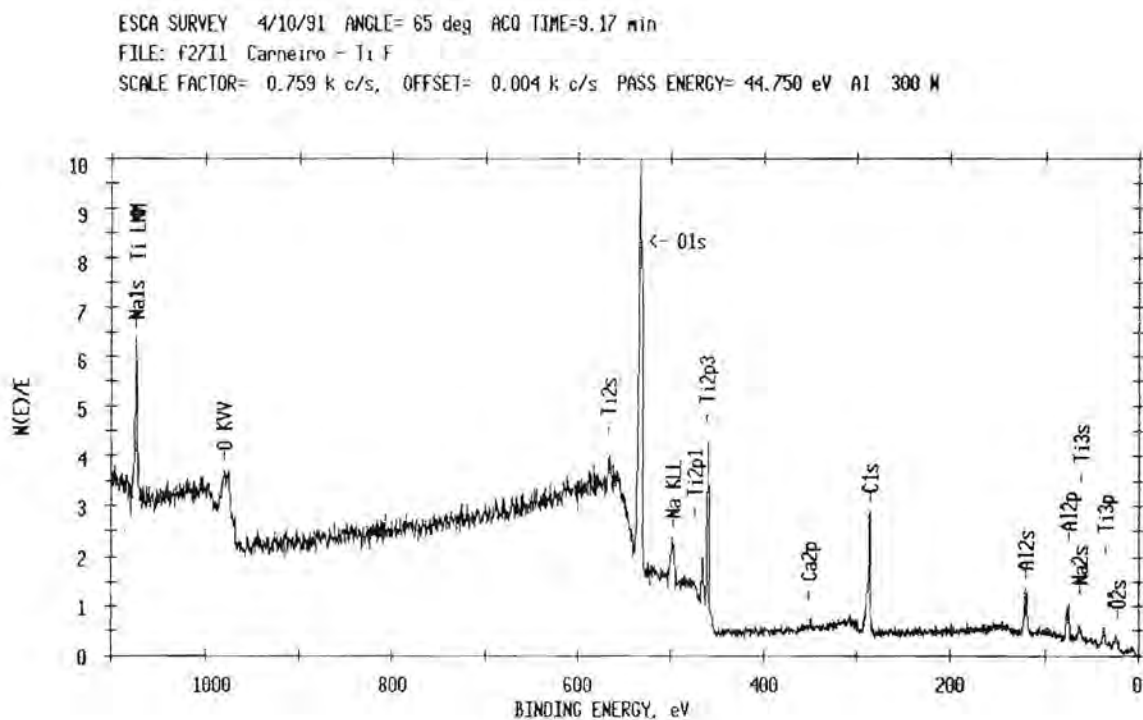


Fig 5-1: XPS survey spectra for cpTi cast control sample surface before RFGDT

ESCA SURVEY 4/10/91 ANGLE= 65 deg ACQ TIME=9.17 min
FILE: f27H1 Carneiro - Ti FG
SCALE FACTOR= 0.903 k c/s, OFFSET= 0.004 k c/s PASS ENERGY= 44.750 eV Al 300 W

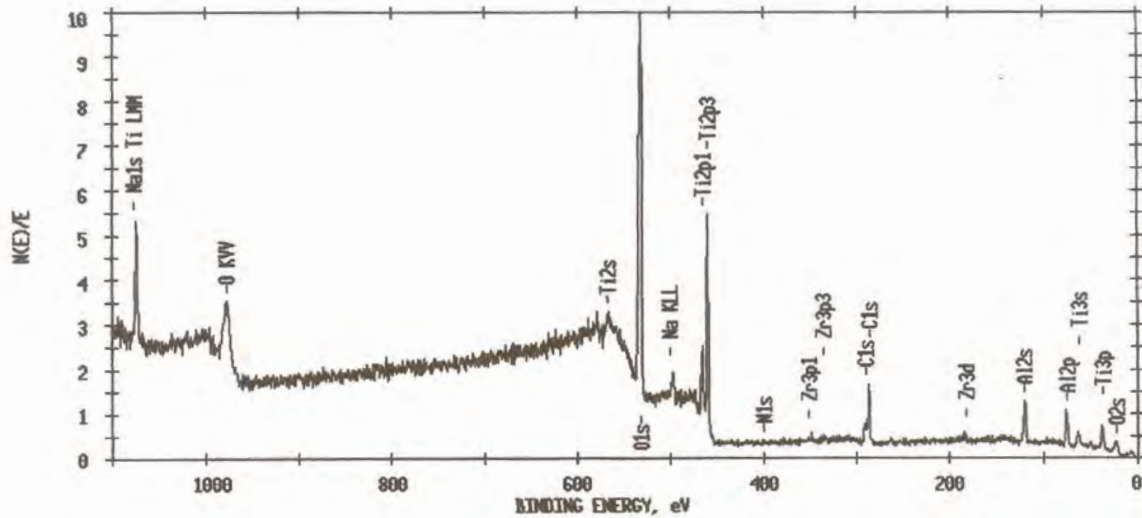


Fig 5-2: XPS survey spectra for cpTi cast control sample surface after RFGDT

Differences in the survey spectra of RFGDT cpTi machined and cast and Ti6Al4V machined and cast samples of control surfaces are shown in Fig 5-3 and Fig 5-4 (see p78), respectively.

ESCA SURVEY 4/10/91 ANGLE= 65 deg ACQ TIME=9.17 min
FILE: f27H1 Carneiro - Ti FG
SCALE FACTOR= 0.903 k c/s, OFFSET= 0.004 k c/s PASS ENERGY= 44.750 eV Al 300 W

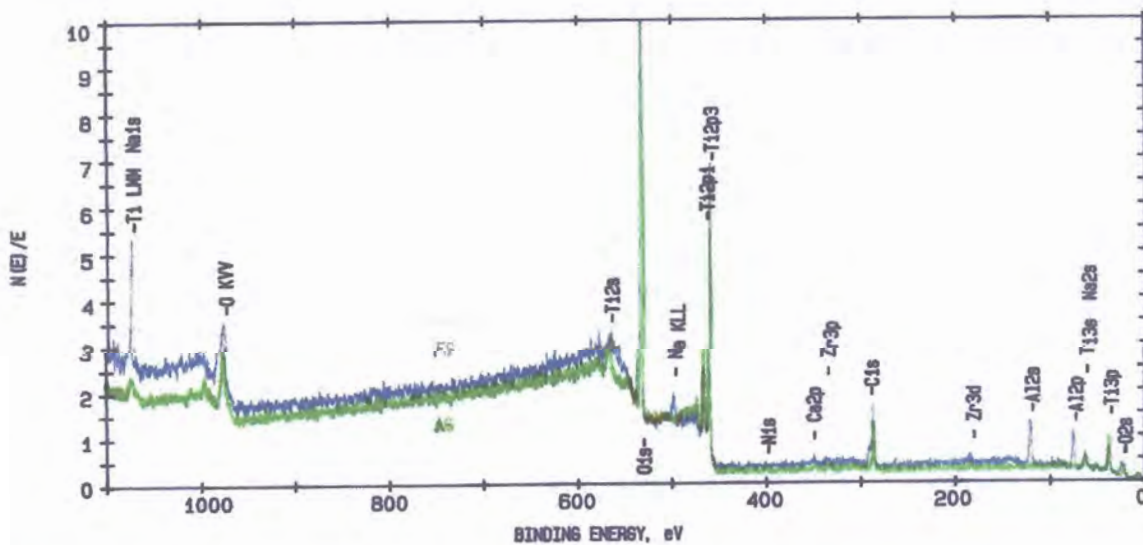


Fig 5-3: XPS survey spectra of cpTi machined RFGDT sample (AG=green) and cpTi cast RFGDT sample (FG=blue) of control surfaces

ESCA SURVEY 4/15/91 ANGLE= 65 deg ACG TIME=14.67 min
 FILE: f32C3 Carneiro - Ti alloy cast HG
 SCALE FACTOR= 0.682 k c/s, OFFSET= 0.005 k c/s PASS ENERGY= 44.750 eV AI 300 W

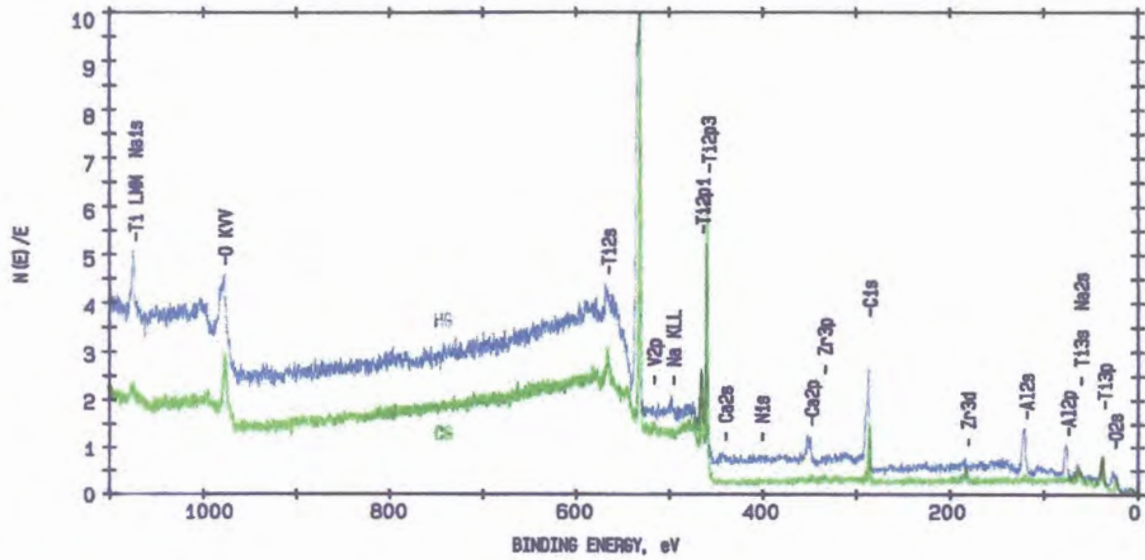


Fig 5-4: XPS survey spectra of Ti6Al4V machined RFGDT sample (CG=green) and Ti6Al4V cast RFGDT sample (HG=blue) of control surfaces

Carbon

Data of the atomic percent concentration of Carbon for all samples before and after RFGDT is shown in Fig 5-5.

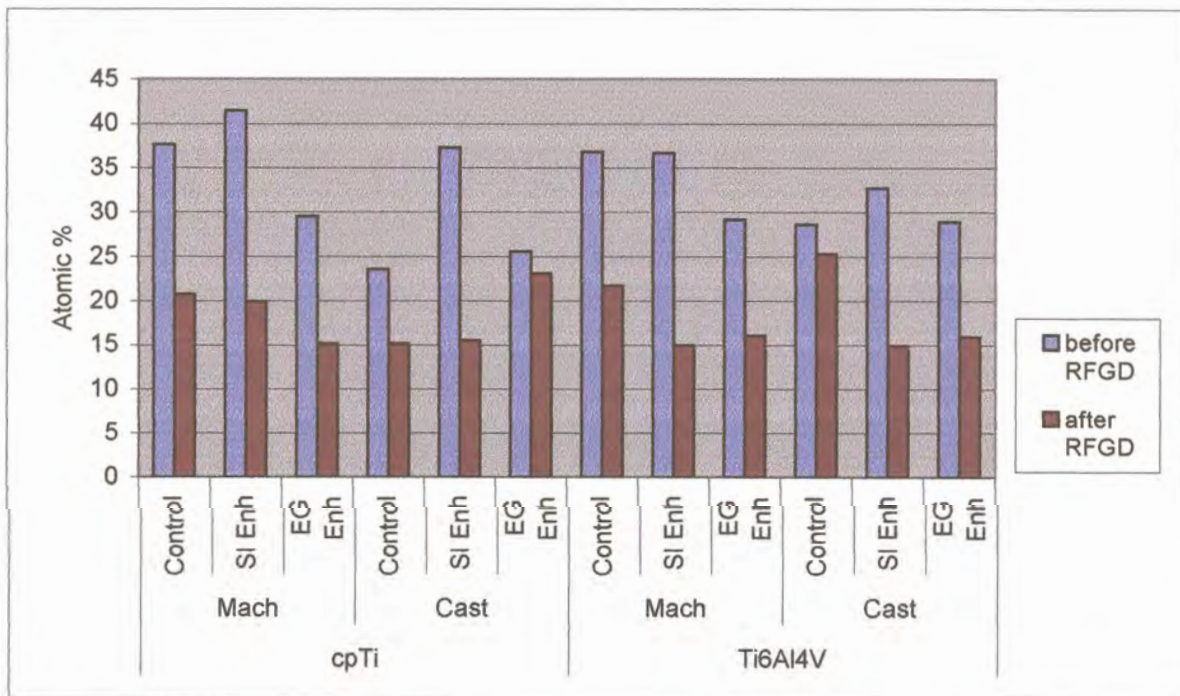


Fig 5-5: Atomic percent concentration of Carbon before and after RFGDT of sample surfaces

On average RFGDT significantly reduced the surface Carbon atomic percent concentration from 32.4% to 18.2% ($p < 0.05$). An interaction between RFGDT and surface enhancement showed that the untreated control and SI enhanced samples had significantly higher surface Carbon content than treated samples ($p = 0.02$).

No significant differences were observed in Carbon atomic percent concentration between the different materials used, method of fabrication employed or surface enhancement procedures other than RFGDT.

Oxygen

The surface Oxygen atomic concentration percent of samples before and after RFGDT is shown in Fig 5-6 (see p80).

A significant difference in surface Oxygen atomic percent concentration was observed between samples that were differently enhanced ($p = 0.0025$). On average the SI enhanced samples had significantly lower surface Oxygen atomic percent (49.9%) compared to ES enhanced and control samples (53.5% and 53.2% respectively).

RFGDT significantly enhanced the average surface Oxygen level from 49.0% to 55.4 % ($p < 0.05$). A significant interaction was observed between surface enhancement and RFGDT ($p = 0.0045$) depicting that enhanced surfaces that were treated had significantly higher surface Oxygen content than untreated enhanced samples.

No significant difference in the Oxygen content was observed between materials used or fabrication procedures adopted.

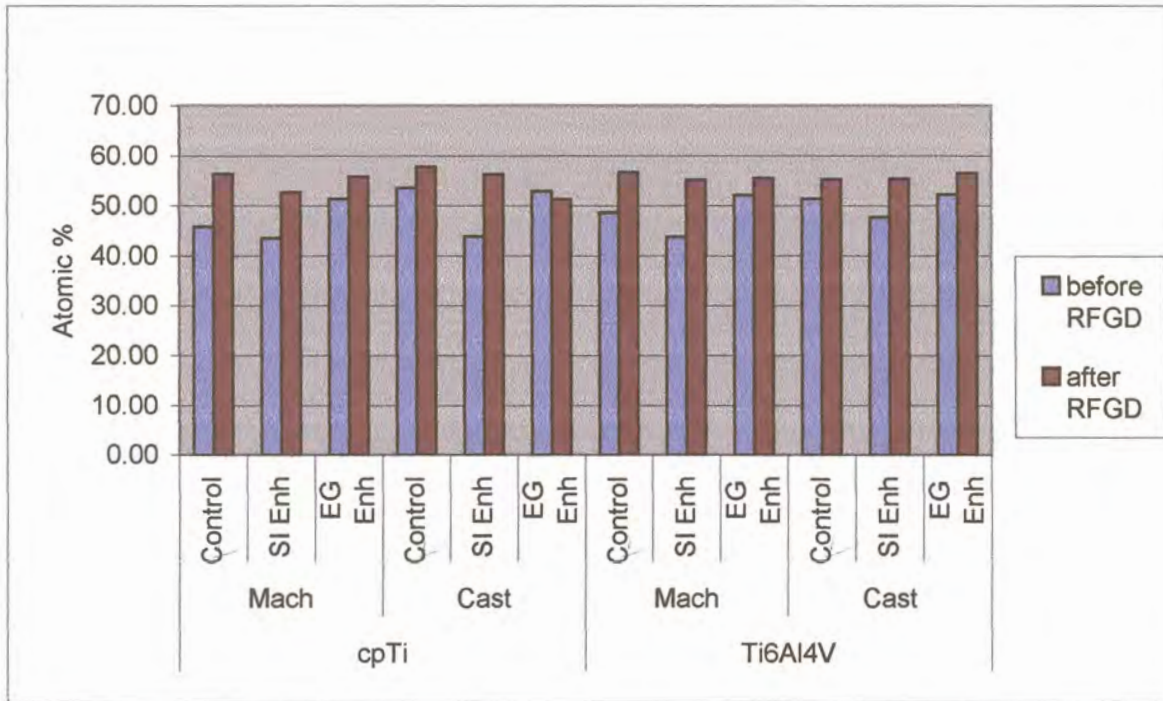


Fig 5-6: Atomic percent concentration of Oxygen before and after RFGDT of sample surfaces

Titanium

Fig 5-7 (see p81) shows the atomic percent concentration of Titanium for the different samples.

The fabrication procedure significantly decreased Titanium levels ($p=0.0004$). On average higher Titanium atomic percent concentration was measured on the surfaces of machined samples (11.8%) than cast samples (8.4%). RFGDT samples had on average significantly higher measured Titanium percentages on their surfaces (13.3%) compared to untreated samples (6.9%). There was an interaction between the method of fabrication and surface enhancement ($p=0.0005$) and machined control samples had on average significantly higher measured surface Titanium percentages (15.5%) than the enhanced machined surfaces (SI and ES) or cast samples.

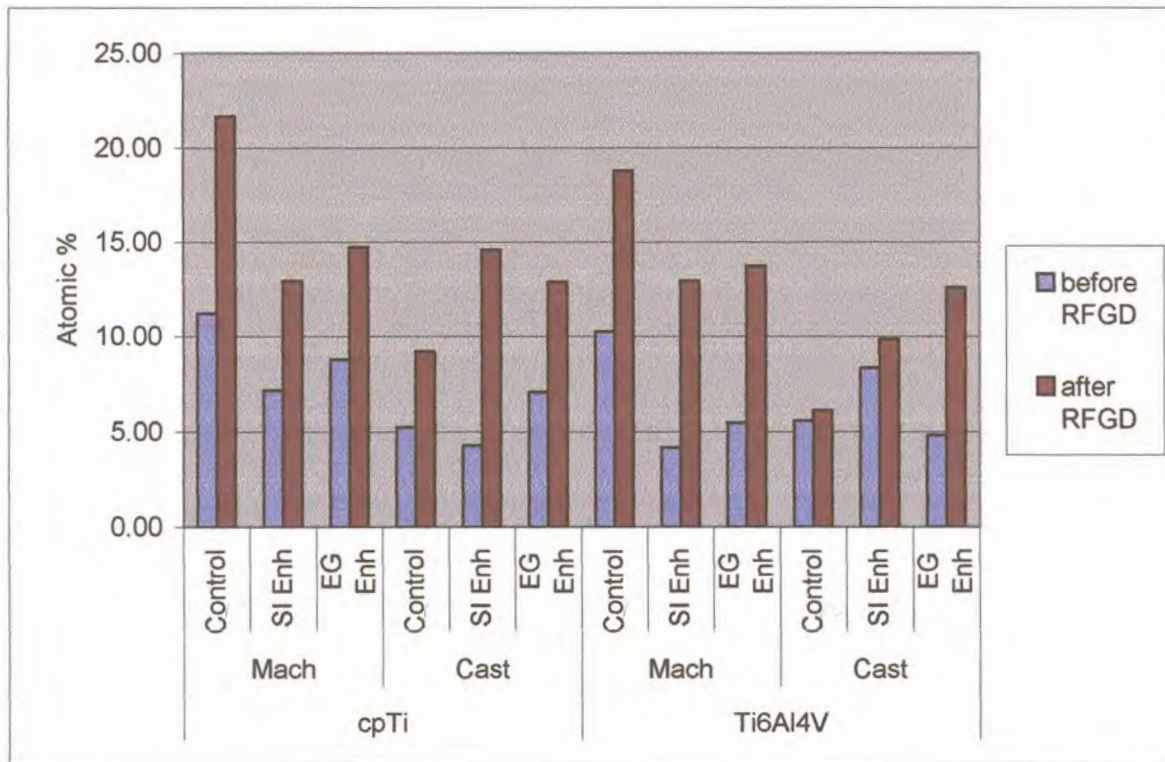


Fig 5-7: Atomic percent concentration of Titanium before and after RFGDT of sample surfaces

Aluminium

The observed XPS values for the Aluminium atomic percent concentration of samples are shown in Fig 5-8 (see p82).

The surface Aluminium atomic percent concentration increased significantly with method of fabrication ($p < 0.05$). On average cast sample surfaces (10.5%) showed significantly higher Aluminium concentrations than machined sample surfaces (5.6%). Surface enhancement significantly affected the Aluminium surface concentration ($p = 0.005$). Enhanced surfaces recorded significantly higher Aluminium than control surfaces. Interaction between method of fabrication and surface enhancement ($p = 0.0002$) showed that on average machined control surfaces (0.6%) have significantly lower Aluminium content compared to cast control sample (11.4%) and other sample surfaces. Material used for fabrication or RFGDT did not have any significant effect on the surface Aluminium content in samples.

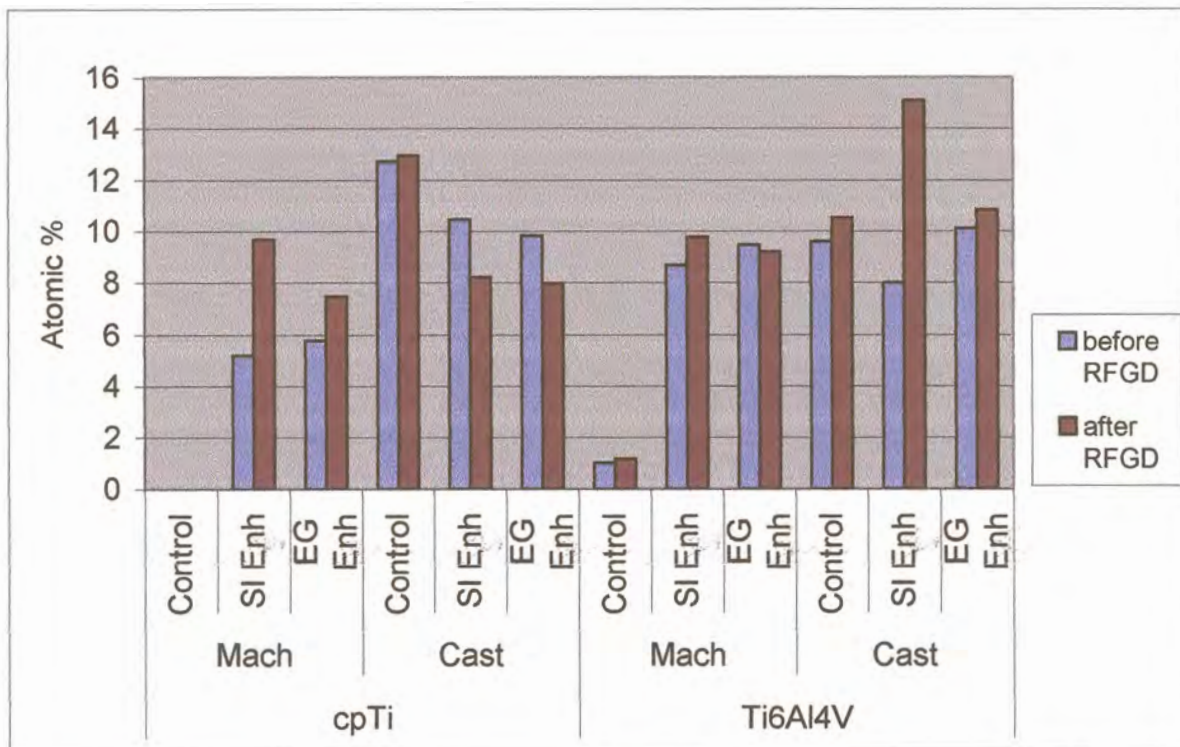


Fig 5-8: Atomic percent concentration of Aluminium before and after RFGDT of sample surfaces

Sodium

Fig 5-9 (see p83) shows the atomic percent concentration of Sodium for the different samples.

The method of fabrication of samples significantly increased the Sodium surface concentration. On average cast samples (3.1%) had significantly higher surface Sodium content than machined samples (1.0%) ($p=0.0002$). SI enhanced samples (3.1%) had significantly higher surface Sodium concentration compared to other enhanced samples ($p=0.02$). There was an interaction between material used and fabrication procedure adopted ($p=0.0039$). On average cpTi machined samples were observed to have significantly lower surface Sodium concentration (0.0%) compared to Ti6Al4V machined and cast samples (3.7%). The interaction between material employed and surface enhancement showed that on average Ti6Al4V SI enhanced surfaces (4.4%) had significantly higher surface Sodium concentration compared to other samples ($p=0.0079$). When the fabrication process was related to surface enhancement it was significant that

machined control and experimental enhanced samples had lower surface Sodium concentration compared to other samples (p=0.0147).

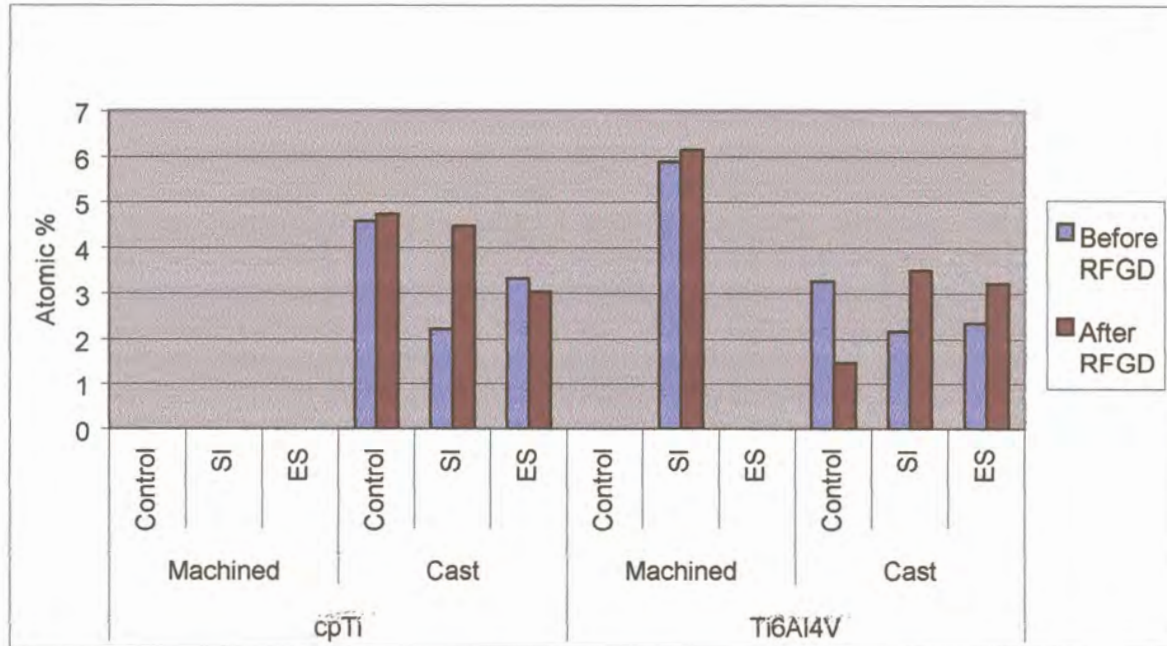


Fig 5-9: Atomic percent concentration of Sodium before and after RFGDT of sample surfaces

5.1.1.2 Curve Fitting

Carbon sub peaks

Deconvolution of high-resolution spectra of the Carbon 1s peak revealed four components for most samples. Table 5-2 (see p84) shows the contribution of each individual sub peak to the Carbon envelope for samples.

The major sub peak of Carbon for most sample surfaces was at ~285eV indicating adventitious Carbon. The remaining sample surfaces had peaks at ~286eV that can be assigned to Carbon bonded with Oxygen or Nitrogen (Moulder et al, 1992). Other sub peaks were recorded between ~287 and 290eV. The peak at ~286eV can also be assigned to hydroxyls (C-OH), while the peaks between ~288-290eV can be assigned to carboxyl (Louw, 1997).

Table 5-2: Deconvoluted Carbon 1s envelope with respective sub peak positions (Bold figures indicate highest peak).

Element	Peak I	Peak II	Peak III	Peak IV
cpTi machined control surface	286.0	287.3	289.8	
cpTi machined control surface RFGDT	285.8	287.2	289.6	
cpTi machined SI Enhanced	285.7	286.7	288.1	289.6
cpTi machined SI Enhanced RFGDT	285.7	286.9	288.6	289.8
cpTi machined ES Enhanced	285.9	287.4	289.7	
cpTi machined ES Enhanced RFGDT	285.9	287.5	289.8	
Ti6Al4V machined control surface	285.8	287.3	289.7	
Ti6Al4V machined control surface RFGDT	285.8	287.4	289.7	
Ti6Al4V machined SI Enhanced	285.9	286.9	288.3	290.2
Ti6Al4V machined SI Enhanced RFGDT	285.5	286.6	288.6	289.9
Ti6Al4V machined ES Enhanced	285.9	287.4	288.6	289.8
Ti6Al4V machined ES Enhanced RFGDT	285.6	286.6	288.4	289.9
cpTi cast control surface	286.4	287.8	290.3	
cpTi cast control surface RFGDT	286.4	287.8	290.4	
cpTi cast SI Enhanced	286.0	287.0	288.3	289.9
cpTi cast SI Enhanced RFGDT	285.7	286.7	288.3	289.8
cpTi cast ES Enhanced	285.7	286.9	287.9	289.6
cpTi cast ES Enhanced RFGDT	285.7	286.8	288.4	289.7
Ti6Al4V cast control surface	286.1	287.4	288.8	289.9
Ti6Al4V cast control surface RFGDT	286.2	287.3	288.4	289.6
Ti6Al4V cast SI Enhanced	285.8	286.4	287.4	289.3
Ti6Al4V cast SI Enhanced RFGDT	285.5	286.7	288.1	289.7
Ti6Al4V cast ES Enhanced	285.7	287.0	288.2	289.5
Ti6Al4V cast ES Enhanced RFGDT	285.5	286.7	288.5	290.0

Fig 5-10 shows a representative plot of the Carbon 1s envelope with its curve fit.

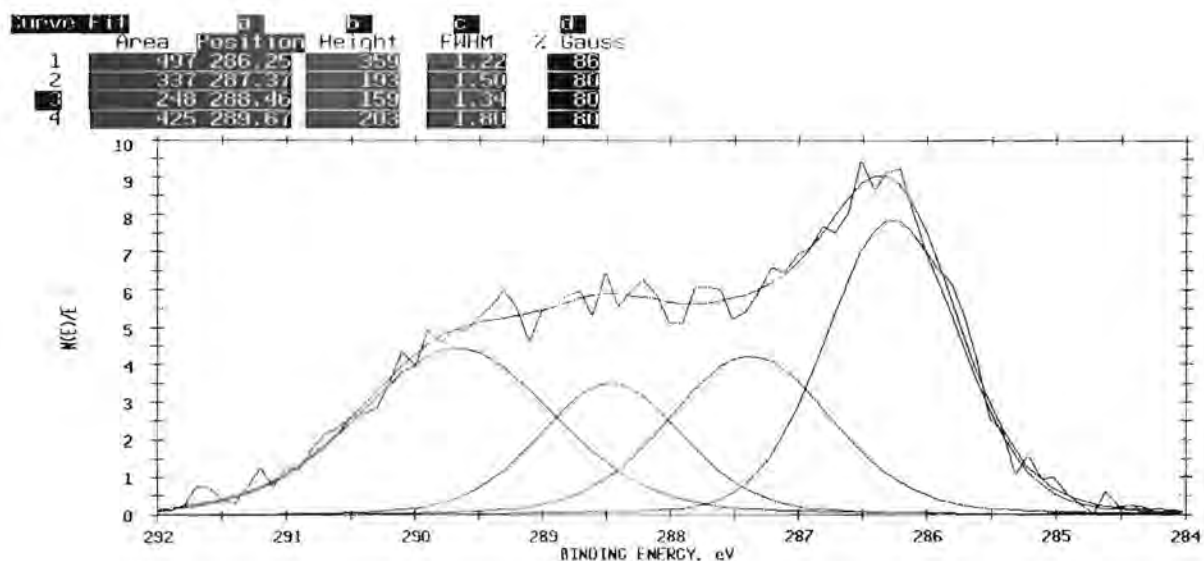


Fig 5-10: Deconvolution of XPS Carbon envelope of Ti6Al4V cast control RFGDT sample surface

Oxygen sub peaks

The respective Oxygen 1s sub peaks within its respective envelope are shown in Table 5-3. Most samples had four components with the exception of Ti6Al4V cast control RFGDT sample that had five component peaks. RFGDT reduced the number of peaks of cpTi and Ti6Al4V machined control samples from three to two.

Table 5-3: Deconvoluted Oxygen 1s envelope with respective sub peak positions (Bold figures indicate highest peak).

Element	Peak I	Peak II	Peak III	Peak IV	Peak V
cpTi machined control surface	529.8	531.2	532.1	533.5	
cpTi machined control surface RFGDT	530.0	531.4			
cpTi machined SI Enhanced	529.7	530.7	531.7	532.9	
cpTi machined SI Enhanced RFGDT	529.4	530.3	531.3	532.5	
cpTi machined ES Enhanced	529.6	530.6	531.6	532.6	
cpTi machined ES Enhanced RFGDT	529.3	530.0	531.0	532.6	
Ti6Al4V machined control surface	530.0	531.8	533.2		
Ti6Al4V machined control surface RFGDT	530.0	531.3			
Ti6Al4V machined SI Enhanced	529.5	530.9	531.8	533.2	
Ti6Al4V machined SI Enhanced RFGDT	529.4	530.4	531.4	533.1	
Ti6Al4V machined ES Enhanced	529.5	530.9	531.9	533.0	
Ti6Al4V machined ES Enhanced RFGDT	529.5	530.4	531.2	532.3	
cpTi cast control surface	529.6	530.9	531.9	533.1	
cpTi cast control surface RFGDT	529.5	530.5	531.8	533.2	
cpTi cast SI Enhanced	529.4	530.5	531.7	532.9	
cpTi cast SI Enhanced RFGDT	529.3	530.0	531.2	532.6	
cpTi cast ES Enhanced	529.6	530.7	531.7	532.9	
cpTi cast ES Enhanced RFGDT	529.4	530.5	531.4	532.9	
Ti6Al4V cast control surface	529.3	530.7	532.2	533.8	
Ti6Al4V cast control surface RFGDT	529.7	530.6	531.5	532.9	534.6
Ti6Al4V cast SI Enhanced	529.6	530.8	531.8	533.2	
Ti6Al4V cast SI Enhanced RFGDT	529.4	530.8	531.9	533.6	
Ti6Al4V cast ES Enhanced	529.6	530.8	531.9	533.0	
Ti6Al4V cast ES Enhanced RFGDT	529.4	530.2	531.4	533.0	

The major sub peak of the different samples varied considerably. For most samples it was at ~529eV, occasionally ~531eV and sometimes ~532eV. Some sub peaks had more or less the same peak height as was observed in Ti6Al4V cast control RFGDT sample. Metal oxides (529-531eV) and hydroxides (531-532eV) mainly contributed to the Oxygen sub peaks. Carbonates could also be present at ~531eV. Besides the different metal oxides of Titanium (TiO_2 -529.7-530.2eV; TiO -530.6eV; Ti_2O_3 -

529.6eV), Aluminium oxide could also have been contributory (Al_2O_3 -528-532eV) to the metal oxide peak detected (Lausmaa et al, 1990).

Deconvoluted high-resolution spectra sub peaks within its respective Oxygen envelope is shown in Fig 5-11.

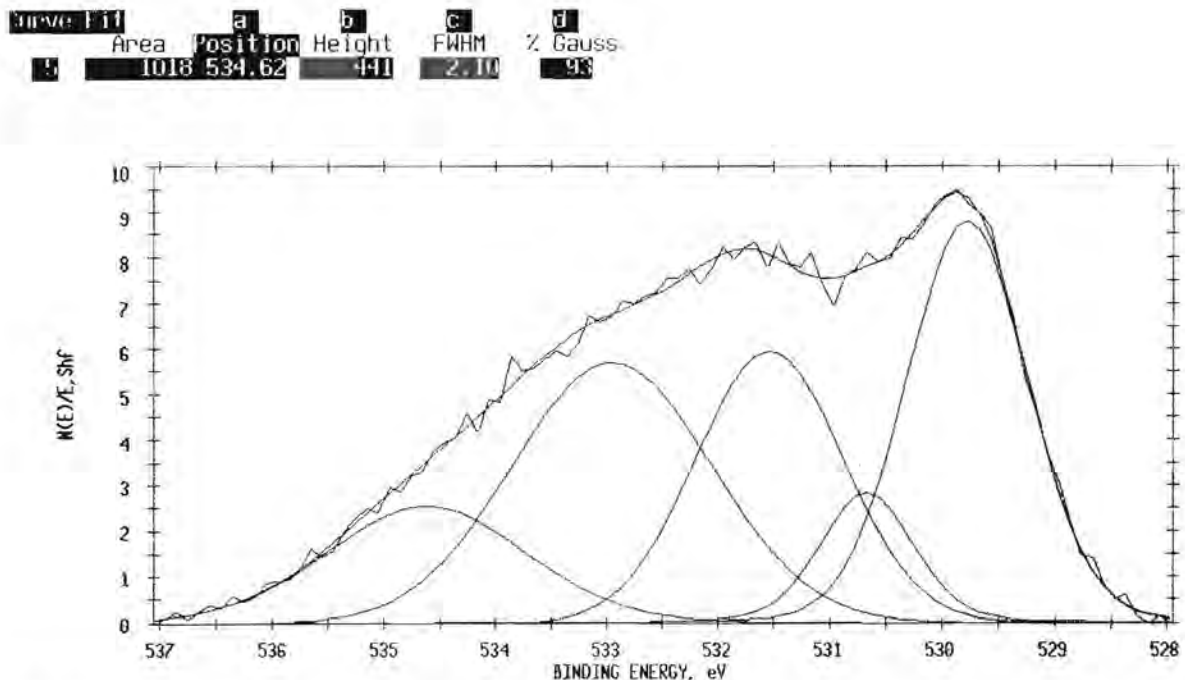


Fig 5-11: Deconvolution of XPS Oxygen envelope of Ti6Al4V cast control RFGDT sample surface

Titanium sub peaks

On most sample surfaces, only one major peak was detected, but deconvolution of the Ti2p peak on cpTi and Ti6Al4V machined control samples revealed two sub peaks, at 458eV and 457eV (see Table 5-4, p87). The major peak detected at 458eV indicates that the sample surfaces constituted mostly of TiO_2 . The oxide layer on some samples though, may rather consist of Ti_2O_3 as indicated by the 457eV peak.

A high-resolution spectrum for Titanium is shown in Fig 5-12 (see p87) with the peak centre at 458eV.

Table 5-4: Deconvoluted Titanium 2p envelope with respective sub peak positions (Bold figures indicate highest peak).

Element	Peak I	Peak II
cpTi machined control surface	458.3	
cpTi machined control surface RFGDT	458.6	457.9
cpTi machined SI Enhanced	458.2	
cpTi machined SI Enhanced RFGDT	458.0	
cpTi machined ES Enhanced	458.1	
cpTi machined ES Enhanced RFGDT	457.8	
Ti6Al4V machined control surface	458.4	
Ti6Al4V machined control surface RFGDT	458.5	457.7
Ti6Al4V machined SI Enhanced	457.9	
Ti6Al4V machined SI Enhanced RFGDT	457.9	
Ti6Al4V machined ES Enhanced	458.0	
Ti6Al4V machined ES Enhanced RFGDT	458.0	
cpTi cast control surface	458.1	
cpTi cast control surface RFGDT	458.1	
cpTi cast SI Enhanced	457.9	
cpTi cast SI Enhanced RFGDT	457.9	
cpTi cast ES Enhanced	458.1	
cpTi cast ES Enhanced RFGDT	458.0	
Ti6Al4V cast control surface	458.1	
Ti6Al4V cast control surface RFGDT	458.2	
Ti6Al4V cast SI Enhanced	458.1	
Ti6Al4V cast SI Enhanced RFGDT	457.9	
Ti6Al4V cast ES Enhanced	458.1	
Ti6Al4V cast ES Enhanced RFGDT	458.0	

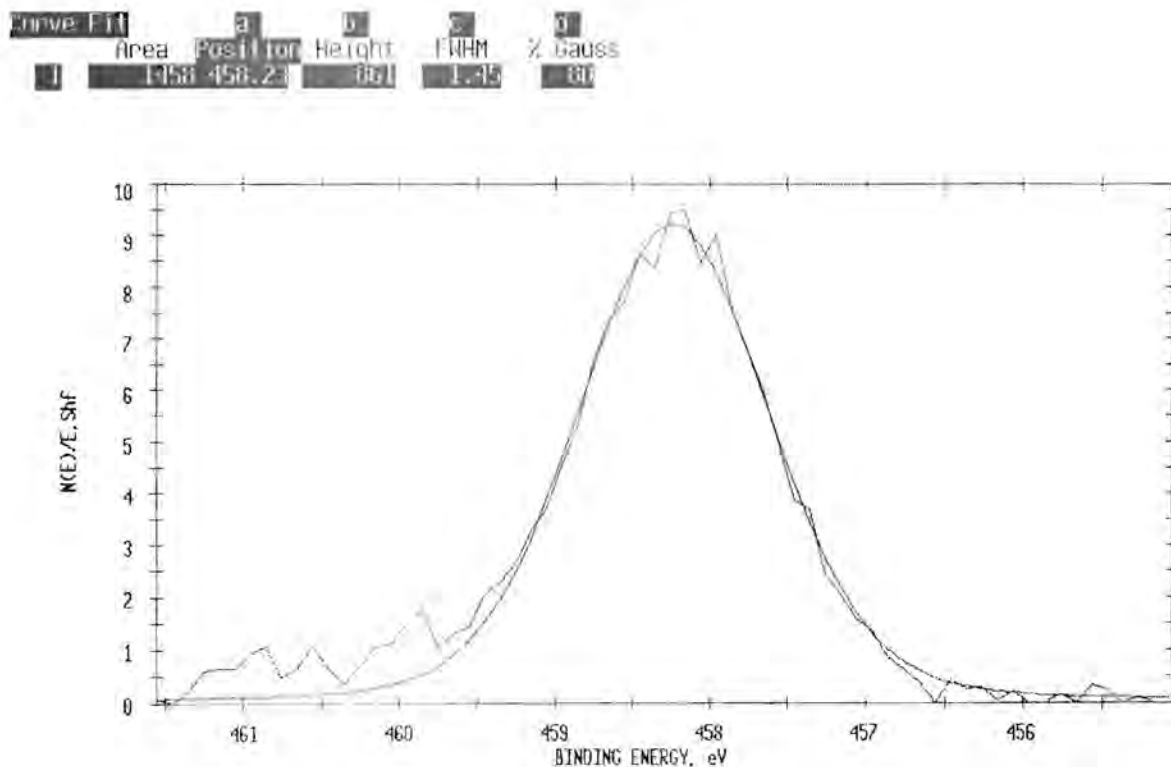


Fig 5-12: Deconvolution of XPS Titanium envelope of Ti6Al4V cast control RFGDT sample surface

Aluminium sub peaks

Fig 5-13 shows the deconvolution of XPS Aluminium envelope for the Ti6Al4V cast control surface.

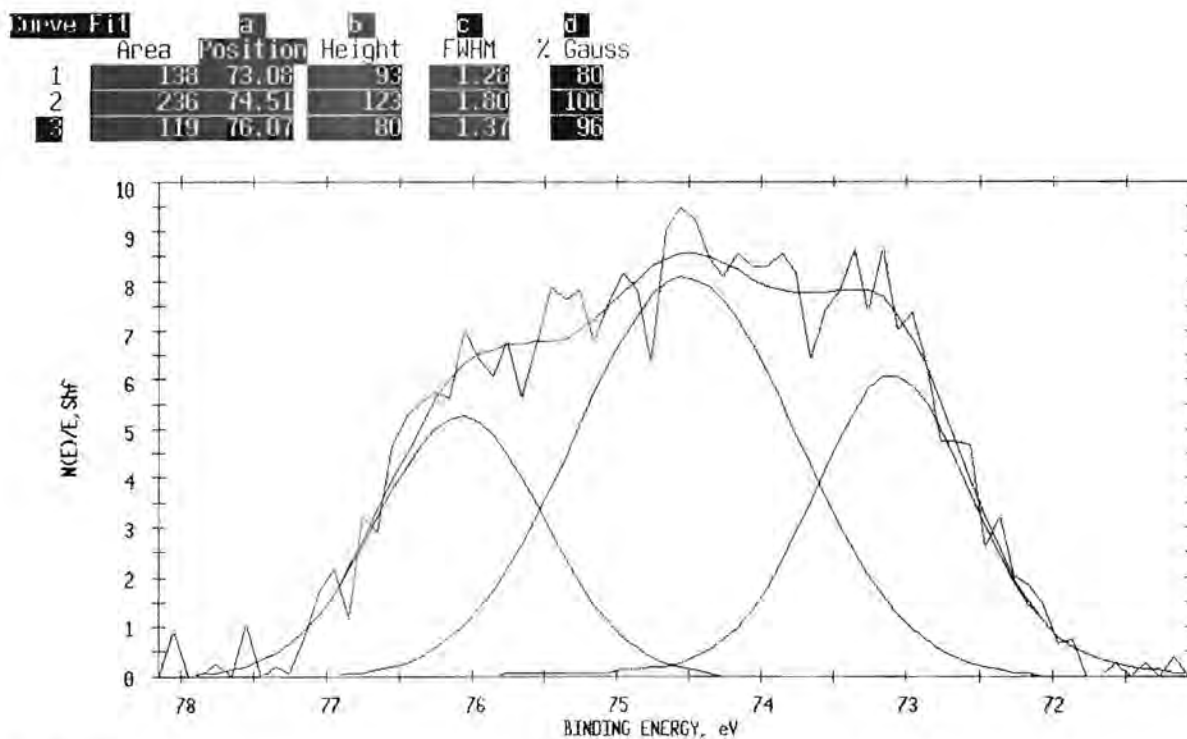


Fig 5-13: Deconvolution of Aluminium envelope for Ti6Al4V cast control surface

A deconvoluted high-resolution spectrum within the Aluminium envelope shows three main sub peaks. The sub peak at 73.03eV was attributed to Aluminium metal while the 74.51eV sub peak was attributed to Aluminium oxides. The 76.07eV peak was probably a Halide form of Aluminium (Moulder et al, 1992).

Sodium sub peaks

The presence of Sodium was detected together with Titanium at 1072eV using the Na (1s) peak and no attempts were made to further deconvolute the Sodium and Titanium peak.

5.1.2 Surface Roughness

5.1.2.1 Area Analysis

Representative 3D images of samples scanned using the Atomic Force Microscope are shown in Fig 5-14 to 5-17 (see p89-90).

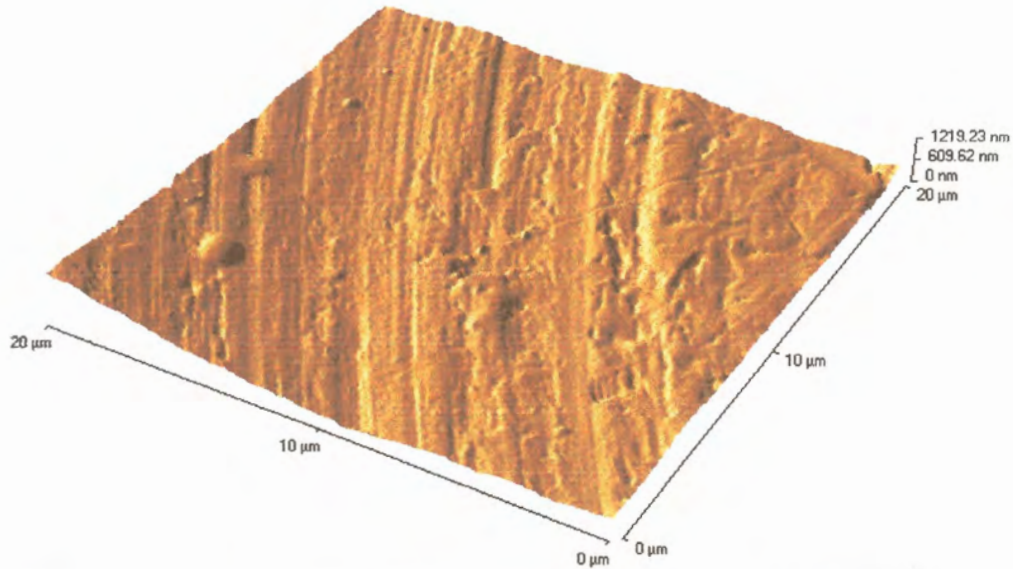


Fig 5-14: AFM 3D images of 20μm scans of cpTi machined control sample surface

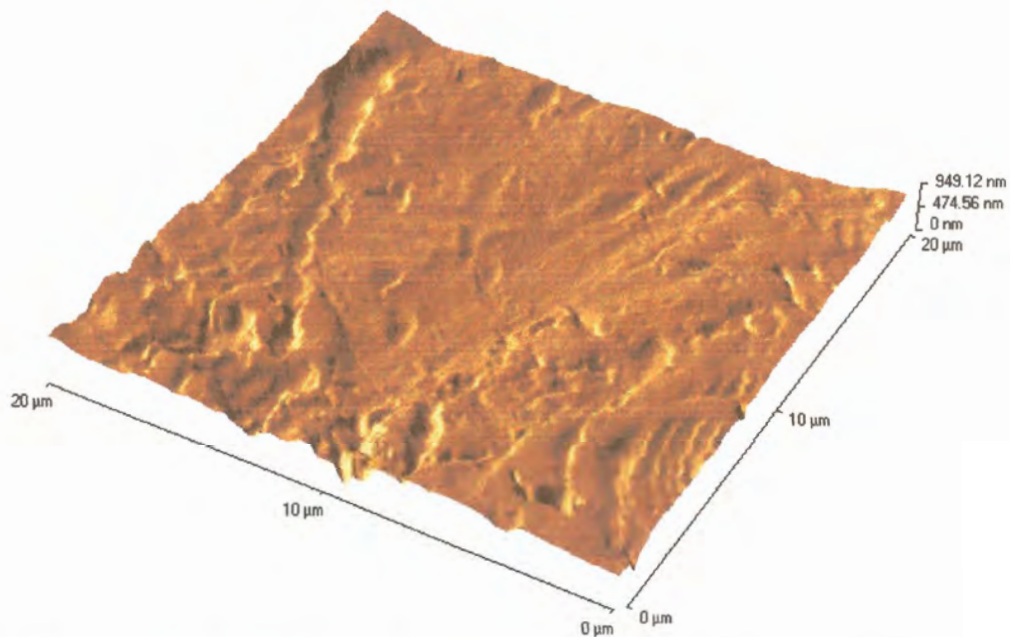


Fig 5-15: AFM 3D images of 20μm scans of Ti6Al4V machined control sample surface

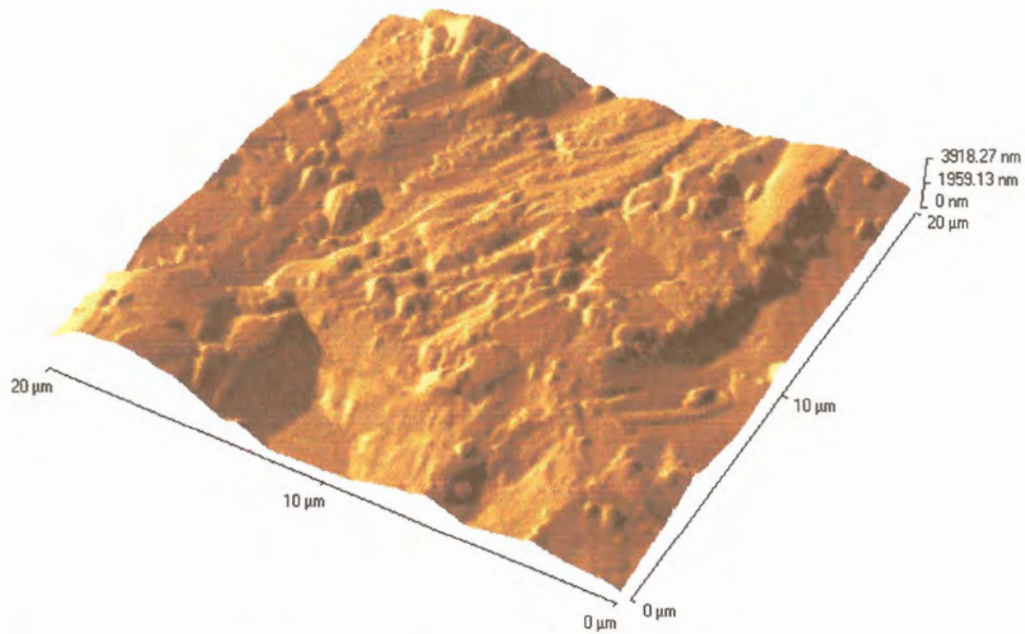


Fig 5-16: AFM 3D images of 20μm scans of cpTi cast control sample surface

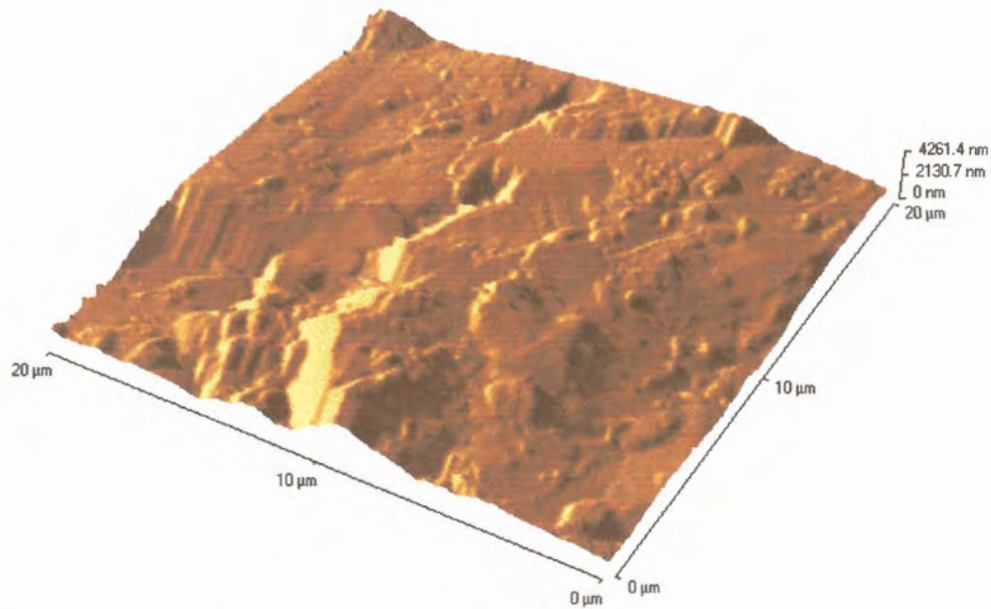


Fig 5-17: AFM 3D images of 20μm scans of Ti6Al4V cast control sample surface

The quantitative data obtained from the surfaces of 3D Atomic Force micrographs were analyzed and averages of the different measures of Area analysis for the 20μm (see Table 5-5, p91) and 5μm (see Table 5-6, p92) are shown (see Addendum C, p180-182)

Table 5-5: Average tabulated values of the surface topography of samples for 20 μ m scans (N=5).

Material	Ra \pm SD	RMS \pm SD	Maximum Height \pm SD	Average Range \pm SD	Surface Area \pm SD
CpTi machined control surface	0.14 \pm 0.04	0.17 \pm 0.05	0.58 \pm 0.15	1.04 \pm 0.16	416.18 \pm 4.09
CpTi machined control surface & RFGDT	0.09 \pm 0.02	0.12 \pm 0.04	0.43 \pm 0.22	0.95 \pm 0.29	416.34 \pm 5.77
Ti6Al4V machined control surface	0.08 \pm 0.03	0.11 \pm 0.04	0.63 \pm 0.29	0.92 \pm 0.35	415.00 \pm 3.18
Ti6Al4V machined control surface & RFGDT	0.14 \pm 0.02	0.18 \pm 0.03	0.53 \pm 0.07	1.20 \pm 0.14	425.02 \pm 6.49
cpTi cast control surface	0.51 \pm 0.1	0.65 \pm 0.12	1.88 \pm 0.52	3.94 \pm 0.62	531.92 \pm 24.25
cpTi cast control surface & RFGDT	0.64 \pm 0.19	0.79 \pm 0.22	2.20 \pm 1.03	4.55 \pm 1.21	559.14 \pm 60.88
Ti6Al4V cast control surface	0.44 \pm 0.19	0.55 \pm 0.24	1.74 \pm 0.84	3.30 \pm 1.38	508.26 \pm 55.34
Ti6Al4V cast control surface & RFGDT	0.41 \pm 0.10	0.52 \pm 0.14	1.92 \pm 0.81	3.67 \pm 0.99	535.26 \pm 65.83

The mean of the different analyses of surface roughness for both the 20 μ m and 5 μ m scans are observed to be higher for the surfaces of cast samples than for the machined samples.

Table 5-6: Average tabulated values of the surface topography of samples for 5 μ m scans (N=5).

Material	Ra \pm SD	RMS \pm SD	Maximum Height \pm SD	Average Range \pm SD	Surface Area \pm SD
CpTi machined control surface	0.05 \pm 0.02	0.07 \pm 0.02	0.26 \pm 0.13	0.51 \pm 0.16	27.1 \pm 0.75
CpTi machined control surface & RFGDT	0.06 \pm 0.05	0.08 \pm 0.06	0.21 \pm 0.12	0.42 \pm 0.28	26.56 \pm 1.0
Ti6Al4V machined control surface	0.08 \pm 0.02	0.10 \pm 0.03	0.34 \pm 0.24	0.52 \pm 0.25	27.31 \pm 1.17
Ti6Al4V machined control surface & RFGDT	0.10 \pm 0.03	0.12 \pm 0.03	0.31 \pm 0.06	0.67 \pm 0.16	28.04 \pm 0.96
cpTi cast control surface	0.26 \pm 0.15	0.32 \pm 0.17	0.68 \pm 0.33	1.61 \pm 0.55	32.85 \pm 3.32
cpTi cast control surface & RFGDT	0.27 \pm 0.14	0.33 \pm 0.15	0.80 \pm 0.45	1.78 \pm 0.53	34.26 \pm 4.46
Ti6Al4V cast control surface	0.25 \pm 0.11	0.31 \pm 0.14	0.75 \pm 0.38	1.63 \pm 0.73	34.94 \pm 5.01
Ti6Al4V cast control surface & RFGDT	0.2 \pm 0.13	0.24 \pm 0.16	0.58 \pm 0.29	1.31 \pm 0.79	32.39 \pm 5.82

Area Ra and RMS

Surface roughness is representative of both Ra and RMS values and results are reported together. RMS is the root mean square of Ra and therefore predicted to be a more reliable measure of assessment (see 2.6.2.1, p33). Ra and RMS values of samples for the 20 μ m scan are shown in Fig 5-18 (see p93).

For the 20 μ m scans the respective average Ra and RMS values of surfaces of cast samples (0.50 μ m and 0.65 μ m) were significantly higher than machined samples (0.11 μ m and 0.14 μ m).

No significant differences in the Ra or RMS values were observed between material used (cpTi or Ti6Al4V) and treatment rendered.

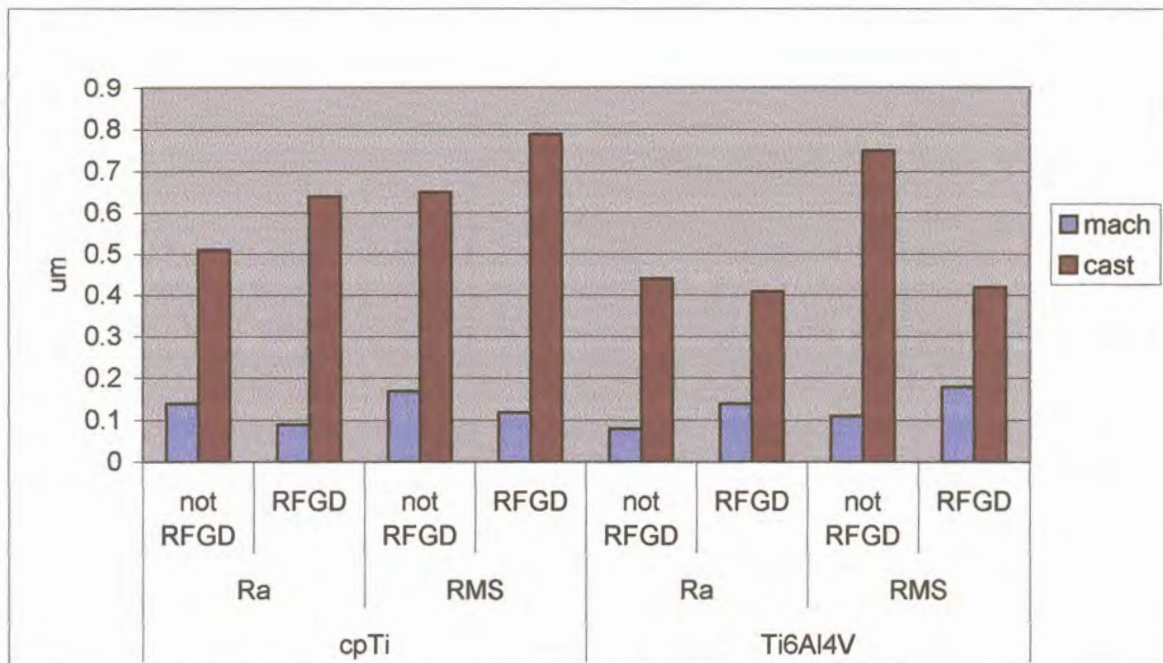


Fig 5-18: Average roughness (Ra and RMS) of the different sample surfaces by material employed and RFGDT for 20 μ m scan

Ra and RMS values of the 5 μ m scans are showed in Fig 5-19 (see p94). Surfaces of cast samples showed on average a significantly higher Ra (0.20 μ m) and RMS (0.30 μ m) values compared to the machined samples (Ra=0.08 μ m and RMS=0.09 μ m). Materials used or treatment rendered was of no significance in terms of Ra or RMS values.

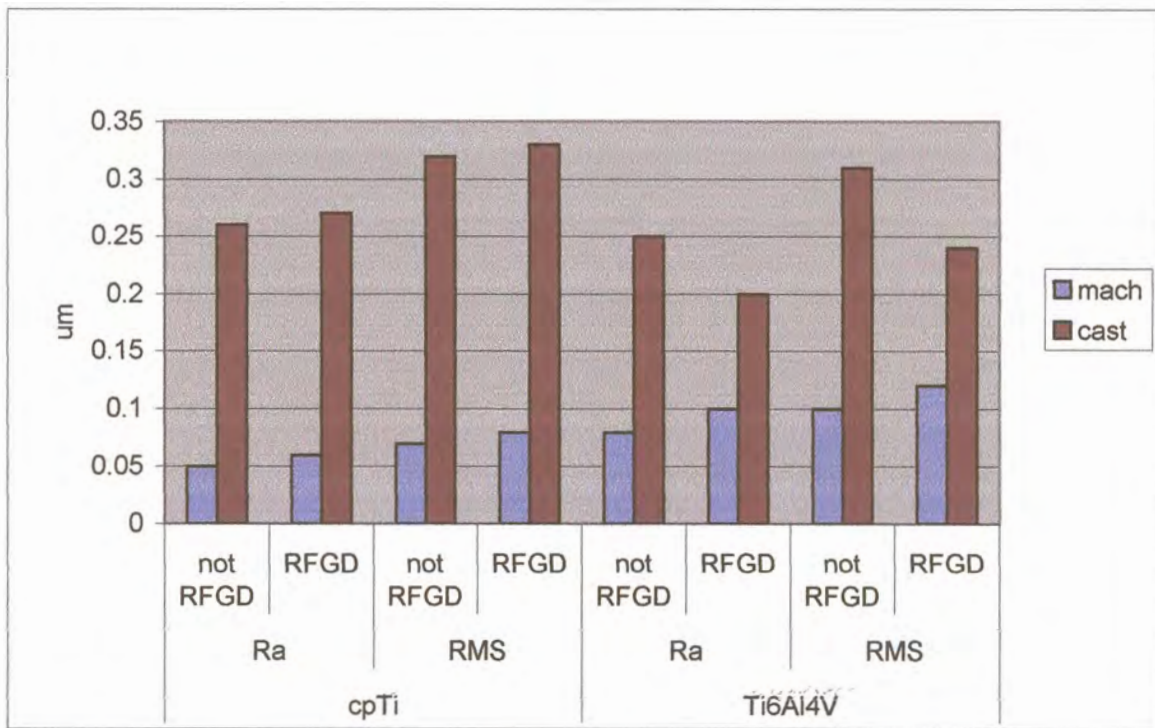


Fig 5-19: Average roughness (Ra and RMS) of the different sample surfaces by material employed and RFGDT for 5 μ m scan

Average height and Maximum range

Average height is the highest point from the zero value of the surface scanned while the Maximum range reveals how the surface topography is related in terms of highest and lowest point of scanned surface (see 2.6.2.1, p33). The Average height and Maximum range for the 20 μ m scans and 5 μ m scans are shown in Fig 5-20 and 5-21 (see p95).

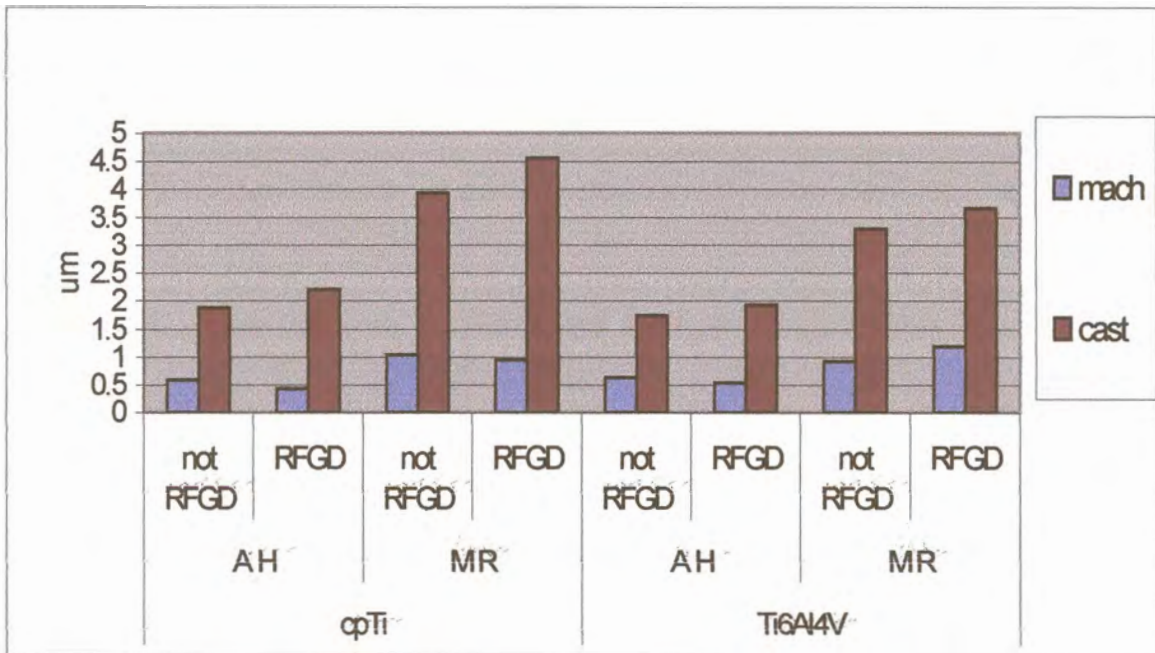


Fig 5-20: Average height and Maximum range for 20µm scans of sample surfaces

For the 20µm scan the respective Average height and Maximum range on average were significantly higher for the surfaces of cast samples (1.93µm and 3.86µm) than that observed for the machined samples (0.54µm and 1.03µm).

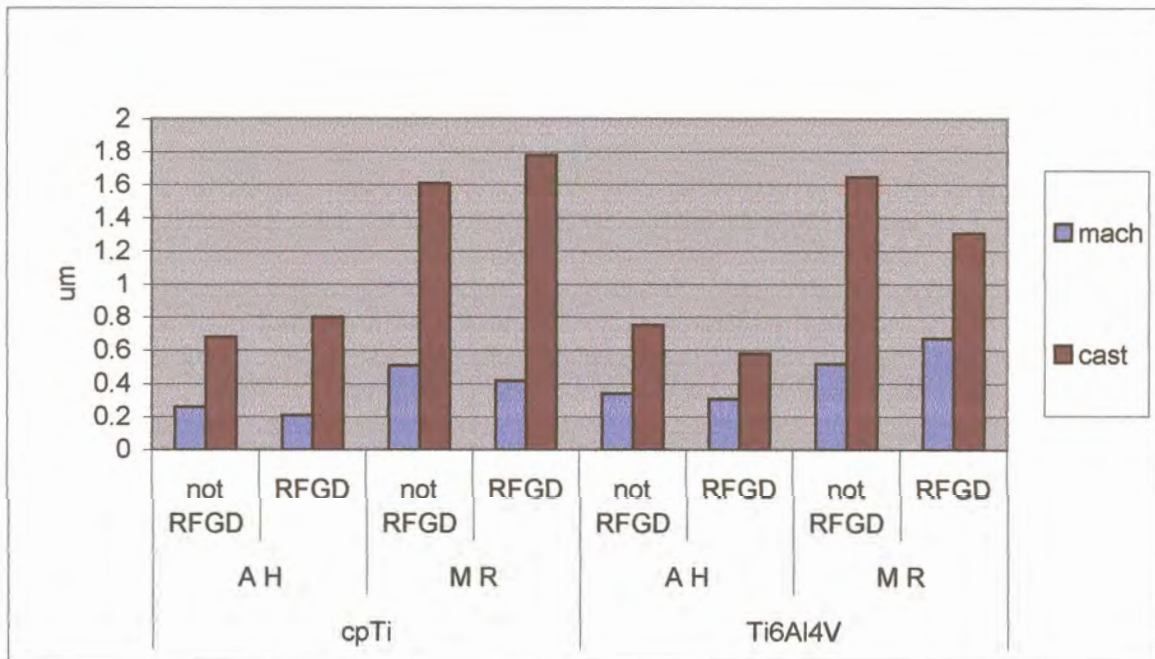


Fig 5-21: Average height and Maximum range for 5µm scans of sample surfaces

For the 5 μ m scans the Maximum range on average for the surfaces of cast samples (1.59 μ m) was significantly higher than machined samples (0.53 μ m) and similarly the Average range was significantly higher for surfaces of cast (0.70 μ m) than machined (0.28 μ m) samples.

Surface Area

Surface area or the projected area denotes the probable contact area of the sample surface (see 2.6.2.1, p33) and the projected surface area is the increase in area as a result of surface topography.

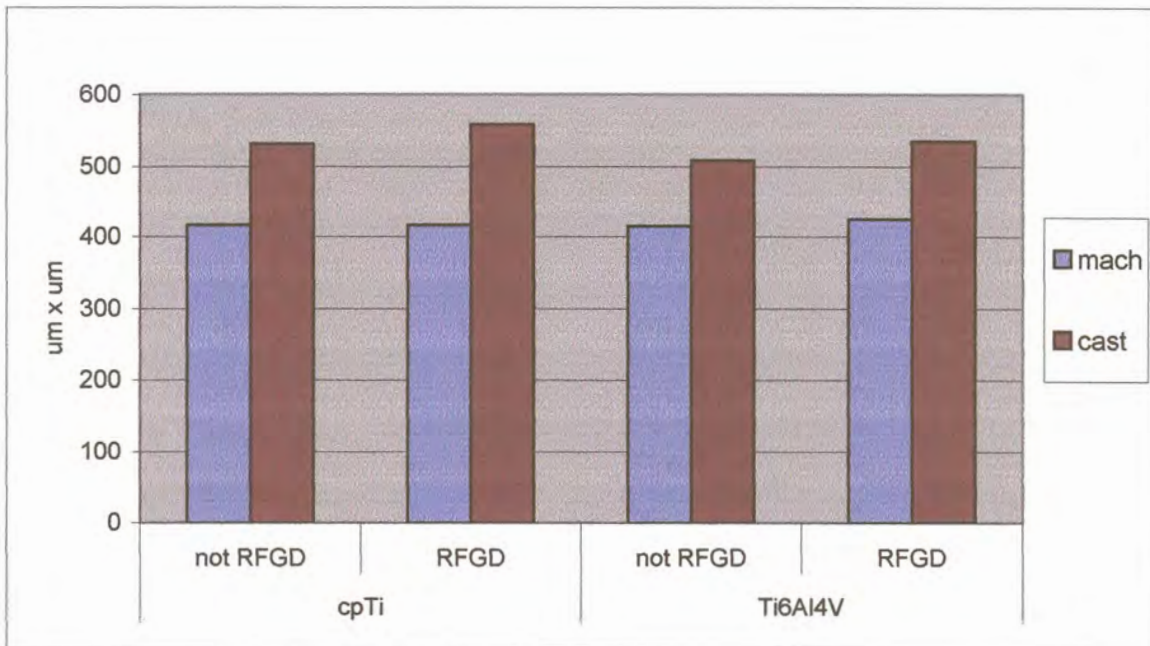


Fig 5-22: Average projected surface area of the 20 μ m scans for sample surfaces

Fig 5-22 shows the average surface area for the 20 μ m scan and surfaces of cast samples display on average a significant surface area increase (533.65 μ m²) compared to machined samples (418.14 μ m²) ($p < 0.05$). RFGDT significantly increased the surface area from 467.84 μ m² to 483.94 μ m² ($p = 0.03$). Material used for fabrication did not significantly modify the projected surface area.

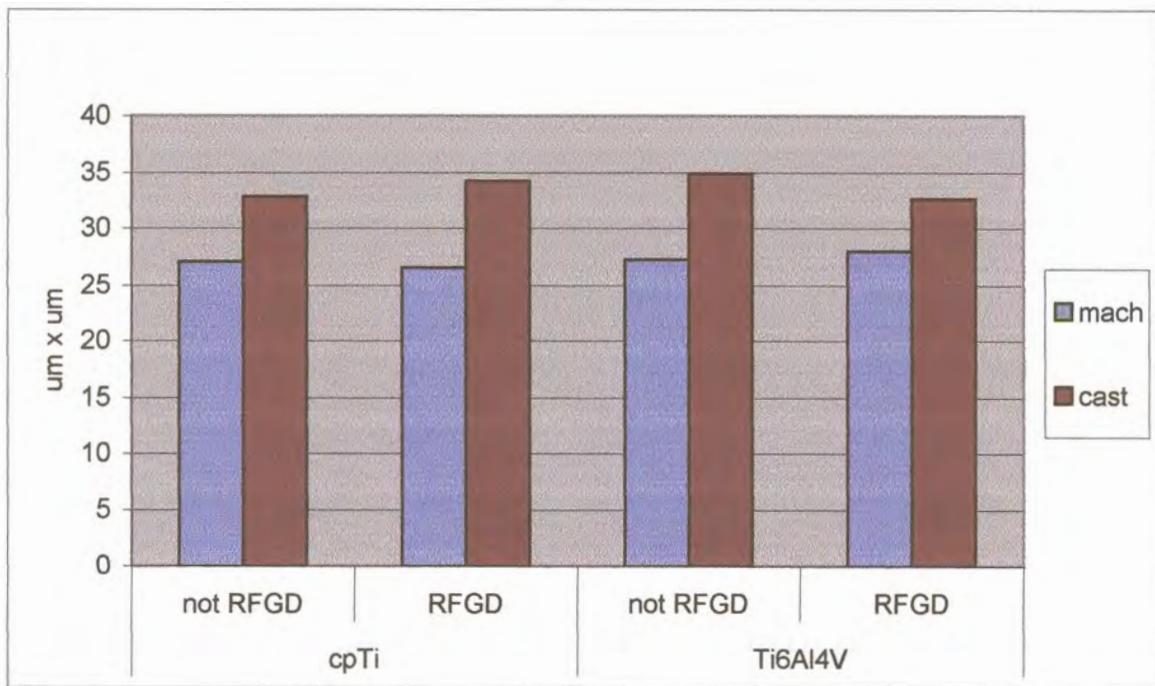


Fig 5-23: Average Projected surface area of the 5µm scans for sample surfaces

Average surface area for the 5µm scans is shown in Fig 5-23. The effect of RFGDT or material used was not obvious but on average surfaces of cast samples ($33.59\mu\text{m}^2$) had a significantly higher projected surface area than machined samples ($27.26\mu\text{m}^2$) ($p=0.0001$).

For a smooth surface with an absolute flat surface topography the projected surface area for a $20 \times 20\mu\text{m}$ scan is assumed to be $400\mu\text{m}^2$ and is equated to a 100% projected surface area. Table 5-7 (see p98) shows the projected surface area of samples as a percentage increase in terms of the projected surface area of the $20 \times 20\mu\text{m}$ scans.

Table 5-7: Projected surface area of samples with their relative percent increase.

Material	Surface area (μm^2)	Percentage increase
cpTi machined control surface	416.18 \pm 4.09	4.04
cpTi machined control surface & RFGDT	416.34 \pm 5.77	4.08
Ti6Al4V machined control surface	415.00 \pm 3.18	3.75
Ti6Al4V machined control surface & RFGDT	425.02 \pm 6.49	6.25
cpTi cast control surface	531.92 \pm 24.25	32.75
cpTi cast control surface & RFGDT	559.14 \pm 60.88	39.78
Ti6Al4V cast control surface	508.26 \pm 55.34	27.06
Ti6Al4V cast control surface & RFGDT	535.26 \pm 65.83	33.81

Fig 5-24 shows the percentage increase of the projected surface area for the different samples.

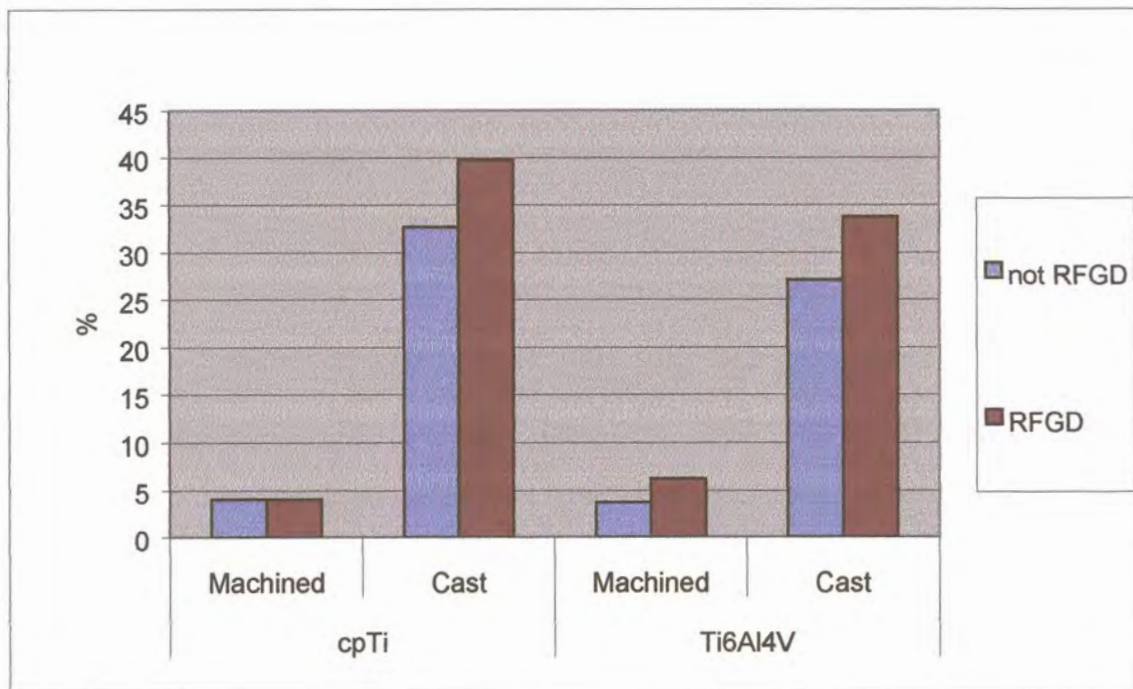


Fig 5-24: Percentage increase in Projected surface area of samples for 20 μm scans

The percentage increase of 33.4% in Projected surface area for surfaces of cast samples was significantly higher than the 4.5% increase in Projected surface area for machined samples ($p < 0.05$). RFGDT on average significantly increased the surface area of samples from 116.90% to 120.98% ($p = 0.03$). Material

used or treatment rendered did not significantly change the percent increase in surface area.

5.1.2.2 Line Analysis

The 20µm scan line analysis of for the different sample surfaces of the three predetermined lines drawn on the 2D images are shown in Figures 5-25 to 5-28 (see p99-101).

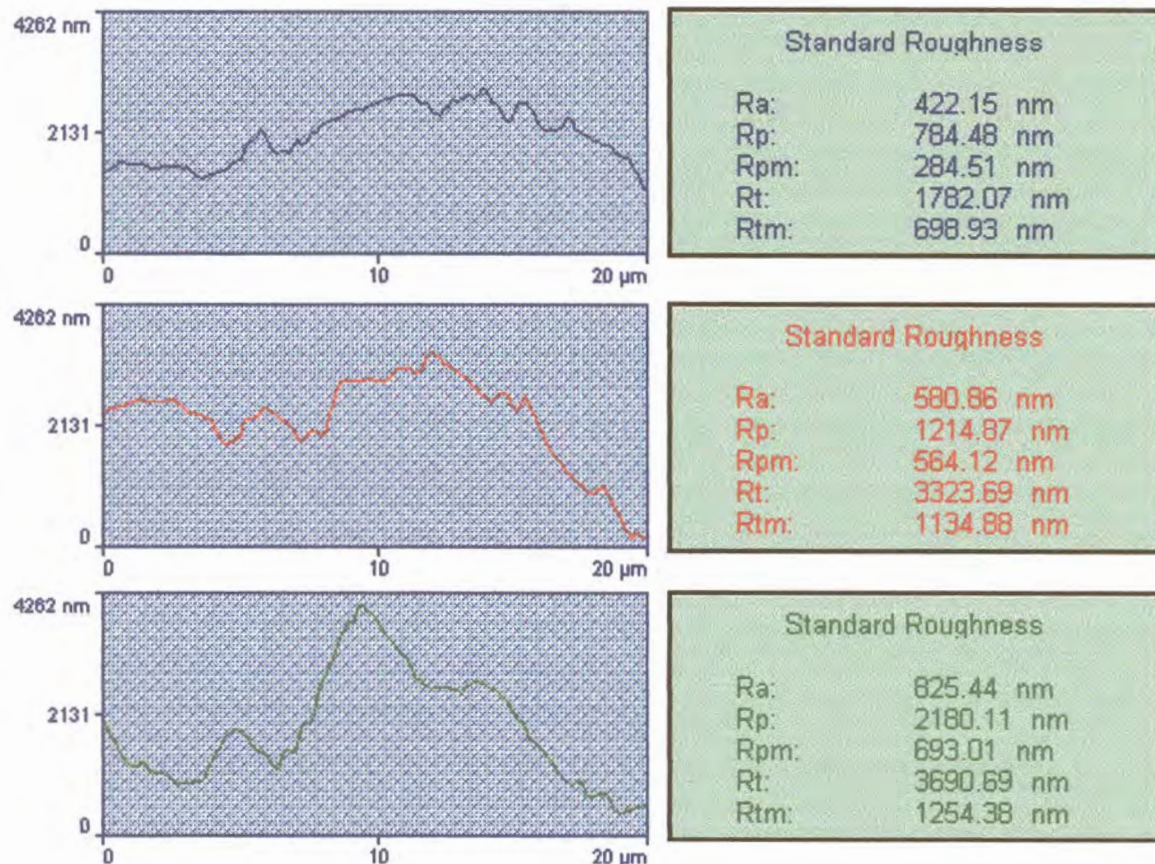


Fig 5-25: Line analysis of the 20µm scans of cpTi machined control sample surface

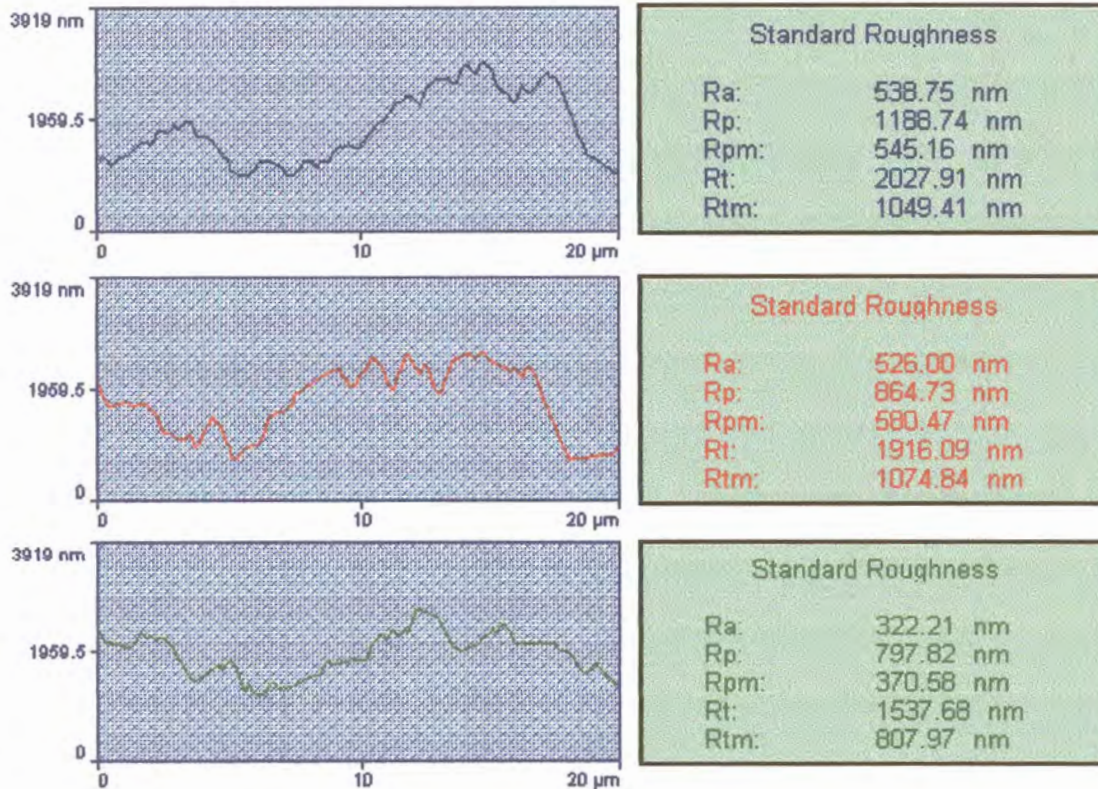


Fig 5-26: Line analysis of the 20µm scans of cpTi cast control sample surface

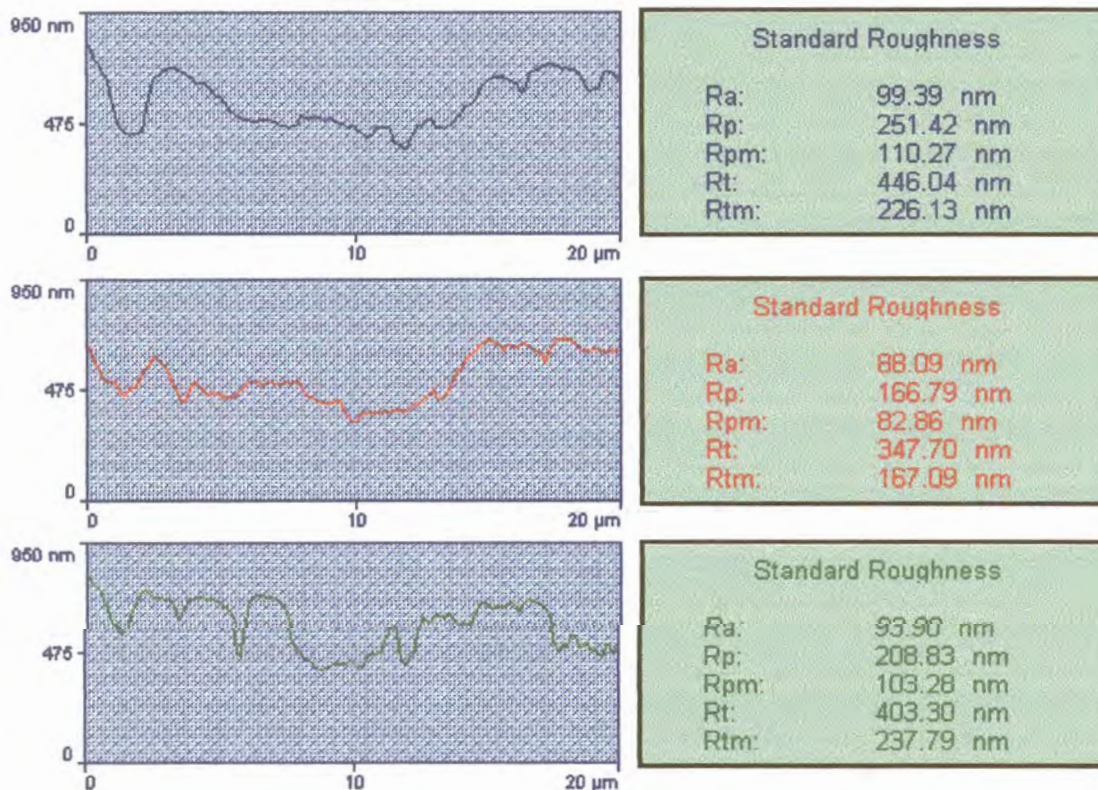


Fig 5-27: Line analysis of the 20µm scans of Ti6Al4V machined control sample surface

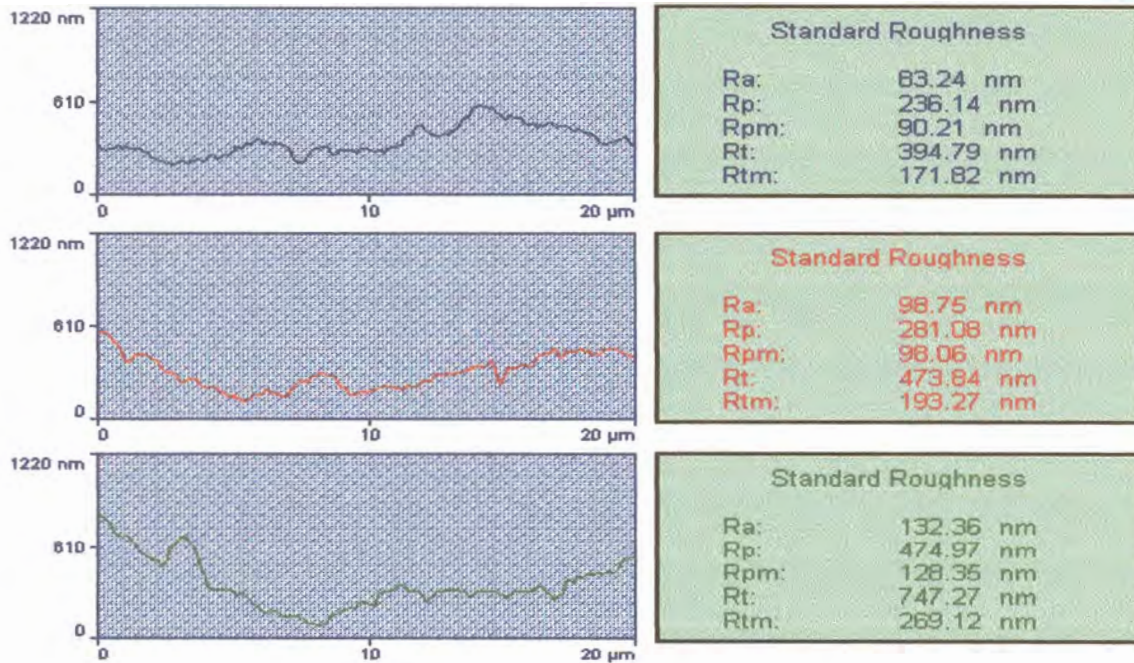


Fig 5-28: Line analysis of the 20µm scans of Ti6Al4V cast control sample surface

For each line drawn that traversed the whole 2D image the computer software produced processed values of Ra, Rtm, Rt, Rpm and Rp, the averages of which are shown in Table 5-8 for the 20µm scans (see Addendum D, p183-187).

Table 5-8: Averages of the line analysis done for the different sample surfaces for the 20µm scan.

Material	Ra	Rtm	Rt	Rpm	Rp
cpTi machined control surface	0.12	0.23	0.56	0.11	0.25
cpTi machined control surface & RFGDT	0.08	0.23	0.47	0.11	0.24
Ti6Al4V machined control surface	0.08	0.19	0.40	0.08	0.18
Ti6Al4V machined control surface & RFGDT	0.12	0.31	0.64	0.15	0.31
cpTi cast control surface	0.40	1.02	2.15	0.50	0.98
cpTi cast control surface & RFGDT	0.59	1.26	2.87	0.63	1.47
Ti6Al4V cast control surface	0.39	0.87	2.00	0.40	0.83
Ti6Al4V cast control surface & RFGDT	0.34	0.87	1.88	0.43	0.98

Similar predetermined lines were drawn for the 5µm scans and the line analyses for the different sample surfaces are shown in Figures 5-29 to 5-32 (see p102-103).

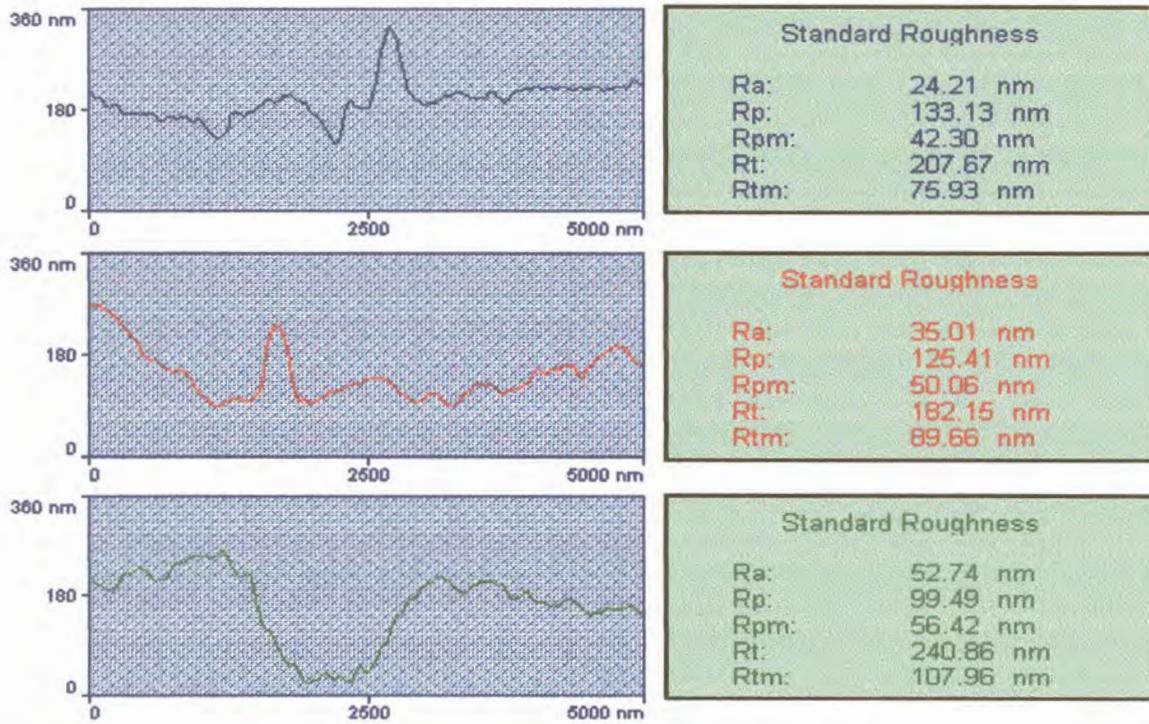


Fig 5-29: Line analysis of the 5µm scans of cpTi machined control sample surface

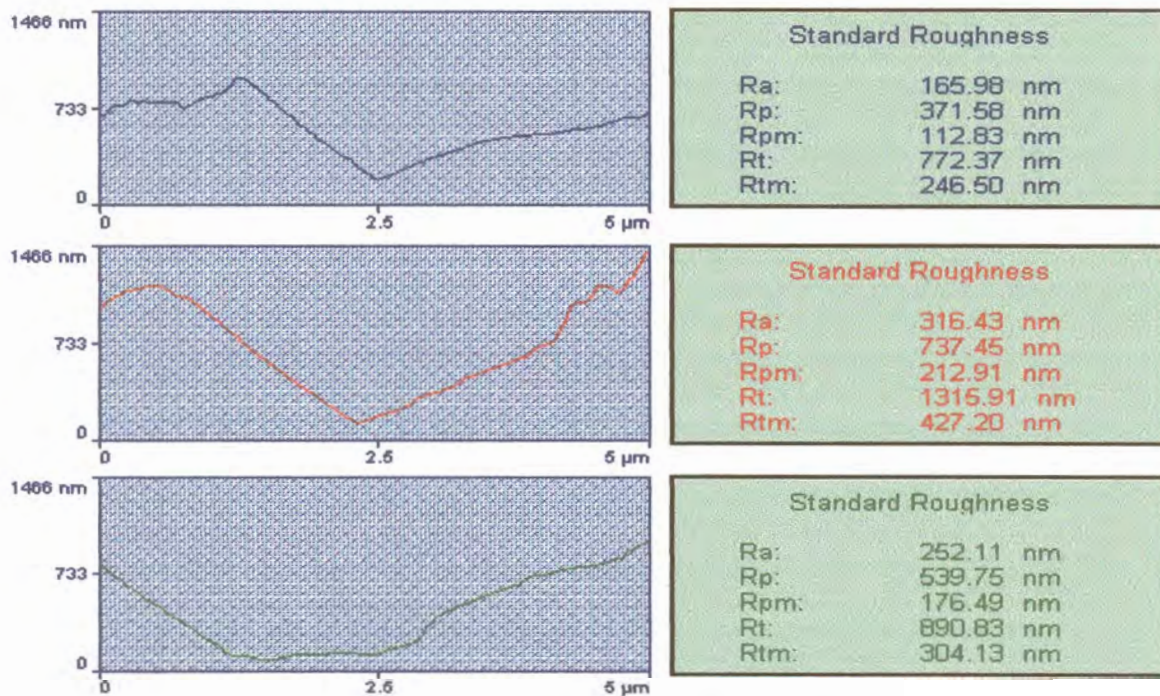


Fig 5-30: Line analysis of the 5µm scans of cpTi cast control sample surface

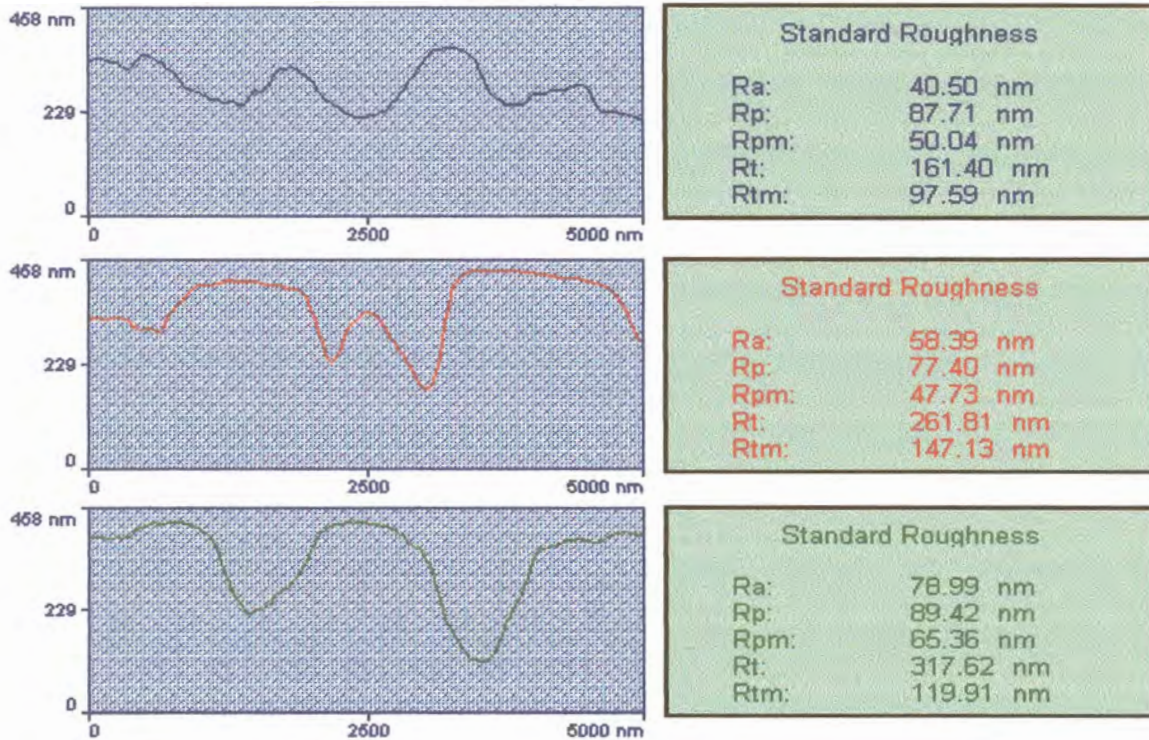


Fig 5-31: Line analysis of the 5 μ m scans of Ti6Al4V machined control sample surface

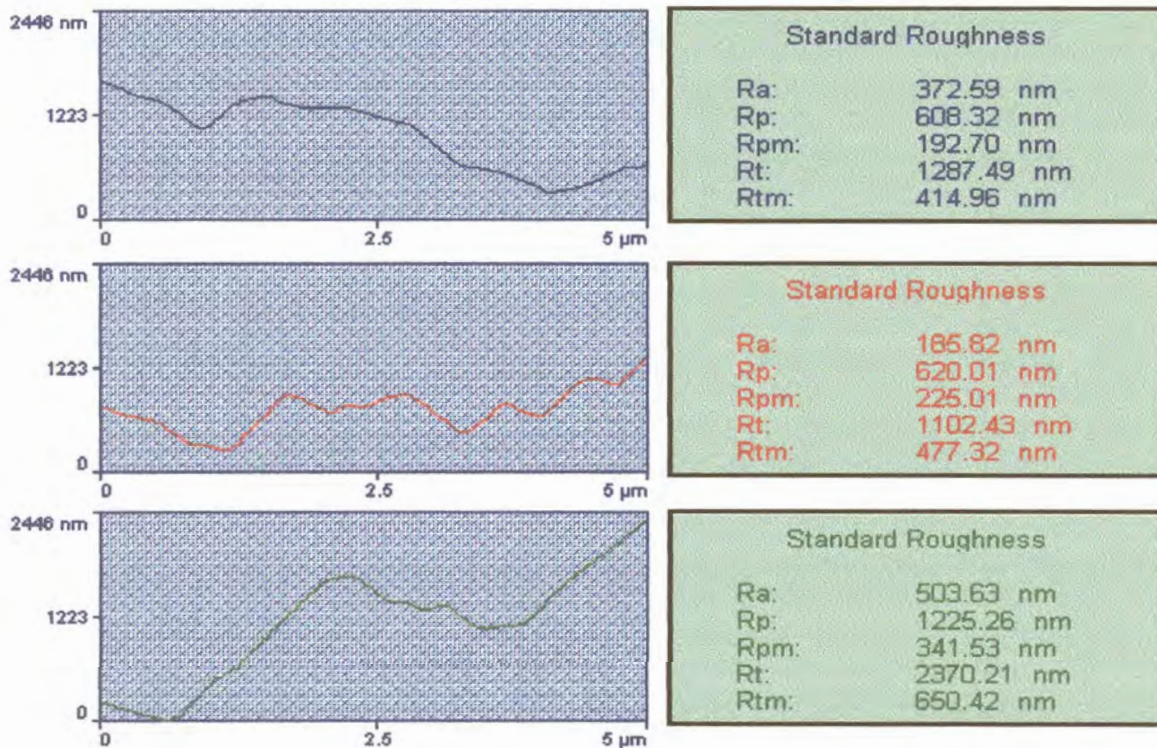


Fig 5-32: Line analysis of the 5 μ m scans of Ti6Al4V cast control sample surface

The means of the different Line analyses values for the 5 μ m scans are shown in Table 5-9 (see Addendum E, p188-192). Even at a smaller scan the surfaces of cast samples had higher values compared to machined samples.

Table 5-9: Averages of the line analysis done for the different sample surfaces for the 5 μ m scan.

Material	Ra	Rtm	Rt	Rpm	Rp
cpTi machined control surface	0.05	0.10	0.24	0.04	0.12
cpTi machined control surface & RFGDT	0.05	0.10	0.24	0.04	0.13
Ti6Al4V machined control surface	0.07	0.13	0.29	0.06	0.11
Ti6Al4V machined control surface & RFGDT	0.07	0.15	0.33	0.07	0.18
cpTi cast control surface	0.26	0.37	1.06	0.19	0.58
cpTi cast control surface & RFGDT	0.22	0.35	0.98	0.17	0.48
Ti6Al4V cast control surface	0.24	0.37	1.05	0.18	0.52
Ti6Al4V cast control surface & RFGDT	0.15	0.26	0.66	0.13	0.32

Ra

Ra is the average distance of the profile from the mean line (see 2.6.2.1, p33) Generally a smooth surface will have a very small value, as the distance from the mean is nearly absent. For both scans the Ra value was determined by the fabrication procedure and not by the material employed or treatment rendered. The mean Ra for the 20 μ m and 5 μ m scans of surfaces of cast samples was 0.31 μ m and 0.18 μ m and this value was significantly higher than that for surfaces of machined samples (0.10 μ m and 0.06 μ m).

Rt

The Rt value shows us the distance between the highest peak and lowest valley recorded (see 2.6.2.1, p33). For both the 20 μm and 5 μm scans there was a significantly higher peak for the surfaces of cast samples (1.66 μm and 0.77 μm) when compared with machined samples (0.52 μm and 0.28 μm). No significant differences were observed between the different materials used or the type of treatment rendered.

Rtm

Rtm is a measure of the peak to valley height (see 2.6.2.1, p34). The Rtm value of 0.76 μm for the surfaces of cast samples was significantly higher than machined samples (0.24 μm) for 20 μm scans ($p=0.0042$). The 5 μm scan had a similar significantly higher measure for the surfaces of cast samples (0.29 μm) compared to machined surfaces (0.12 μm). Rtm was determined solely by the fabrication process.

Rp

Rp is the measure of the single highest peak recorded on the image scan (see 2.6.2.1, p34) and for the 20 μm scan it was significantly higher for the surfaces of cast samples (0.77 μm) than the machined samples (0.24 μm). Interestingly for the 20 μm scans RFGDT significantly ($p=0.04$) increased the Rp value of the surfaces of cast samples to 0.62 μm and machined samples to 0.39 μm . For the 5 μm scan fabrication determined the Rp value which was significantly higher for the surfaces of cast samples (0.40 μm) compared to machined samples (0.13 μm).

Rpm

Rpm is the measure of the mean peak heights on an image scan (see 2.6.2.1, p34). The Rpm for the surfaces of cast samples was 0.37 μm (20 μm scan) and 0.14 μm (5 μm scans) and was

significantly higher than machined samples (0.11 μm and 0.05 μm).

Fabrication procedures adopted significantly influenced line analysis of sample surfaces for the 20 μm scans and a summary of the different values is shown in Fig 5-33.

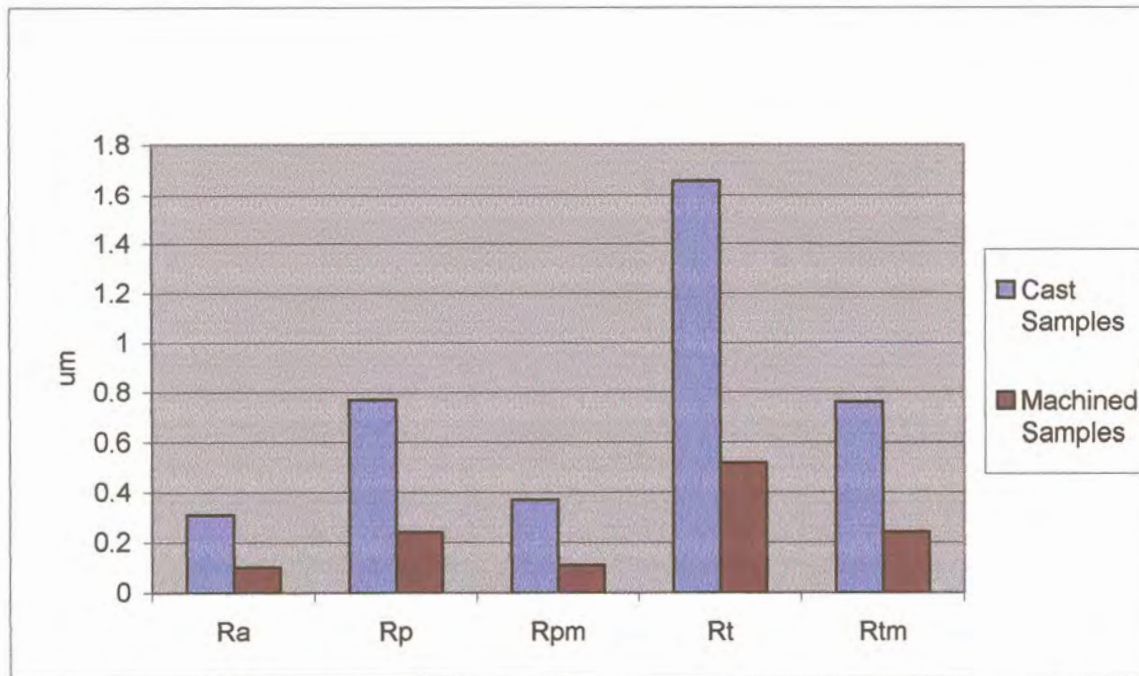


Fig 5-33: Different values of line analysis of sample surfaces as related to fabrication procedures for the 20 μm scan

5.1.3 Depth Profile

Depth profiles depict the oxide thickness (see 2.6.3, p35). It is the distance between the outside or exterior of the sample and the bulk material.

Fig 5-34 (see p107) shows a tracing of the depth profile for the Ti6Al4V cast control RFGDT sample. Depth profiles of other samples are shown in Addendum G (see p196-199). As the overlying oxide is sputtered away, the O1s and Ti2p peaks from the oxide decreases and the O1s and Ti2p peaks from the substrate increases. The Oxygen signal from the substrate originates from dissolved Oxygen in the Titanium or Titanium alloy matrix (Louw, 1997).

S140x40.pro: UP CSIR
 2001 Dec 21 Al mono 20.0 W 100.0 μ 45.0° 46.95 eV 1.2588e+004 max
 O1s/Area20: Sample HG (Binom3)

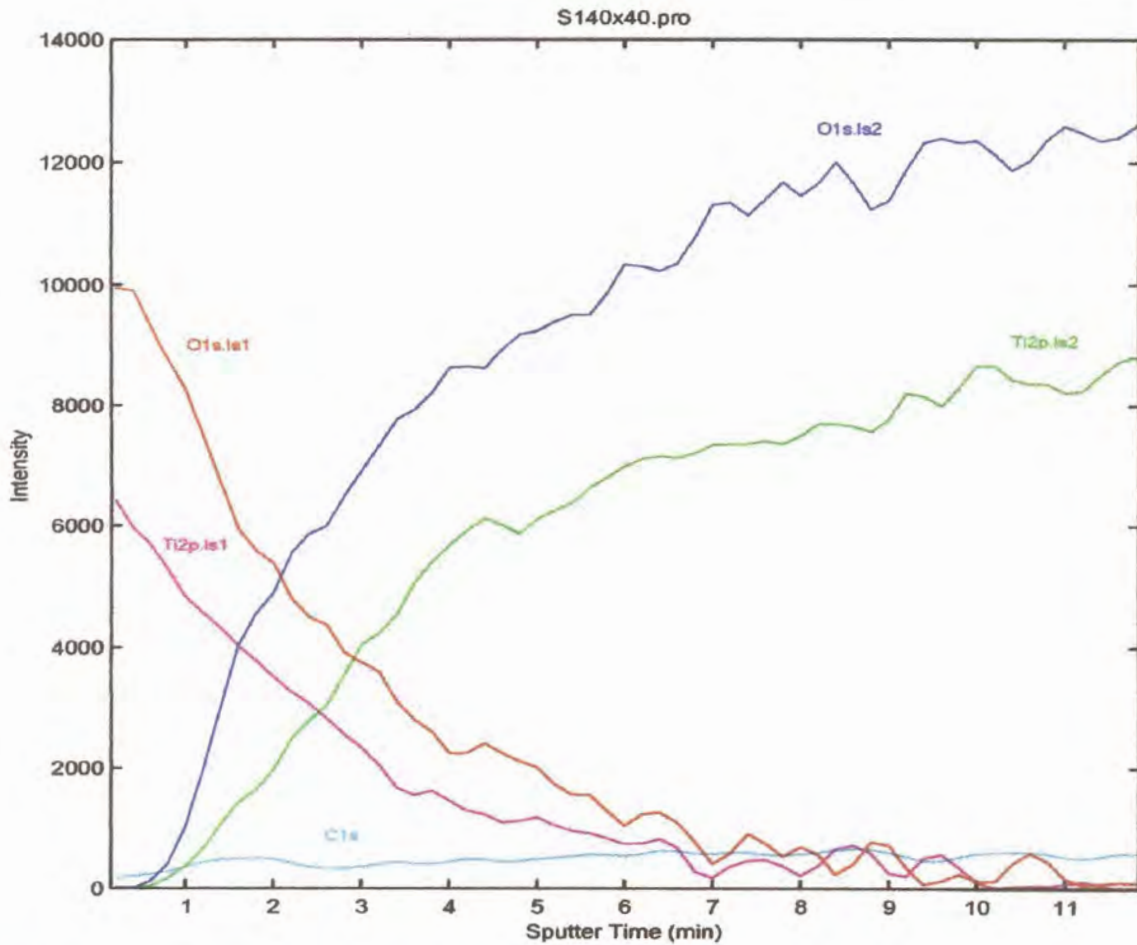


Fig 5-34: Tracing of the depth profile of Ti6Al4V cast control RFGDT sample

From the depth profile tracing the sputter time required for the oxygen peak to reach half its background concentration regardless of its initial intensity was recorded for each sample (see Table 5-10, p108). The oxide thickness was then calculated from the known sputter rate of $3.5\text{nm}\cdot\text{sec}^{-1}$ (see 4.4.3, p65).

Table 5-10: Sputter time and Oxide thickness of samples

Sample	sputter time (min)	Oxide thickness (nm)
cpTi machined control surface	0.8	2.8
cpTi machined control surface RFGDT	1.2	4.2
cpTi machined SI Enhanced	1.2	4.2
cpTi machined SI Enhanced RFGDT	2.2	7.7
cpTi machined ES Enhanced	1.6	5.6
cpTi machined ES Enhanced RFGDT	2.4	8.4
Ti6Al4V machined control surface	0.5	1.9
Ti6Al4V machined control surface RFGDT	0.8	2.8
Ti6Al4V machined SI Enhanced	1.8	6.3
Ti6Al4V machined SI Enhanced RFGDT	1.9	6.7
Ti6Al4V machined ES Enhanced	1.8	6.3
Ti6Al4V machined ES Enhanced RFGDT	2.0	7.0
cpTi cast control surface	1.8	6.3
cpTi cast control surface RFGDT	1.8	6.3
cpTi cast SI Enhanced	1.6	5.6
cpTi cast SI Enhanced RFGDT	2.4	8.4
cpTi cast ES Enhanced	1.5	5.3
cpTi cast ES Enhanced RFGDT	2.4	8.4
Ti6Al4V cast control surface	1.5	6.0
Ti6Al4V cast control surface RFGDT	2.1	7.4
Ti6Al4V cast SI Enhanced	1.2	4.2
Ti6Al4V cast SI Enhanced RFGDT	1.6	5.6
Ti6Al4V cast ES Enhanced	1.7	6.0
Ti6Al4V cast ES Enhanced RFGDT	2.4	8.4

Fig 5-35 (see p109) shows the oxide depth of the different samples analyzed before and after RFGDT. With the exception of the Ti6Al4V machined ES sample all other ES enhanced samples had similar oxide thicknesses of 8.4nm. cpTi cast SI sample also had a similar oxide thickness of 8.4nm.

The analysis showed that the method of fabrication employed had a significant effect on the oxide thickness of samples ($p=0.0062$) and it was higher for cast samples (6.47nm) than machined samples (5.32nm). Surface enhancement significantly increased the oxide thickness ($p=0.0006$). Control surfaces had a thinner oxide (4.70nm) compared to enhanced surfaces (SI=6.08nm and ES=6.91nm). On average the oxide thickness was significantly thicker on RFGDT samples (6.77nm) than untreated samples (5.03nm) ($p=0.0002$). There was an interaction between the method of fabrication and surface enhancement and machined control surfaces had significantly lower oxide thicknesses

(2.93nm) compared to other samples ($p=0.0011$). Material used for sample preparation had no apparent influence on the oxide thickness.

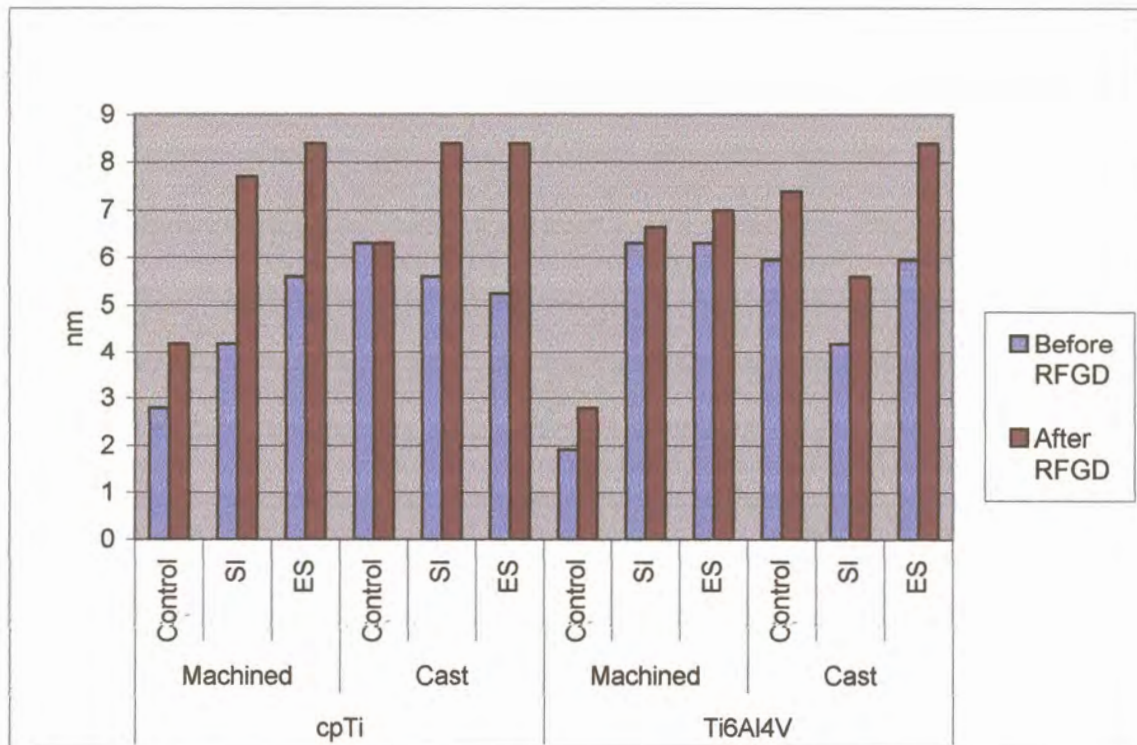


Fig 5-35: Oxide thickness of sample surfaces

5.2 Cell Culturing

5.2.1 Cell Attachment

5.2.1.1 Fibroblasts

At time zero, fibroblasts of $10.58 \times 10^4 \text{ cells.ml}^{-1}$ concentration were inoculated on cpTi and Ti6Al4V samples and Tissue Culture plastic, as a control. At time intervals of 1 day, 2 days, 14 days and 28 days the cells were counted and their % attachment efficiency and proliferation determined (see Addendum A, p178).

A comparison of the mean % attachment efficiency and proliferation of fibroblasts on samples showed that there was

no significant difference between day 1 (40.21%) and 2 (47.11%), but a significant difference was noted between day 1 and 2 and day 14 (79.94%). Day 14 was also significantly lower than day 28 (130.07%).

When fibroblasts were analyzed for their % attachment efficiency and proliferation on the different surfaces no significant differences were observed between samples regardless of surface characteristics. The machined Ti6Al4V control sample had the highest % attachment efficiency and proliferation for fibroblasts (88.743%) compared even to the control surface of tissue culture plastic (86.55%). The lowest % attachment efficiency and proliferation of fibroblasts was on cpTi cast control surface (58.52%) ($p > 0.05$).

Fig 5-36 shows a line graph for the % attachment efficiency and proliferation for fibroblasts on the different sample surfaces prepared from cpTi by machining. It is seen that fibroblasts behave similarly up to day 14, where the machined cpTi ES samples showed a higher % attachment efficiency and proliferation, even to the control. At 28 days the machined cpTi SI sample had the lowest % attachment efficiency and proliferation compared to the other machined cpTi control and ES samples ($p < 0.05$).

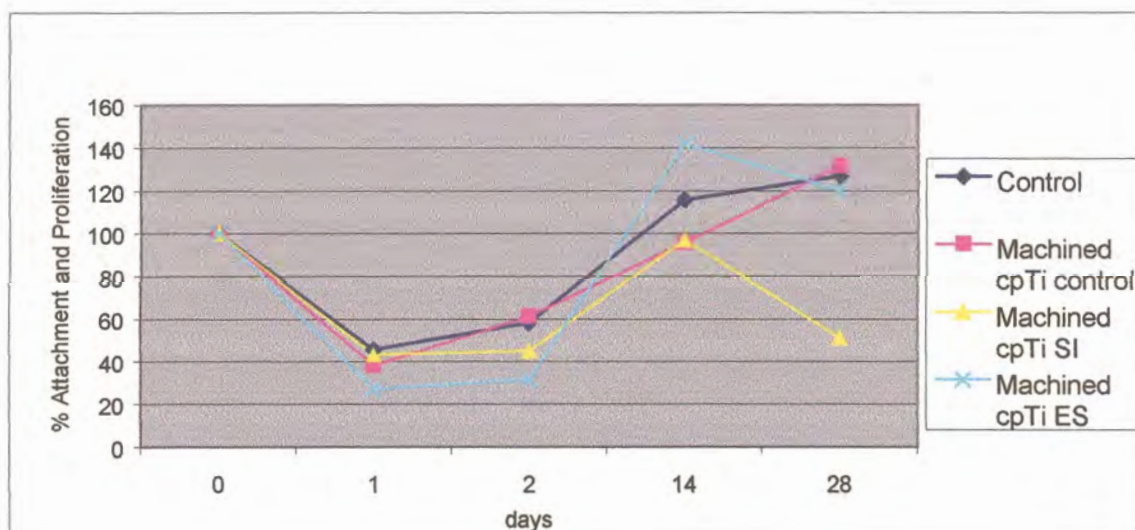


Fig 5-36: Percent attachment efficiency and proliferation of fibroblasts on machined cpTi samples

A line graph of the % attachment efficiency and proliferation of fibroblasts on machined Ti6Al4V samples (see Fig 5-37), shows that the samples had a similar trend, up to day 14, where samples were more or less similar in % attachment and proliferation. At day 28 the machined Ti6Al4V control sample maintained a much higher % attachment efficiency and proliferation that was similar to the control, and about double the % attachment and proliferation rate of the SI and ES samples ($p>0.05$).

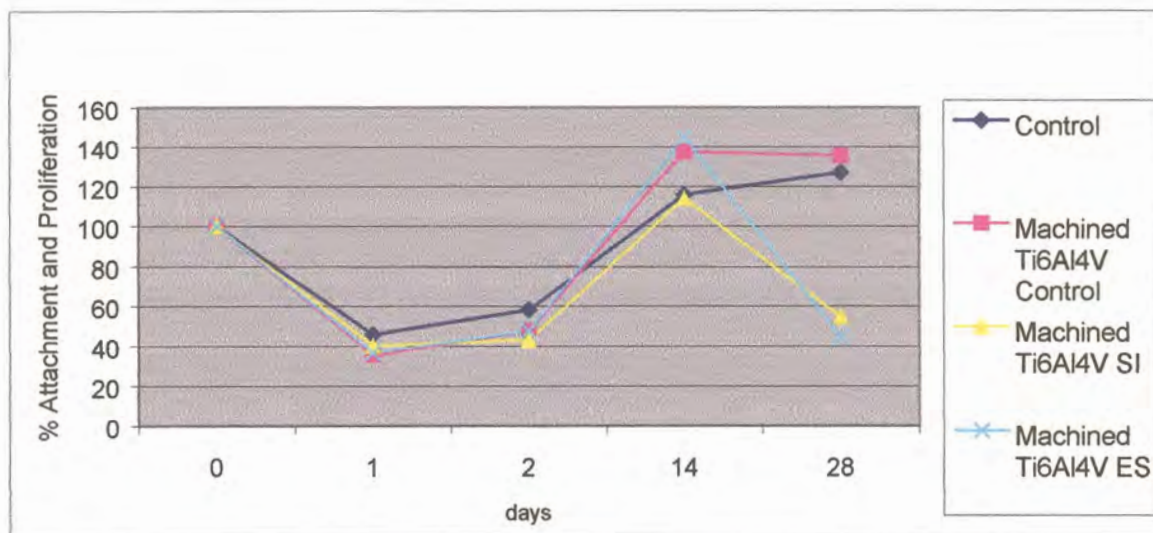


Fig 5-37: Percent attachment efficiency and proliferation of fibroblasts on machined Ti6Al4V samples

Fig 5-38 (see p 112) is a line graph for fibroblast cells exposed to surfaces of cast cpTi samples. No results were reported for the cast cpTi SI surface due to contamination. Cast cpTi control and ES samples had a much lower % attachment efficiency and proliferation than the control, with the cast cpTi control surface having the lowest % attachment efficiency and proliferation ($p>0.05$).

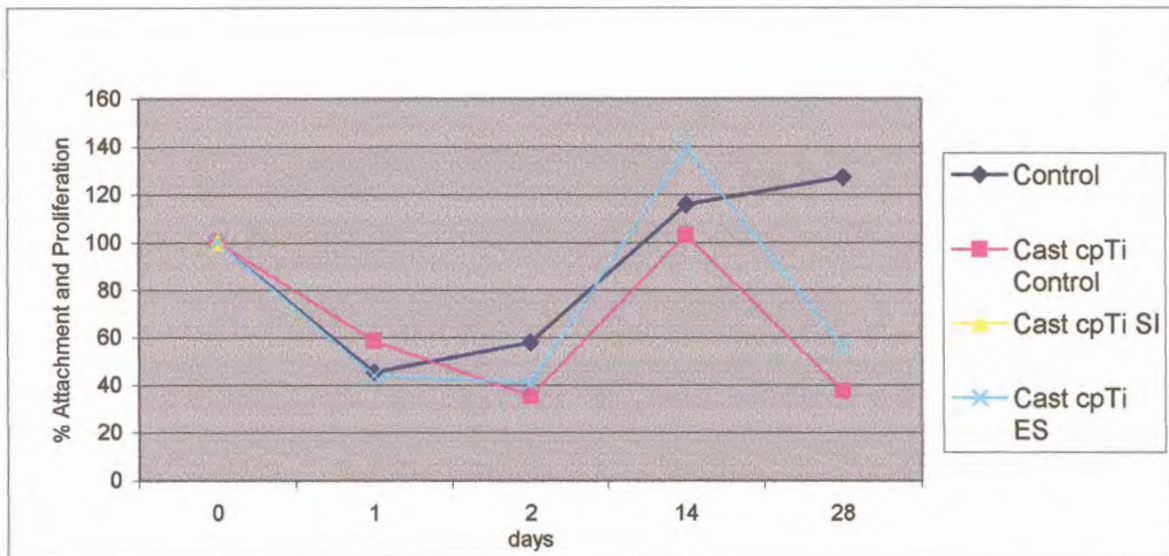


Fig 5-38: Percent attachment efficiency and proliferation of fibroblasts exposed to cast cpTi samples

When surfaces of cast Ti6Al4V samples were analyzed (see Fig 5-39), the % attachment efficiency and proliferation of fibroblasts was seen to be similar up to day 2. At day 14, a spike in % attachment efficiency and proliferation is seen for the cast Ti6Al4V control sample, which is much higher than the control ($p > 0.05$). The cast Ti6Al4V control, SI and ES samples at 28 days had a much lower % attachment efficiency and proliferation of fibroblasts than the control ($p > 0.05$).

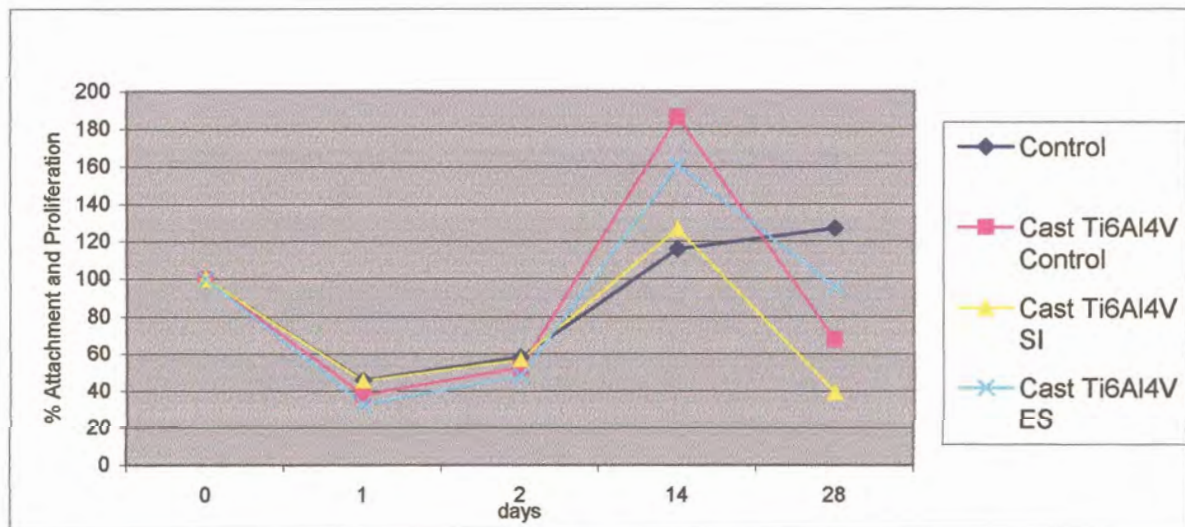


Fig 5-39: Percent attachment efficiency and proliferation of fibroblasts exposed to cast Ti6Al4V samples

Fig 5-40 shows the % attachment efficiency and proliferation of fibroblasts on the surfaces of all machined samples. The % attachment efficiency and proliferation of samples followed a similar trend up to 14 days with different maximum percentages. At 28 days the machined cpTi SI, machined Ti6Al4V SI and machined Ti6Al4V ES samples were observed to have a lower % attachment efficiency and proliferation compared to other samples. The machined cpTi and Ti6Al4V control and the machined cpTi ES samples had a % attachment efficiency and proliferation similar to the control that was much higher than the other samples ($p>0.05$).

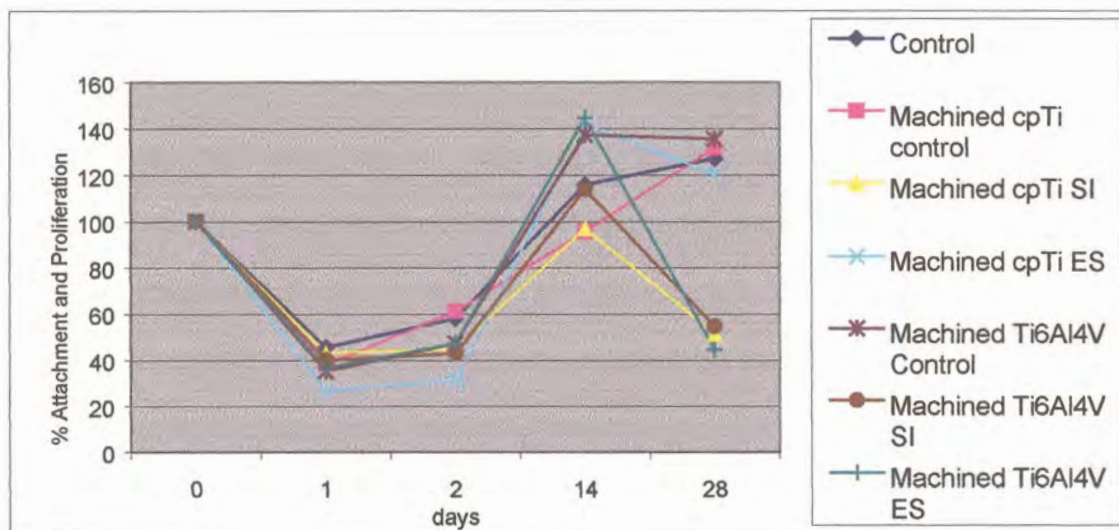


Fig 5-40: Percent attachment efficiency and proliferation of fibroblasts exposed to machined samples

Fig 5-41 (see p114) shows the line graph for fibroblasts on surfaces of cast samples. Cast samples behaved in a similar manner up to day 2. From day 2 to day 14, there was an increased in % attachment efficiency and proliferation of cells, but at different rates. The cast Ti6Al4V control recorded nearly double the % attachment efficiency and proliferation than the cast cpTi control sample ($p>0.05$). A decline was observed in comparison to the control at 28 days. Cast cpTi control and cast Ti6Al4V SI samples had the lowest % attachment efficiency and proliferation compared to other cast samples ($p>0.05$).

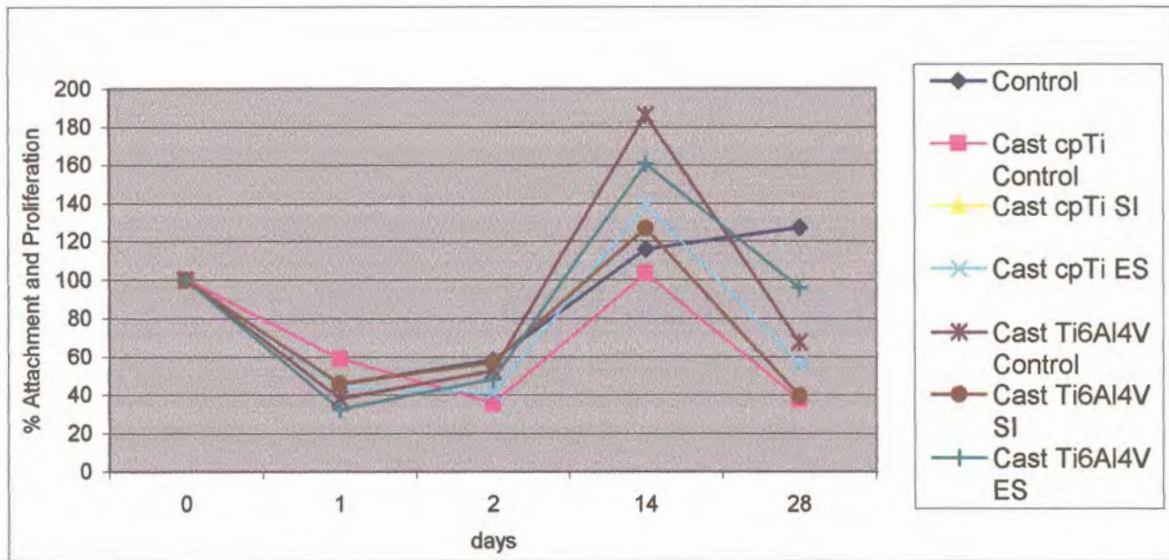


Fig 5-41: Percent attachment efficiency and proliferation of fibroblasts exposed to cast samples

Fig 5-42 shows the % attachment efficiency and proliferation of fibroblasts on fabricated control samples. Though the % attachment efficiency and proliferation was similar for day 1 and 2, at day 14 cast Ti6Al4V samples showed the highest % attachment efficiency and proliferation in comparison to the other samples and the control ($p > 0.05$). At day 28 the % attachment efficiency and proliferation for the machined control samples was higher than the cast control samples ($p > 0.05$).

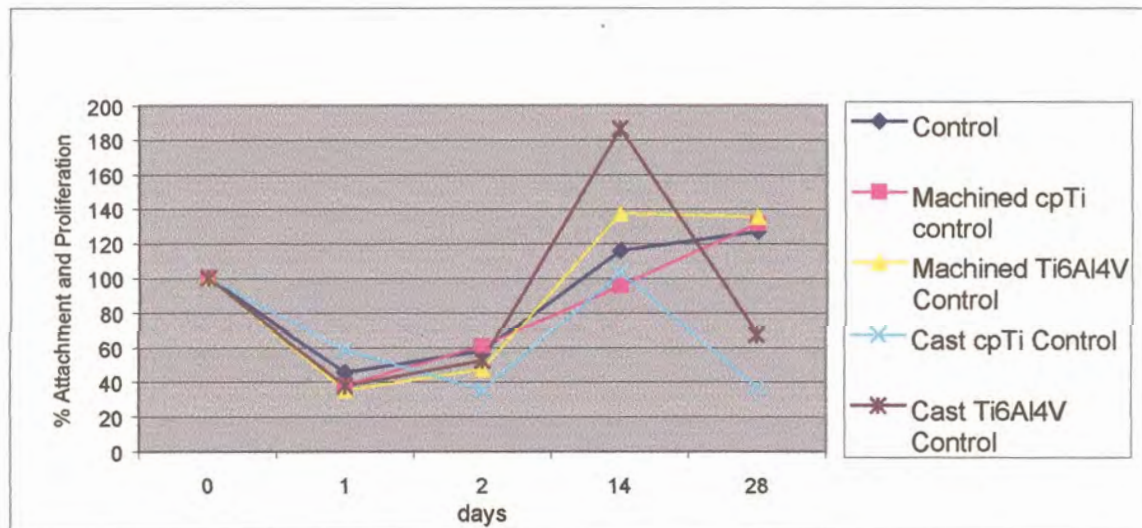


Fig 5-42: Percent attachment efficiency and proliferation of fibroblasts exposed to different control samples

Fig 5-43 shows the % attachment efficiency and proliferation of fibroblasts on surfaces of SI enhanced samples. Regardless of the material or fabrication procedure, the SI enhanced samples showed a similar trend, but at 28 days they had a much lower % attachment efficiency and proliferation compared to the control ($p>0.05$).

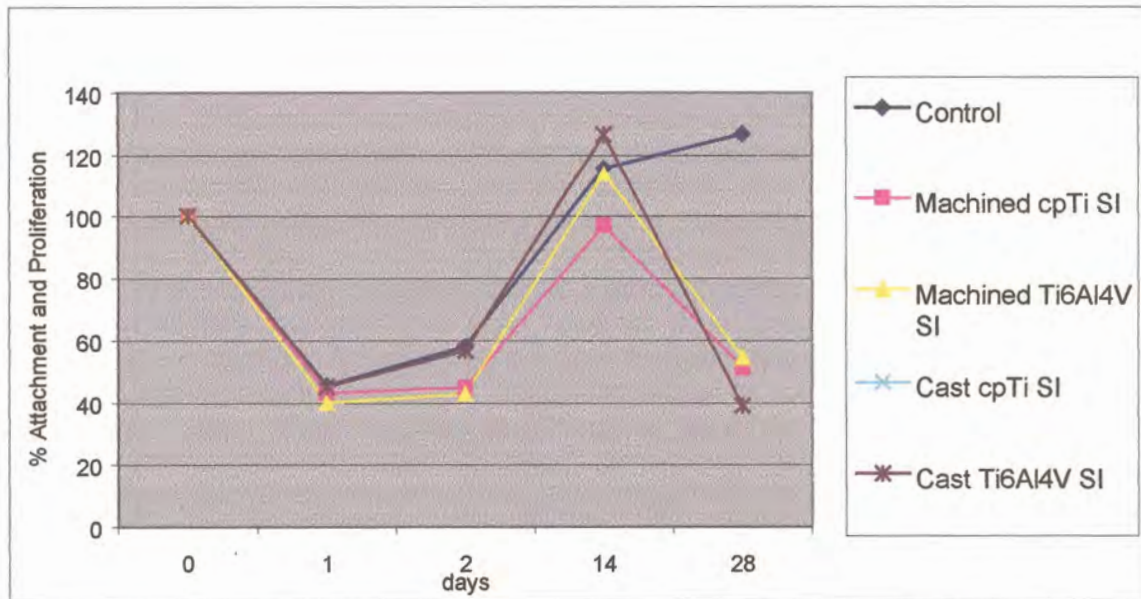


Fig 5-43: Percent attachment efficiency and proliferation of fibroblasts exposed to SI enhanced samples

The % attachment efficiency and proliferation of fibroblasts on surfaces of ES samples is shown in Fig 5-44 (see p116). The samples had a similar trend of % attachment efficiency and proliferation up to day 2. At day 14 all samples had a higher % attachment efficiency and proliferation than the control ($p>0.05$). The cast Ti6Al4V ES had a higher % attachment efficiency and proliferation than the control ($p>0.05$). The machined cpTi ES sample was closer in % attachment efficiency and proliferation to the control than the other samples at 28 days ($p>0.05$).

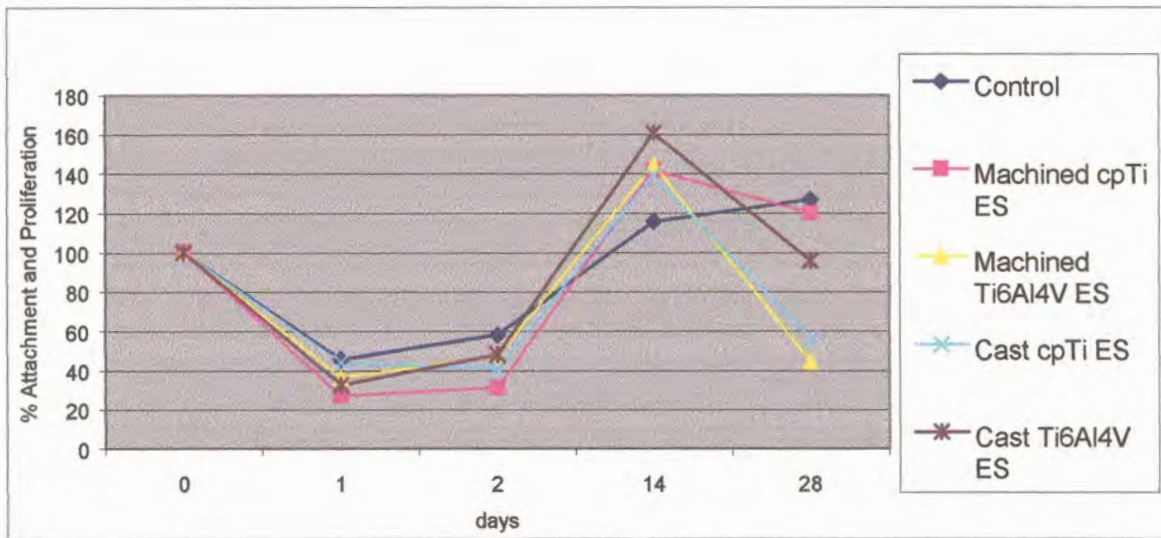


Fig 5-44: Percent attachment efficiency and proliferation of fibroblasts exposed to ES samples

5.2.1.2 Osteoblast-like Cells

At time zero osteoblasts-like cells of $11.0 \times 10^4 \text{ cells.ml}^{-1}$ concentration were inoculated on cpTi and Ti6Al4V samples and Tissue Culture plastic, as a control. At time intervals of 2 days, 14 days and 28 days the cells were counted and their % attachment efficiency and proliferation determined. Counts of day 1 were lost due to infection (see Addendum B, p179).

A comparison of mean % attachment efficiency and proliferation showed that day 14 (163.75%) was significantly higher than day 2 and day 28 ($p=0.0004$). Day 2 (98.05%) and day 28 (79.00%) showed no differences ($p>0.05$).

When surfaces were analyzed for their % attachment efficiency and proliferation for osteoblasts-like cells, no significant differences were observed between the different samples regardless of surface characteristics, but the % attachment efficiency and proliferation on the surface of cast cpTi control sample (77.37%) was about half that on machined Ti6Al4V SI sample (145.09%) ($p>0.05$). The osteoblasts-like cells on different samples were observed to have a % attachment efficiency and proliferation that was either higher or lower than the control (109.58%) ($p>0.05$).

Fig 5-45 shows the % attachment efficiency and proliferation of osteoblasts-like cells on the surfaces of machined cpTi samples. The machined cpTi SI and ES samples maintained more or less a steady growth from day 2 to day 14. The machined cpTi control sample had a much higher % attachment efficiency and proliferation than the other machined cpTi samples but lower than the control surface ($p > 0.05$). The % attachment efficiency and proliferation of osteoblasts-like cells on machined cpTi SI sample was stable to day 28 unlike other samples that showed a decline at day 28 ($p > 0.05$). At day 28 samples were still having a higher % attachment efficiency and proliferation than the control ($p > 0.05$).

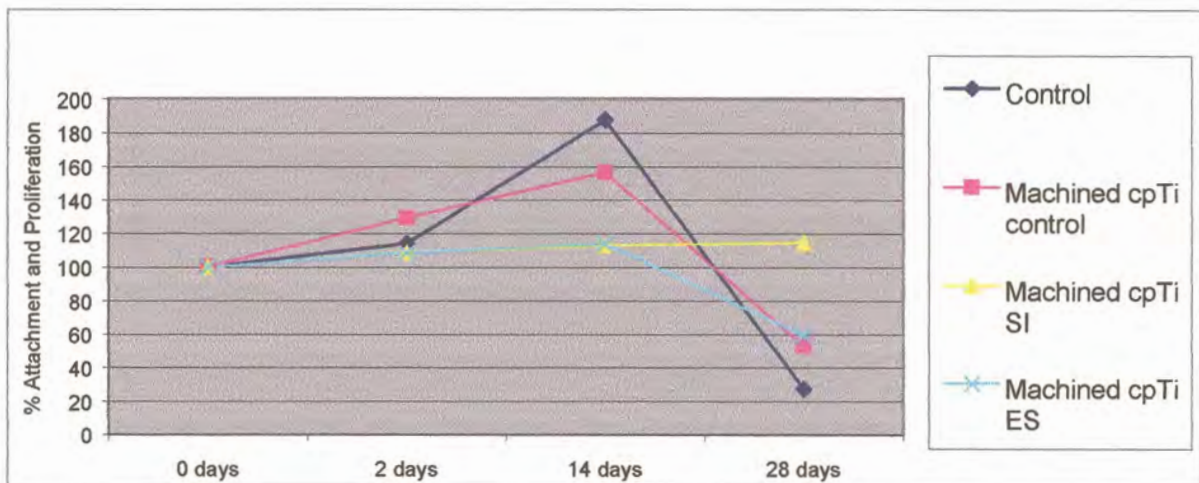


Fig 5-45: Percent attachment efficiency and proliferation of osteoblasts-like cells exposed to machined cpTi samples

Fig 5-46 (see p118) shows the % attachment efficiency and proliferation of osteoblasts-like cells on surfaces of machined Ti6Al4V samples. The % attachment efficiency and proliferation varied between samples at day 2. At day 14, there was an increase in % attachment efficiency and proliferation for all samples with the machined Ti6Al4V SI sample having a similar count as the control ($p > 0.05$). At day 28 the machined Ti6Al4V SI sample was about 10 fold higher in % attachment efficiency and proliferation than the other

samples that showed a decline in % attachment efficiency and proliferation to below 50% ($p>0.05$).

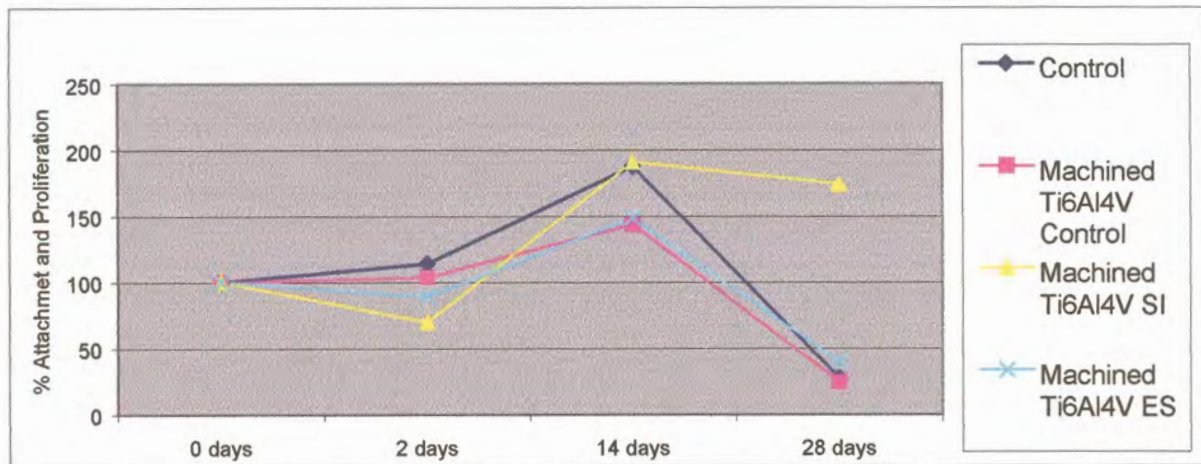


Fig 5-46: Percent attachment efficiency and proliferation of osteoblasts-like cells exposed to machined Ti6Al4V samples

The % attachment efficiency and proliferation of osteoblasts-like cells on surfaces of cast cpTi samples is shown in Fig 5-47. Although samples behaved more or less the same at day 2, at day 14, other samples and the control had a higher % attachment efficiency and proliferation compared to cast cpTi control sample which was more or less similar to day 2 ($p>0.05$). All samples showed a decline in % attachment efficiency and proliferation at day 28 ($p>0.05$).

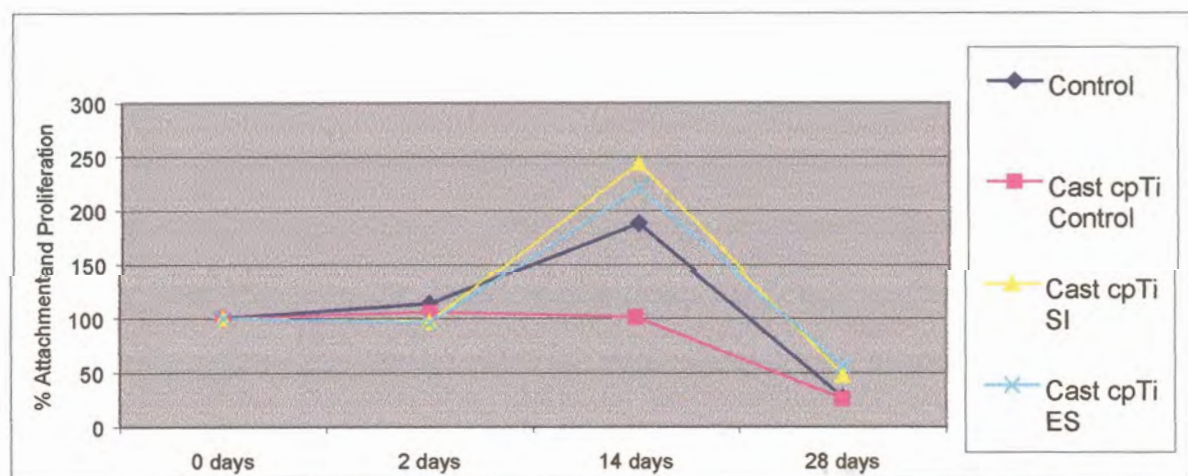


Fig 5-47: Percent attachment efficiency and proliferation of osteoblasts-like cells exposed to cast cpTi samples

Fig 5-48 shows the % attachment efficiency and proliferation of osteoblasts-like cells on surfaces of cast Ti6Al4V samples. The cast Ti6Al4V control sample showed an increase in % attachment efficiency and proliferation over time. The cast Ti6Al4V SI declined similar to the control at day 28. The cast Ti6Al4V ES sample maintained a % attachment efficiency and proliferation of over 150% at day 28 that was much higher than the control and cast Ti6Al4V SI samples ($p>0.05$).

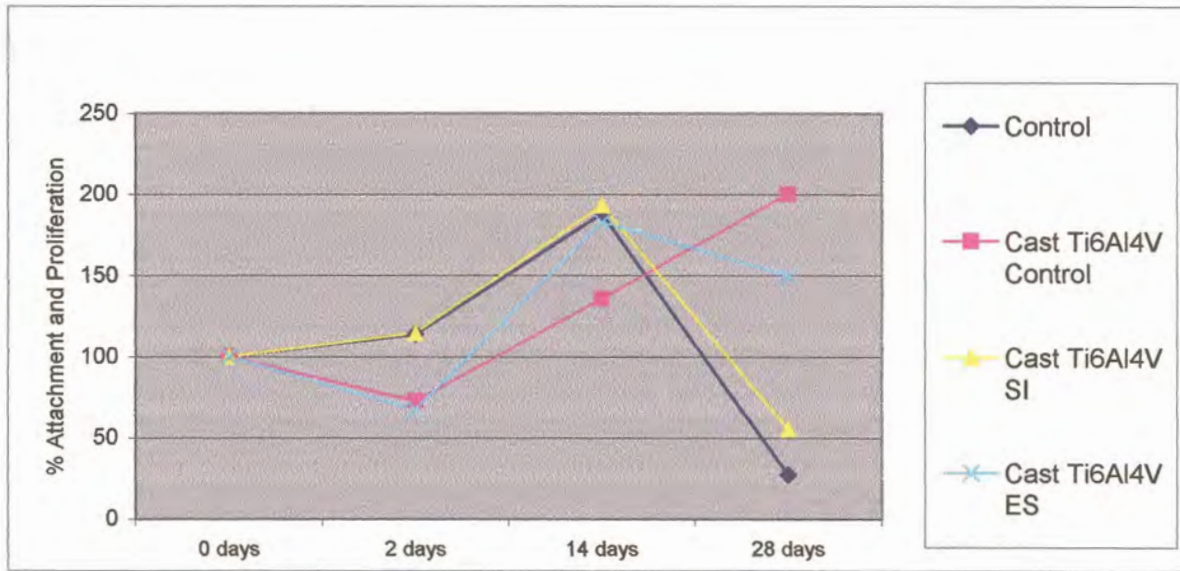


Fig 5-48: Percent attachment efficiency and proliferation of osteoblasts-like cells exposed to cast Ti6Al4V samples

Fig 5-49 (see p120) shows the % attachment efficiency and proliferation of osteoblasts-like cells on surfaces of machined samples. The machined Ti6Al4V SI sample had the lowest % attachment efficiency and proliferation at day 2 compared to other samples. At day 14 it had increased to the same % as the control and at day 28 it still had the highest % attachment efficiency and proliferation of over 150% ($p>0.05$). The machined cpTi SI sample maintained a steady % attachment efficiency and proliferation over time. All other samples including the control dropped in % attachment efficiency and proliferation at 28 days ($p>0.05$).

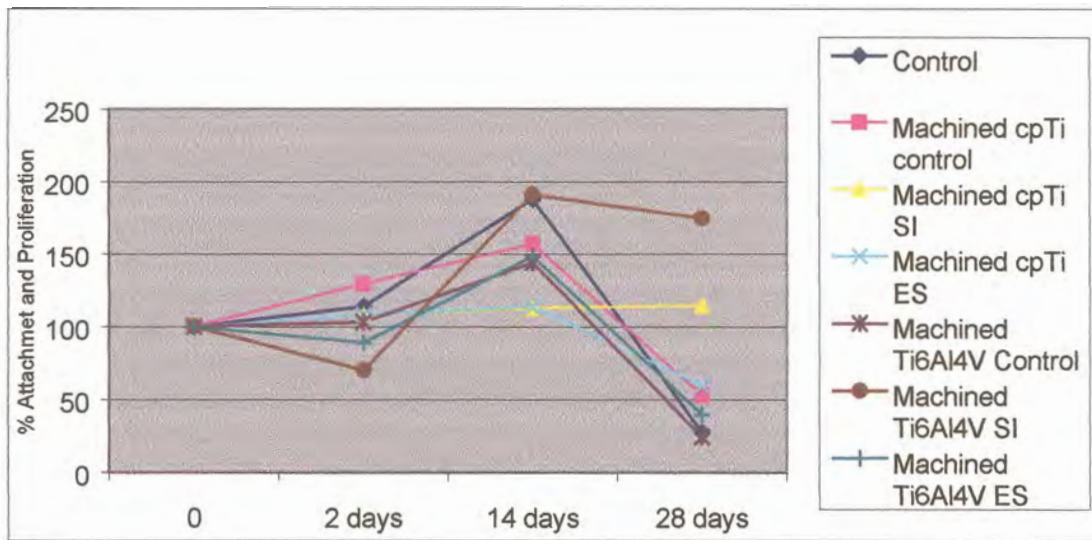


Fig 5-49: Percent attachment efficiency and proliferation of osteoblasts-like cells exposed to machined samples

Fig 5-50 (see p121) shows the % attachment efficiency and proliferation of osteoblasts-like cells on surfaces of cast samples. Cast cpTi control sample maintained a constant % attachment efficiency and proliferation to day 14 after which it declined to have the lowest % attachment efficiency and proliferation at day 28 ($p > 0.05$). At day 14, the cast cpTi SI surface had the highest % attachment efficiency and proliferation compared to other samples and showed a decline in % attachment efficiency and proliferation at 28 days ($p > 0.05$). At day 28, the cast Ti6Al4V control sample had the highest proliferation rate followed by the cast cpTi ES surface though both showed an initial decrease in % attachment efficiency and proliferation at day 2 ($p > 0.05$).

Fig 5-51 (see p121) shows the % attachment efficiency and proliferation for osteoblasts-like cells on control surfaces of samples. The cast Ti6Al4V control had an initial decline at day 2, followed by a steady increase to day 14 and day 28. At day 28, it had the highest % attachment efficiency and proliferation of 200% compared to other surfaces ($p > 0.05$). All other samples had a low % attachment efficiency and proliferation at day 28 ($p > 0.05$).

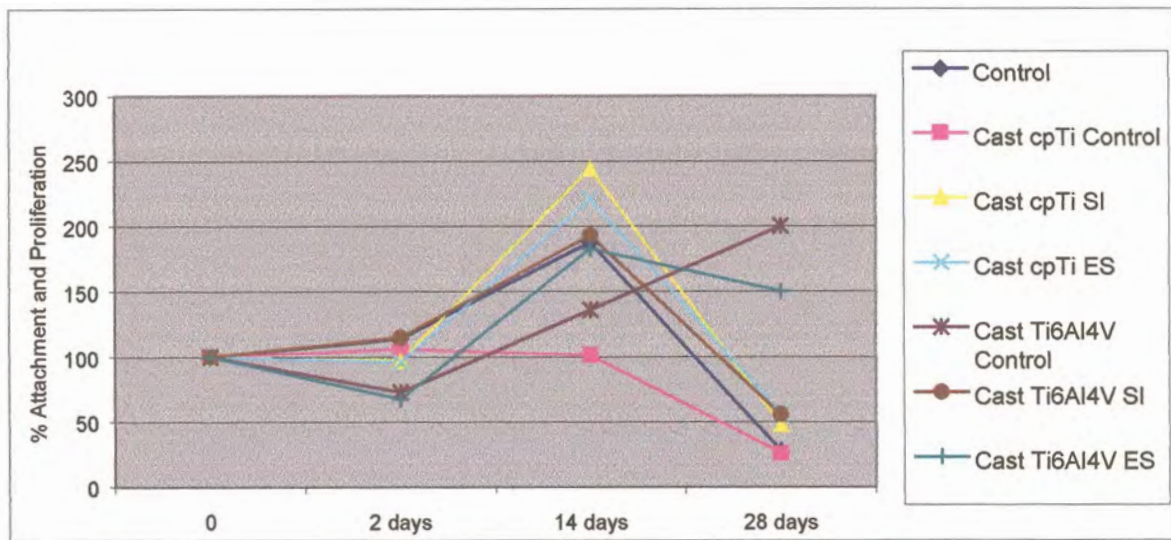


Fig 5-50: Percent attachment efficiency and proliferation of osteoblasts-like cells exposed to cast samples

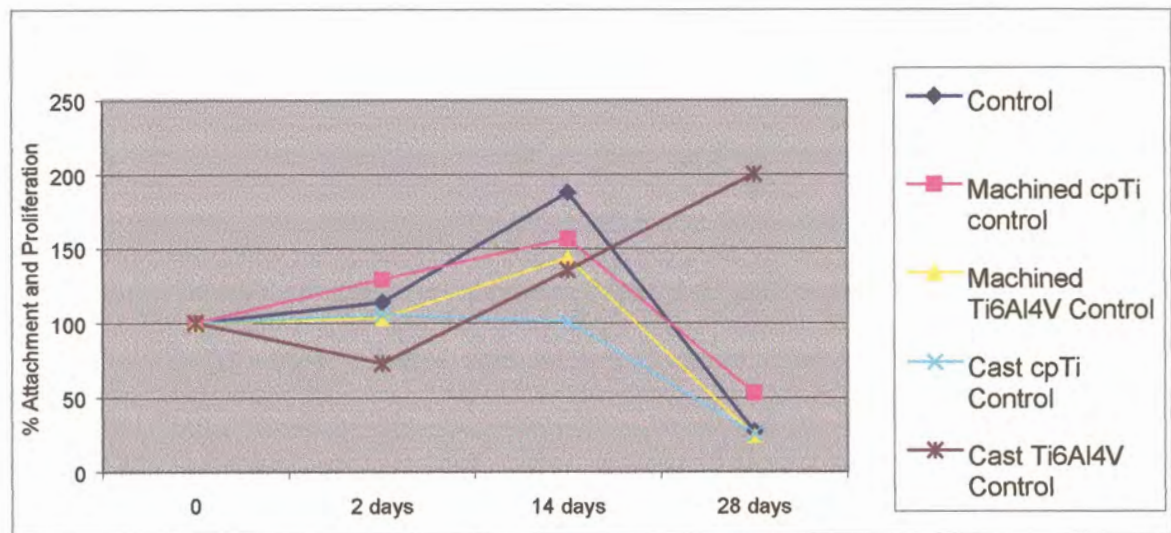


Fig 5-51: Percent attachment efficiency and proliferation of osteoblasts-like cells exposed to control surfaces of samples

Fig 5-52 (see p122) shows the % attachment efficiency and proliferation of osteoblasts-like cells on surfaces of SI samples. A steady % attachment efficiency and proliferation was maintained over time on machined cpTi SI samples. The machined Ti6Al4V SI sample had an initial decrease in percent attachment efficiency and proliferation at day 2 but the highest at day 28 ($p > 0.05$). At day 14, cast cpTi SI samples had the highest % attachment efficiency of over 200% but decreased to about 50% by day 28 ($p > 0.05$).

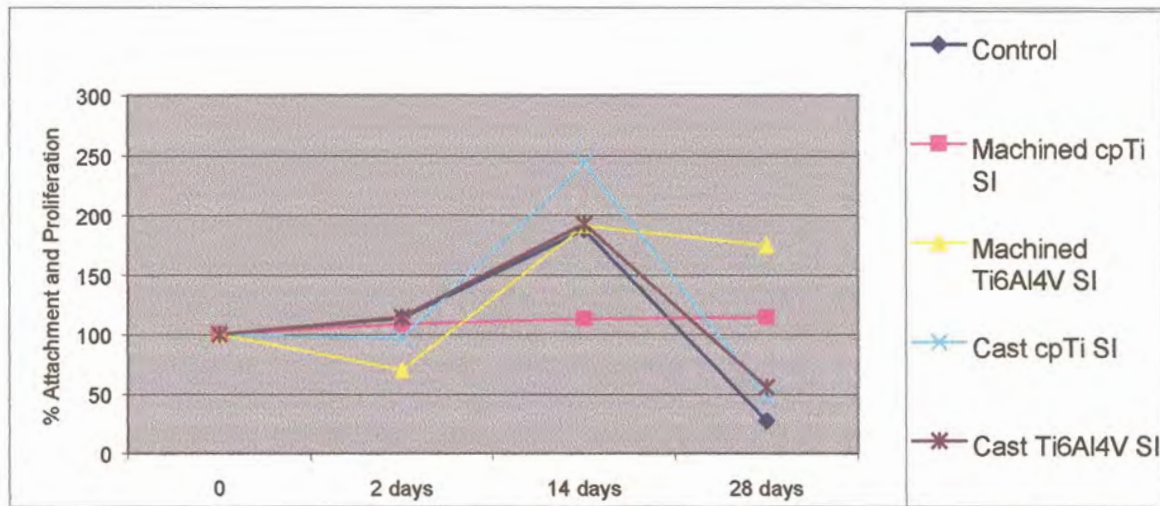


Fig 5-52: Percent attachment efficiency and proliferation of osteoblasts-like cells exposed to SI samples

Fig 5-53 shows the % attachment efficiency and proliferation of osteoblasts-like cells on surfaces of ES samples. The cast Ti6Al4V ES sample had the highest % attachment efficiency and proliferation at 28 days compared to other samples, but initially showed a decline at day 2. The cast cpTi ES sample had the highest % attachment efficiency and proliferation of over 200% at day 14 but declined to about 50% at day 28. Results show that up to day 14 machined cpTi ES samples maintained a constant % attachment efficiency and proliferation after which a decline was observed at day 28.

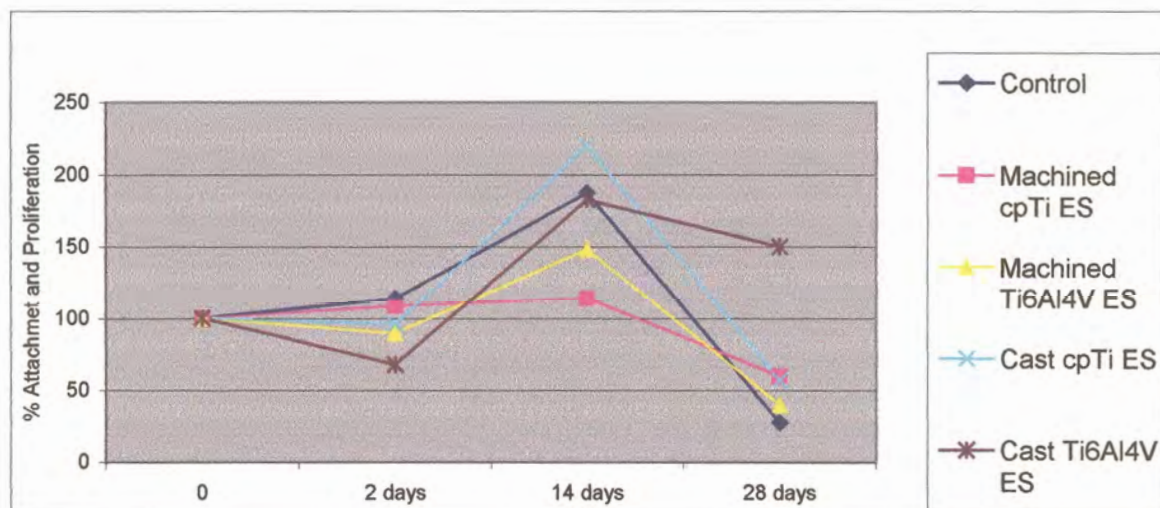


Fig 5-53: Percent attachment efficiency and proliferation of osteoblasts-like cells exposed to ES samples

5.2.2 Scanning Electron Microscope Analysis

5.2.2.1 Fibroblasts

Two days

Following seeding, the fibroblasts were seen to attach and spread, displaying an extremely flat configuration, in an apparent attempt to colonize the entire substrate surface (see Fig 5-54 and 5-55, p124). The cells were seen to be in close contact with the surface of the sample discs and though a network of cells is seen over the surface, there are still areas where cells have not spread or attached. The neighboring cells maintained contact with one another in a haphazard manner through multiple extensions, varying from extremely short to relative long extensions. The machined Ti6Al4V control sample was the only sample that had a monolayer of cells on its surface after 2 days and it appeared more intense than the control sample (see Fig 5-55, p124). With the proliferation and spreading of cells it was difficult to identify individual cells within the continuous sheet.

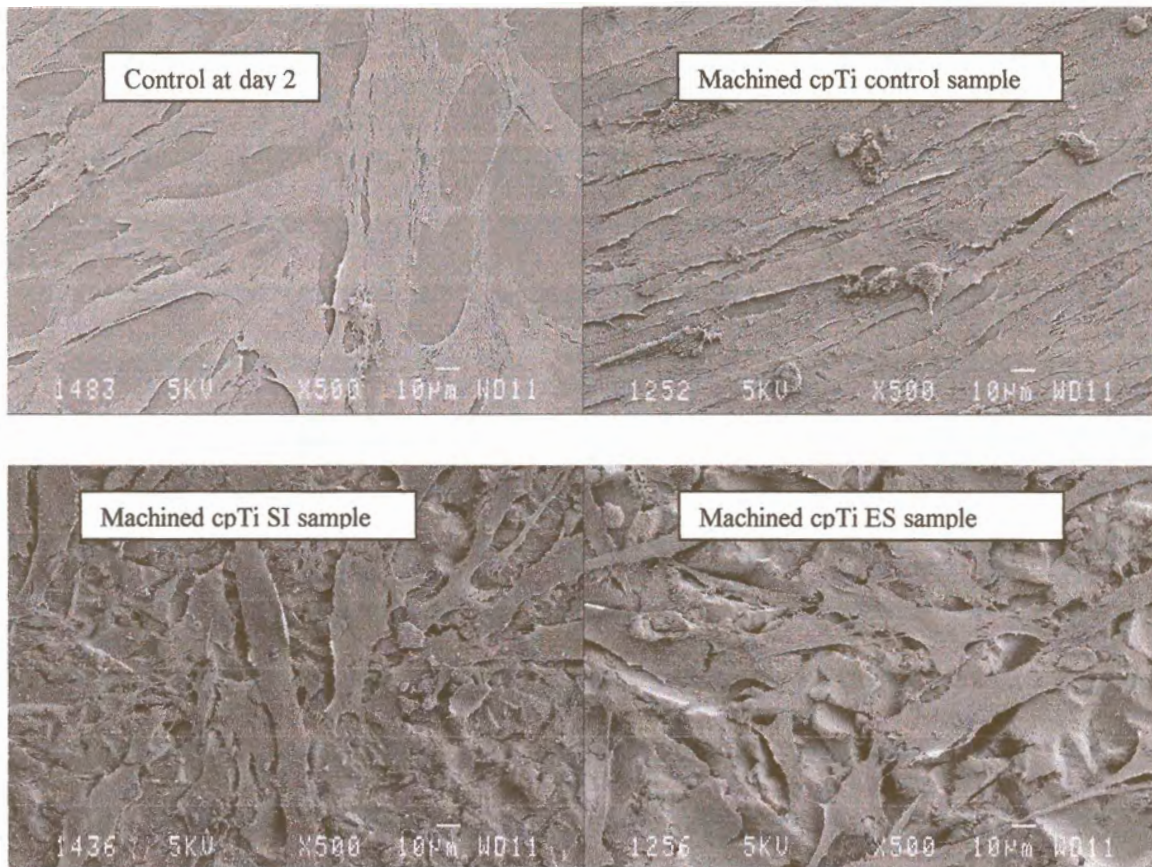


Fig 5-54: Growth of fibroblasts on surfaces of machined cpTi samples after 2 days incubation

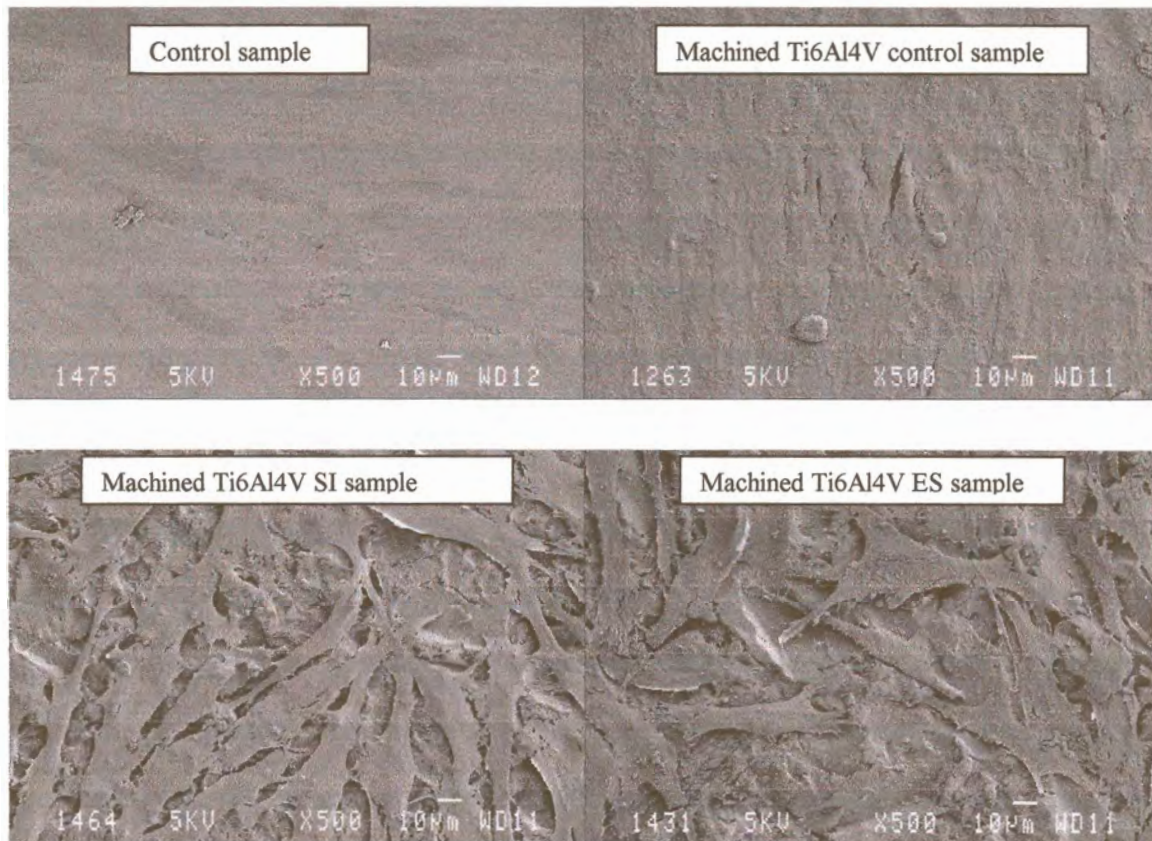


Fig 5-55: Growth of fibroblasts on surfaces of machined Ti6Al4V samples after 2 days incubation

On machined control surfaces fibroblasts were observed to have spread at a much faster rate and appeared to follow the topography created by the machining grooves (see Fig 5-56).

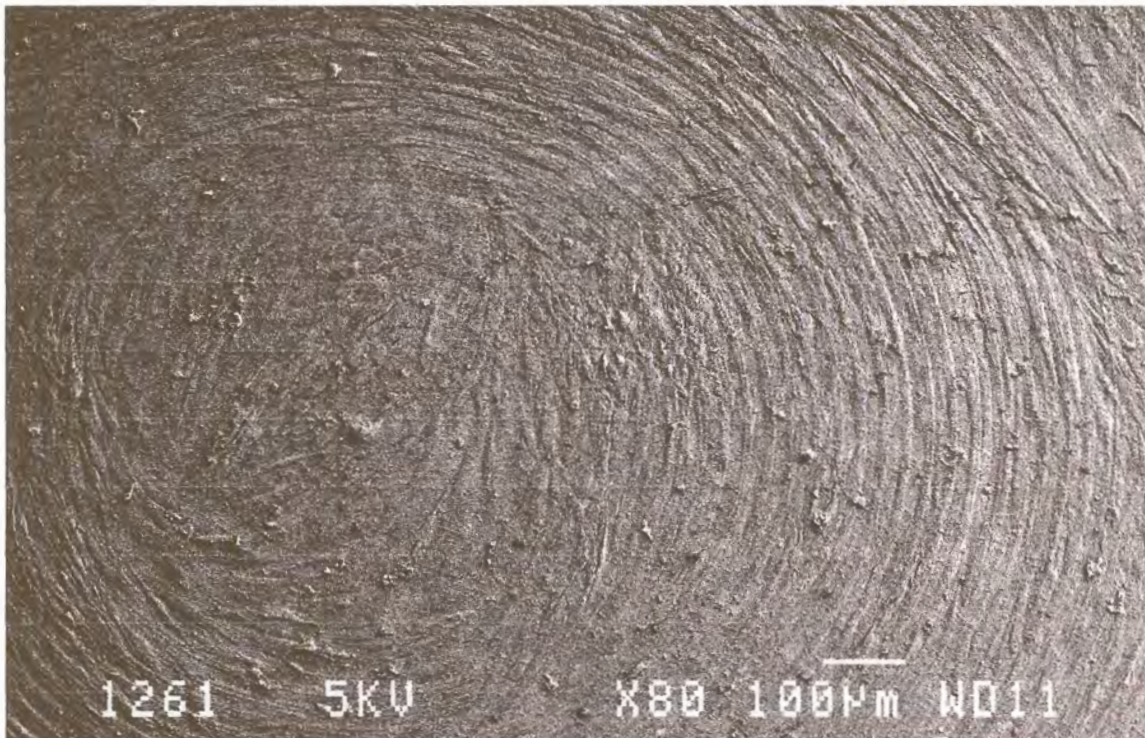


Fig 5-56: Fibroblasts aligned according to the grooves created by machining on surface of machined Ti6Al4V control sample

Fibroblasts on cast samples had a similar appearance to the machined enhanced samples (see Fig 5-57). Cells were flattened and polygonal in shape. Some parts of the surface were still visible between the spread cells.

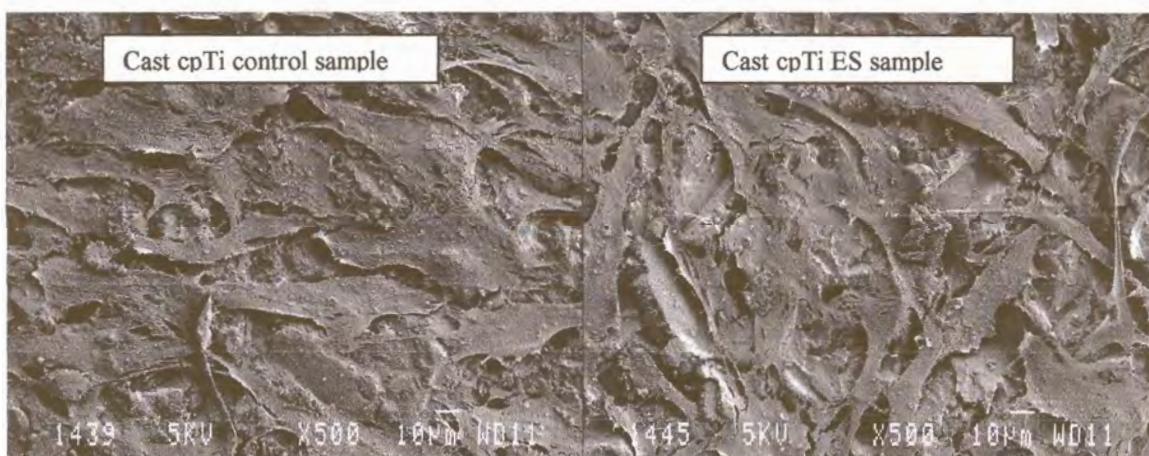


Fig 5-57: Growth of fibroblasts on surfaces of cast cpTi samples after 2 days incubation

Fig 5-58 shows fibroblasts on the surfaces of cast Ti6Al4V and the control samples. Regardless of type of surface preparation, fibroblasts spread on all surfaces with a similar intensity. On the cast Ti6Al4V ES sample long filopodial extensions are seen amidst the spread cells.

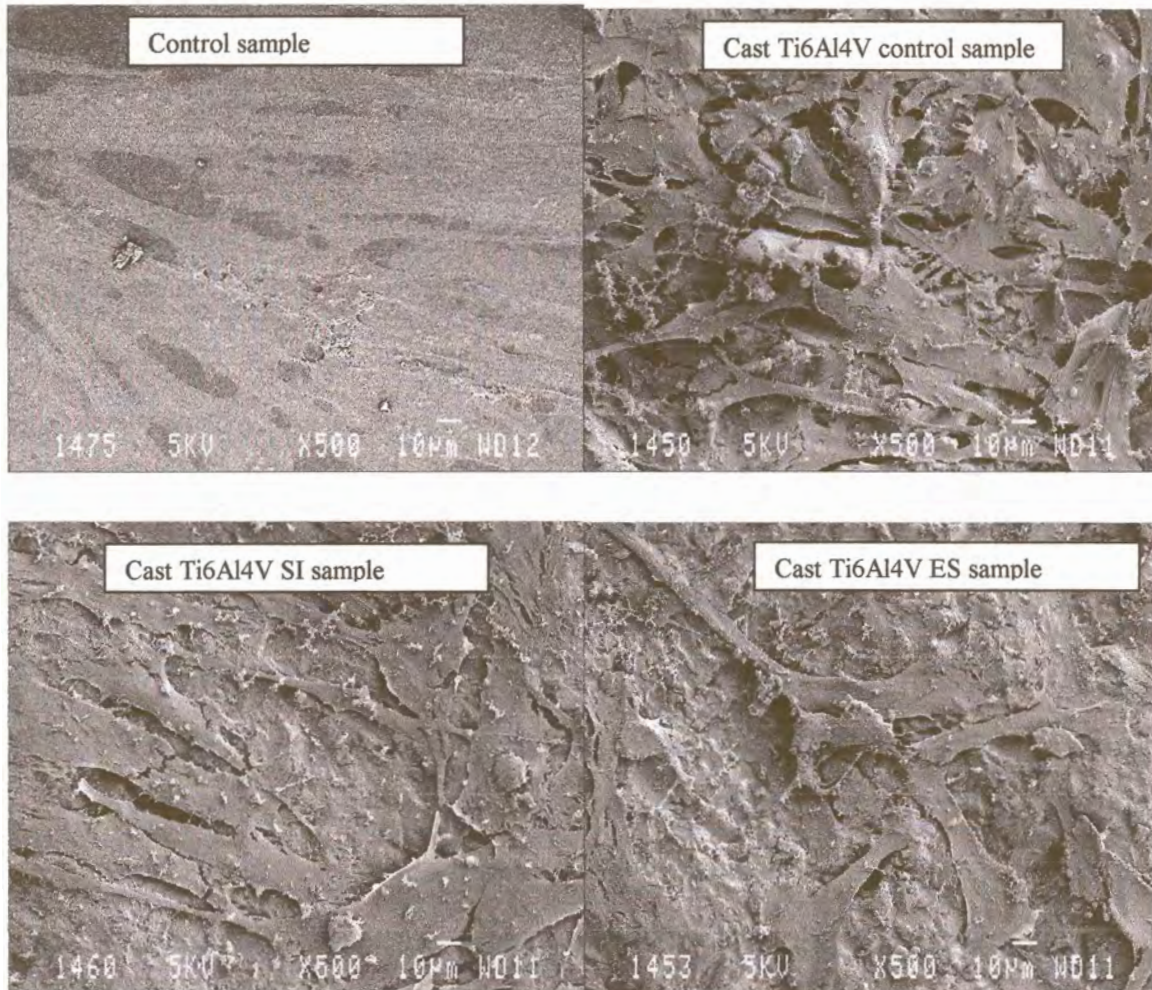


Fig 5-58: Growth of fibroblasts on surfaces of cast Ti6Al4V samples after 2 days incubation

Twenty-eight days

When the control samples are viewed together (see Fig 5-59, p127) no obvious difference can be seen between the fibroblasts. All surfaces are made up of more than a layer of cells and an intercellular matrix of interconnecting fibrils. On the surface cells are seen in the process of dividing and spreading.

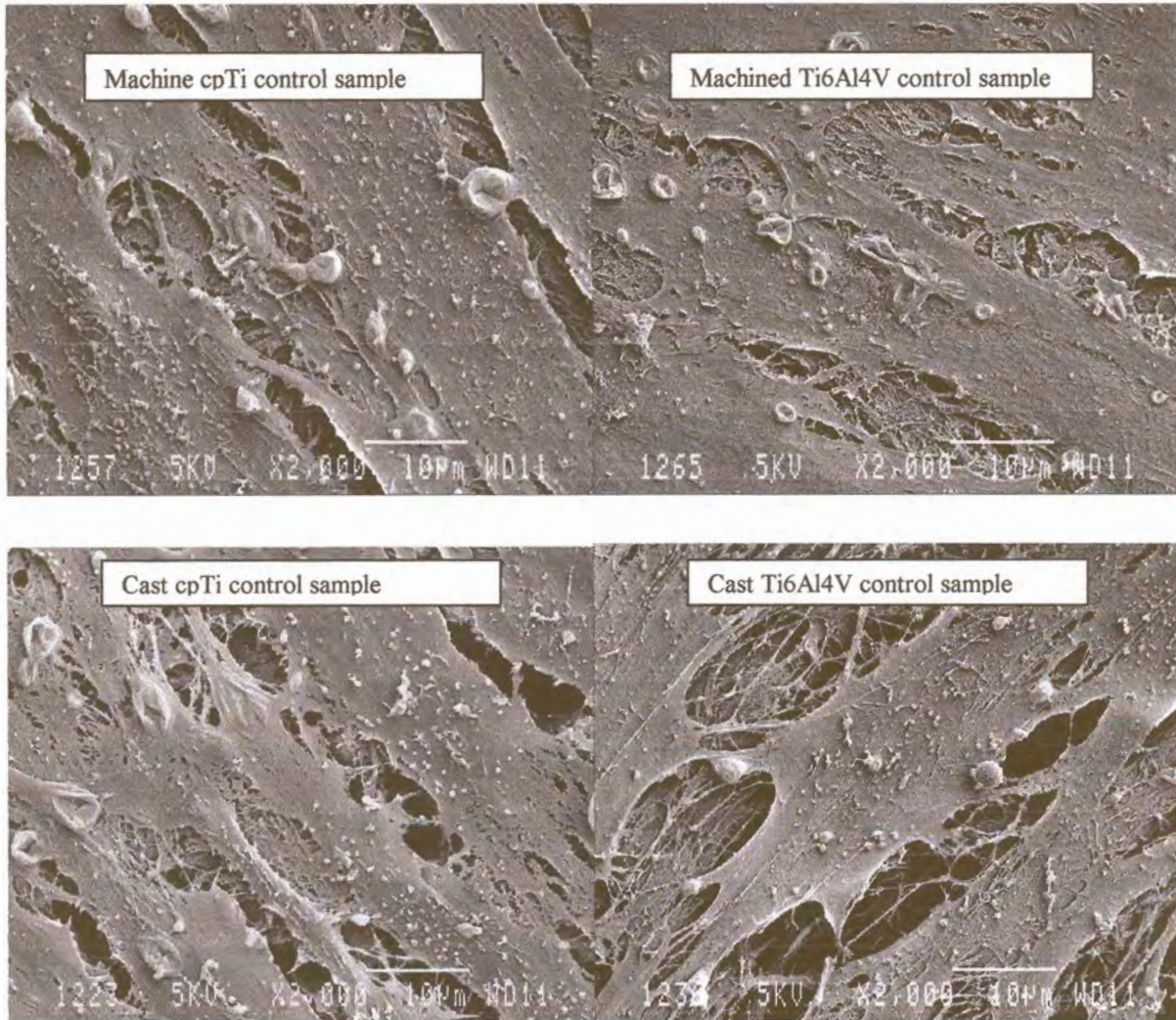


Fig 5-59: Growth of fibroblasts on surfaces of control samples after 28 days incubation

Fig 5-60 (see p128) shows fibroblasts on the surfaces of experimentally enhanced samples. An intense monolayer of cells is seen on all surfaces resulting in failure to distinguish the underlying surface topography of samples. After the formation of a cellular layer, the valleys are completely obliterated as can be seen from the image of the machined Ti6Al4V ES sample whose cell layer was torn, probably during processing.

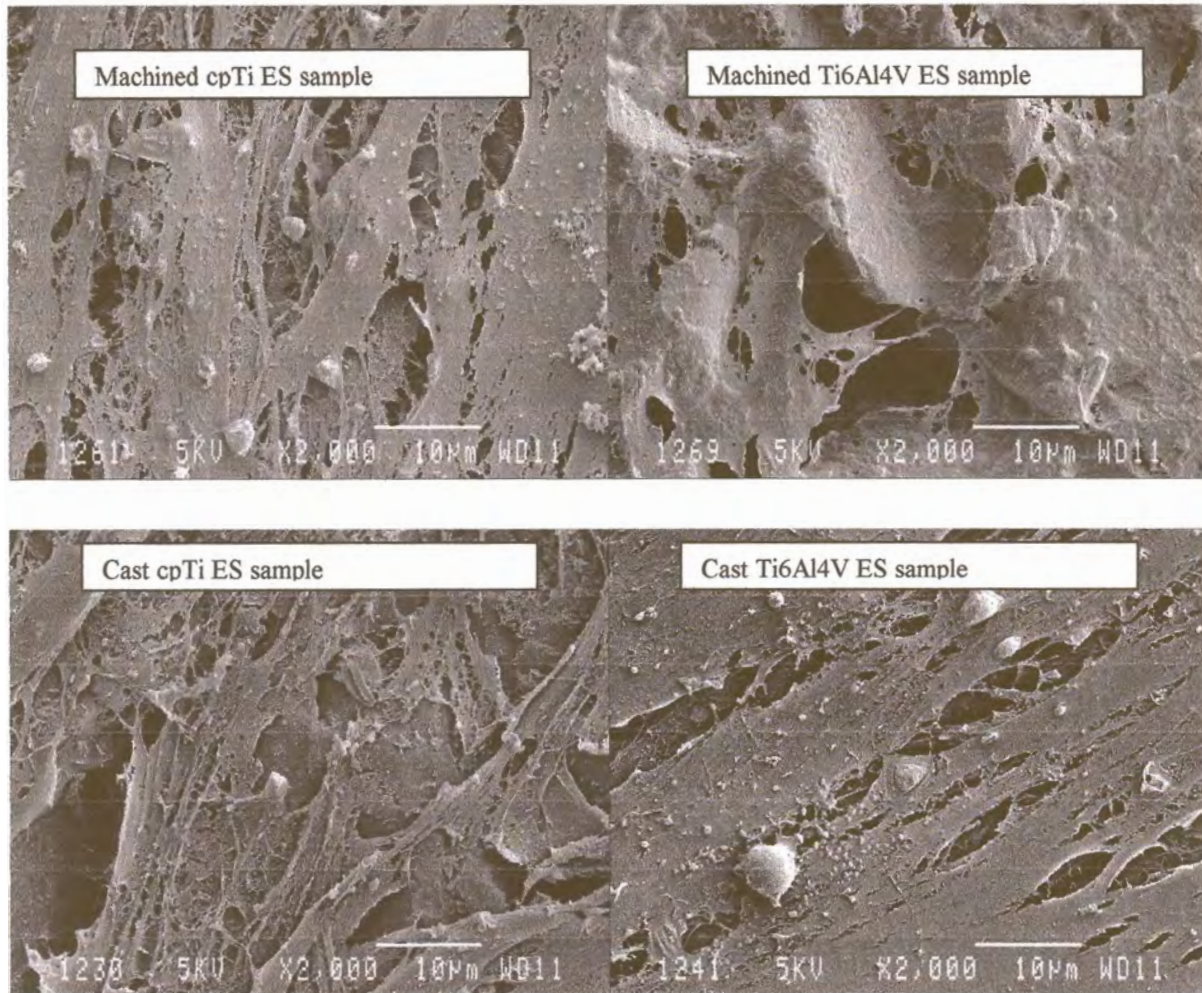


Fig 5-60: Growth of fibroblasts on surfaces of enhanced samples after 28 days incubation

The surfaces of SI enhanced samples also have a similar appearance to experimentally enhanced surfaces (see Fig 5-61, p129). The surface topography is completely obliterated by a carpet of cells. Dividing and spreading cells are seen over the surface. On the control sample a fibroblast is seen with a thickened rounded filopodia extending away from the body of the cell, while on the other samples cells display a flatter appearance of attached filopodia.

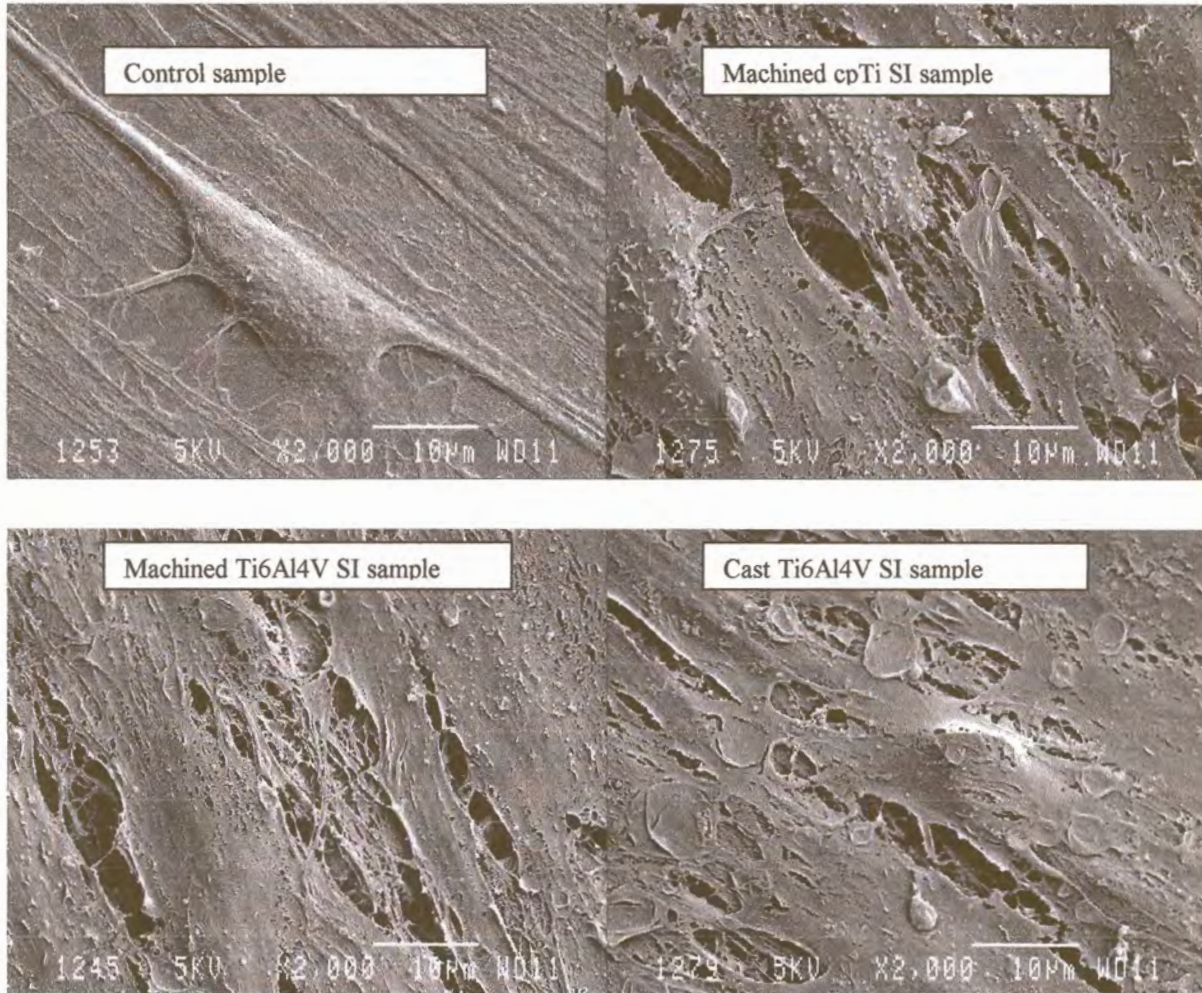


Fig 5-61: Growth of fibroblasts on surfaces of SI enhanced samples after 28 days incubation

5.2.2.2 Osteoblast-like Cells

Two days

Fig 5-62 (see p130) shows the surface of machined cpTi and Ti6Al4V control samples with osteoblasts-like cells completely covering the surface. Flattened cells together with cells that have divided and in the process of attachment and spreading are seen covering the surfaces. The underlying surface topography of machining grooves is displayed.

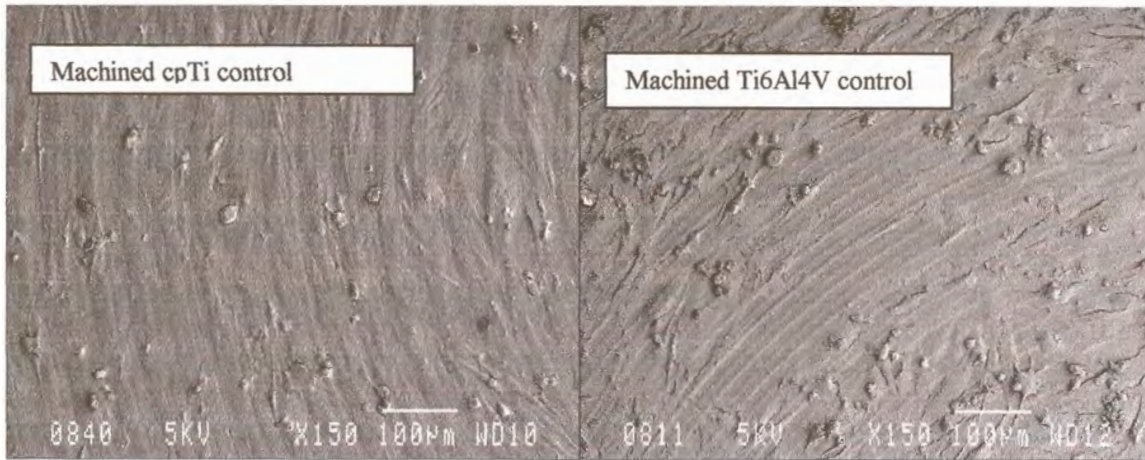


Fig 5-62: Osteoblast-like cells have completely covered the surface of the machined cpTi and Ti6Al4V control sample after 2 days incubation

Regardless of material or surface preparation, machined samples had a similar cell presentation (see Fig 5-63, p131). Osteoblast-like cells had already spread after 2 days as was evidenced by the absence of visible nuclei body within flattened cells. The flattened cells appear polygonal to irregular in shape with complete cytoplasmic extensions of the cell body on the surface (very heterogeneous in appearance). The osteoblasts-like cells spanned across pits and depressions, mostly contacting prominent features of the surface before flattening. Cells that have divided are in the process of attachment as seen over the spread cells.

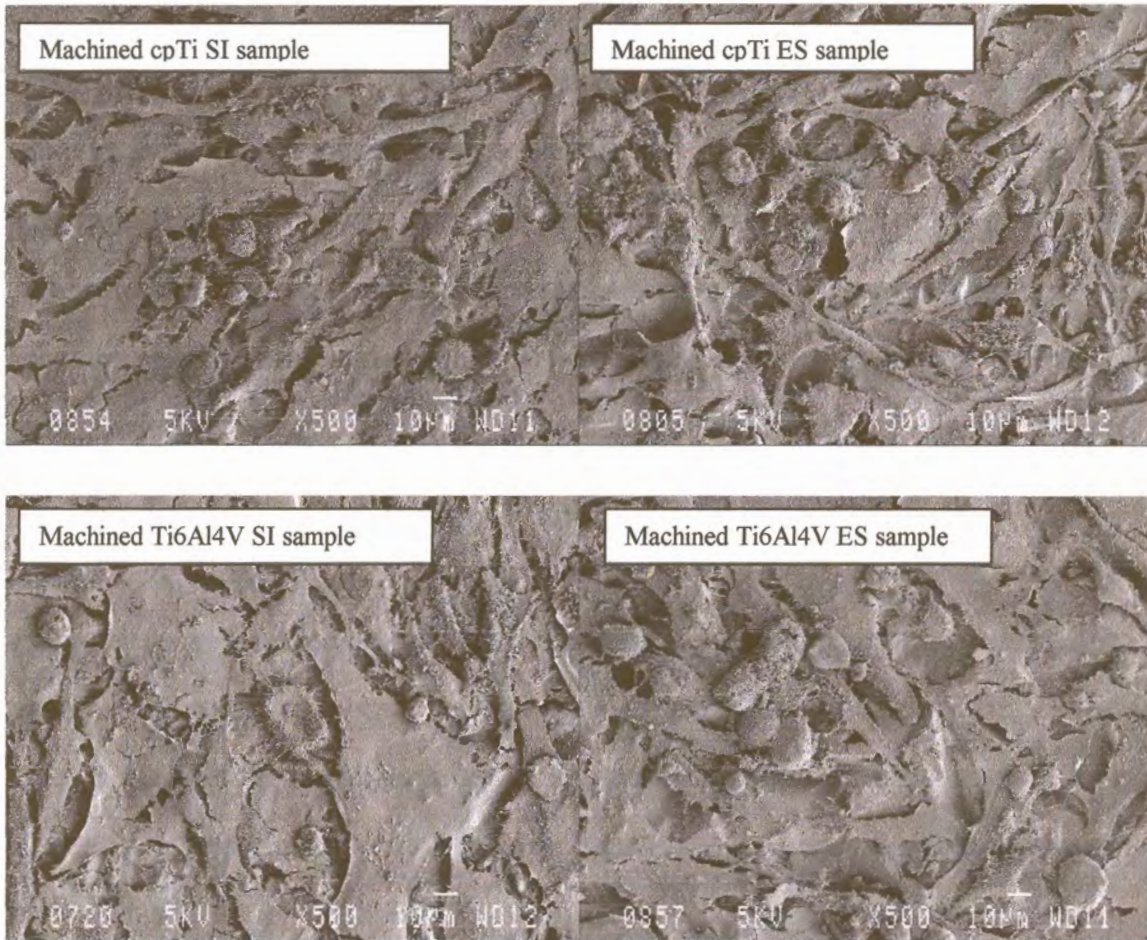


Fig 5-63: Growth of osteoblasts-like cells on surfaces of machined enhanced samples after 2 days incubation

Fig 5-64 shows the surfaces of cast control samples. Osteoblast-like cells are seen to have spread and attached to the peaks. The cell bodies are lifted from the underlying depressions to form a carpet of cells at the surface.

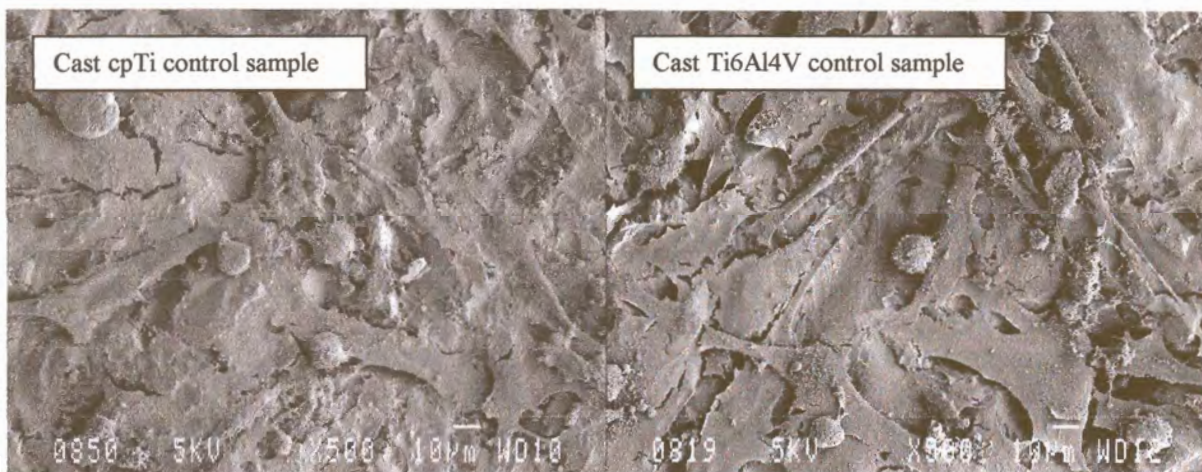


Fig 5-64: Growth of osteoblasts-like cells on surfaces of cast control samples after 2 days incubation

Osteoblast-like cells on surfaces of cast enhanced samples are also seen to adhere to peaks and lift off the base to form a layer of cells at the surface (Fig 5-65).

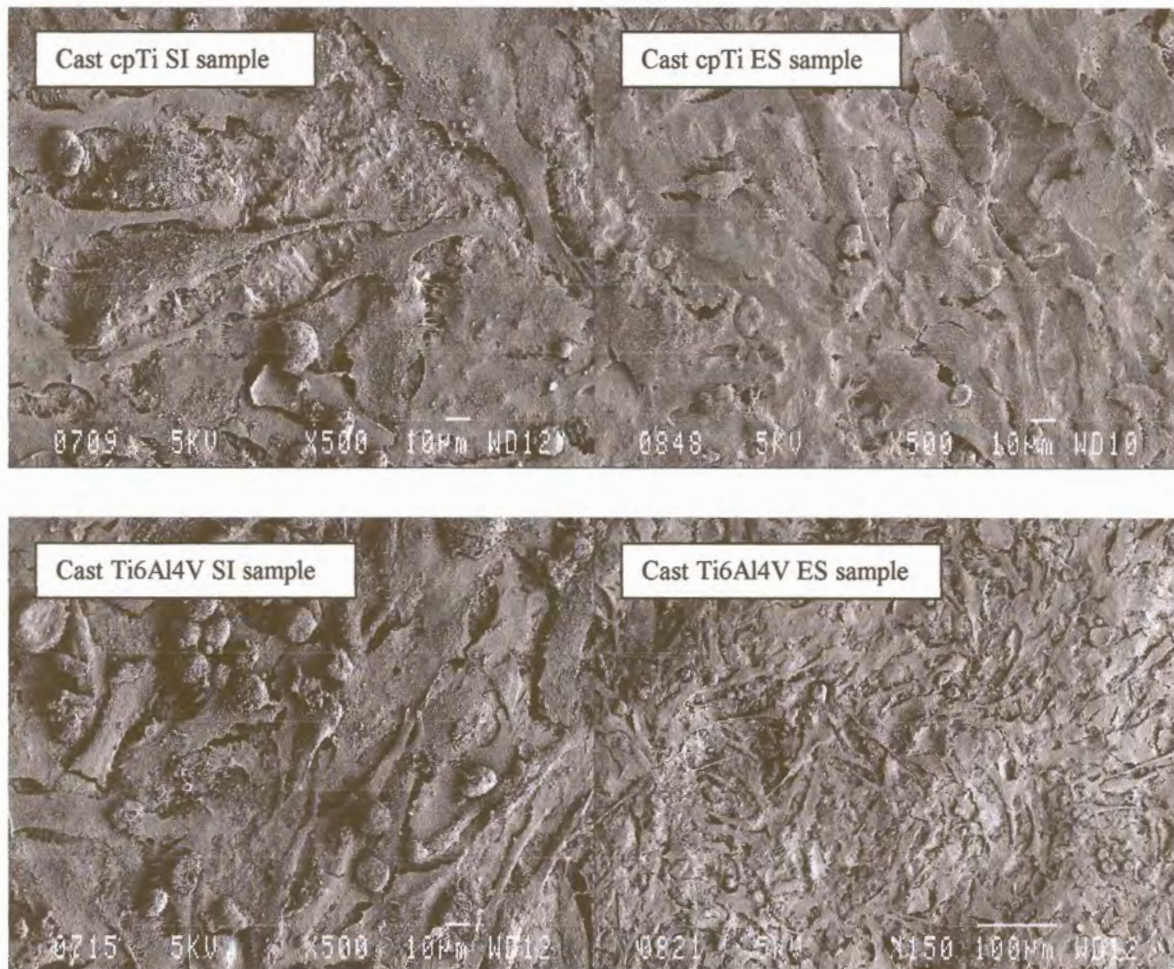


Fig 5-65: Growth of osteoblasts-like cells on surfaces of cast enhanced samples after 2 days incubation

Fig 5-66 (see p133) shows an individual osteoblasts-like cell attached to the surfaces of different samples. Regardless of the surface it is in contact with, the cell has a similar appearance. It is spherical in appearance with its nucleus still very prominent. The cell surface appears rough with foldings and displays numerous microvilli-like projections that anchor the cell to the surfaces. Some of the cells show extensive branching with many smaller filopodia extending in all directions.

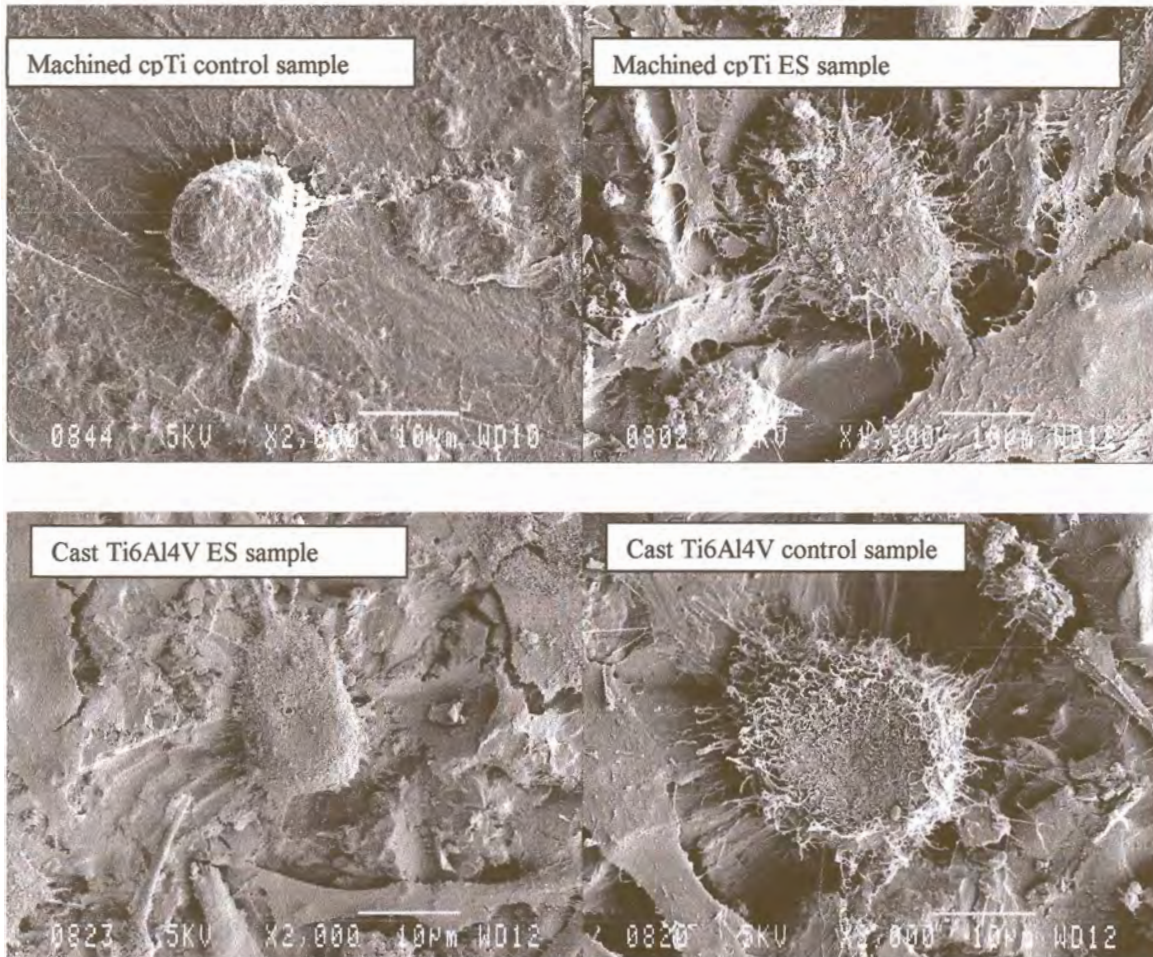


Fig 5-66: Attached osteoblasts-like cell seen on the different Titanium surfaces

Twenty-eight days

Though the cell counts showed a decline in cell growth at 28 days, SEM images shows that the osteoblasts-like cells on surfaces of either machined or cast samples are still in abundance and one surface can not be told apart from another (see Fig 5-67 and 5-68, p134-135). There is a mixture of attached and unattached cells seen over the surfaces. With the exception of the machined control surfaces where cells appeared to lay over the surface in a longitudinal manner, other samples have cells that appear polygonal. While some surfaces are observed to have lots of extracellular deposits (cast cpTi ES and Ti6Al4V SI and machined cpTi SI and Ti6Al4V SI) other samples appear to have numerous cells lying over the surface with some in the process of attachment. More than one layer of cells is obvious.

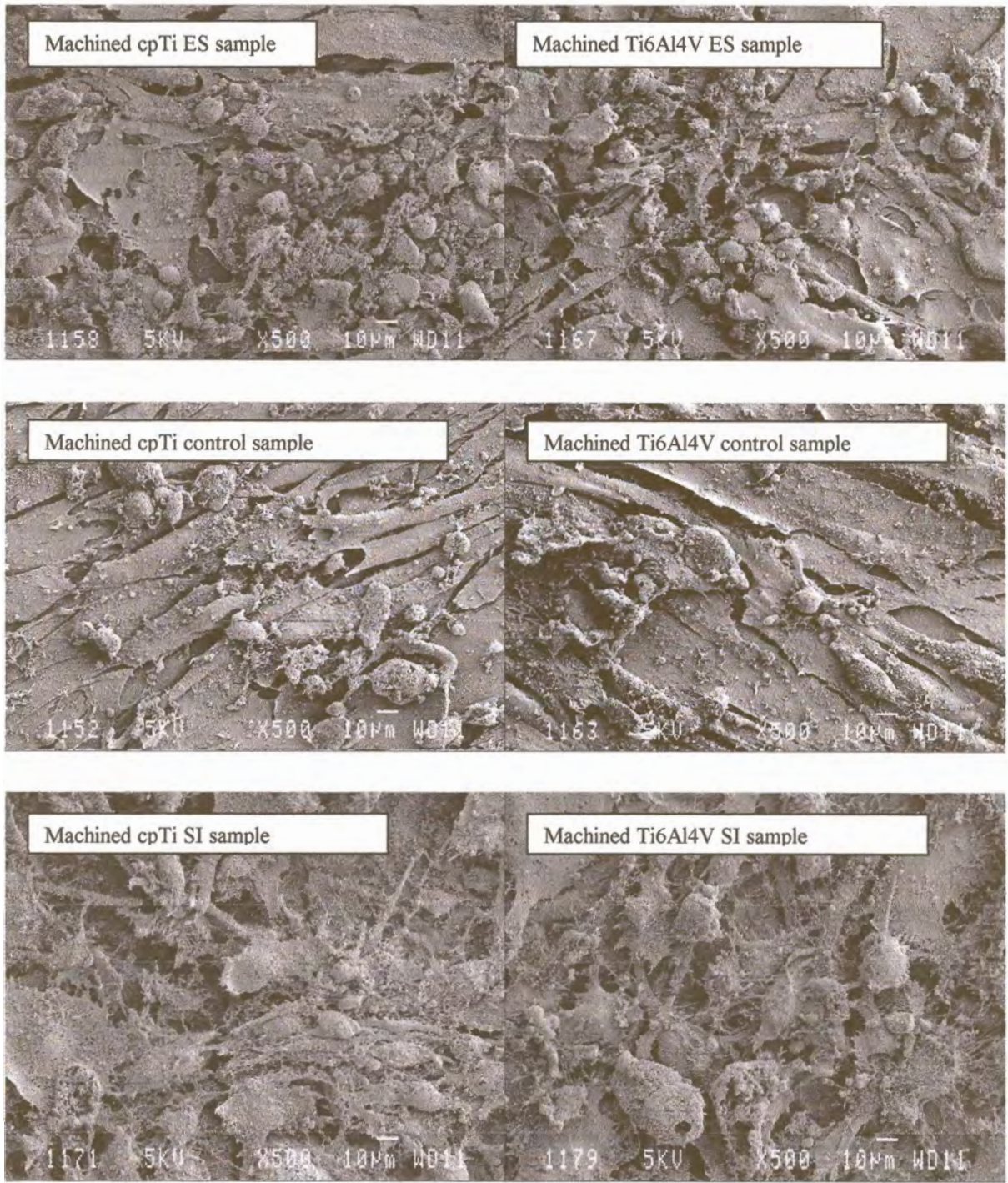


Fig 5-67: Growth of osteoblasts-like cells on surfaces of machined samples after 28 days incubation

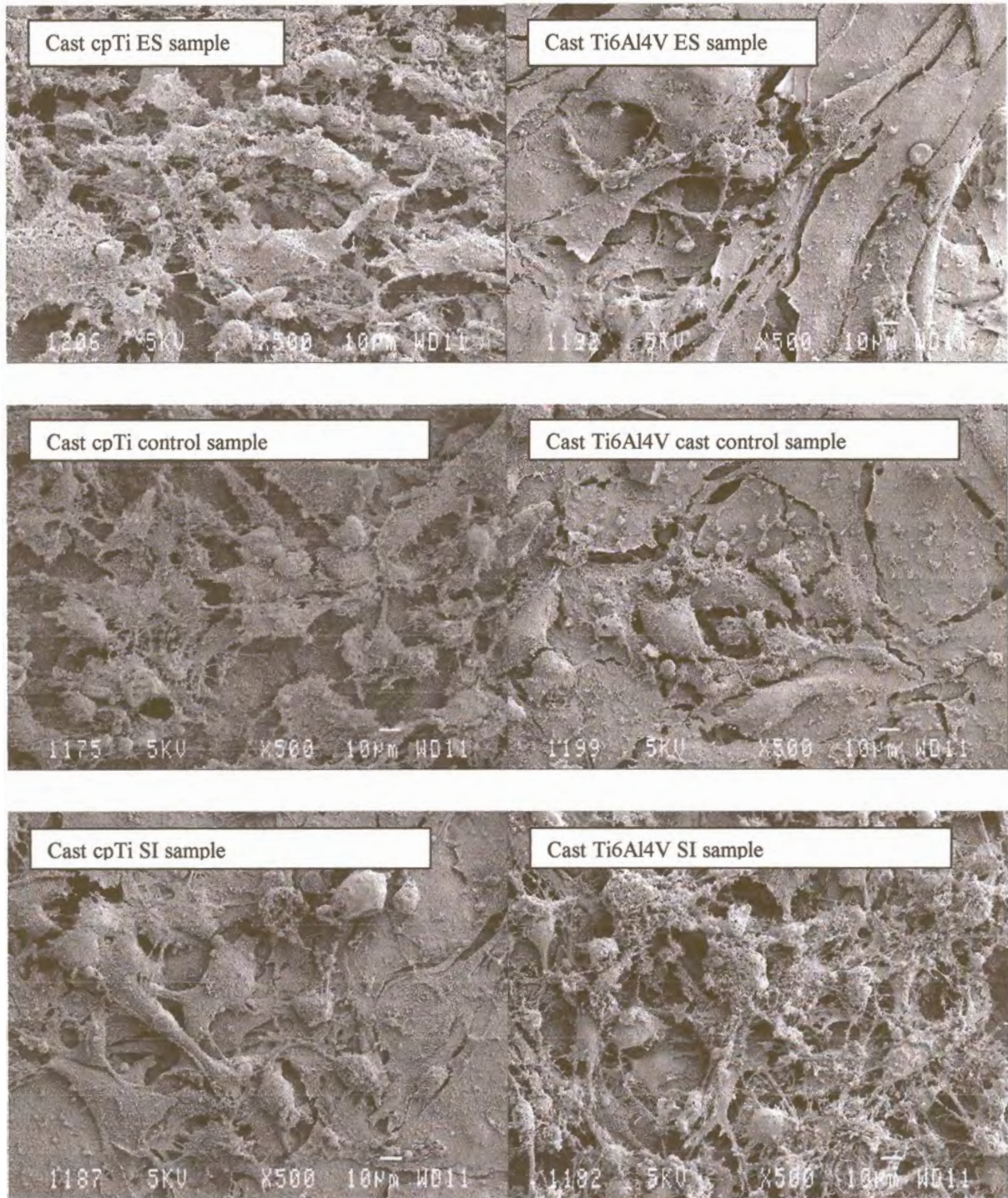


Fig 5-68: Growth of osteoblasts-like cells on surfaces of cast samples after 28 days incubation

In an attempt to migrate on the surface, cells overlapped and superimposed not only with their borders, but often with more extensive involvement of their cell bodies (see Fig 5-69, p136). A network of cell bodies spanned the surface forming a carpet of intertwined cells.

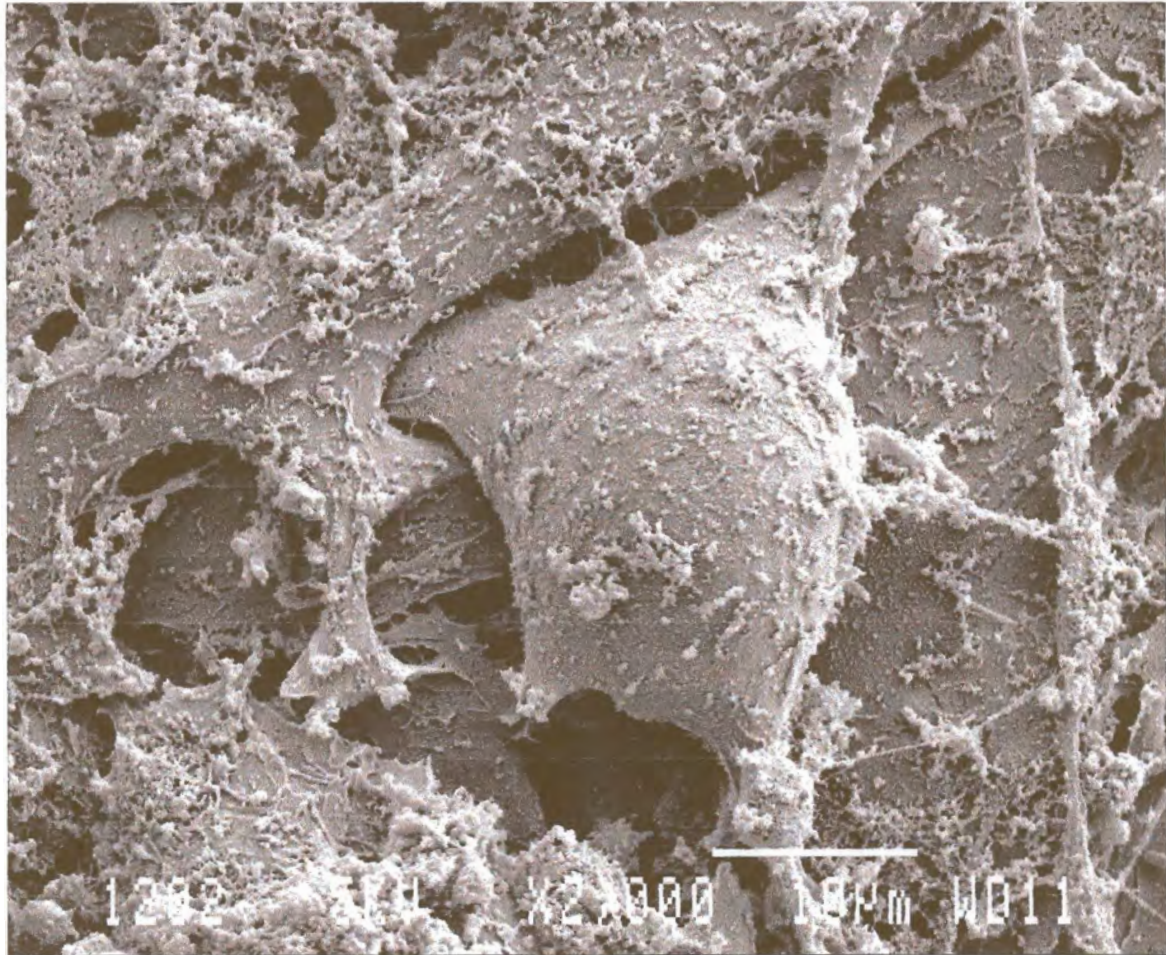


Fig 5-69: Network of osteoblasts-like cells formed on surface of cast Ti6Al4V control samples after 28 days incubation

CHAPTER 6 DISCUSSION

Bio-acceptability is a complex issue involving all the phenomena that contribute to the interfacial reactions between host tissues and implant. The bio-acceptability of Titanium has been attributed to its physical and chemical characteristics and the stable oxide layer that forms on its surface (Kasemo, 1983).

Most metals form oxide layers when exposed to the atmosphere and Titanium and its alloys are no exception. Many of the Titanium alloys in which Titanium is present in concentrations of 85% to 95% maintain the passivity of pure Titanium (Parr *et al*, 1985).

Due to the reactive nature of Titanium (see 2.1.5, p8) the oxide formed on its surface is dependent on the conditions under which it gets oxidized. Any substance that comes into contact with the implant surface has the potential to modify the oxide layer (Lausmaa *et al*, 1990; Hellsing, 1997).

Assuming that a true clean metal surface is available, the first stage is adsorption of the Oxygen on the metal surface, usually considered as a chemisorption process, which is assumed to involve a process of dissociation and at least partial ionization of the Oxygen leading to the formation of ordered superlattice domains or sub-oxide platelets within the metal. So called "oxide nuclei" form at the surface of many metals and these may grow together to form a continuous layer of oxide. These initial stages of the oxidation process depend on the cleanliness of the surface, which in turn depends on the gaseous environment and the purity of the metal. It also critically depends on the surface orientation and the roughness of the surface. Further complexities are introduced after the growth of a continuous layer of oxide on the metal surface, since the oxide provides a barrier between reactants. If the layer is compact, diffusion processes dominate and in

the case of a porous oxide, the reaction may be controlled by phase-boundary processes. The initial stage of oxidation, if a continuous oxide layer is already present, is still adsorption of gaseous species (Louw, 1997).

The incorporation of Oxygen into the oxide generally depends on the defect structure of the oxide. Diffusion of cations and anions across the oxide film is much slower than the electron transfer and can lead to space charge layers that may modify the transport process. The driving force for the diffusion of metal or Oxygen ions may be either the strong electric field set up across thin films of oxides, and/or the chemical potential gradient across thicker oxide films or scales. The reaction will also normally be a function of temperature, Oxygen pressure and the crystal structure and physical properties of the oxide on the metal (see 2.1.6, p10) (Louw, 1997).

Before the advent of Titanium Casting machines, Titanium products were available in the wrought form and either machined or plastic formed to the desired shape (see 2.2, p12). Casting of Titanium opened up a new era in the fabrication of implants. Pure Titanium has a hexagonal close-packed structure to a body-centred cubic phase that remains stable up to the melting point. Titanium alloy microstructure is made up of two phases the alpha phase and smaller amounts of beta phase (see 2.1.4, p7). Casting involves heat treatment and with the increase in temperature, a different crystalline structure is produced to the wrought form (Louw, 1997). Miyakawa *et al* (1996) claims that surface contaminants introduced as a result of casting or surface processing may influence Titanium's biocompatibility and resistance to corrosion negatively. Chemical interactions are known to occur between investment materials and cast samples and it is therefore necessary to grit blast cast surfaces to remove refractory material that adheres to the casting after

devesting (Curtis, 1998). According to Miyakawa *et al* (1989) the surfaces of Titanium castings exhibit a layered structure. Grit blasting with larger size particles may be considered to improve the mechanical bonding of cast Titanium (Papadopoulos *et al*, 1999) and grit blasting with 250µm Alumina (Al_2O_3) has the potential to remove significant amounts of substances that could affect the end result of the prosthesis, in this instance its bio-acceptability (Watanabe *et al*, 1999).

As it is the oxide layer of implants that makes contact with body tissues (see 2.4, p19), allowing direct apposition of bone to the implant surface enhancing osseointegration (Branemark *et al*, 1977), different treatments including tailoring of the oxide thickness, chemical composition and roughness, have been developed by implant companies according to proprietary preparations (Buser *et al*, 1991; Martin *et al*, 1995; Boyan *et al*, 1996; Schwartz *et al*, 1996; Arys *et al*, 1998). However as yet, overall *in vitro*, animal and clinical studies do not yield compelling conclusions about the role of surface composition and texture with respect to bone response at the interface (Brunski *et al*, 2000).

Bio-acceptability of the different samples in terms of materials used, fabrication procedures employed and surface preparations adopted will be discussed in relation to the different surface characterizations.

6.1 Chemical Composition

cpTi and Ti6Al4V showed no significant differences in their surface chemical composition in quantitative (atomic %) and qualitative (composition) terms in disagreement to Kasemo & Lausmaa, (1991) who mentioned major differences between cpTi and Ti6Al4V.

Chemical analysis of sample surfaces showed had dominant signals for Carbon, Oxygen and Titanium, in agreement to other

studies (Lausmaa *et al*, 1990; Keller *et al*, 1994; Placko *et al*, 2000). The atomic % concentration of Carbon reflects the amount of residues or contamination on the surface (Hellsing, 1997) and can be assigned mainly to surface contamination by adsorbed carbon containing (organic) molecules, which is a normal observation for air-exposed surfaces (Lausmaa *et al*, 1990). RFGDT significantly reduced Carbon indicating that the majority of it was present as a surface contaminant and that its presence was not related to the materials employed, fabrication procedures or surface enhancement. Baier & De Palma (1970) also reported that strongly bound hydrocarbon layers, the most common residual contamination on solid surfaces, could be efficiently stripped by RFGDT.

The concentration and XPS binding energy determination of the different oxygen peaks are important in determining the chemical make up of the oxide. Similar to findings by Placko *et al*, (2000) the O1s peak had a characteristic peak for TiO₂ at ~531eV. Other peaks were of metal oxides of Aluminium and other oxygen containing species. The significant increase in Oxygen concentration with RFGDT could be attributed to the process of plasma cleaning itself as immediately after the Argon plasma treatment the samples were oxidized *in situ* in pure Oxygen at room temperature (Aronsson *et al*, 1997). In this study the atomic percent concentration of Oxygen was significantly influenced by RFGDT and was not related to cpTi or Ti6Al4V material employed or the machining and casting procedures or the differently enhanced surface preparations.

The dominant Titanium peak at 457-458eV indicates that the oxide is mainly made up of TiO₂ and some Ti₂O₃, as found in other studies (Lausmaa *et al*, 1989; Machnee *et al* 1993; Sittig *et al* 1999; Kilipadi *et al*, 2000). The absence of a Titanium metal peak at 454eV indicates that the oxide thickness is greater than the escape depth of photoelectrons from the underlying Titanium substrate and intermediate layer, meaning

that the bulk material was not exposed (Lausmaa *et al*, 1990). A lower Titanium surface concentration is measured on the cast and surface enhanced samples. This can probably be attributed to the remnants of grit blasting over surfaces of samples. The Titanium surface concentration detected on cpTi and Ti6Al4V samples was similar but the significant increase in Titanium surface concentration after RFGDT can be explained by the consequent significant decrease of Carbon on the surfaces of samples.

The relatively high Aluminium concentration detected on the surfaces of samples can be attributed mostly to the Aluminium oxide used in the grit blasting procedures of surface enhancement. RFGDT was not able to influence the Aluminium concentration indicating that it was either strongly embedded into the surface or because the particles were too huge to be sputtered of the surface (see 2.6.4.1, p39). In agreement with results of this study, Wennerberg *et al* (1996) also found relatively high atomic % levels of Aluminium (17%) on the surfaces of blasted implants. Darvell *et al* (1995) indicated the presence of up to 10% atomic concentration of Aluminium on the surfaces of castings after blasting was done. According to Kononen *et al*, (1992) Aluminium is generally known to be biocompatible though it has been associated with irreversible enzymatic disturbance (Bruneel & Helsen, 1988) as well as inhibition of the mineralization process of bone (Pilliar, 1998).

The presence of Sodium on samples is related to the process of fabrication and surface enhancement and its concentration was not affected by RFGDT. Small amounts of Sodium on implant surfaces do not cause problems in implant use (Klauber *et al*, 1990) and its presence may be important in the initial attachment of cells to the surface of the implant, especially due to its interaction with other inorganic elements within body tissues.

Most of the other inorganic contamination (Calcium, Lead, Zinc, Nitrogen and Vanadium) that was introduced in smaller quantities as a result of surface preparation was eliminated by RFGDT. RFGDT also reduced the Carbon contamination with a resultant increase in the Oxygen and Titanium concentrations, but had no effect on the Aluminium or Sodium concentrations, in agreement with results reported by Aronsson, *et al*, (1997). The Sodium and Aluminium did not change with RFGDT probably because they are incorporated into the oxide layer by the surface preparation methods employed. The elimination of contaminants by RFGDT indicates that most of the contaminants were present at the outer most surface layer only. According to Aronsson *et al*, (1997) normal contamination layers are typically restricted to one monolayer of atoms or molecules or less. Probably explaining why most of the contaminants disappear after RFGDT.

According to Baun (1982) contaminants in the oxide layer may arise from the bulk composition through heat treatment processes that facilitate diffusion of the lighter elements to the surface and could be the explanation as to why after RFGD treatment only cast samples were detected as having Zirconium. During the recovery of Titanium from its ore a number of zirconium products are used and probably explains its presence (Beder & Ploger, 1959).

Absence of traces of Silicon on any of the samples analyzed can be related to the storing of samples under Argon in polypropylene containers after RFGDT. Silicon contamination is normally observed on samples stored in glass vials but not in polypropylene vials (Esposito *et al*, 1999).

The fact that differences in chemical composition are negligible amongst samples after RFGDT could be due to the high stability of the oxide formed during the RFGDT (Taborelli *et al*, 1997). As in accordance with the criteria for RFGDT (Aronsson *et al*, 1997) the plasma cleaning process did not

introduce any new impurities to the surface. The reoxidation *in situ* in pure oxygen passivates the surface and minimizes the subsequent formation of unintentional surface reaction layers (Aronsson *et al*, 1997).

The oxide layer of cast and machined enhanced samples had similar elements detected that relates to the adopted procedure of grit blasting. Buser *et al* (1991) also found levels of Aluminium and Sodium on their sandblasted samples.

As it is the oxide layer and not the metal itself that determines the chemical properties of the implant, the chemical "quality" of the Titanium oxide superficial layer together with other related factors become the determining factors of bio-acceptability (see 2.6.4, p37). The concentration of the Aluminium and Sodium from cast and enhanced samples could probably be reduced by meticulous post blasting using air to dislodge the loosely adhered particles followed by an ultrasonic bath using distilled water for 30 min. As no significant differences were observed between the different samples with regard to material, fabrication procedure or surface enhancement, it was difficult to relate if bio-acceptability was influenced by the presence of the different elements.

6.2 Surface Roughness

A major consideration in designing implants has been to produce surfaces that promote desirable responses in the cells and tissue contacting the implant. In an attempt to improve cell attachment various forms of dental implants are available with differing surface characteristics that range from relatively smooth machined surfaces to more roughened surfaces created by coatings, blasting by various substances, by acid treatments, or by employing combinations of these mentioned treatments (Cochran, 1999). Currently, virtually all dental

implant manufacturers market implants that feature some form of roughened surface (Cochran, 1999).

Area analysis was determined from a 3D image scan of the surface while Line analysis was determined from a line drawn across a 2D image scan. The importance of each value in the determination of surface topography is discussed separately (see 2.6.2.1, p33-34).

6.2.1 Area Analysis

Both addition and subtraction methods can increase the surface area of an implant, but they do not necessarily make the implant surface rougher (Klokkevold, 2002). The surface topography of samples was introduced by the fabrication procedure adopted and was not related to the material employed. The Ra values of cast samples ($0.50\mu\text{m}$) were much higher than machined samples ($0.11\mu\text{m}$). Larsson *et al*, (1997) measured a Ra value of $0.05\mu\text{m}$ for machined Titanium surfaces and Buser *et al*, (1998) reported a Ra value of $2.0\mu\text{m}$ for the SLA surface and a Ra of $1.3\mu\text{m}$ for the Osseotite surface. Zhu *et al*, (2002) reported a Ra value of $0.340 \pm 0.01\mu\text{m}$ before being anodized and after anodizing with a voltage of 391V, surfaces had a Ra value of $0.516 \pm 0.037\mu\text{m}$ that was similar to the observed Ra value of cast samples in this study. Most studies only specify the Ra values as a measure of surface roughness, which is totally inadequate as the Ra value is the average deviation of the profile from the mean line and has no ability to differentiate between peaks and valleys. RMS that is the root mean square of the Ra value is inadequate when reported with the Ra value or alone. It is important therefore to report other area analysis values for proper interpretations to be made (see 2.6.2.1, p33).

Cast samples analyzed had a Ra value of $0.50\mu\text{m}$ and a RMS value of $0.65\mu\text{m}$ together with an average height of $1.93\mu\text{m}$ and a Maximum range of $3.86\mu\text{m}$ while machined samples had significant

lower values of Ra (0.11 μ m), RMS (0.14 μ m), Average height (0.54 μ m) and Maximum range (1.03 μ m). The surfaces of machined samples showed typical features of grooves that were preferentially oriented in the machining direction while cast samples showed a relatively irregular topography of peaks and valleys. The spatial relationship was different for the machined and cast samples and this difference may have contributed to the surface roughness parameters being much higher for cast samples.

The irregularities resulting from grit-blasting treatment typically range from submicron size to approximately 10 microns (Pilliar, 1998). Wennerberg *et al* (1996) concluded that surfaces created by blasting with Al₂O₃ were isotropic and they recommended a surface roughness with a Ra of 1-1.4 μ m as being suitable for good bone to metal fixation. Samples that were fabricated by casting also had an isotropic surface but with a much lower Ra value than that recommended by Wennerberg *et al*, (1996). Grit blasting and casting are both methods of surface creation that are based on forming processes leading to isotropic surfaces. The machined surfaces also displayed a similar topography because the surfaces were not really produced by turning but by cutting into the discs. Machining of implants normally entails a turning procedure (anisotropic surface) (see 2.6.2, p29). Therefore, though our results show that the machined surfaces and the cast surfaces are similar, it should be remembered that the overall topography could differ.

Grit blasting not only takes away material but also creates depression on the surface. The blasting pressure together with the size of the grit particles used could be a determining factor to the surface roughness of the cast samples. Cast surfaces were observed to have deep depressions in comparison to their high peaks resulting in the increase in surface area. According to Scacchi (2000), the requirements for an oral

implant design include maximum surface area for attachment and primary stability.

The significant increase in surface area for the 20 μ m scan with RFGDT can be related to the intentional oxidation that is done after removal of contaminants during the RFGDT (Kasemo & Lausmaa, 1988b). Vargas *et al*, (1992) hypothesized that after removal of contaminants the remaining oxide is leveled but this study found a significant build up of oxide especially over the peaks. At 5 μ m scan only few peaks are present in comparison to the 20 μ m scan hence oxide needles thus formed from the oxidation process were probably too few to have a significant effect on surface area.

6.2.2 Line Analysis

Taborelli *et al* (1997) found distinct topographies introduced by surface preparation that could be identified by their peak to valley values of micro roughness.

In this study parameters of line analysis were definitely higher for cast samples compared to machined samples. For cast samples the Ra value of 0.31 μ m was nearly the same as the Rpm values of 0.37 μ m indicating that the distance of the profile from the mean was actually contributed to by the peaks. The Rt values of 1.66 μ m were also approximately double the Rp value of 0.77 μ m for cast samples, implying that the peaks and valleys on the surface were of approximately similar distances from the mean. The Rt and Rp values contributed to the Rtm being nearly double the Rpm. The ratio of Rpm/Rtm for cast samples was 1:2 signifying a surface that is relatively rough as a low ratio normally is preferred for bearing surfaces. Wong *et al* (1995) noted that the presence of many small peaks resulted in more effective fixation of bone than a smaller number of higher peaks. We did not determine the number of peaks or valleys within a line scan and it would have contributed to a better surface topographical analysis, though

it is accepted that reported values are representative (see 2.6.2.1, p33-34).

The R_p value for cast samples was significantly increased by RFGDT and the increase can be explained by the oxide protrusions that occurred over the peaks in agreement with Solar *et al* (1979).

Similar to our findings, Abron *et al*, (2001) in their study reported that the average surface roughness values (R_a) and the average peak to valley distance (R_p-v) were similar regardless of blasting and acid etching or incomplete blasted surfaces, indicating that the deviation from the mean surface plane in the form of a peak or the deviation in the form of a valley were practically the same. As explained (see 2.6.2.1, p33) the R_a value does not differentiate peaks from valleys.

Although the critical level of roughness magnitudes that influence biological response has not yet been established, it is possible that cells tend to respond most actively to structures that approach their size. This was the reason why analysis of 20 μ m scans for surface topography were performed. Smaller points of attachments were evaluated from the 5 μ m scans. Determining the number of peaks and valleys within a line scan could be an added indicator of bio-acceptability as it was observed that the presence of peaks is necessary for cell attachment. From this investigation it is indicative that surface topography can be manipulated for better bio-acceptability.

6.3 Depth Profile

Titanium dioxide is indeed the definitive material that governs the interaction between host tissue and the implant surface in contact with the body tissues, allowing the direct apposition of bone to the implant surface, enhancing

osseointegration (Branemark *et al*, 1977; Kasemo, 1983; Branemark *et al*, 1985).

The oxide thickness between cpTi and Ti6Al4V showed no significant differences in this study though Keller *et al* (1994) found that the oxide thickness on Titanium alloy oxidized surface was approximately 2.5 times thicker than the oxides on cpTi. Differences, if any, between the surface oxides formed on the alloy Ti6Al4V and on unalloyed cpTi might play a role in the acceptance (and integration) by the host tissue (Ask *et al*, 1988) (see 2.6.3, p34-35).

After RFGDT the machined control surfaces were found to have the lowest oxide thickness compared to other samples that were either cast or enhanced, suggesting that the fabrication method and surface enhancement were the determining reasons for the significantly higher oxide thickness. Machnee *et al* (1993) did not find any significant differences in oxide thickness between the differently prepared samples they studied while Binon *et al* (1992) found that the oxide thickness of the implants investigated greatly depended on the manufacturing process and conditions. Lausmaa *et al* (1990) and Sittig *et al* (1999) in their studies measured oxide thickness of 2-6nm depending on method of sterilization. Placko *et al* (2000), in their study estimated the thickness of oxides to be about 3nm, similar to that found by Ong *et al* (1993). The reported difference in oxide thickness by authors could be partly attributed to the different equipment and methodologies adopted to measure the Titanium oxide layer.

RFGDT surfaces had a significantly thicker oxide than untreated surfaces. In agreement, Aronsson *et al* (1997) reported that reoxidation of surfaces produces oxide thicknesses of about 2-150nm and RFGDT treatment normally produced a stoichiometric TiO₂ surface oxide of uniform thickness with no traces from earlier treatments.

The ideal oxide thickness that is required for bio-acceptability has not been delineated by this study. In disagreement to Kasemo & Lausmaa (1986) and Albrektsson *et al* (1981) who reported that the oxide layer is assumed to grow over time after implantation, Wennerberg *et al* (1996) found that after implantation and removal of the screws, the 75 μ m blasted implants had become smoother than before implantation but were still distinguishable from the 25 μ m implants in terms of roughness. Arys *et al* (1998) also found that the TiO₂ overlay on failed implants was considerably reduced in thickness or absent and speculated it to being stripped away either by mechanical stress, or being chemically modified and dissolved in the microenvironment. Another explanation of the absence of the Titanium oxide layer onto implanted implants is the possibility that osteoclast cells phagocytosed the oxide, as osteoclasts are essential cells in bone remodeling (Davies *et al*, 1989). The importance of a stoichiometric oxide layer that is not prone to the phagocytosis activity of the osteoclast is thus emphasized.

The overall chemical reaction involved in the oxidation process or formation of the oxide layer can be described in terms of three layers: (i) a metal/oxide interface containing suboxides (with the metal in a lower oxidation state), (ii) a uniform crystalline oxide layer, and (iii) a thin outer layer where the metal is in its highest oxidation state. For alloys, the selective oxidation of the alloy components combined with competing ion movement govern the growth and subsequent structure of the oxide layer (Louw, 1997).

Cast samples had a significantly thicker oxide than machined samples and can be related to the fabrication process of the cast samples. The stoichiometric composition of the oxide layer formed by casting could be entirely different from that formed by machining, resulting in a variation between samples. Other characteristics like grain size and crystal orientation

could also be contributory (see 2.1.4, p7). According to Low *et al* (2001) the thicker oxide layer of cast samples is related to the heavy reaction layers formed during the casting process and increased surface area introduced by grit blasting.

Defective oxides that are formed as a result of other elements bonded to Oxygen and the Oxygen chemisorbed on the surface could lead to its breakdown causing failure in bio-acceptability. The type of oxide formed, amorphous in relation to stoichiometric could be another determinant of bio-acceptability as the surface charge at the peak may be dependent on the type of crystalline structure.

6.4 Cell Culturing

Assessing the attachment and growth of various cell types to a biomaterial *in vitro* offers a well-controlled, quantitative and cost effective model of interactions at the tissue-implant-interface. Using the direct contact method, cells are cultured directly onto the material under investigation and observed over a period of time relative to their morphologic and functional features (see 2.7, p41).

Fibroblasts were obtained from human gingival biopsies, according to the method by Kononen *et al* (1992) and Botha (1995) while the osteoblasts-like cells used in the study were from a human osteosarcoma cell line. Since human cells are more reliable as test systems than other tissues and species in culture the use of human cells was motivated.

Viable cells were counted at predetermined times using a Neubauer haemocytometer and the Trypan-blue exclusion method (Botha, 1995). The percent attachment and proliferation was then determined from the counts. While some researchers counted the unattached cells using a Coulter Counter (Bowers *et al*, 1992), others counted the attached cells (Morra &

Cassinelli, 1997). None of these methods distinguished viable from non-viable cells. In this investigation it was regarded as an important consideration to distinguish between viable and non viable cells (see 2.7.5, p48).

For comparison of data a base-line control is necessary and tissue culture plastic was used as a control because of its suitable characteristics. Keller et al (1990) demonstrated that after one hour, more than 90% of the inoculated cell population had attached to the tissue culture plastic. Tissue culture plastic is plasma treated to promote cell adhesion and growth (Amstein & Hartman, 1975).

The percent attachment efficiency and proliferation of both fibroblasts and osteoblasts-like cells displayed a significant difference with time. They both reached their peak proliferation by day 14, with osteoblasts-like cells reaching a maximum of 180% and fibroblasts a maximum of 120%. At day 28, the fibroblasts on the control surface showed a significant rise in % attachment efficiency and proliferation while the osteoblasts-like cells showed a significant decline. The % attachment efficiency and proliferation of fibroblasts on the surfaces of machined cpTi and Ti6Al4V control samples was observed to be similar to the control unlike the cast and enhanced samples that showed a decline in relation to the control. This observation was probably related to the type of surface topography (see 2.6.2, p30-31). Over time, the % attachment efficiency and proliferation for osteoblasts-like cells was observed to decline for most samples similar to the control, with the exception of the cast Ti6Al4V control sample that displayed an increase in % attachment efficiency and proliferation as from day 2 to day 28 and machined cpTi SI sample that maintained a steady % attachment efficiency and proliferation. Cast Ti6Al4V ES sample and machined Ti6Al4V SI sample showed a very slight decline in % attachment efficiency and proliferation of fibroblasts from day 14 to 28. The array

in the display of results could not be explained from either the chemical or topographical analysis but is probably related to the phenomena of attachment and spreading. From this investigation it appears that spreading and attachment are two different phenomena of cells that are determined by different factors.

There were no significant differences in the % attachment efficiency and proliferation of fibroblasts or osteoblasts-like cells between the different materials used (cpTi and Ti6Al4V), fabrication employed (machined and cast) or surface enhancement procedures (control, SI and ES) and the control. This observation could have been contributed to by the limitations of funds that permitted only two readings of cell counts per sample. Statistical analysis thus performed was not able to detect differences and deductions made from these results should be interpreted as possible trends.

The % attachment efficiency and proliferation of fibroblasts did not show any statistical difference between materials used. Machined control samples were similar to the control while cast and enhanced samples had a different % attachment efficiency and proliferation that was much lower than the control. Mustafa *et al* (1998) showed that smooth surfaces favour fibroblast attachment and least attachment occurs on rough surfaces (see 2.6.2, p30). The % attachment efficiency and proliferation of fibroblasts on all SI samples and machined Ti6Al4V ES and cast cpTi ES was much lower than the control while the machined cpTi ES and cast Ti6Al4V ES samples nearly matched the control. These results imply a possible trend that the SI surfaces are not compatible for the proliferation of fibroblasts. It is possible that the reduced % attachment efficiency and proliferation of fibroblasts was related to the delay in finding attachment points, as the surface was probably smoother than other samples.

The % attachment efficiency and proliferation for osteoblasts-like cells did not show any significant differences between samples. Machined SI samples were observed to have a higher % attachment efficiency and proliferation of osteoblasts-like cells compared to other machined samples and the control. This observation was probably related to the way the machined SI samples were manufactured and the topography they displayed. The cast samples had a similar presentation to the controls with the exception of cast Ti6Al4V control and cast cpTi ES samples that had a much higher % attachment efficiency and proliferation ($p > 0.05$). It is possible that these surfaces were smoother than the other cast surfaces but it could also be related to the hardness of the cast alloy material (see 2.1.4, p6) and the blasting procedure that produced a different surface topography conducive to osteoblasts-like cell proliferation. Numerous studies have associated increased surface roughness with greater osteoblastic activity (Michaels *et al*, 1989; Bowers *et al*, 1992; Keller *et al*, 1994; Walivaara *et al*, 1994; Trisi *et al*, 1999). Though other studies (Mustafa *et al*, 1998; Larsson *et al*, 1997) found that bone derived cells behave differently to fibroblast cells we found a similarity between the behaviour of fibroblast and osteoblasts-like cells. Fibroblast and osteoblasts-like cells are anchorage dependant cells (Brunette, 1988; Zreigat *et al*, 1996) and therefore it can be assumed that their behaviour would be similar.

The tendency of cells to proliferate on a surface appears to be dependent on the surface topography (see 2.6.2, p29). From this investigation smoother surfaces have been observed to enhance proliferation and spreading probably because of the presence of focal contacts while on rougher surfaces % proliferation and attachment was related to the presence of filopodia.

6.5 Scanning Electron Microscopy

Scanning Electron Microscopy of samples revealed that the fibroblast and osteoblasts-like cells had a similar mechanism of attachment and proliferation depending on the surface encountered. On surfaces with smoother topography cells were observed to be in close contact with each other and formed very close contact with the surface adapting to the underlying topography. On surfaces with a rougher topography the spread or suspended cells exhibited irregular polygonal shapes with gaps or spaces where there was no area of contact. As the adhered cells formed a layer of differently shaped suspended cells over the surface it was difficult to determine the underlying topography. On surfaces that were observed to have a lower % proliferation scanning electron micrographs revealed that there were a lot of empty spaces between the attached cells (see Fig 5-58, p126).

After inoculation, cells settled on the surface of samples by gravitation. Though we did not view the different stages of cell adhesion, it can be hypothesized that once cells settle they react to the encountered surface by the production of filopodia. Extensions of filopodia are indicative of cell spreading (Keller *et al*, 1994). Possibly the filopodia that are produced by the cell have specific functions, namely for exploratory purposes and attachment purposes. The attachment filopodia are presumably shorter in length and used for suspending the cell once it has attached to a point while the exploratory filopodia are normally longer and thicker. The length of the exploratory filopodia is probably determined by the absence of attachment sites within the vicinity of the cell stimulating the cell to continue the search for attachment sites. It is possible that along the path that the exploratory filopodia takes, attachment filopodia are formed when contact points are met. Bagambisa & Joos (1990) have

reported filopodia of as long as 120 μ m over the surfaces they studied (regular surface).

On smooth surfaces it is assumed that filopodial extension of a cell move in all directions in search of points to adhere. After a failed attempt to find points of attachment on the smooth surface the filopodia are seen to coalesce together by the spread of the cytoplasm to the filopodia causing the cell to flatten maintaining a circular shape. The circular shape of the cell is probably a result of absence of points of tension within the cell that cause the cytoplasm to move in different directions. After the cell has flattened there are still few filopodia that emerge and probably still in search for a point of attachment to which it can attach itself. According to Brunette (1986b) filopodia were found to increase in length with time and have been found to play an important role in cell spreading and that contact however was not required for cell spreading as most isolated cells became fully spread. As the number of spread cells increased it was difficult to differentiate one cell from another as cells on the surface were viewed as a unit of cytoplasm that was in close contact to the underlying topography of the surface. Shelton *et al* (1988) also observed that cells on smooth surfaces eventually formed very close contact with the surface adapting to the underlying topography. Since cells are not attached but just spread over the underlying surface, proliferation is probably an easy task as the cells do not have to detach before proliferation, explaining why the smoother surfaces had a higher % of proliferated cells.

On irregular surfaces that consisted of peaks and valleys filopodia were observed around the entire surface of the cells and extending in all directions (see Fig 5-66, p133). It is presumed that for a cell to adhere to a surface there must be areas (points) to which the filopodia can attach and these points are assumed to be the peaks. Filopodia observed were of

different types, some were short and attached to nearby peaks while others were tapered and some even extended over depression and valleys in search of attachment sites. Ohara & Buck (1979) found that cells did not follow the finer surface contours but bridged over the grooved areas. Where there was no area of contact the cytoplasmic extensions continued over the surface until they found a place to attach. When cells that had settled encountered a surface that had surrounding peaks most of its filopodia were observed to attach to these peaks. After attachment of the filopodia to the peaks the cell cytoplasm was observed to lift off the surface and spread between its filopodia. Depending on the number of attachment points that also acted as tension points the cell was observed to acquire its shape. Using these attached filopodia the cell was then able to suspend itself to the surface creating a gap or space beneath. It is probably the tension that is created within the cell that causes the cell to lift off the surface.

Since most of man's functions are determined by impulses due to different charges generated, it is also assumed that for an attraction to occur between two surfaces they must be of different charge. It is possible that the filopodia are of a different charge to the peaks that they seek. According to Tengvall & Lundstrom (1992) Titanium is covered by a surface layer of oxide which is only weakly negatively charged under physiological conditions. It also appears that the filopodia are rigid enough to bridge over surfaces in search of the opposite charge. When a flat or smooth surface is encountered there probably is no charge on the surface explaining why the cell spreads but does not attach. According to Weiss (1978) most biosurfaces carry a net negative surface charge and net positively charged surfaces are not encountered in mammals.

Many researchers (Thomas *et al*, 1987; Mustafa *et al*, 1998; Ellingsen, 1998; Lazzara *et al*, 1999; Abron *et al*, 2001) have reported higher bone-implant-contact for the rougher surfaces

compared to the smoother surfaces and the probable reason could be the many adhesion points over a rough surface in comparison to the smooth surface where cells were spread more but with no contact.

The data from this study indicates that numerous parameters can be measured or identified as an indicator for potential bio-acceptability. Since there were no significant differences in the bio-acceptability between samples it was difficult to relate the effects of chemical analysis of samples investigated. Probably the time interval of the study was not adequate enough to determine the effects of the different elements found on the surfaces of samples with emphasis on Sodium and Aluminium that was introduced by the process of grit blasting (see 6.1, p140). The immediate effect of the oxide thickness was also not obvious but the importance of an oxide of adequate thickness and stoichiometric make up is emphasized, as it will prevent the dissolution of elements (see 2.1.5, p10). It is also probably the oxide crystals that determine the surface charge of the peaks that is necessary for cell attachment. Surface topography was able to display its immediate effects from the % proliferation and attachment of cells.

6.6 Bio-acceptability

The bio-acceptability of machined and cast cpTi and Ti6Al4V from results of this investigation showed no significant differences in terms of % attachment efficiency and proliferation. Surface enhancement that was used as a tool to increase the surface topography also was not able to display any significant differences between the control surfaces and the enhanced surfaces in terms of % attachment efficiency and proliferation. Scanning electron micrographs were able to emphasize the difference in cell morphology as seen on smooth and rough surfaces. Cells (as determined by surface analysis)

were found to attach rather than to spread on the rougher surfaces investigated. The chemical analysis of cast and enhanced samples was similar, probably because the grit blasting process influenced the outer surface of these samples. Grit blasting was used as a method of surface enhancement and for the devesting of cast samples. The oxide layer was significantly thicker for the cast and enhanced surfaces than for the machined control surfaces but no differences were observed in terms of bio-acceptability. RFGDT was significantly able to reduce all contaminants that were introduced from the different sample processing methods with the exception of Sodium and Aluminium that were not affected. The effect of Sodium and Aluminium concentration on bio-acceptability was not noted probably due to the time interval of the study.

Using the results from this investigation that has confirmed the bio-acceptability of cast surfaces, the fabrication of cost effective implants using Titanium alloy is possible. The desired strength that the alloy possesses together with its ease in availability and affordable custom made appliances prepared by casting would have the same results in bio-acceptability. The bio-acceptability of the fabricated cast Titanium alloy implants could also be enhanced employing grit blasting of specific size to ensure the desired surface topography that will determine the peaks and valleys. RFGDT could be utilized as a method of producing a stoichiometric oxide for even better bio-acceptability.

CHAPTER 7 CONCLUSIONS AND RECOMMENDATIONS

7.1 Conclusions

From this study that investigated the surface characteristics and *in vitro* bio-acceptability of Titanium and Titanium alloy the following can be concluded:

1. Chemical Analysis:

- a) Chemical and elemental composition of cpTi and Ti6Al4V surfaces showed no significant differences when analysed for their atomic % concentration and the curve fitting for the different elements detected on their surface.
- b) Casting of samples introduced Sodium and Aluminium to the surface in comparison to the machining of samples that did not have these elements on their surfaces. The Oxygen peak of cast samples showed more sub peaks from peak fitting compared to the machined samples and the Titanium peak indicated mostly TiO₂.
- c) Surface enhancement of samples regardless of the size of grit particles used introduced the presence of Sodium and Aluminium onto the surface of the samples.

2. Surface topography

- a) Materials used (cpTi and Ti6Al4V) in the fabrication of samples were of no significance in determining the surface topography of the samples.
- b) Surface topography was determined by the fabrication procedure and the cast samples were found to have a

significantly rougher surface topography compared to machined samples.

3. Depth profiles

- a) The oxide thickness of the different materials used (cpTi and Ti6Al4V) for the preparation of samples was not statistically different.
- b) The cast samples had a significantly higher oxide thickness than the machined samples.
- c) Surface enhancement significantly increased the oxide thickness.

4. Radio Frequency Glow Discharge Treatment (RFGDT)

- a) There was a significant reduction in the surface Atomic % concentration of Carbon and a resultant significant increase in Oxygen and Titanium with RFGDT. Aluminium and Sodium were not affected by RFGDT but most of the smaller signals from Calcium, Zinc, Lead, Nitrogen, etc were removed from surfaces by RFGDT.
- b) Surface area of samples and the R_p value of the 20 μ m scan were significantly increased by RFGDT.
- c) The oxide thickness was significantly increased by RFGDT.

5. Bio-acceptability

- a) Fibroblasts were observed to increase their % attachment efficiency and proliferation (%AEP) with time while osteoblasts-like cells were observed to decrease their %AEP with time.

- b) The reaction of fibroblasts and osteoblasts-like cells to cpTi and Ti6Al4V showed no significant differences between the materials.
- c) Though no significant differences were found between the machined and cast samples in terms of %AEP of fibroblasts and osteoblasts-like cells, machined samples were observed to have a higher %AEP than cast samples.
- d) Surface enhancement of samples showed no significant differences in the %AEP of fibroblasts and osteoblasts-like cells. Machined cpTi ES enhanced samples had a similar %AEP of fibroblasts to the control, unlike the other enhanced samples that had a much lower %AEP. Machined Ti6Al4V SI and cast Ti6Al4V control samples had relatively higher %AEP for osteoblasts-like cells than the other samples.
- e) Scanning Electron Micrographs revealed that cells over the machined control samples had spread and proliferated more than the other samples showing the underlying topography of the sample. Cells on the cast and enhanced surfaces were observed to have attached to the peaks and were not in contact with the underlying surface but suspended over the surface and of irregular shapes.
- f) After different surface characterization processes, cast cpTi and Ti6Al4V samples showed similar results in terms of bio-acceptability when compared to the proprietary innovative characterized implant surfaces.

7.2 Recommendations

The results from this study identified numerous opportunities for future research:

- 1) Further development and testing of the cast surfaces are needed to optimise the blasting particle size for the devesting of cast samples and to determine the degree of roughness desired for better osseointegration.
- 2) The long-term effect of the blasting particles (Aluminium) that get embedded onto the surface should be analysed for their effect on bio-acceptability.
- 3) Alternative methods of devesting of cast samples should be evaluated.
- 4) The optimal oxide thickness and the stoichiometry of the cast samples should be defined and evaluated.
- 5) Increased used of cast Titanium in the dental fraternity will depend on clinical trials to compare the effectiveness of cast Titanium as an equivalent or superior design for osseointegration.
- 6) As casting changes the crystalline structure, further investigations should link the relationship of the oxide formed to the underlying crystalline structure.
- 7) Further study of cellular and tissue responses, particularly long-term studies of expression of cell phenotype, would help explicate the importance of surface micro-morphology on biological response.
- 8) The difference between cell attachment and spreading should be defined, as there may be a difference between contact, initial adhesion, later adhesion and detachment before mitosis.

- 9) The optimal RFGDT of cast samples for better bio-acceptability should be elucidated.
- 10) Histomorphometric analysis of cast samples following defined surface topography.
- 11) Further studies are warranted to determine the effect of surface roughness on osteoblasts attachment and proliferation.
- 12) Comparative biological evaluation of cast samples in relation to machined samples using epithelial cells will indicate its bio-acceptability in terms of the cast surface.
- 13) Defining the peak and valley heights and distance on the surface of cast samples will help to determine the optimal deviation for improved attachment of cells.



CHAPTER 8 REFERENCES

- Aaboe M, Schou S, Hjorting-Hanssen E, Helbo M & Vikjaer D (2000) Osseointegration of subperiosteal implants using bovine bone substitute and various membranes. *Clinical Oral Implants Research*, 11:51-58.
- Abron A, Hopfensperger M, Thompson J & Cooper LF (2001) Evaluation of a predictive model for implant surface topography effects on early osseointegration in a rat tibia model. *Journal of Prosthetic Dentistry*, 85:40-46.
- Albrektsson T & Jacobsson M (1987) Bone-metal interface in osseointegration. *Journal of Prosthetic Dentistry*, 57:597-607.
- Albrektsson T (1989) In vivo performance of metallic dental implants. In: Satcos JC, Williams KJ. Transactions of the Academy of Dental Materials. Proceedings of conference on correlations between in-vitro and in-vivo performance of dental materials, Trinity College, Dublin, Ireland. 2:143-147.
- Albrektsson T (1993) On long term maintenance of the osseointegrated response. *Australian Prosthodontic Journal*, 7:15-24 (Suppl).
- Albrektsson T, Branemark P-I, Hansson H-A & Lindstrom J (1981) Osseointegrated titanium implants. Requirements for ensuring a long lasting direct bone-to-implant anchorage in man. *Acta Orthopaedica Scandinavica*, 52:155-170.
- Albrektsson T, Branemark P-I, Hansson H-A, Kasemo B, Larsson K, Lundstrom I, McQueen DH & Skalak R (1983) The interface zone of inorganic implants in vivo: Titanium implants in bone. *Annals of Biomedical Engineering*, 11:1-27.
- Albrektsson T (1985) The response of bone to titanium implants. *CRC Critical Reviews of Biocompatibility*, 1:53-84.
- Al-Mesmar HS, Morgano SM & Mark LE (1999) Investigation of the effect of 3 sprue designs on the porosity and the completeness of titanium cast removable partial denture frameworks. *Journal of Prosthetic Dentistry*, 82:15-21.
- Amstein CF & Hartman PA (1975) Adaptation of plastic surfaces for tissue culture by glow discharge. *Journal of Clinical Microbiology*, 2:46-54.
- Anonymous (1991) Advanced Arc-casting System, CYCLARC, Operational Instructions, Vol 2. Kyoto, J Morita Corporation.
- Anonymous (1996) Visualizing the Micro World, Santa Clara, USA.
- Anselme K, Bigerelle M, Noel B, Dufresne E, Judas D, Tost A & Hardouin P (2000) Qualitative and quantitative study of human osteoblast adhesion on materials with various surface roughness. *Journal of Biomedical Materials Research*, 49:155-166.
- Aronsson B-O, Lausmaa J & Kasemo B (1997) Glow discharge plasma treatment for surface cleaning and modification of metallic biomaterials. *Journal of Biomedical Materials Research*, 35:49-73.
- Arys A, Philippart C, Dourov N, He Y, Le QT & Pireaux JJ (1998) Analysis of titanium dental implants after failure of osseointegration: combined histological, electron microscopy, and x-ray photoelectron spectroscopy approach. *Journal of Biomedical Materials Research*, 43:300-312.



- Ask M, Lausmaa J & Kasemo B (1988) Preparation and surface spectroscopic characterization of oxide films on Ti6Al4V. *Applied Surface Science*, **35**:283-301.
- ASTM (1995) Annual Book of ASTM Standards. F 67-95: Standard Specification for Unalloyed Titanium for surgical Implant applications. Volume F4. Section F04.12. Philadelphia: American Society For Testing and Biomaterials, p 1-3.
- ASTM (1997) Annual Book of ASTM Standards. F 86-91: Standard practice for surface preparation and marking of metallic surgical implants. Volume 13, Section 13.01. Philadelphia: American Society For Testing and Biomaterials, p 6-8.
- ASTM (1999) Annual Book of ASTM Standards. B 348-99: Standard Specification for Titanium and Titanium Alloy Bars and Billets. Volume 10, Section 10.01. Philadelphia: American Society For Testing and Biomaterials, p 201.
- Bagambisa FB & Joos D (1990) Preliminary studies on the phenomenological behaviour of osteoblasts cultured on hydroxyapatite ceramics. *Biomaterials*, **11**:50-56.
- Baier RE & De Palma VA (1970) Electrodeless glow discharge cleaning and activation of high energy substrates to insure their freedom from organic contamination and their receptivity for adhesives and coatings. Calspan Corporation, Advanced Technology Centre, NY, Report No. 176.
- Baier RE & Meyer AE (1988) Implant surface preparation. *International Journal of Oral & Maxillofacial Implants*, **3**:9-20.
- Baier RE, Meyer AE, Akers CK, Natiella JR, Meenaghan M & Carter JM (1982) Degradative effects of conventional steam sterilization on biomaterial surfaces. *Biomaterials*, **3**:241-245.
- Baier RE, Meyer AE, Natiella JR, Natiella RR & Carter JM (1984) Surface properties determine bioadhesive outcomes: methods and results. *Journal of Biomedical Materials Research*, **18**:327-355.
- Baun WL (1982) Analysis of metal surfaces by ion spectroscopy in surface analysis and pretreatment of metals and plastics. Brewis DM (ed.), McMillan, New York. P45-72.
- Beder CE & Ploger WJ (1959) Intraoral titanium implants. *Journal of Oral Surgery, Oral Medicine & Oral Pathology*, **12**:787-799.
- Bellows CG, Aubin JE, Heersche JN & Antosz ME (1986) Mineralised bone nodules formed in vitro from enzymatically released rat calvaria cell populations. *Calcified Tissue International*, **38**:143-154.
- Bessing C & Bergman M (1992) The castability of unalloyed titanium in three different casting machines. *Swedish Dental Journal*. **16**:109-113.
- Binon P, Weir D & Marshall S (1992) Surface analysis of an original Branemark implant and three related clones. *International Journal of Oral & Maxillofacial Implants*, **7**:168-175.
- Botha SJ (1995) The definition and the implementation of an in vitro fibroblast model to evaluate the bio-acceptability of titanium surfaces in dentistry. PhD thesis, Faculty of Dentistry University of Pretoria, p 44-46, 115-136.
- Bowers KT, Keller JC, Randolph BA, Wick DG & Michaels CM (1992) Optimization of surface micromorphology for enhanced osteoblast response in vitro. *International Journal of Oral & Maxillofacial Implants*, **7**:302-310.



- Boyan BD, Hummert TW, Dean DD & Schwartz Z (1996) Role of material surfaces in regulating bone and cartilage cell response. *Biomaterials*, 17:137-146.
- Boyd DW & Kustin K (1984) Vanadium: A versatile biochemical effector with an elusive biological function. *Advances in Inorganic Biochemistry*, 6:411-465.
- Branemark PI (1983) Osseointegration and its experimental background. *Journal of Prosthetic Dentistry*. 50:399-410.
- Branemark PI, Hansson BO, Adell R, Breine U, Lindstrom, Hallen O & Ohman A (1977) Osseointegrated implants in the treatment of the edentulous jaw. Experience from a ten-year period. *Scandinavian Journal of Plastic and Reconstructive Surgery, Suppl* 16:1-132.
- Branemark P-I, Zarb G & Albrektsson T (1985) *Tissue integrated Prosthesis: Osseointegration in Clinical Dentistry*. Chicago:Quintessence Publ. Co.
- Bruneel N & Helsen JA (1988) In vitro simulation of biocompatibility of Ti-Al-V. *Journal of Biomedical Materials Research*, 22:203-214.
- Brunette DM (1986a) Spreading and orientation of epithelial cells on grooved substrata. *Experimental Cell Research*, 167:203-217.
- Brunette DM (1986b) Fibroblasts on micromachined substrata orient hierarchically to grooves of different dimensions. *Experimental Cell Research*, 164:11-26.
- Brunette DM (1988) The effects of implant surface topography on the behavior of cells. *International Journal of Oral & Maxillofacial Implants*, 3:231-246.
- Brunette DM, Melcher AH & Moe HK (1976) Culture and origin of epithelium-like and fibroblast-like cells from porcine periodontal ligament explants and cell suspensions. *Archives of Oral Biology*, 21:393-400.
- Brunski JB, Puleo DA & Nanci A (2000) Biomaterials and biomechanics of oral and maxillofacial implants: Current status and future developments. *International Journal of Oral & Maxillofacial Implants*, 15:15-46.
- Bullock GR & Petrusz P (1985) *Techniques in Immunochemistry*. London: Academic Press.
- Buser D (1999) Effects of various titanium surface configurations on osseointegration and clinical implant stability. *Proceedings of the 3rd European Workshop on Periodontology, Implant*. Quintessence Publ. p 88-101.
- Buser D, Nydegger T, Hirt HP, Cochran DL & Nolte L-P (1998) Removal torque values of titanium implants in the maxilla of miniature pigs. *International Journal of Oral & Maxillofacial Implants*, 13:611-619.
- Buser D, Schenk RK, Steinemann S, Fiorellini JP, Fox CH & Stich H (1991) Influence of surface characteristics on bone intergration of titanium implants. A histomorphometric study in miniature pigs. *Journal of Biomedical Materials Research*, 25:889-902.
- Calandrelli L, Immirzi B, Malinconico M, Orsello G, Volpe MG, Ragione FD, Zappia V & Oliva A (2002) Biocompatibility studies on biodegradable polyester-based composites of human osteoblasts: a preliminary screening. *Journal of Biomedical Materials Research*, 59:611-617.
- Carlsson LV, Albrektsson T & Berman C (1989) Bone response to plasma-cleaned titanium implants. *International Journal of Oral and Maxillofacial Implants*, 4:199-204.
- Chehoudi B, Gould TRL & Brunette DM (1989) Effect of surface topography on epithelial and connective tissue attachment. *Journal of dental Research*, 68:306 (Abstr. 998) (Special Issue).



- Chen WT (1981) Surface changes during retraction induced spreading of fibroblasts. *Journal of Cell Science*, 49:1-13.
- Cheung HS & Haak MH (1989) Growth of osteoblasts on porous calcium phosphate ceramic: an in vitro model for biocompatibility study. *Biomaterials*, 10:63-67.
- Clavin TJ, Keller NC, Wick DG & Stanford CM (1990) Development of a model for cell attachment. *Journal of Dental Research*, 69:369.
- Cochran DL (1999) A comparison of endosseous dental implant surfaces. *Journal of Periodontology*, 70:1523-1539.
- Cooper LF, Handelman B, McCormack SM & Guckes AD (1993) Binding of murine osteoblastic cells to titanium discs and collagen I gels: implications for alternative interpretations of Osseointegration. *International Journal of Oral & Maxillofacial Implants*, 8:264-272.
- Cooper LF, Matsuda T, Ylisaukka-Kala PK & Felton DA (1998) Generalizations regarding the process and the phenomenon of osseointegration. Part II. In vitro studies. *International Journal of Oral & Maxillofacial Implants*, 13:163-74.
- Culp LA (1978) Biochemical determinants of cell adhesion. In *Current Topics in membranes and transport*, Volume II. Academic press, Inc. p.327-396.
- Curtis RV (1998) Stress-strain and thermal expansion characteristics of a phosphate bonded investment mould material for dental super plastic forming. *Journal of Dentistry*, 26:251-258.
- Darvell BW, Samman N, Luk WK, Clark RKF & Tideman H (1995) Contamination of titanium castings by aluminium oxide blasting. *Journal of Dentistry*, 23:319-322.
- Davies JE (1988) In vitro assessment of bone biocompatibility. *International Endodontic Journal*, 21:178-187.
- Davies JE (1989) In vitro and vivo performance of non-metallic dental implants. Proceedings on conference on correlation between in vitro and in vivo performances of dental materials. June 2:148-166. Held at Trinity College, Dublin, Ireland.
- Davies JE (1998) Mechanism of endosseous integration. *International Journal of Prosthodontics*, 11:391-401.
- Davies JE, Lowenberg B & Shiga A (1990) The bone-titanium interface in vitro. *Journal of Biomedical Materials Research*, 24:1289-1306.
- Davies JE, Price NM & Matsuda T (1989) In vitro biocompatibility assays which employ bone derived cells. In *Oral Implantology and Biomaterials*, ed Kawahara H. Elsevier Science Publishers B.V., Amsterdam, Printed in the Netherlands, p 197-203.
- Dmytryk JW, Fox SC & Moriarty JD (1990) The effects of scaling titanium implant surfaces with metal and plastic instruments on cell attachment. *Journal of Periodontology*, 61:491-496.
- Donachie MH (1984) Titanium: A technical guide. Metal Park, OH: ASM International. p 43-51.
- Doundoulakis JH (1987) Surface analysis of titanium after sterilization: Role in implant-tissue interface and bioadhesion. *Journal of Prosthetic Dentistry*, 58:471-478.
- Dowben P (1994) In "Surface Segregation Phenomena", In: Dowben P & Miller A., eds. Ch 6. Ann Arbor:CRC Press.
- Ellingsen JE (1998) Surface configurations of dental implants. *Periodontology 2000*, 17:36-46.



- Esposito M, Lausmaa J, Hirsch J-M & Thomsen P (1999) Surface analysis of failed oral implants. *Journal of Biomedical Materials Research*, 48:559-568.
- Fassel V (1978) Quantitative elemental analysis by emission spectroscopy. *Science*, 202:183-191.
- Frandsen PA, Christoffersen H, & Madsen T (1984) Holding power of different screws in the femoral head. A study in human cadaver hips. *Acta Orthopaedica Scandinavica*, 55:349-351.
- Gail MH & Boone CW (1972) Cell substrate adhesivity - a determinant of cell motility. *Experimental Cell Research*, 70:33-40.
- Glantz P-O (1998) The choice of alloplastic materials for oral implants: Does it really matter? *The International Journal of Prosthodontics*, 11:402-7.
- Gotfredsen K, Harder F, Hildestad P & Hjorting-Hansen E (1988) Explanation of ITI implants type F. *Danish Dental Journal*, 92:102-5.
- Gotfredsen K, Nimh L, Hjorting-Hansen E, Jensen JS & Holmen A (1992) Histomorphometric and removal torque analysis for TiO₂-coated titanium implants. An experimental study on dogs. *Clinical Oral Implants Research*, 3:77-84.
- Grinnel F & Bennett MH (1981) Fibroblast adhesion on collagen substrata in the presence and absence of plasma fibronectin. *Journal of Cell Science*, 48:19-34.
- Grinnell F, Milam M & Sate PA (1973) Adhesion of baby hamster kidney cells. *Journal of Cell Biology*, 56(3):659-665.
- Groessner-Schreiber B & Tuan RS (1992). Enhanced extracellular matrix production and mineralization by osteoblasts cultured on titanium surfaces in vitro. *Journal of Cell Sciences*. 101:209-217.
- Guy SC (1976) *Essentials of Material Science*. New York, McGraw-Hill Book Co., pp 328-330.
- Guy SC, McQuade MJ, Scheidt MJ, McPherson JC, Rossmann JA & Van Dyke TE (1993) In vitro attachment of human gingival fibroblasts to endosseous implant materials. *Journal of Periodontology*, 64:542-546.
- Hahn H & Palich W (1970) Preliminary evaluation of porous metal surfaced titanium for orthopedic implants. *Journal of Biomedical Materials Research* 4:571-577.
- Hakkinen L, Yli-Urpo A, Heino J & Larjava H (1988) Attachment and spreading of human gingival fibroblasts on potentially bioactive glasses in vitro. *Journal of Biomedical Materials Research*, 22:1043-1059.
- Ham AW (1969) *Histology*. Lippincott, Philadelphia, pp 388-391.
- Hamanaka H, Doi H, Yoneyama T & Okuno O (1989) Dental casting of titanium and Ni-Ti alloys by a new casting machine. *Journal of Dental Research*, 68:1529-1533.
- Harris M (1959) Growth measurements on monolayer cultures with an electronic cell counter. *Cancer Research*. 19:1020-1024.
- Hartman LC, Meenaghan MA, Schaaf NG & Hawker PB (1989) Effects of pretreatment sterilization and cleaning methods on materials properties and osseointegrativity of a threaded implant. *International Journal of Oral & Maxillofacial Implants*, 4:11-18.
- Heckmann M & Krieg T (1989) Biological and pharmacological modulations of fibroblast functions. *Skin Pharmacology*, 2:125-137.



- Helsing M. (1997). Comparative surface analysis of four dental implant systems. *Journal of the Dental Association of South Africa*, 52:399-402.
- Hobo S, Ichida E & Garcia LT (1989) Osseointegration and occlusal rehabilitation. Chicago: Quintessence. P 3-104.
- Ida K, Tsutsumi S & Togaya T (1984) Titanium or titanium alloys for dental casting. *Journal of Dental Research*, 63:985-993.
- Inoue T, Cox JE, Pilliar RM & Melcher AH (1987) Effect of the surface geometry of smooth and porous-coated titanium alloy on the orientation of fibroblasts in vitro. *Journal of Biomedical Research*, 21:107-126.
- Ishaug SL, Crane GM, Miller RJ, Pasko AW, Yaszemski MJ & Mikos AG (1997) Bone formation by three-dimensional stromal osteoblast culture in biodegradable polymer scaffolds. *Journal of Biomedical Materials Research*, 36:17-28.
- Itakura Y, Kosugi A, Sudo H, Yamamoto S & Kumegawa M (1988) Development of a new system for evaluating the biocompatibility of implant materials using an osteogenic cell line (MC3T3-E1). *Journal of Biomedical Materials Research*, 22:613-622.
- Ito A, Okazaki Y, Tabeiishi T & Ito Y (1995) In vitro biocompatibility, mechanical properties and corrosion resistance of Ti-Zr-Nb-Ta-Pd and Ti-Sn-Nb-Ta-Pd alloys. *Journal of Biomedical Materials Research*, 29:893-900.
- Ivanoff CJ, Sennethy L & Lekholm U (1996) Influence of soft tissue contamination on the integration of titanium implants. An experimental study in rabbits. *Clinical Oral Implantology Research*, 7:128-132.
- Kamen PR (1988) Attachment of oral fibroblasts to HTR polymer. *Compendium Continuing Education Dentistry*, Suppl No 10:3350-352.
- Kamen PR (1989) Attachment of human Oral fibroblasts to a granular polymeric implant for hard tissue replacement. *Journal of Oral Implantology*, XV:52-56.
- Kasemo B & Lausmaa J (1986) Surface science aspects on inorganic biomaterials. *CRC Critical Reviews on Biocompatibility*, 2:335-380.
- Kasemo B & Lausmaa J (1988b) Biomaterial and implant surfaces: on the role of cleanliness, contamination and preparation procedures. *Journal of Biomedical Materials Research*, 22:145-158 (Suppl. A2).
- Kasemo B & Lausmaa J (1988a). Biomaterial and implant surfaces: A surface science approach. *International Journal of Oral & Maxillofacial Implants*, 3:247-259.
- Kasemo B & Lausmaa J (1991) The biomaterial-tissue interface and its analogues in surface science and technology. In *Bone Biomaterial Interface*. ed. Davies JE. University of Toronto Press, Toronto. p27.
- Kasemo B (1983) Biocompatibility of titanium implants: Surface science aspects. *Journal of Prosthetic Dentistry*, 49(6):832-837.
- Kasten FH, Solleau K & Meffert RM (1990) Quantitative evaluation of human gingival epithelial cell attachment to implant surfaces in vitro. *International Journal of Periodontics & Restorative Dentistry*, 10:69-79.
- Kawahara H, Yamagami A & Nakamura M (1968) Biological testing of dental materials by means of tissue culture. *International Dental Journal*, 18:443-467.



- Keller JC, Draughn RA, Wightman JP, Dougherty WJ & Melatiou SD (1990) Characterization of sterilized cp titanium implant surfaces. *International Journal of Oral & Maxillofacial Implants*, 5:360-67.
- Keller JC, Stanford CM, Wightman JP, Draughn RA & Zaharias R (1994) Characterization of titanium implants surfaces. III. *Journal of Biomedical Materials Research*, 28:939-946.
- Keller JC, Wightman JP, Draughn RA & Dougherty WJ. (1989). Characterization of acid passivated cpTi surfaces. *Journal of Dental Research*, 68:872.
- Kieswetter K, Schwartz Z, Dean DD & Boyan BD (1996) The role of implant surface characteristics in the healing of bone. *Critical Reviews of Oral Biology and Medicine*, 7:329-345.
- Kieswetter K, Schwartz Z, Rummert TW, Cochran DL, Simpson J, Dean DD & Boyan BD (1996) Surface roughness modulates the local production of growth factors and cytokines by osteoblast-like MG-63 cells. *Journal of Biomedical Materials Research*, 32:55-63.
- Kilpadi DV, Lemons JE, Liu J, Raikar GN, Weimer JJ & Vohra Y (2000) Cleaning and heat-treatment effects on unalloyed titanium implant surfaces. *International Journal of Oral & Maxillofacial Implants*, 15:219-230.
- Kilpadi DV, Raikar GN, Liu J, Lemons JE, Vohra Y, & Gregory JC (1998a) Effect of surface treatment on unalloyed titanium implants: Spectroscopic analysis. *Journal of Biomedical Materials Research*. 40:646-659.
- Kilpadi DV, Weimer JJ, Lemons JE (1998b) Effects of passivation and dry heat-sterilization, surface energy and topography of unalloyed titanium implants. *Colloids and Surfaces A: Physicochemical and engineering aspects*, 135:89-101.
- Kittel C (1996) Introduction to the solid state physics. Chp 7 and 11. 7th ed J Wiley & Sons.
- Klauber C, Lenz LJ & Henry PJ (1990) Oxide thickness and surface contamination of six endosseous dental implants determined by electron spectroscopy for chemical analysis: A preliminary report. *International Journal of Oral & Maxillofacial Implants*, 5:264-271.
- Klokkevold P (2002) Surface enhancement to optimize the success of dental implants. *Dental Implantology Update*. 13:17-23.
- Kononen M, Hormia M, Kivilathi J, Hautaniemi J & Thesleff I (1992) Effect of surface processing on the attachment, orientation and proliferation of human gingival fibroblasts on titanium. *Journal of Biomedical Materials Research*, 26:1325-1341.
- Krozer A, Hall J & Ericsson I (1999) Chemical treatment of machined titanium surfaces. An in vitro study. *Clinical Oral Implants Research*. 10:204-211.
- Kurachi T, Nagao H, Nagura H & Enomoto S (1997) Effect of a titanium surface on bone marrow-derived osteoblastic cells in vitro. *Archives of Oral Biology*, 42:465-8.
- Larsson C (2000) The interface between bone and implants with different surface oxide properties. *Applied Osseointegration Research*, 1:9-14.
- Larsson C, Emanuelsson L, Thomsen P, Ericson E, Aronsson B.-O, Kasemo B & Länsmää J (1997) Bone response to surface modified titanium implants- Studies on the tissue response after 1 year to machined and electropolished implants with different oxide thickness. *Journal of Material Sciences: Materials in Medicine*, 8:721-729.



- Lausmaa J, Ask M, Halander U & Kasemo B (1989) Preparation and analysis of Ti surfaces used in the evaluation of biological response. *Mater Res Soc Symp Proc*, 110:647-653.
- Lausmaa J, Kasemo B & Mattsson H (1990) Surface spectroscopic characterization of Titanium implant materials. *Applied Surface Science*, 44:133-144.
- Lausmaa J, Kasemo B, & Hansson S (1985) Accelerated oxide growth on titanium implants during autoclaving caused by fluorine contamination. *Nanomaterials*, 6:23-27.
- Lazzara RJ, Testori T, Tripi P, Porter SS & Weinstein RL (1999) A human histological analysis of osseointegration and machined surfaces using implants with 2 opposing surfaces. *International Journal Periodontics & Restorative Dentistry*, 19:117-129.
- Lemons J (1986) Implant dentistry forefront '85. Surface evaluation of materials. *Journal of Oral Implantology*, 12:396-405.
- Lemons JE (1990) Interactions of dental biomaterials with bone. Proceedings of conference on Enamel-Dentine-Pulp Bone-Periodontal tissue interactions with dental materials. 3:96-109. Transactions of the Academy of Dental materials.
- Lim YJ, Oshida Y, Andree CJ & Barco MT (2001) Surface characterizations of variously treated titanium materials. *International Journal of Oral & Maxillofacial Implants*, 16:333-342.
- Linder L (1985) High-resolution microscopy of the implant tissue interface. *Acta Orthopaedica Scandinavica*, 56:269-272.
- Low CW (1997) The oxidation of titanium and its alloys. Phd Thesis. University of Orange Free State, Bloemfontein, South Africa. p44,45,125.
- Low D, Sumii T & Swain M (2001) Thermal expansion coefficient of titanium casting. *Journal of Oral Rehabilitation*, 28:239-242.
- Lugowski S, Smaith DC & van Loon JC (1987) The determination of titanium and vanadium in whole blood. *Trace Elements in Medicine*, 4:28-35.
- Lumbikanonda N & Sammons R (2001) Bone cell attachment to dental implants of different surface characteristics. *International Journal of Oral & Maxillofacial Implants*, 16:627-636.
- Machnee CH, Wagner WC, Jaarda MJ & Lang BR (1993) Identification of oxide layers of commercially pure titanium in response to cleaning procedures. *International Journal of Oral & Maxillofacial Implants*, 8:529-533.
- Maniopoulos C, Sodek J & Melcher AH (1988) Bone formation in vitro by stromal cells obtained from bone marrow of young adult rats. *Cell and Tissue Research*, 254:317-330.
- Marmary Y, Brunette DM & Heersche JNM (1976) Differences in vitro between cells derived from periodontal ligament and skin of *Macaca irus*. *Archives of Oral Biology*, 21:709-716.
- Martin JY, Schwartz Z, Hummert TW, Schraub DM, Simpson J, Lankford J, Jr, Dean DD, Cochran DL & Boyan BD (1995) Effect of titanium surface roughness on proliferation, differentiation and protein synthesis of human osteoblast-like cells (MG63). *Journal of Biomedical Materials Research*, 29:389-401.
- Matsuda T, Yamauchi K & Ito G (1987) The influence of bioglass on the growth of fibroblasts. *Journal of Biomedical Materials Research*, 21:499-507.



- Matsuda T, Yliheikka PK, Felton DA & Coopers LF (1998) Generalizations regarding the process and phenomenon of osseointegration. Part 1: In vivo studies. *International Journal of Oral & Maxillofacial Implants*, 13:17-29.
- Mattsson H (1990) Oxidation of titanium in aqueous solutions, Ph.D. thesis, Calmers University of Technology, Goteborg, Sweden.
- Meffert RM (1986) Endosseous dental implantology from the Periodontist's viewpoint. *Journal of Periodontology*, 57:531-536.
- Meffert RM (1997) Do implant surfaces make a difference? *Current Opinion in Periodontology*, 4:104-108.
- Mesaros MG (1989) Osseointegration and the dental endosseous titanium implant interface. *Journal of the Michigan Dental Association*, 71:269-275.
- Michaels CM, Keller JC, Stanford CM & Solursh M (1989) In vitro cell attachment of osteoblast-like cells to titanium. *Journal of Dental Research* (Special Issue), 68:376.
- Mittal KL (1979) "Surface contamination: An overview" in surface contamination: Genesis, detection and control, Vol 1, KL Mittal (ed.), Plenum Press, NewYork. p3-46.
- Miyakawa O, Watanabe K, Okawa S, Kanatani M, Nakano S & Kobayashi M (1996) Surface contamination of titanium by abrading treatment. *Dental Materials Journal*, 15:11-21.
- Miyakawa O, Watanabe K, Okawa S, Nakano S, Kobayashi M & Shiohara N (1989) Layered structure of cast titanium surface. *Dental Materials Journal*, 8:175-185.
- Mori T, Jean-Louis M, Yahugami M & Togaya T (1994) The effect of investment type on the fit of titanium crowns. *Australian Dental Journal*, 39:348-352.
- Morra M & Cassinelli C (1997) Organic surface chemistry on titanium surfaces via thin film deposition. *Journal of Biomedical Materials Research*, 37:198-206.
- Mouhy J, Sennerby L & Van Reck J (2000) The soft tissue response to contaminated and cleaned titanium surfaces using CO₂ laser, citric acid and hydrogen peroxide. *Clinical Oral Implant Research*, 11:93-98.
- Moulder JF, Stickle WF, Sobol PE & Bomben KD (1992) A Reference Book of Standard Spectra for Identification and Interpretation of XPS Data. Perkin-Elmer Corporation, Physical Electronics Division, Prairie, Minnesota. USA.
- Mugnolo G & Filliponi H (2001) Osseointegration of tissue functional rough TiO₂-blasted titanium implants: One year follow-up of 100 implants. *Dental Implantology Update*, 12:9-15.
- Mummery L (1992) Parameters Chapter 3 and Chapter 1 Surfaces. In: Surface Texture Analysis The Handbook. West Germany, Hommelwerke GmbH. THYSSEN. p 1-7; 23-33.
- Murai K, Takeshita F, Ayukawa Y, Kiyoshima T, Suetsugu T & Tanaka T (1996) Light and electron microscopic studies of bone-titanium interface in the tibia of young and mature rats. *Journal of Biomedical Materials Research*, 30:523-533.
- Mustafa K, Silva Lopez B, Hultenby K, Wennerberg A & Arvidson K (1998) Attachment and proliferation of human oral fibroblasts to titanium surfaces blasted with TiO₂ particles. *Clinical Oral Implants Research*, 9:195-207.



- Mustafa K, Wennerberg K, Wroblewski J, Hultenby K, Silva Lopez B, & Arvidson K (2001) Determining optimal surface roughness of TiO₂ blasted titanium implant material for attachment, proliferation and differentiation of cells derived from human mandibular alveolar bone. *Clinical Oral Implant Research*, 12:515-525.
- Mustafa K, Wroblewski J, Hultenby K, Silva Lopez B & Arvidson K (2000) Effects of titanium surfaces blasted with TiO₂ particles on the initial attachment of cells derived from human mandibular bone. A scanning electron microscopic and histomorphometric analysis. *Clinical Oral Implant Research*, 11:116-120.
- Nevins M & Langer B (1993) The successful application of osseointegrated implants to the posterior jaw: a long term retrospective study. *International Journal of Oral & Maxillofacial Implants*, 8:428-432.
- Oakley C & Brunette DM (1993) The sequence of alignment of microtubules, focal contacts and actin filaments in fibroblast spreading on smooth and grooved titanium substrata. *Journal of Cell Science*, 106:343-354.
- Ohara PT & Buck RC (1979) Contact guidance in vitro: A light transmission, and scanning electron microscopic study. *Experimental Cell Research*, 121:235-249.
- Ong JL & Lucas LC (1998) Auger electron spectroscopy and its use for characterization of titanium and hydroxyapatite surfaces. *Biomaterials*, 19:455-464.
- Ong JL, Lucas LC, Rånkäär GM & Gregory JC (1993) Electrochemical corrosion analyses and characterization of surface modified titanium. *Applied Surface Science*, 72:7-13.
- Orsini G, Assenza B, Scarano A, Piattelli M & Piattelli A (2000) Surface analysis of machined versus sandblasted and acid etched titanium implants. *International Journal of Oral & Maxillofacial Implants*, 15:779-784.
- Osborn JF & Newsley H (1980) Dynamics aspects of the implant-bone interface. In: Heimke G (ed.) *Dental Implants Materials and Systems*. Munich: Carl Haner. p. 111-123.
- Papadopoulos T, Tsetsekou A & Eliades G (1999) Effect of aluminium oxide sandblasting on cast commercially pure titanium surfaces. *European Journal of Prosthodontics & Restorative Dentistry*, 7:15-21.
- Parr GR, Gardner LK & Toth RW (1985) Titanium: The mystery metal of implant dentistry. Dental materials aspect. *Journal of Prosthetic Dentistry*, 54:410-414.
- Pilliar RM (1991) Modern metal processing for improved load-bearing surgical implants. *Biomaterials*, 12:95-100.
- Pilliar RM (1998) Overview of surface variability of metallic endosseous dental implants: Textured and porous surface-structured designs. *Implant Dentistry*, 7:305-314.
- Pilliar RM, Deporter DA, Watson PA, & Valiquette N (1991) Dental implant design-Effect on bone remodeling. *Journal of Biomedical Materials Research*. 25(4):459-465.
- Placko HE, Mishra S, Weimer JJ & Lucas LC (2000) Surface characterization of titanium-based implant materials. *International Journal of Oral & Maxillofacial Implants*, 15:355-363.
- Predecki P, Stephan JE, Auslaender BA, Mooney VL & Kirkland K (1972) Kinetics of bone growth into cylindrical channels in aluminium oxide and titanium. *Journal of Biomedical Materials Research*, 6:375-400.



- Puleo DA & Nanci A (1989) Understanding and controlling the bone-implant interface. *Biomaterials*, 20: 2311-2321.
- Rajaraman R, Rounds DE, Yen SP & Rembaum A (1974) A scanning electron microscope study of cell adhesion and spreading in vitro. *Experimental Cell Research*, 88:327-339.
- Ratner BD (1983) Surface characterization of biomaterials by electron spectroscopy for chemical analysis. *Annals of Biomedical Engineering*, 11:313-336.
- Ratner BD (1988) Biomaterial surfaces. *Journal of Biomedical Materials Research*, 21:59-90.
- Renner AM (2001) The versatile use of titanium in implant prosthodontics. *Quintessence of Dental Technology*, p 188-197.
- Rieger MR, Adams WR, Kinzel GL & Brose MO (1989) Finite element analysis of bone-adapted and bone-bonded endosseous implants. *Journal of Prosthetic Dentistry*, 62:436-440.
- Rodan GA & Martin TJ (1981) Role of osteoblasts in hormonal control of bone resorption - a hypothesis. *Calcified Tissue International*, 33:349-351.
- Saltzman WM, Parsons-Wingerter P, Leong KW & Lin S (1991) Fibroblast and hepatocyte behaviour on synthetic polymer surfaces. *Journal of Biomedical Materials Research*, 25:741-759.
- Scacchi M (2000) The development of the ITI® DENTAL IMPLANT SYSTEM. Part I: A review of the literature. *Clinical and Oral Implants Research*, 11:8-21(Suppl)
- Schmidt C, Kaspar D, Sarkar NR, Claes LE & Ignatius AA (2002) A scanning electron microscopy study of human osteoblasts morphology on five orthopedic metals. *Journal of Biomedical Materials Research*, 63:252-261.
- Schutz RW & Thomas DE (1987) Corrosion of titanium and titanium alloys, in metals Handbook, 9th ed., Vol 13:Corrosion, ASM International Ohio, p669-706.
- Schwartz Z, Martin JY, Dean DD, Simpson J, Cochran DL & Boyan BD (1996) Effect of titanium surface roughness on chondrocyte proliferation, matrix production and differentiation depends on the state of cell maturation. *Journal of Biomedical Materials Research*, 30:145-155.
- Shelton RM, Rasmussen AC & Davies JE (1988) Protein adsorption at the interface between charged polymer substrata and migrating osteoblasts. *Biomaterials*, 9:24-29.
- Shelton RM, Whyte IM & Davies JE (1987) Interaction between primary bone cell cultures and biomaterials. Part 4: Colonization of charged polymer surfaces. *Biomaterials and Clinical applications*. ed. Pizzoferrato A, Marchetti PG, Ravaglioli A & Lee AJC. Elsevier Science Publishers B.V., Amsterdam. Printed in The Netherlands. p597-602.
- Shirkhanzadeh M (1995) XRD-XPS characterization of super plastic TiO₂ coatings prepared on Ti6Al4V surgical alloy by an electrochemical method. *Journal of Materials Science: Materials in Medicine*, 6:206-210.
- Sigma Cell Culture Reagents. (1992) p215,216,217,273.
- Sigma Cell Culture Reagents. (1993), p 13
- Sittig C, Textor M, Spencer ND, Wieland M & Vallotton P-H (1999) Surface characterization of implant materials cpTi, Ti-6Al-7Nb and Ti-6Al-4V with different pretreatments. *Journal of Materials Science: Materials in Medicine*, 10:35-46.



- Smith DC (1988) Future directions for research on materials and design of dental implants. *Journal of Dental Education*, 52:815-820.
- Smith DC (1991) Surface Characterization of implant materials: Biological implications. In *The Bone biomaterial interface* Davies JE. University of Toronto press, USA. p3-18.
- Smith DC, Pilliar BR & Chernicky R (1991) Dental implant materials. Part I. Some effects of preparative procedures on surface. *Journal of Biomedical Materials Research*, 25(9):1045-1068.
- Solar RJ, Pollack SR & Korostoff E (1979) In vitro corrosion testing of titanium surgical implant alloys: An approach to understanding titanium release from implants. *Journal of Biomedical Materials Research*, 13:217-250.
- Steinemann SG (1998) Titanium - the material of choice? *Periodontology* 2000, 17:7-21.
- Sudo H, Kodama H, Amagai Y, Yamamoto S & Kasai S (1983) In vitro differentiation and calcification in a new clonal osteogenic cell line derived from newborn mouse calvaria. *Journal of Cell Biology*, 96:191-198.
- Taborelli M, Jobin M, Francois P, Vaudaux P, Tonetti M, Szukler-Moncler S, Simpson JP & Desseigne F (1997) Influence of surface treatments developed for oral implants on physical and biological properties of titanium (I) Surface Characterization. *Clinical Oral Implant Research*, 8:208-216.
- Takarada H, Cattoni M & Rose GG (1975) Ultrastructural studies of human gingival. V. Microfibrils of elastic nature and their direct penetration of the basal lamina in chronic periodontitis. *Journal of Periodontology*, 46:294-301.
- Tengvall P & Lundstrom I (1992) Physico-chemical considerations of titanium as a biomaterial. *Clinical Materials*, 9:115-134.
- The Colgate Oral Care Report, A Summary *Journal of Advances in Dentistry and Oral Health Care*. Volume 10, number 2, 2000, p4
- Thom D, Powell AJ & Rees DA (1979) Mechanisms of cellular adhesion. IV. Role of serum glycoproteins in fibroblast spreading on glass. *Journal of Cell Science*, 35:281-305.
- Thomas KA, Kay JF, Cook SD & Jarcho M (1987) The effect of surface macrotexture and hydroxyapatite coating on the mechanical strengths and histologic profiles of titanium implant materials. *Journal of Biomedical Materials Research*, 21:1395-1414.
- Trisi P, Rao W & Rebaudi A. (1999). A histometric comparison of smooth and rough titanium implants in human low-density jawbone. *International Journal of Oral & Maxillofacial Implants*, 14:689-698.
- Urist MR, De Lange RJ & Finerman GAM (1983) Bone cell differentiation and growth factors. *Science*, 220:680-686.
- Van Steenberghe D (1988) Periodontal aspects of osseointegrated oral implants modum Branemark. *Dental Clinics of North America*, 32:355-370.
- Vargas E, Baier RE & Meyer AE (1992) Reduced corrosion of cpTi and Ti6Al4V alloy endosseous dental implants after glow discharge treatment: A preliminary report. *International Journal of Oral & Maxillofacial Implants*, 7:338-344.
- Verschueren H (1985) Interference reflection microscopy in cell biology: methodology and applications. *Journal of Cell Science*, 75:279-301.



- Verseik P (1984) Trace element analysis - a plea for accuracy. *Trace Elements in Medicine*, 1:2-12.
- Walivaara B, Aronsson B-O, Rodahl M, Lausmaa J & Tengvall P (1994) Titanium with different oxides: In vitro studies of protein adsorption and contact activation. *Biomaterials*, 15:827-834
- Wang RR & Fenton A (1996) Titanium for prosthodontic applications: A review of the literature. *Quintessence International*, 27:401-8.
- Watanabe I, Kurtz KS, Babcenell JL & Okabe T (1999) Effect of sandblasting and silicoating on bond strength of polymer-glass composite to cast titanium. *Journal of Prosthetic Dentistry*, 82:462-7.
- Weiss L & Kapes DL (1966) Observation on cell adhesion and separation following enzyme treatment. *Experimental Cell Research*, 41:601-608.
- Weiss L (1978) Cell adhesion. *International Dental Journal*, 28:7-17.
- Wennerberg A, Albrektsson T, Ulrich H & Krol J (1992) An optical three-dimensional technique for topographical descriptions of surgical implants. *Journal of Biomedical Engineering*, 14:412-418.
- Wennerberg A, Albrektsson T & Lausmaa J (1996) Torque and histomorphometric evaluation of c.p titanium screws blasted with 25- and 75- μ m sized particles of Al₂O₃. *Journal of Biomedical Materials Research*, 30:251-260.
- William DF (1981) Titanium and Titanium alloys. Vol I. In *Biocompatibility of Clinical Implant Materials*. CRC Press, Inc., Boca Raton, Florida, p10-11,14,23.
- Williams DF (1982) Tissue reaction to metallic corrosion products and wear particles in clinical orthopaedics implants. Boca Raton, FL: CRC Press, p231-248.
- Winship KA (1992) Toxicity of aluminium: A historical review, part I. *Adverse Drug Reactions & Toxicological Reviews*, 11:123-141.
- Wong M, Eulenberger J, Schenk R, Hunziker E (1995) Effects of surface topology on the osseointegration of implant materials in trabecular bone. *Journal of Biomedical Materials Research*, 29:1567-1575.
- Worthington P (1988) Current implant usage. *Journal of Dental Education*, 52:692-695.
- Young FA (1988) Future directions for dental implant materials research. *Journal of Dental Education*, 52:770-774.
- Young L (1972) Anodic oxide films, Academic Press, London and New York. Chap 20.
- Zarb GA & Albrektsson T (1993) Current interpretations of the osseointegrated response of clinical significance. *International Journal of Prosthodontics*, 6(2):95-105.
- Zarb GA, Branemark P-I & Albrektsson (1985) *Tissue Integrated Prosthesis: Osseointegration in Clinical Practice*. Quintessence, Chicago.
- Zhu X, Kim K, Ong JL, & Jeong Y (2002) Surface analysis of anodic oxide films containing phosphorus on titanium. *International Journal of Oral & Maxillofacial Implants*. 17:331-336.
- Zinelis S (2000) Effect of pressure of helium, argon, krypton and xenon on the porosity, microstructure and mechanical properties of commercially pure titanium castings. *Journal of Prosthetic Dentistry*, 84:575-582.
- Zrelqat H, Standard CO, Gengenbach JG, Steele J & Howlett CR (1996) The role of surface characteristics in the initial adhesion of human bone-derived cells on ceramics. *Cells Materials*, 6:45-56.

LORD,

Thank you for being at my side and

holding my hand.

Sometimes the road seemed long,

but LORD,

You were always there

to give me strength and

guide me on my way.

ADDENDUM A

Fibroblasts counts X dilution factor X 10⁴

Seeding concentration was 10.58 X 10⁴ cells.ml⁻¹.

178

Time Sample	Day 1				Day 2				Day 14				Day 28			
	Mic 1	Mic 2	Ave	%	Mic 1	Mic 2	Ave	%	Mic 1	Mic 2	Ave	%	Mic 1	Mic 2	Ave	%
Control	4.76	4.86	4.82	45.52	5.94	6.32	6.13	58.01	13.08	11.58	12.29	115.72	13.54	13.34	13.42	126.96
cpTi mach cont	3.26	4.76	4.01	37.81	6.22	6.66	6.44	60.91	9.42	10.75	10.80	95.36	13.40	14.40	13.90	131.38
cpTi mach SI	4.00	5.12	4.56	43.06	4.22	5.26	4.74	44.76	11.00	9.50	10.26	96.88	6.44	4.40	5.42	51.25
cpTi mach ES	2.00	3.66	2.84	26.78	3.14	3.42	3.28	31.06	16.40	13.60	15.00	141.78	13.60	11.80	12.70	120.04
Ti6Al4V mach cont	2.66	4.47	3.70	35.05	5.20	4.80	5.00	47.26	16.60	12.44	14.52	137.26	11.40	17.26	14.32	135.40
Ti6Al4V mach SI	4.44	4.00	4.22	39.91	3.56	5.50	4.52	42.80	11.50	12.60	12.06	113.89	7.78	3.76	5.76	54.48
Ti6Al4V mach ES	2.00	5.72	3.86	36.46	5.12	4.88	5.00	47.26	17.80	12.80	15.30	144.61	4.40	5.00	4.70	44.42
cpTi cast cont	6.00	6.40	6.20	58.60	3.72	3.76	3.74	35.28	9.78	12.00	10.88	102.92	2.88	5.00	3.94	37.28
cpTi cast SI																
cpTi cast ES	4.00	5.34	4.66	44.11	3.26	5.40	4.32	40.88	14.20	15.20	14.70	138.94	7.12	4.76	5.94	56.05
Ti6Al4V cast cont	3.12	4.86	3.98	37.66	4.50	6.58	5.54	52.32	19.20	20.20	19.70	186.20	7.76	6.50	7.12	67.34
Ti6Al4V cast SI	5.80	3.78	4.78	45.26	7.00	5.00	6.00	56.71	13.80	13.00	13.40	126.65	3.60	4.66	4.14	39.07
Ti6Al4V cast ES	4.00	2.86	3.42	32.41	5.60	4.58	5.08	48.07	17.20	16.80	17.00	160.68	10.00	10.26	10.12	95.70

ADDENDUM B

Osteoblasts counts X dilution factor X 10⁴

Seeding concentration was 11.0 X 10⁴ cells.ml⁻¹.

Time	2 days				14 days				28 days			
	Mic 1	Mic 2	Ave	%	Mic 1	Mic 2	Ave	%	Mic 1	Mic 2	Ave	%
Control	11.2	13.7	12.5	113.8	22.8	18.4	20.6	187.7	2.9	3.1	3.0	27.3
cpTi mach cont	12.2	16.2	14.2	129.1	16.8	17.6	17.2	156.4	4.2	7.4	5.8	52.8
cpTi mach SI	10.7	13.2	12.0	108.5	12.0	12.8	12.4	112.7	14.2	11.0	12.6	114.6
cpTi mach ES	11.3	12.6	11.9	108.4	14.4	10.6	12.5	113.4	6.6	6.4	6.5	59.3
Ti6Al4V mach cont	10.9	11.8	11.3	103.1	21.6	10.0	15.8	143.6	3.3	2.0	2.7	24.2
Ti6Al4V mach SI	7.1	8.3	7.7	69.8	22.0	20.0	21.0	190.9	18.8	19.6	19.2	174.6
Ti6Al4V mach ES	8.3	11.3	9.8	89.0	19.2	13.4	16.3	148.2	3.6	5.1	4.3	39.5
cpTi cast cont	9.7	13.6	11.6	105.8	12.4	9.8	11.1	100.9	2.0	3.6	2.8	25.5
cpTi cast SI	8.8	12.5	10.7	96.8	34.4	19.2	26.8	243.6	5.3	5.1	5.2	47.5
cpTi cast ES	10.2	10.9	10.5	95.9	28.2	20.2	24.2	220.0	6.2	6.2	6.2	56.5
Ti6Al4V cast cont	7.3	8.7	8.0	7.7	18.0	11.8	14.9	135.4	25.8	18.2	22.0	200.0
Ti6Al4V cast SI	11.2	14.0	12.6	114.6	20.0	22.4	21.2	192.7	5.8	6.4	6.1	55.4
Ti6Al4V cast ES	8.8	6.0	7.4	67.3	21.8	18.4	20.1	182.7	18.6	14.4	16.5	150.0

ADDENDUM C

Area Analysis

Area Ra values of the different samples analysed - 20 μ m scan

Samples	I	II	III	IV	V	Aver
cpTi mach cont	0.076	0.19	0.146	0.176	0.113	0.1402
cpTi mach cont RFGDT	0.13	0.086	0.062	0.085	0.126	0.0978
Ti6Al4V mach cont	0.082	0.089	0.083	0.143	0.045	0.0884
Ti6Al4V mach cont RFGDT	0.12	0.107	0.17	0.162	0.16	0.1438
cpTi cast cont	0.422	0.685	0.541	0.531	0.419	0.5196
cpTi cast cont RFGDT	0.702	0.524	0.538	0.97	0.5	0.6468
Ti6Al4V cast cont	0.597	0.195	0.311	0.682	0.463	0.4496
Ti6Al4V cast cont RFGDT	0.454	0.366	0.268	0.555	0.417	0.412

Area Ra values of the different samples analysed - 5 μ m scan

Samples	I	II	III	IV	V	Aver
cpTi mach cont	0.051	0.045	0.041	0.112	0.049	0.0596
cpTi mach cont RFGDT	0.156	0.035	0.033	0.061	0.041	0.0652
Ti6Al4V mach cont	0.082	0.071	0.105	0.105	0.047	0.082
Ti6Al4V mach cont RFGDT	0.111	0.075	0.157	0.117	0.071	0.1062
cpTi cast cont	0.319	0.161	0.222	0.499	0.108	0.2618
cpTi cast cont RFGDT	0.427	0.123	0.213	0.432	0.159	0.2708
Ti6Al4V cast cont	0.185	0.089	0.32	0.351	0.333	0.2556
Ti6Al4V cast cont RFGDT	0.402	0.244	0.05	0.176	0.132	0.2008

Area RMS values of the different samples analysed -20 μ m scan

Samples	I	II	III	IV	V	Aver
cpTi mach cont	0.093	0.219	0.176	0.219	0.153	0.172
cpTi mach cont RFGDT	0.173	0.106	0.08	0.11	0.167	0.1272
Ti6Al4V mach cont	0.103	0.108	0.106	0.175	0.059	0.1102
Ti6Al4V mach cont RFGDT	0.15	0.136	0.218	0.195	0.209	0.1816
cpTi cast cont	0.562	0.835	0.673	0.676	0.522	0.6536
cpTi cast cont RFGDT	0.877	0.609	0.682	1.14	0.651	0.7918
Ti6Al4V cast cont	0.736	0.227	0.393	0.832	0.584	0.5544
Ti6Al4V cast cont RFGDT	0.578	0.467	0.329	0.711	0.525	0.522

Area RMS values of the different samples analysed - 5 μ m scan

Samples	I	II	III	IV	V	Aver
cpTi mach cont	0.076	0.057	0.061	0.112	0.063	0.0738
cpTi mach cont RFGDT	0.2	0.051	0.04	0.077	0.05	0.0836
Ti6Al4V mach cont	0.098	0.087	0.122	0.144	0.056	0.1014
Ti6Al4V mach cont RFGDT	0.146	0.097	0.178	0.138	0.089	0.1296
cpTi cast cont	0.402	0.214	0.272	0.58	0.14	0.3216
cpTi cast cont RFGDT	0.512	0.173	0.267	0.497	0.233	0.3364
Ti6Al4V cast cont	0.238	0.104	0.381	0.441	0.405	0.3138
Ti6Al4V cast cont RFGDT	0.497	0.297	0.062	0.212	0.166	0.2468

Surface Area values of the different samples analysed – projected area of 400 μ m² scan

Samples	I	II	III	IV	V	Aver
cpTi mach cont	412.7	413.8	418.1	422.5	413.8	416.18
cpTi mach cont RFGDT	425.5	412.8	410.6	417.8	415	416.34
Ti6Al4V mach cont	415.8	417.2	415.9	416.7	409.4	415
Ti6Al4V mach cont RFGDT	426.9	420.2	417.2	433.8	427	425.02
cpTi cast cont	532	568.7	534.1	523.2	501.6	531.92
cpTi cast cont RFGDT	573.2	499.1	602.7	627.9	492.8	559.14
Ti6Al4V cast cont	570.3	434.3	472.1	547.6	517	508.26
Ti6Al4V cast cont RFGDT	585.7	559.9	424.8	579	526.9	535.26

Surface Area values of the different samples analysed – projected area of 25 μ m² scan

Samples	I	II	III	IV	V	Aver
cpTi mach cont	27.51	26.66	26.72	28.24	2.64	27.15
cpTi mach cont RFGDT	28.29	26.01	25.8	26.58	26.13	26.56
Ti6Al4V mach cont	27.26	27.0	27.9	28.79	25.6	27.31
Ti6Al4V mach cont RFGDT	28.6	27.2	27.0	29.3	21.8	28.04
cpTi cast cont	36.87	30.87	31.17	35.94	29.43	32.86
cpTi cast cont RFGDT	40.66	29.42	33.83	36.42	31.01	34.2
Ti6Al4V cast cont	31.88	28.26	36.76	41.35	36.47	34.94
Ti6Al4V cast cont RFGDT	39.3	37.71	25.75	29.74	29.45	32.39

Maximum range values of the different samples analysed - 20 μ m scan

Samples	I	II	III	IV	V	Aver
cpTi mach cont	0.812	0.963	1.022	1.19	1.22	1.0414
cpTi mach cont RFGDT	1.24	1.017	0.47	0.897	1.136	0.952
Ti6Al4V mach cont	0.817	0.949	0.752	1.518	0.602	0.9276
Ti6Al4V mach cont RFGDT	1.001	1.237	1.137	1.319	1.341	1.207
cpTi cast cont	4.046	4.607	3.918	4.201	2.93	3.9404
cpTi cast cont RFGDT	5.856	2.826	4.702	5.448	3.951	4.5566
Ti6Al4V cast cont	4.525	1.152	2.737	4.261	3.83	3.301
Ti6Al4V cast cont RFGDT	3.838	3.509	2.063	4.483	4.477	3.674

Maximum range values of the different samples analysed - 5 μ m scan

Samples	I	II	III	IV	V	Aver
cpTi mach cont	0.699	0.333	0.512	0.647	0.359	0.51
cpTi mach cont RFGDT	0.917	0.351	0.199	0.423	0.25	0.428
Ti6Al4V mach cont	0.46	0.463	0.528	0.942	0.242	0.527
Ti6Al4V mach cont RFGDT	0.972	0.591	0.632	0.616	0.571	0.6764
cpTi cast cont	1.843	1.152	1.466	2.47	1.14	1.6142
cpTi cast cont RFGDT	2.516	1.138	1.666	2.108	1.489	1.7834
Ti6Al4V cast cont	1.487	0.51	1.693	2.446	2.124	1.652
Ti6Al4V cast cont RFGDT	2.347	1.846	0.314	1.097	0.972	1.3152

Average height values of the different samples analysed - 20 μ m scan

Samples	I	II	III	IV	V	Aver
cpTi mach cont	0.535	0.633	0.614	0.779	0.363	0.5848
cpTi mach cont RFGDT	0.83	0.348	0.241	0.36	0.416	0.439
Ti6Al4V mach cont	0.509	0.569	0.485	1.151	0.459	0.6346
Ti6Al4V mach cont RFGDT	0.499	0.627	0.437	0.519	0.579	0.5322
cpTi cast cont	1.948	2.185	1.821	2.415	1.042	1.8822
cpTi cast cont RFGDT	3.463	1.245	2.311	2.926	1.102	2.2094
Ti6Al4V cast cont	2.583	0.509	1.274	1.99	2.35	1.7412
Ti6Al4V cast cont RFGDT	1.583	1.639	0.905	2.921	2.562	1.922

Average height values of the different samples analysed - 5 μ m scan

Samples	I	II	III	IV	V	Aver
cpTi mach cont	0.455	0.195	0.126	0.365	0.187	0.2656
cpTi mach cont RFGDT	0.421	0.244	0.108	0.204	0.114	0.2182
Ti6Al4V mach cont	0.271	0.312	0.281	0.763	0.106	0.3466
Ti6Al4V mach cont RFGDT	0.361	0.258	0.359	0.232	0.355	0.313
cpTi cast cont	0.83	0.429	0.587	1.184	0.377	0.6814
cpTi cast cont RFGDT	1.495	0.451	0.842	0.91	0.326	0.8048
Ti6Al4V cast cont	0.626	0.192	0.724	1.055	1.164	0.7522
Ti6Al4V cast cont RFGDT	0.898	0.811	0.144	0.501	0.572	0.5852

ADDENDUM D

Line Analysis - 20 μ m scans

Ra values of 20 μ m scan line analysis

	I	II	III	IV	V	VI	VII	VIII	IX	X	XI	XII	XIII	XIV	V	Aver
cpTi mach cont	0.04	0.06	0.06	0.18	0.18	0.20	0.16	0.09	0.12	0.20	0.11	0.10	0.8	0.09	0.13	0.12
cpTi mach cont RFGDT	0.1	0.10	0.09	0.07	0.07	0.06	0.07	0.04	0.05	0.13	0.05	0.09	0.15	0.12	0.08	0.08
Ti6Al4V mach cont	0.09	0.07	0.06	0.09	0.08	0.09	0.10	0.69	0.05	0.14	0.13	0.12	0.05	0.03	0.03	0.08
Ti6Al4V mach cont RFGDT	0.16	0.10	0.10	0.08	0.07	0.11	0.03	0.10	0.21	0.18	0.13	0.12	0.13	0.14	0.14	0.12
cpTi cast cont	0.54	0.30	0.17	0.22	0.52	0.48	0.53	0.52	0.32	0.26	0.69	0.56	0.28	0.16	0.50	0.40
cpTi cast cont RFGDT	0.53	0.71	0.78	0.51	0.60	0.46	0.33	0.66	0.42	0.62	0.79	1.16	0.68	0.42	0.20	0.59
Ti6Al4V cast cont	0.52	0.50	0.57	0.17	0.18	0.20	0.22	0.16	0.33	0.42	0.58	0.82	0.29	0.43	0.43	0.39
Ti6Al4V cast cont RFGDT	0.32	0.44	0.46	0.28	0.40	0.39	0.19	0.08	0.30	0.52	0.26	0.51	0.39	0.30	0.24	0.34

Rp values of 20 μ m scan line analysis

	I	II	III	IV	V	VI	VII	VIII	IX	X	XI	XII	XIII	XIV	V	Aver
cpTi mach cont	0.14	0.13	0.18	0.24	0.24	0.29	0.29	0.16	0.24	0.37	0.20	0.28	2.36	0.28	0.47	0.25
cpTi mach cont RFGDT	0.19	0.23	0.30	0.17	0.19	0.16	0.18	0.17	0.13	0.52	0.13	0.18	0.30	0.44	0.30	0.24
Ti6Al4V mach cont	0.18	0.17	0.20	0.25	0.16	0.20	0.26	0.13	0.12	0.28	0.25	0.22	0.09	0.08	0.09	0.18
Ti6Al4V mach cont RFGDT	0.39	0.26	0.23	0.18	0.27	0.42	0.08	0.18	0.35	0.32	0.39	0.32	0.38	0.29	0.55	0.31
cpTi cast cont	1.30	1.16	0.44	0.87	1.06	0.88	1.18	0.86	0.79	1.01	1.53	1.06	0.61	0.38	1.55	0.98
cpTi cast cont RFGDT	1.10	1.17	1.63	1.34	1.36	1.23	0.090	1.06	1.29	1.32	1.94	2.67	1.74	1.93	0.75	1.47
Ti6Al4V cast cont	1.08	0.96	0.94	0.33	0.36	0.42	0.39	0.26	0.83	0.78	1.21	2.18	0.64	1.23	0.82	0.83
Ti6Al4V cast cont RFGDT	1.04	1.15	2.08	0.91	1.46	1.03	0.34	0.32	0.95	1.10	0.71	1.08	1.19	0.68	0.60	0.98

Rpm values of 20 μm scan line analysis

	I	II	III	IV	V	VI	VII	VIII	IX	X	XI	XII	XIII	XIV	V	Aver
cpTi mach cont	0.07	0.07	0.08	0.11	0.13	0.14	0.11	0.08	0.06	0.24	0.13	0.12	0.09	0.09	0.12	0.11
cpTi mach cont RFGDT	0.12	0.16	0.16	0.08	0.09	0.11	0.08	0.07	0.08	0.16	0.07	0.11	0.17	0.13	0.11	0.11
Ti6Al4V mach cont	0.12	0.10	0.09	0.11	0.08	0.10	0.09	0.09	0.05	0.09	0.10	0.11	0.06	0.03	0.04	0.08
Ti6Al4V mach cont RFGDT	0.24	0.14	0.12	0.10	0.16	0.12	0.02	0.07	0.13	0.23	0.25	0.17	0.16	0.13	0.16	0.15
cpTi cast cont	0.75	0.60	0.28	0.33	0.78	0.50	0.54	0.58	0.37	0.45	0.67	0.58	0.31	0.18	0.64	0.50
cpTi cast cont RFGDT	0.53	0.72	0.72	0.64	0.43	0.50	0.46	0.62	0.58	0.73	0.98	1.19	0.59	0.54	0.25	0.63
Ti6Al4V cast cont	0.63	0.58	0.66	0.16	0.17	0.20	0.17	0.17	0.43	0.28	0.56	0.69	0.38	0.55	0.43	0.40
Ti6Al4V cast cont RFGDT	0.50	0.64	0.71	0.46	0.46	0.53	0.13	0.09	0.28	0.61	0.45	0.31	0.50	0.44	0.35	0.43

Rt values of 20 μm scan line analysis

	I	II	III	IV	V	VI	VII	VIII	IX	X	XI	XII	XIII	XIV	V	Aver
cpTi mach cont	0.26	0.29	0.34	0.68	0.69	0.89	0.65	0.41	0.50	0.84	0.56	0.65	0.39	0.47	0.74	0.56
cpTi mach cont RFGDT	0.52	0.63	0.59	0.32	0.32	0.32	0.35	0.36	0.30	0.77	2.82	0.40	0.67	0.75	0.54	0.47
Ti6Al4V mach cont	0.40	0.40	0.40	0.44	0.34	0.40	0.48	0.5	0.27	0.55	0.53	0.50	0.24	0.21	0.26	0.40
Ti6Al4V mach cont RFGDT	0.76	0.51	0.56	0.45	0.48	0.62	0.14	0.47	0.75	0.82	0.69	0.68	0.86	0.71	1.04	0.64
cpTi cast cont	2.85	1.95	1.30	2.35	3.86	1.94	2.02	1.91	1.53	1.97	3.06	2.63	1.28	0.87	2.68	2.15
cpTi cast cont RFGDT	2.41	4.27	4.10	2.28	2.35	2.52	1.77	2.74	2.76	2.67	3.75	5.07	2.38	2.32	1.64	2.87
Ti6Al4V cast cont	3.61	2.25	2.82	0.77	0.76	0.88	0.94	0.81	1.66	1.78	3.32	3.69	1.96	2.30	2.42	2.00
Ti6Al4V cast cont RFGDT	1.84	2.20	3.06	1.68	2.69	2.09	0.92	0.60	1.43	2.39	1.47	2.44	2.15	2.00	1.26	1.88

R_{tm} values of 20 μm scan line analysis

	I	II	III	IV	V	VI	VII	VIII	IX	X	XI	XII	XIII	XIV	V	Aver
cpTi mach cont	0.15	0.15	0.18	0.26	0.27	0.30	0.23	0.16	0.16	0.52	0.25	0.24	0.17	0.19	0.26	0.23
cpTi mach cont RFGDT	0.29	0.32	0.30	0.17	0.16	0.21	0.18	0.17	0.18	0.32	0.15	0.20	0.29	0.26	0.22	0.23
Ti6Al4V mach cont	0.27	0.21	0.20	0.22	0.16	0.23	0.24	0.24	0.14	0.20	0.21	0.2	0.15	0.10	0.12	0.19
Ti6Al4V mach cont RFGDT	0.45	0.31	0.22	0.24	0.26	0.26	0.04	0.14	0.28	0.49	0.45	0.40	0.39	0.33	0.40	0.31
cpTi cast cont	1.31	1.02	0.65	0.73	1.45	1.13	1.04	1.07	0.80	1.06	1.48	1.14	0.59	0.42	1.34	1.02
cpTi cast cont RFGDT	1.42	1.62	1.55	1.25	0.82	0.98	0.86	1.54	1.13	1.53	1.78	2.11	0.85	0.85	0.57	1.26
Ti6Al4V cast cont	1.25	1.44	1.58	0.33	0.34	0.42	0.38	0.38	0.84	0.69	1.13	1.25	0.80	1.04	1.18	0.87
Ti6Al4V cast cont RFGDT	1.06	1.34	1.32	0.96	0.99	0.96	0.29	0.18	0.45	1.09	0.93	0.75	0.93	0.96	0.77	0.87

ADDENDUM E

Line Analysis - 5 μ m scans

Ra values of 5 μ m scan line analysis

	I	II	III	IV	V	VI	VII	VIII	IX	X	XI	XII	XIII	XIV	V	Aver
cpTi mach cont	0.03	0.03	0.06	0.03	0.04	0.04	0.03	0.02	0.02	0.09	0.12	0.12	0.02	0.03	0.05	0.05
cpTi mach cont RFGDT	0.09	0.21	0.12	0.02	0.02	0.03	0.04	0.02	0.02	0.04	0.03	0.03	0.04	0.03	0.04	0.05
Ti6Al4V mach cont	0.07	0.07	0.07	0.04	0.05	0.07	0.12	0.09	0.10	0.08	0.06	0.08	0.04	0.05	0.05	0.07
Ti6Al4V mach cont RFGDT	0.08	0.12	0.11	0.05	0.08	0.06	0.04	0.02	0.02	0.09	0.08	0.15	0.06	0.06	0.06	0.07
cpTi cast cont	0.19	0.41	0.36	0.17	0.17	0.13	0.16	0.31	0.25	0.52	0.44	0.54	0.04	0.09	0.11	0.26
cpTi cast cont RFGDT	0.26	0.38	0.51	0.06	0.10	0.10	0.13	0.21	0.19	0.34	0.33	0.48	0.10	0.09	0.09	0.22
Ti6Al4V cast cont	0.23	0.09	0.21	0.09	0.08	0.08	0.43	0.25	0.27	0.37	0.18	0.50	0.27	0.26	0.32	0.24
Ti6Al4V cast cont RFGDT	0.21	0.27	0.26	0.16	0.22	0.18	0.05	0.04	0.03	0.16	0.15	0.16	0.13	0.14	0.14	0.15

Rp values of 5 μ m scan line analysis

	I	II	III	IV	V	VI	VII	VIII	IX	X	XI	XII	XIII	XIV	V	Aver
cpTi mach cont	0.08	0.08	0.13	0.09	0.06	0.08	0.11	0.07	0.12	0.16	0.20	0.24	0.13	0.12	0.09	0.09
cpTi mach cont RFGDT	0.18	0.50	0.38	0.10	0.03	0.06	0.10	0.07	0.05	0.06	0.08	0.05	0.05	0.08	0.12	0.12
Ti6Al4V mach cont	0.10	0.11	0.08	0.08	0.07	0.08	0.16	0.15	0.24	0.09	0.11	0.14	0.10	0.09	0.11	0.11
Ti6Al4V mach cont RFGDT	0.22	0.28	0.16	0.17	0.19	0.15	0.10	0.04	0.04	0.28	0.30	0.28	0.16	0.16	0.16	0.16
cpTi cast cont	0.48	0.60	0.59	0.64	0.48	0.33	0.37	0.73	0.53	1.10	1.04	1.16	0.19	0.24	0.21	0.21
cpTi cast cont RFGDT	0.45	0.63	0.90	0.18	0.43	0.27	0.37	0.41	0.31	0.06	0.88	0.87	0.41	0.17	0.22	0.22
Ti6Al4V cast cont	0.68	0.25	0.41	0.23	0.17	0.19	0.73	0.72	0.56	0.60	0.62	1.22	0.40	0.49	0.52	0.52
Ti6Al4V cast cont RFGDT	0.51	0.73	0.48	0.37	0.59	0.34	0.09	0.10	0.07	0.26	0.26	0.24	0.32	0.25	0.20	0.20

Rpm values of 5µm scan line analysis

	I	II	III	IV	V	VI	VII	VIII	IX	X	XI	XII	XIII	XIV	V	Aver
cpTi mach cont	0.03	0.03	0.08	0.05	0.04	0.04	0.03	0.02	0.03	0.03	0.05	0.07	0.04	0.05	0.05	0.04
cpTi mach cont RFGDT	0.04	0.15	0.10	0.02	0.01	0.03	0.05	0.02	0.02	0.03	0.03	0.02	0.03	0.05	0.04	0.04
Ti6Al4V mach cont	0.04	0.07	0.04	0.05	0.04	0.06	0.08	0.08	0.10	0.07	0.05	0.07	0.03	0.03	0.03	0.06
Ti6Al4V mach cont RFGDT	0.07	0.12	0.07	0.07	0.07	0.05	0.04	0.01	0.01	0.12	0.07	0.11	0.08	0.09	0.07	0.07
cpTi cast cont	0.14	0.22	0.27	0.13	0.19	0.07	0.11	0.21	0.17	0.36	0.35	0.37	0.06	0.08	0.13	0.19
cpTi cast cont RFGDT	0.22	0.32	0.33	0.06	0.12	0.11	0.19	0.15	0.13	0.30	0.23	0.26	0.09	0.03	0.04	0.17
Ti6Al4V cast cont	0.19	0.16	0.17	0.08	0.07	0.07	0.28	0.23	0.20	0.19	0.22	0.34	0.12	0.17	0.27	0.18
Ti6Al4V cast cont RFGDT	0.27	0.26	0.22	0.14	0.19	0.14	0.02	0.03	0.03	0.13	0.10	0.06	0.16	0.11	0.10	0.13

Rt values of 5µm scan line analysis

	I	II	III	IV	V	VI	VII	VIII	IX	X	XI	XII	XIII	XIV	V	Aver
cpTi mach cont	0.15	0.16	0.32	0.23	0.21	0.24	0.21	0.13	0.16	0.33	0.39	0.46	0.20	0.18	0.24	0.24
cpTi mach cont RFGDT	0.32	0.82	0.55	0.20	0.06	0.20	0.19	0.12	0.10	0.16	0.17	0.13	0.16	0.18	0.22	0.24
Ti6Al4V mach cont	0.25	0.29	0.13	0.20	0.16	0.26	0.31	0.40	0.37	0.45	0.47	0.34	0.42	0.17	0.17	0.29
Ti6Al4V mach cont RFGDT	0.39	0.50	0.43	0.27	0.38	0.30	0.20	0.11	0.10	0.42	0.41	0.43	0.38	0.34	0.32	0.33
cpTi cast cont	0.91	1.46	1.18	0.95	0.83	0.55	0.77	1.31	0.89	1.76	1.79	2.16	0.30	0.55	0.47	1.06
cpTi cast cont RFGDT	1.21	1.69	2.23	0.29	0.72	0.54	0.75	0.92	0.72	1.33	1.34	1.54	0.60	0.36	0.41	0.98
Ti6Al4V cast cont	0.94	0.58	0.89	0.41	0.34	0.35	1.45	1.34	1.04	1.28	1.10	2.37	1.37	1.11	1.21	1.05
Ti6Al4V cast cont RFGDT	0.97	1.17	1.16	1.02	0.96	0.70	0.20	0.18	0.15	0.56	0.53	0.48	0.59	0.61	0.57	0.66

Rtm values of 5 μ m scan line analysis

	I	II	III	IV	V	VI	VII	VIII	IX	X	XI	XII	XIII	XIV	V	Aver
cpTi mach cont	0.06	0.07	0.17	0.12	0.10	0.12	0.07	0.05	0.06	0.10	0.12	0.15	0.07	0.08	0.10	0.10
cpTi mach cont RFGDT	0.07	0.28	0.20	0.05	0.05	0.08	0.12	0.06	0.05	0.08	0.07	0.04	0.07	0.11	0.10	0.10
Ti6Al4V mach cont	0.08	0.13	0.12	0.09	0.14	0.11	0.17	0.17	0.19	0.21	0.12	0.18	0.06	0.06	0.07	0.13
Ti6Al4V mach cont RFGDT	0.16	0.23	0.18	0.13	0.15	0.12	0.08	0.03	0.04	0.21	0.14	0.25	0.19	0.21	0.14	0.15
cpTi cast cont	0.32	0.48	0.62	0.26	0.35	0.13	0.24	0.42	0.30	0.68	0.68	0.73	0.12	0.20	0.02	0.37
cpTi cast cont RFGDT	0.53	0.67	0.70	0.13	0.26	0.22	0.35	0.29	0.27	0.56	0.46	0.51	0.15	0.07	0.08	0.35
Ti6Al4V cast cont	0.37	0.28	0.31	0.16	0.15	0.16	0.54	0.46	0.35	0.41	0.47	0.65	0.28	0.37	0.55	0.37
Ti6Al4V cast cont RFGDT	0.55	0.43	0.45	0.33	0.34	0.35	0.06	0.07	0.06	0.22	0.21	0.13	0.34	0.22	0.19	0.26

ADDENDUM F

Spreadsheet for the Depth profile and Chemical analysis

MATER	FABRIC	SURFACE	TREAT	DEPTH_P	M2Ti	M2C	M2O	M2Al	M2Na	M2Zn	M2Pb	M2Ca	M2N	M2V	M2Zr
1	1	1	1	2.8	11.23	37.7	45.82	0.1	0	2.72	0.52	0.62	1.38		
1	1	1	2	4.2	21.64	20.75	56.44	0.1	0			0.1	0.8		0.37
1	1	2	1	4.2	7.19	41.47	43.62	5.2	0	0.49		0.36			
1	1	2	2	7.7	12.97	19.94	52.73	9.69	0			0.32			
1	1	3	1	5.6	8.78	29.53	51.43	5.78	0	1.41		0.97			
1	1	3	2	8.4	14.73	15.12	55.91	7.47	0			0.38			
1	2	1	1	6.3	5.26	23.6	53.62	12.71	4.58			0.23			
1	2	1	2	6.3	9.21	15.09	57.86	12.93	4.74			0.35			0.17
1	2	2	1	5.6	4.29	37.31	43.96	10.48	2.22	0.21		0.47	1.07		
1	2	2	2	8.4	14.59	15.52	56.3	8.22	4.47			0.39			0.51
1	2	3	1	5.25	7.09	25.6	52.96	9.84	3.33	0.66		0.52			
1	2	3	2	8.4	12.91	23.09	51.31	7.97	3.04			0.5	0.93		0.25
2	1	1	1	1.925	10.27	36.83	48.68	1.04	0	2.07	0.34	0.32	0.46	0.89	
2	1	1	2	2.8	18.8	21.77	56.69	1.18	0			0.1			0.67
2	1	2	1	6.3	4.19	36.68	43.83	8.68	5.9			0.24	0.48		
2	1	2	2	6.65	12.97	14.94	55.26	9.77	6.16	0.18		0.31			0.4
2	1	3	1	6.3	5.49	29.2	52.19	9.47	0	0.65		0.75			
2	1	3	2	7	13.73	16.05	55.49	9.2	0			0.3			
2	2	1	1	5.95	5.61	28.67	51.42	9.61	3.27			0.44	0.77	0.21	
2	2	1	2	7.4	6.16	25.31	55.36	10.53	1.49			1.03			0.12
2	2	2	1	4.2	8.35	32.68	47.7	8.01	2.17	0.14		0.2	0.74		
2	2	2	2	5.6	9.87	14.86	55.45	15.09	3.51			0.06			0.35
2	2	3	1	5.95	4.84	28.93	52.24	10.11	2.35	0.49		0.6	0.44		
2	2	3	2	8.4	12.61	15.94	56.55	10.85	3.22			0.41			0.41

Spreadsheet for Surface topography

Area analysis

MATER	FABRIC	SURFACE	TREAT	M3Ra	M3RMS	M3HEIG	M3RAN	M3SUR	M3Ra_1	M3RMS_1	M3HEIG_1	M3RAN_1	M3SUR_1
1	1	1	1	0.14	0.17	0.58	1.04	416.18	0.06	0.07	0.27	0.51	27.15
1	1	1	2	0.09	0.13	0.45	0.95	416.34	0.07	0.08	0.22	0.43	26.56
1	2	1	1	0.52	0.65	1.88	3.94	531.92	0.26	0.32	0.68	1.61	32.86
1	2	1	2	0.65	0.9	2.21	4.56	559.14	0.27	0.34	0.8	1.78	34.2
2	1	1	1	0.09	0.11	0.63	0.93	415	0.08	0.1	0.35	0.53	27.31
2	1	1	2	0.14	0.18	0.53	1.21	425.02	0.11	0.13	0.31	0.68	28.04
2	2	1	1	0.45	0.55	1.74	3.3	508.26	0.09	0.31	0.75	1.65	34.94
2	2	1	2	0.41	0.52	1.92	3.67	535.26	0.2	0.25	0.58	1.32	32.39

194

Line analysis

MATER	FABRIC	SURFACE	TREAT	LARA	LARTM	LART	LARPM	LARP	LARA_1	LARTM_1	LART_1	LARPM_1	LARP_1	p_SUR_A
1	1	1	1	0.125	0.237	0.561	0.114	0.254	0.053	0.102	0.245	0.046	0.123	104.04
1	1	1	2	0.089	0.233	0.478	0.117	0.243	0.056	0.1	0.244	0.048	0.131	104.08
1	2	1	1	0.126	0.314	0.641	0.151	0.311	0.077	0.154	0.337	0.076	0.184	132.75
1	2	1	2	0.407	1.02	2.152	0.508	0.983	0.264	0.376	1.063	0.195	0.584	139.78
2	1	1	1	0.085	0.199	0.401	0.089	0.183	0.074	0.132	0.298	0.06	0.118	103.75
2	1	1	2	0.126	0.314	0.641	0.151	0.311	0.077	0.154	0.337	0.076	0.184	106.25
2	2	1	1	0.392	0.874	2.001	0.409	0.833	0.246	0.371	1.057	0.189	0.523	127.06
2	2	1	2	0.344	0.87	1.885	0.436	0.98	0.158	0.268	0.661	0.136	0.326	133.81

Spreadsheet for % attachment efficiency and proliferation

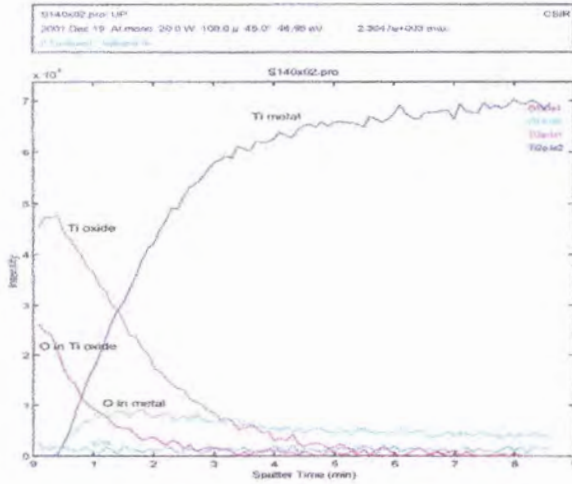
Surface	Time	Fibro	Osteo
1	1	37.81	
1	2	60.91	129.09
1	14	95.36	156.36
1	28	131.38	52.83
2	1	26.78	
2	2	31.06	108.41
2	14	141.78	113.84
2	28	120.04	59.29
3	1	35.05	
3	2	47.26	103.13
3	14	137.26	143.64
3	28	135.4	24.24
4	1	36.46	
4	2	47.26	89.02
4	14	144.61	148.18
4	28	44.42	39.54
5	1	43.06	
5	2	44.76	108.48
5	14	96.88	112.73
5	28	51.25	114.55
6	1	58.6	
6	2	35.28	105.77
6	14	102.92	100.91
6	28	37.28	25.45
7	1	44.11	
7	2	40.88	95.86
7	14	138.94	220.0
7	28	56.05	56.46
8	1	37.66	
8	2	52.32	72.73
8	14	186.2	135.45
8	28	67.34	200.0
9	1	32.41	
9	2	48.07	67.27
9	14	160.68	182.73
9	28	95.7	150.0
10	1		
10	2		96.82
10	14		243.64
10	28		47.47
11	1	45.26	
11	2	56.71	114.55
11	14	126.65	192.73
11	28	39.07	55.43
12	1	39.91	
12	2	42.8	69.82
12	14	113.89	190.91
12	28	54.48	174.55
13	1	45.52	
13	2	58.01	113.81
13	14	115.72	187.67
13	28	126.96	27.27



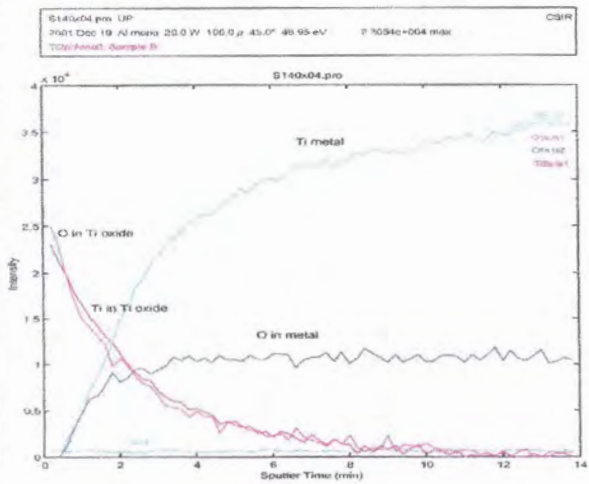
ADDENDUM G

Depth profile

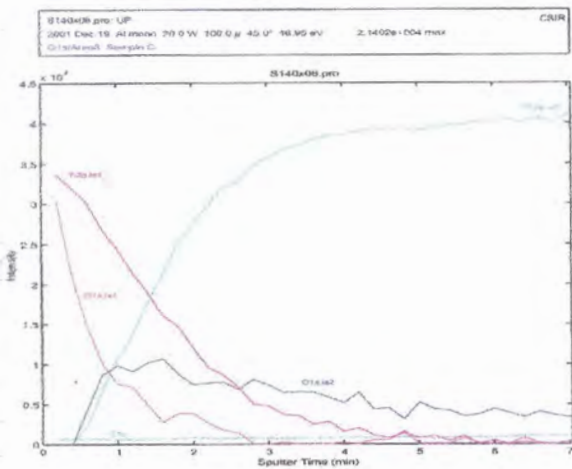
Before RFGDT



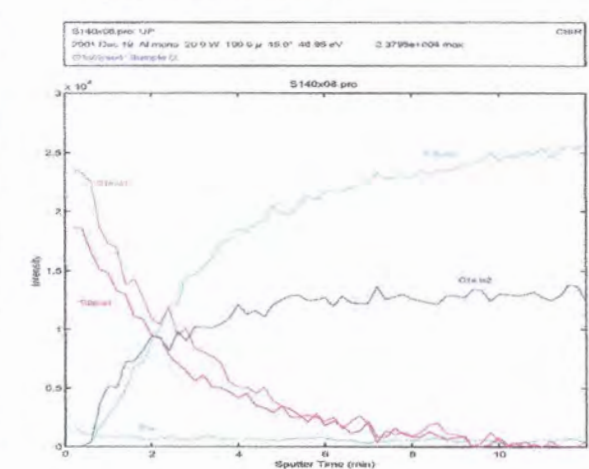
cpTi machined control sample



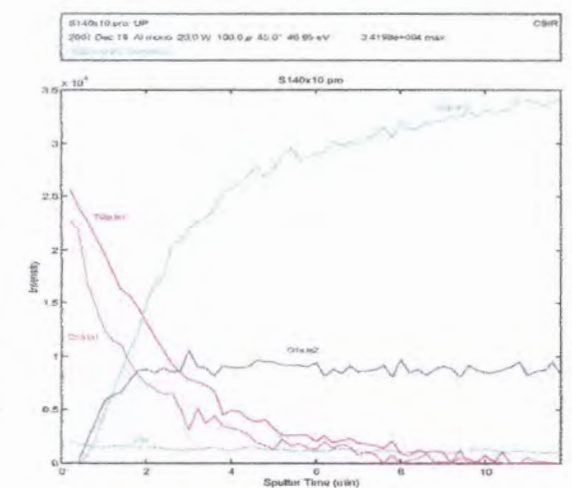
cpTi machined ES sample



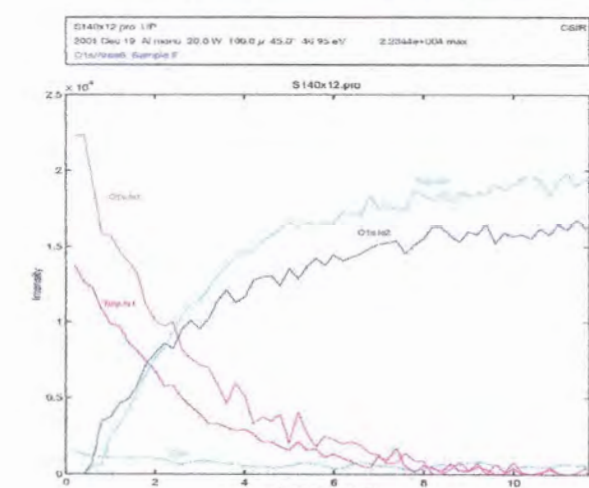
Ti6Al4V machined control sample



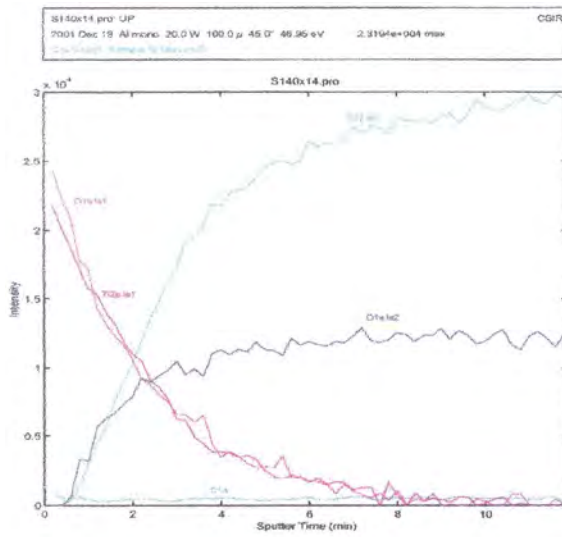
Ti6Al4V machined ES sample



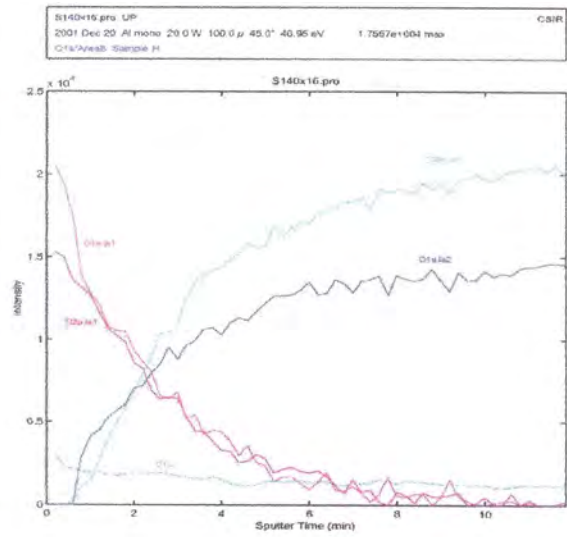
cpTi machined SI sample



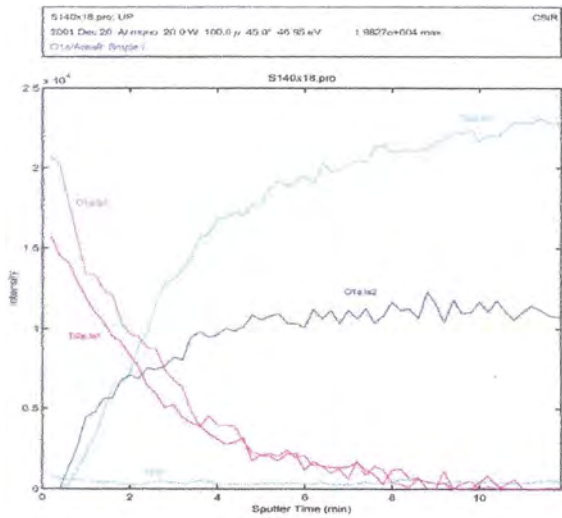
cpTi cast control sample



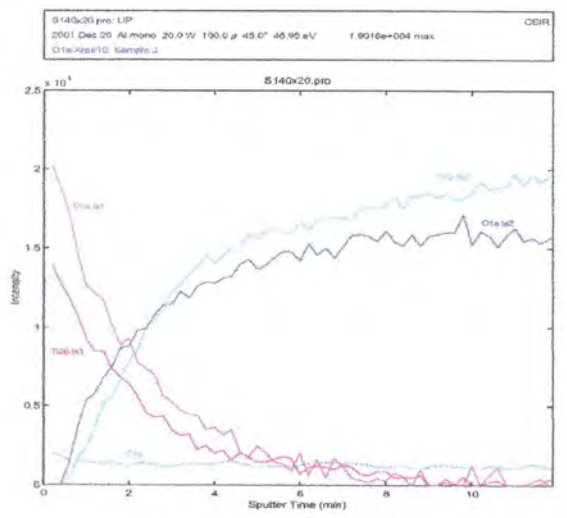
cpTi cast ES sample



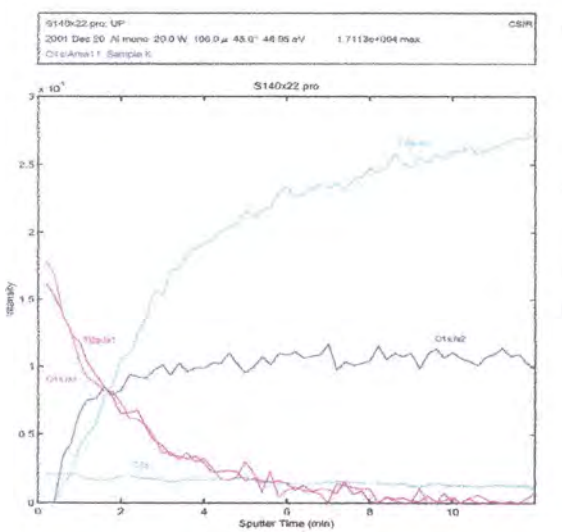
Ti6Al4V cast control sample



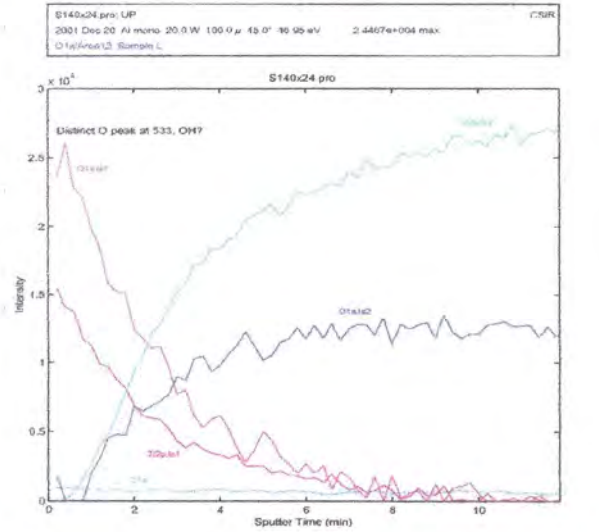
Ti6Al4V cast ES sample



cpTi cast SI sample



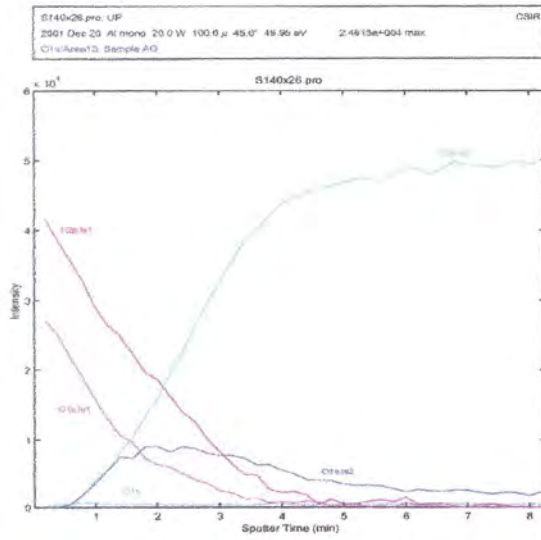
Ti6Al4V cast SI sample



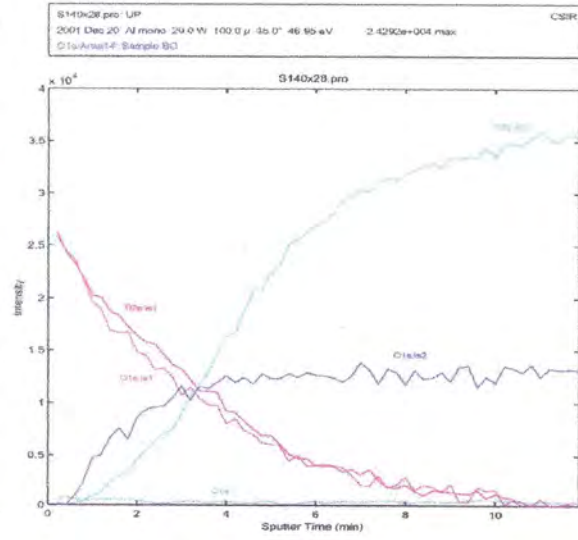
Ti6Al4V machined SI sample



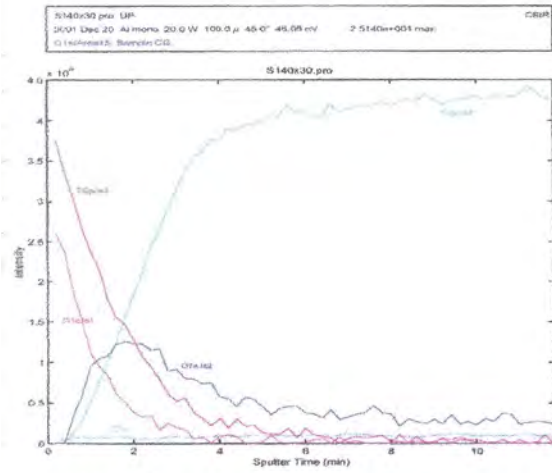
After RFGDT



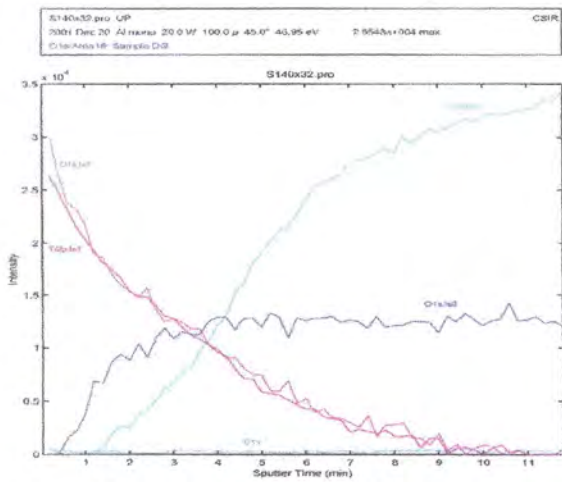
cpTi machined control RFGDT sample



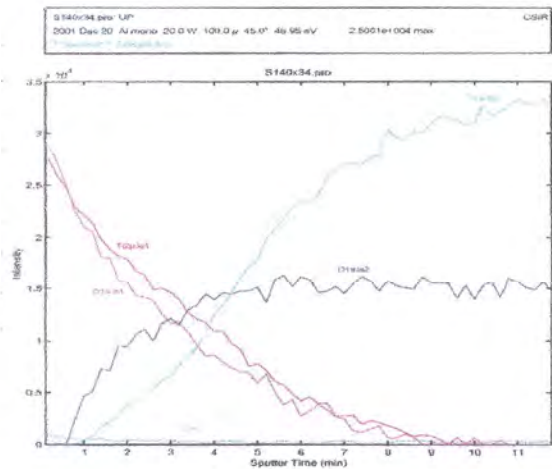
cpTi machined ES RFGDT sample



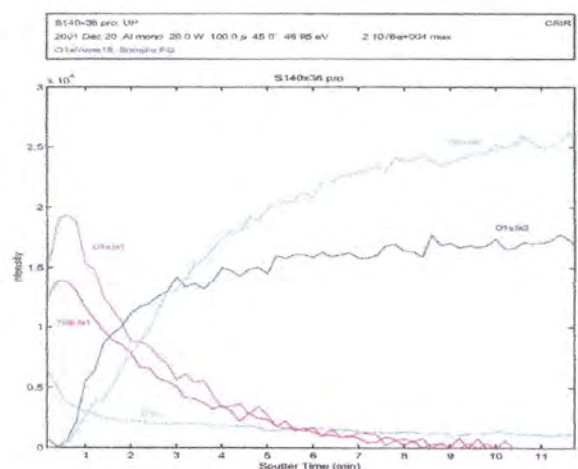
Ti6Al4V machined control RFGDT sample



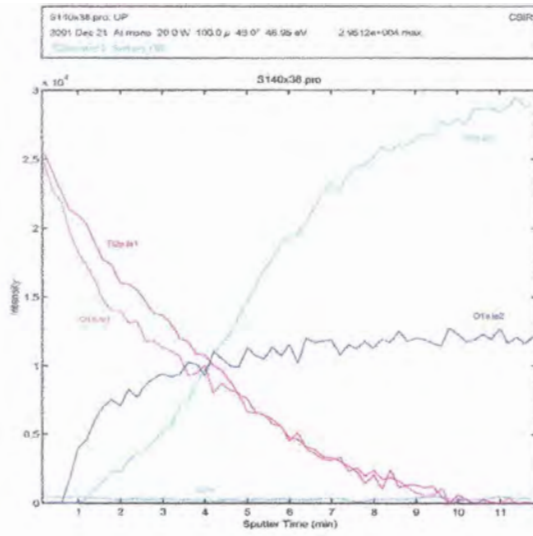
Ti6Al4V machined ES RFGDT sample



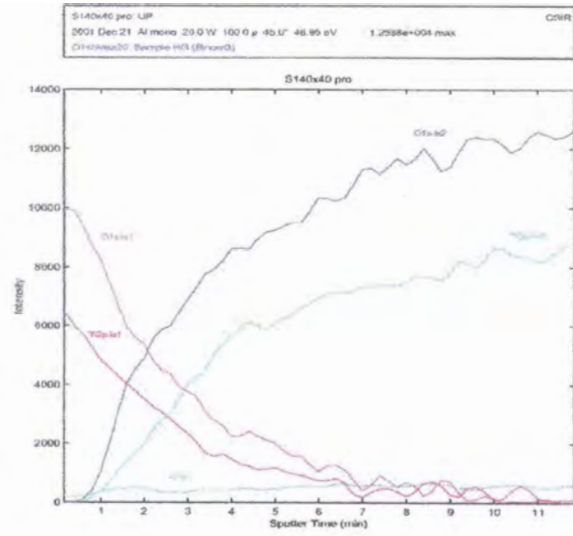
cpTi machined SI RFGDT sample



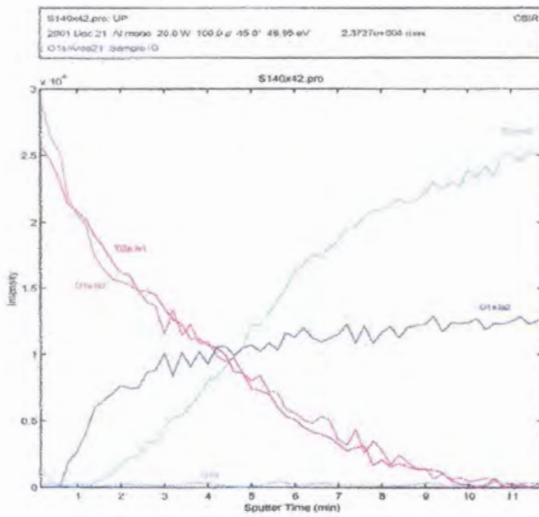
cpTi cast control RFGDT sample



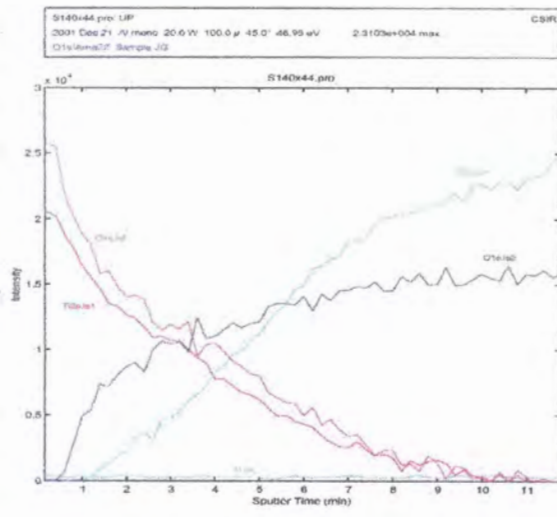
cpTi cast ES RFGDT sample



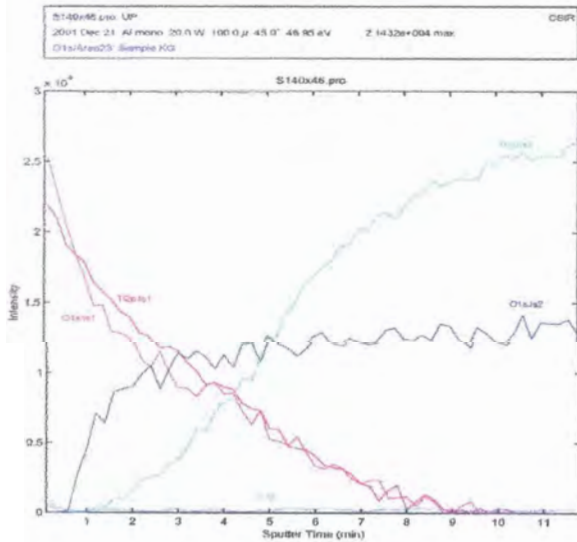
Ti6Al4V cast control RFGDT sample



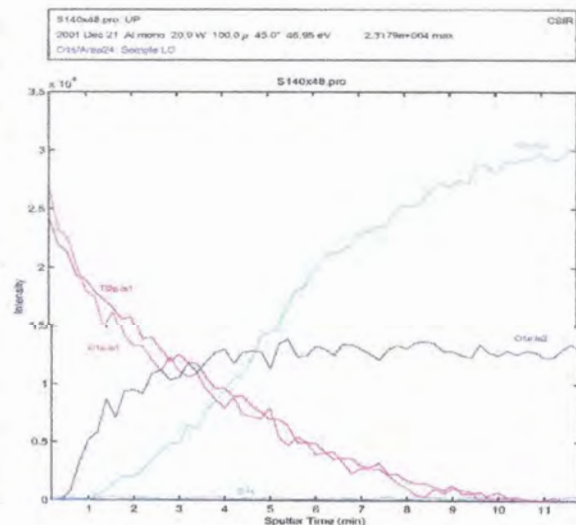
Ti6Al4V cast ES RFGDT sample



cpTi cast SI RFGDT sample



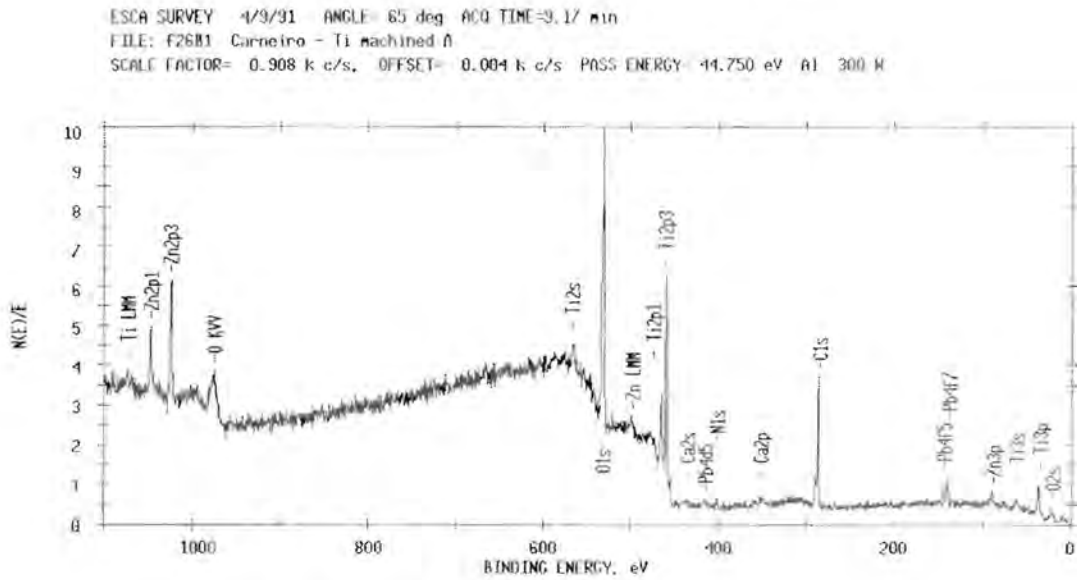
Ti6Al4V cast SI RFGDT sample



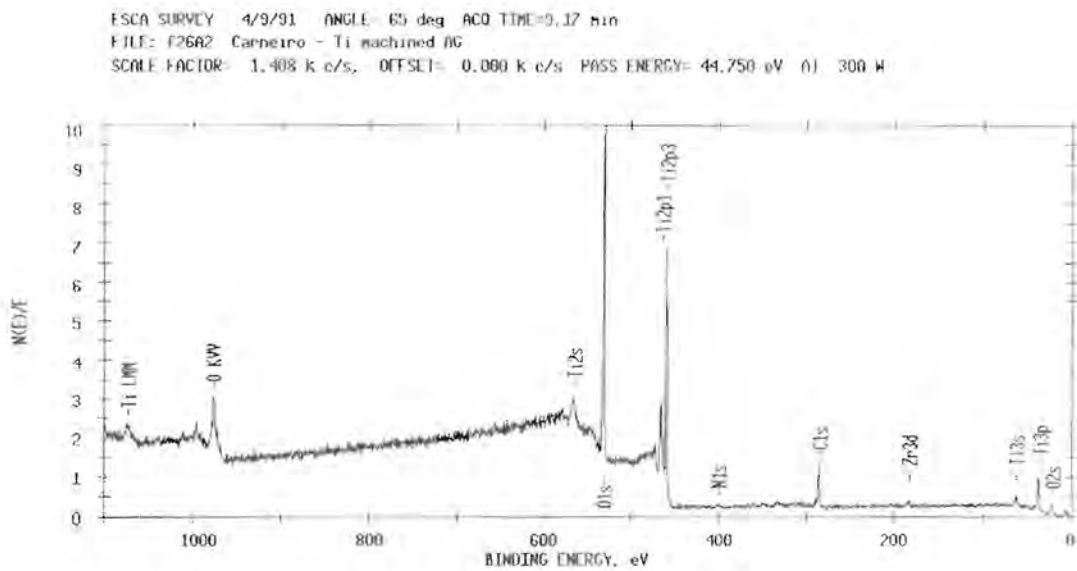
Ti6Al4V machined SI RFGDT sample

ADDENDUM H

XPS Spectra

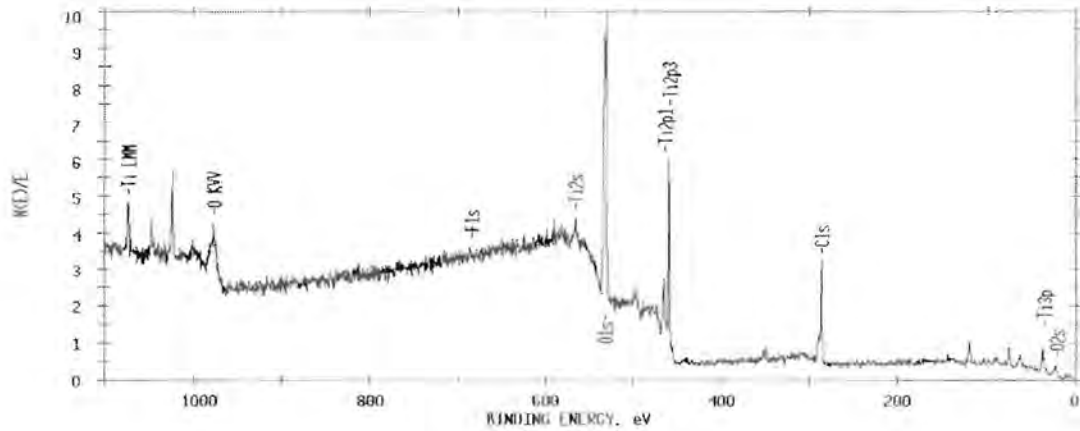


cpTi machined control sample



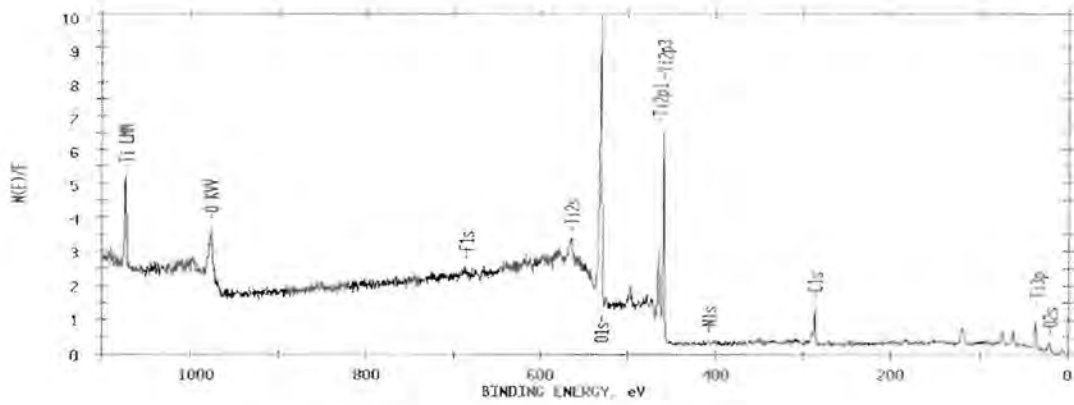
cpTi machined control RFGDT sample

ESCA SURVEY 8/27/91 ANGLE= 65 deg ACQ TIME=9.17 min
FILE: F20A1 LC - B Ti machined enhanced
SCALE FACTOR= 0.940 k c/s, OFFSET= 0.004 k c/s PASS ENERGY= 44.750 eV AI 300 H



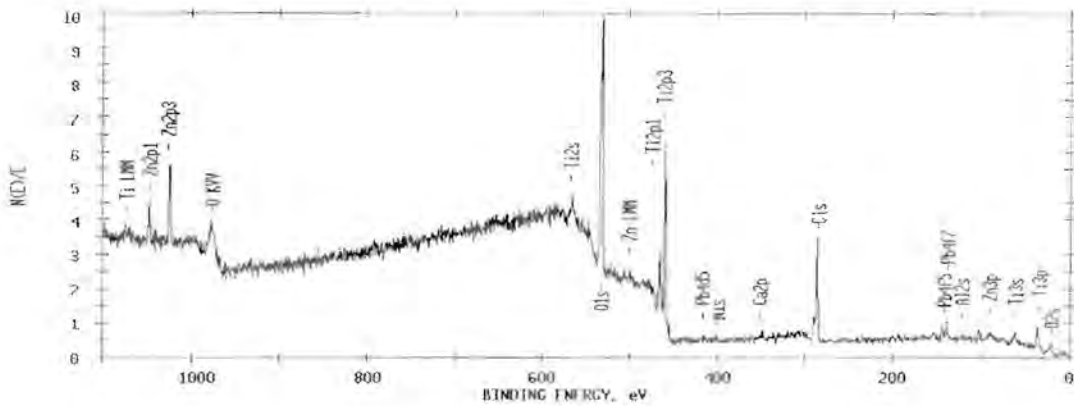
cpTi machined ES control sample

ESCA SURVEY 8/27/91 ANGLE= 65 deg ACQ TIME=9.17 min
FILE: F20B2 LC - B Ti machined enhanced RFGD
SCALE FACTOR= 1.114 k c/s, OFFSET= 0.000 k c/s PASS ENERGY= 44.750 eV AI 300 H



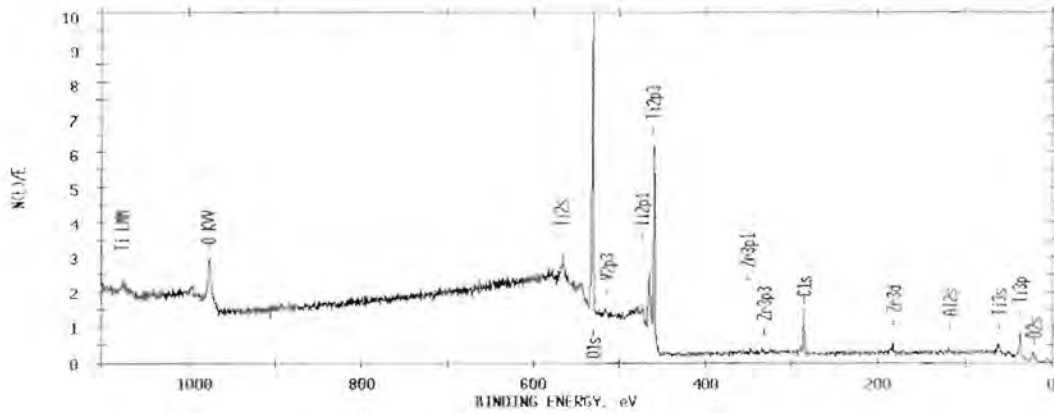
cpTi machined ES control RFGD sample

ESCA SURVEY 4/10/91 ANGLE= 65 deg ACQ TIME=9.17 min
FILE: F27C1 Carneiro - Ti alloy machined C
SCALE FACTOR= 0.885 k c/s, OFFSET= 0.004 k c/s PASS ENERGY= 44.750 eV AI 300 H



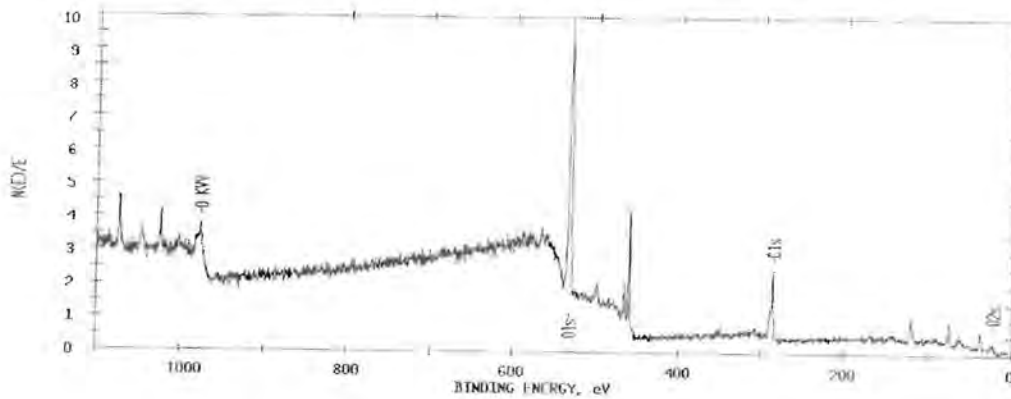
Ti6Al4V machined control sample

ESCA SURVEY 4/10/91 ANGLE= 65 deg ACQ TIME=9.17 min
FILE: F2701 Carneiro - Ti Alloy machined CG
SCALE FACTOR= 1.436 k c/s. OFFSET= 0.000 k c/s PASS ENERGY= 14.750 eV Al 300 W



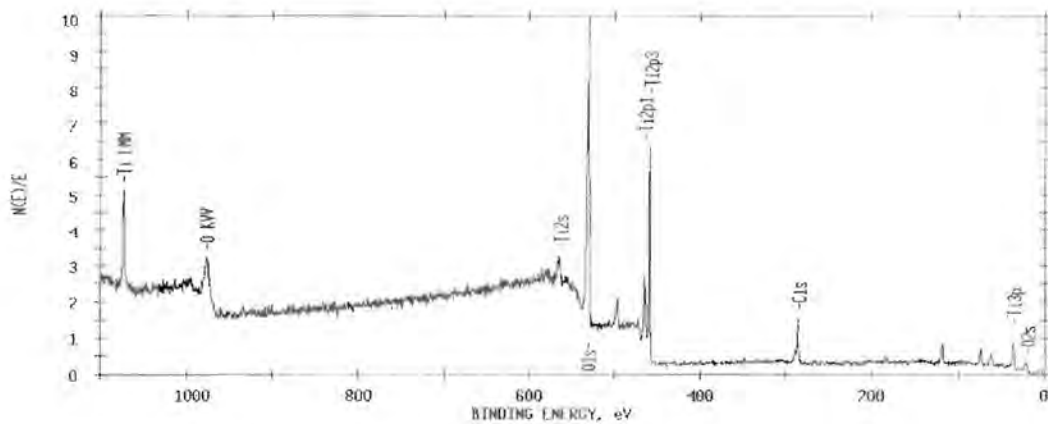
Ti6Al4V machined control RFGDT sample

ESCA SURVEY 8/27/91 ANGLE= 65 deg ACQ TIME= 9.17 min
FILE: F20C1 LC - D Ti alloy machined enhanced
SCALE FACTOR= 0.871 k c/s. OFFSET= 0.000 k c/s PASS ENERGY= 14.750 eV Al 300 W



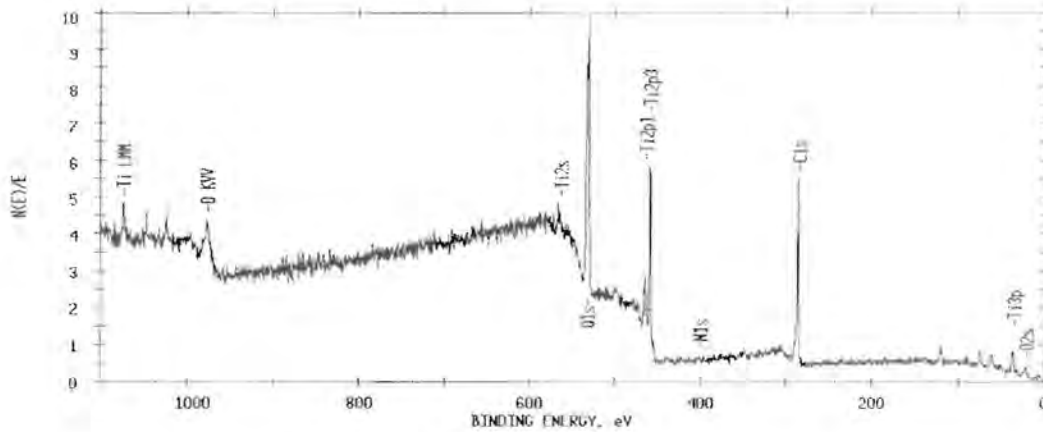
Ti6Al4V machined ES control sample

ESCA SURVEY 8/27/91 ANGLE= 65 deg ACQ TIME=9.17 min
FILE: F2001 LC - DG Ti alloy machined enhanced RFGD
SCALE FACTOR= 1.365 k c/s. OFFSET= 0.000 k c/s PASS ENERGY= 14.750 eV Al 300 W



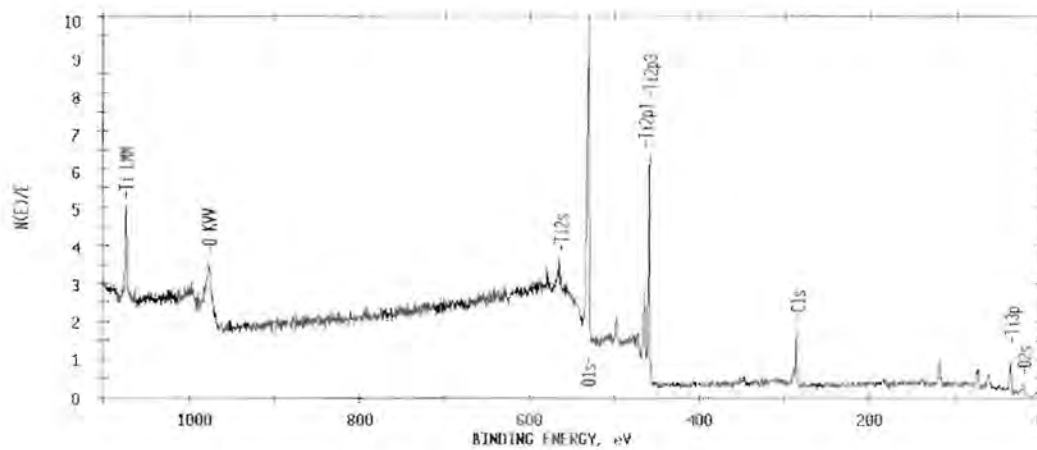
Ti6Al4V machined ES RFGDT sample

ESCA SURVEY 8/27/91 ANGLE= 65 deg ACO TIME=9.17 min
FILE: F20E1 LC - E Ti machined enhanced SI
SCALE FACTOR= 0.916 k c/s, OFFSET= 0.001 k c/s PASS ENERGY= 44.750 eV AI 300 W



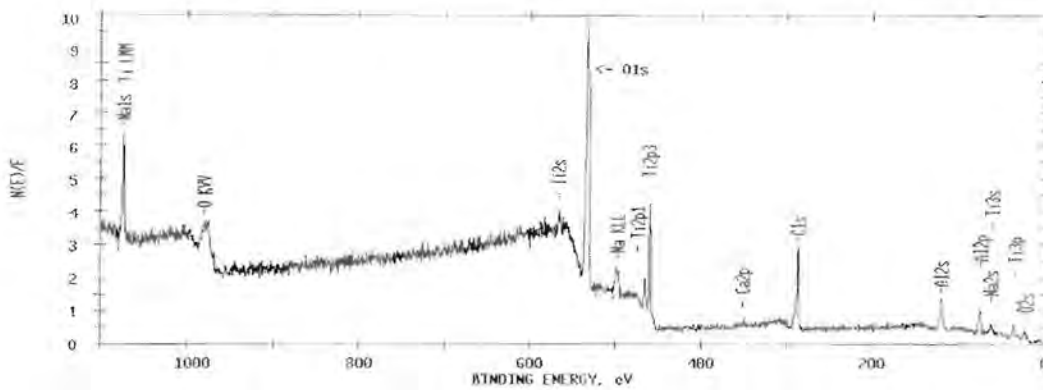
cpTi machined SI sample

ESCA SURVEY 8/27/91 ANGLE= 65 deg ACO TIME=9.17 min
FILE: F20F1 LC - EG Ti machined enhanced SI RFGD
SCALE FACTOR= 1.157 k c/s, OFFSET= 0.000 k c/s PASS ENERGY= 44.750 eV AI 300 W



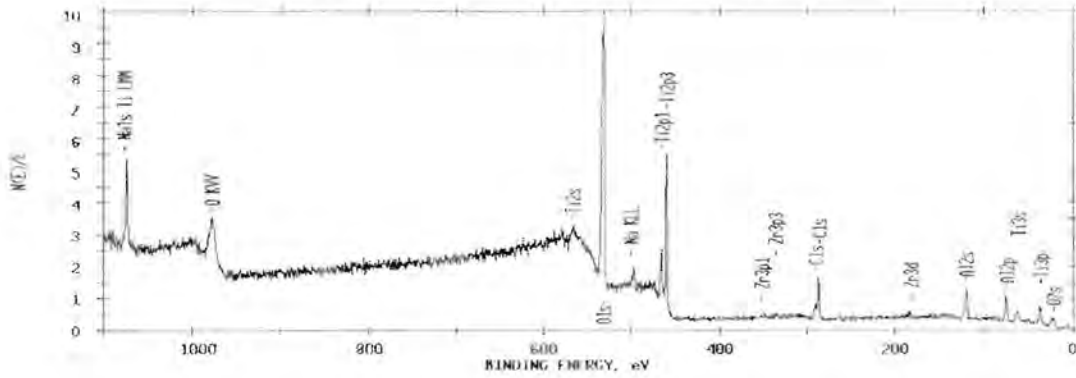
cpTi machined SI RFGD sample

ESCA SURVEY 4/10/91 ANGLE= 65 deg ACO TIME=9.17 min
FILE: F2/11 Carneiro - Ti F
SCALE FACTOR= 0.759 k c/s, OFFSET= 0.004 k c/s PASS ENERGY= 44.750 eV AI 300 W



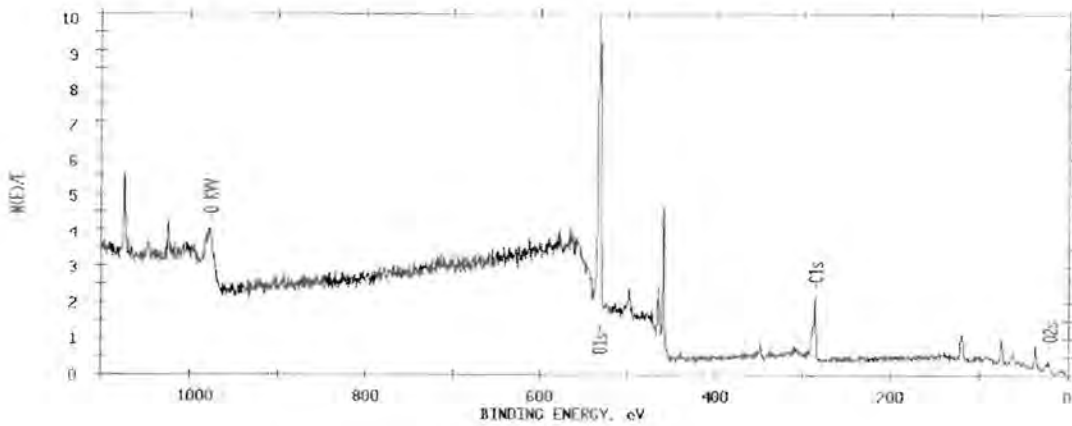
cpTi cast control sample

ESCA SURVEY 4/10/91 ANGLE= 65 deg ACQ TIME= 9.17 min
FILE: F2/H1 Carneiro - Ti FG
SCALE FACTOR= 0.903 k c/s. OFFSET= 0.004 k c/s PASS ENERGY= 44.750 eV AT 300 W



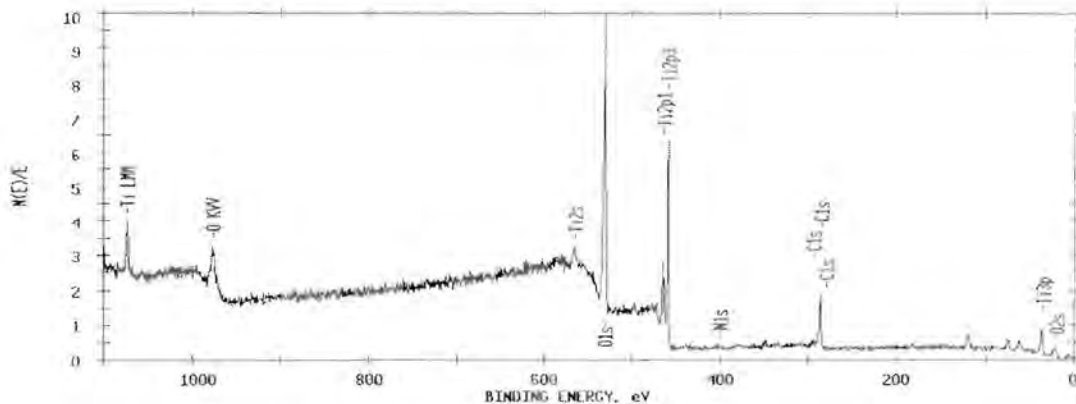
cpTi cast control RFGDT sample

ESCA SURVEY 8/28/91 ANGLE= 65 deg ACQ TIME= 9.17 min
FILE: F21A1 LC - G Ti cast enhanced
SCALE FACTOR= 0.930 k c/s. OFFSET= 0.004 k c/s PASS ENERGY= 44.750 eV AT 300 W



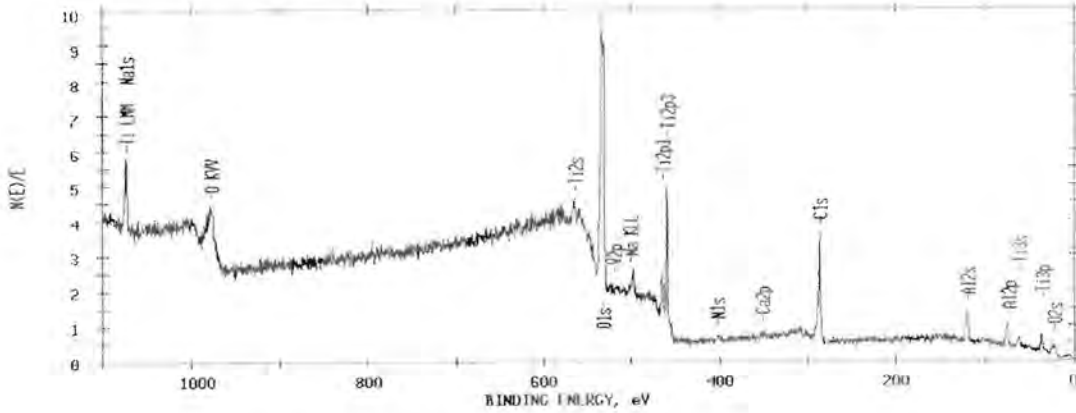
cpTi cast ES sample

ESCA SURVEY 8/28/91 ANGLE= 65 deg ACQ TIME= 9.17 min
FILE: F21B21 LC - GG to cast enhanced RFGD
SCALE FACTOR= 1.142 k c/s. OFFSET= 0.000 k c/s PASS ENERGY= 44.750 eV AT 300 W



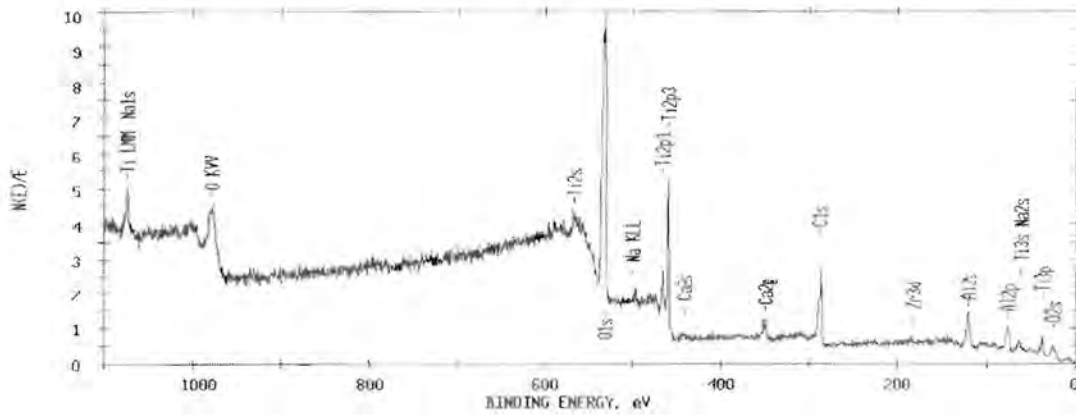
cpTi cast ES RFGDT sample

ESCA SURVEY 4/23/91 ANGLE= 65 deg ACO TIME=9.17 min
FILE: F10A1 Carneiro - Ti cast alloy H repeat
SCALE FACTOR= 0.965 k c/s. OFFSET= 0.012 k c/s PASS ENERGY= 44.750 eV AI 300 W

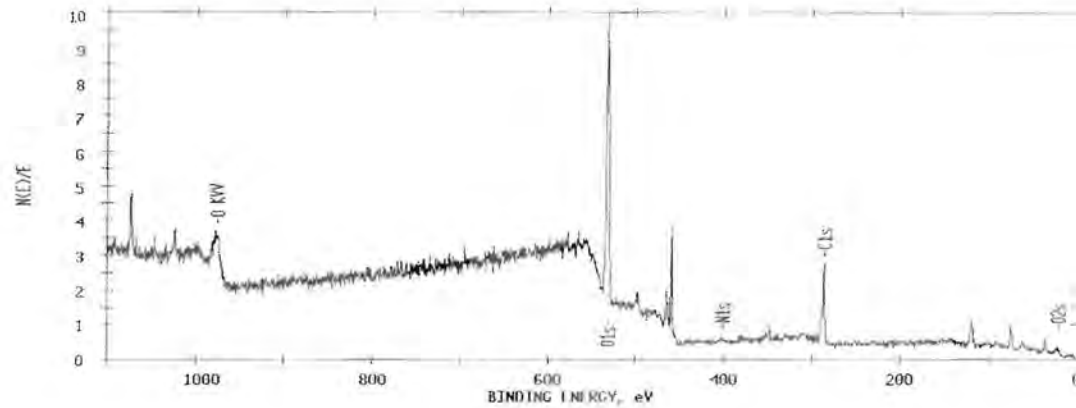


Ti6Al4V cast control sample

ESCA SURVEY 4/15/91 ANGLE= 65 deg ACO TIME=14.67 min
FILE: F32C3 Carneiro - Ti alloy cast HC
SCALE FACTOR= 0.682 k c/s. OFFSET= 0.005 k c/s PASS ENERGY= 44.750 eV AI 300 W

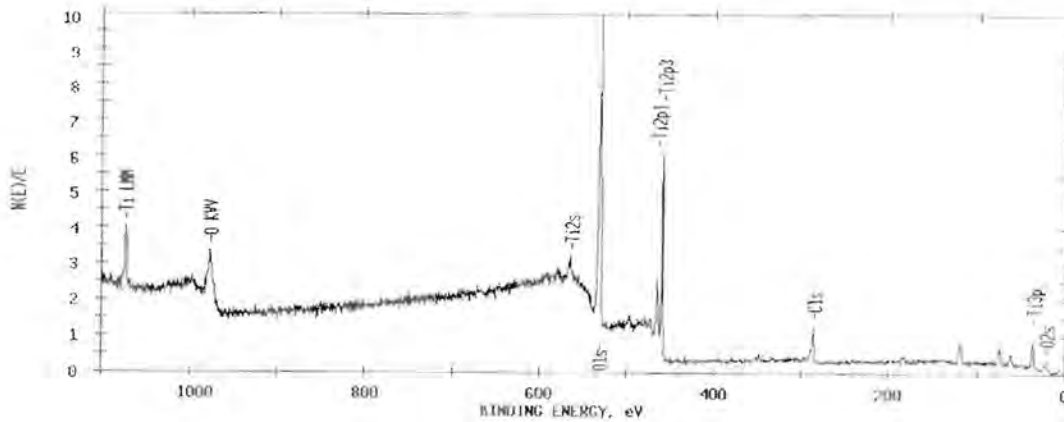


ESCA SURVEY 8/28/91 ANGLE= 65 deg ACO TIME=9.17 min
FILE: F21C1 IC - I Ti alloy cast enhanced
SCALE FACTOR= 0.845 k c/s. OFFSET= 0.000 k c/s PASS ENERGY= 44.750 eV AI 300 W



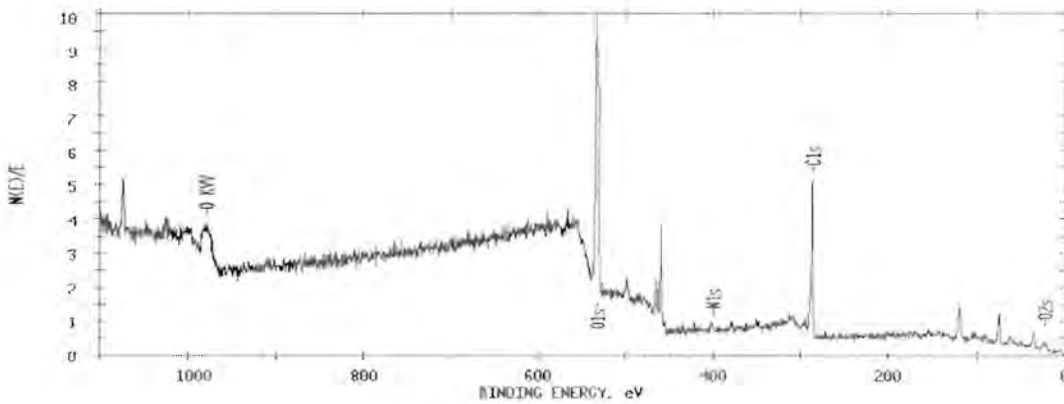
Ti6Al4V cast ES sample

ESCA SURVEY 8/28/91 ANGLE= 65 deg ACO TIME=9.17 min
FILE: F21D1 LC - 16 Ti alloy cast enhanced RFGD
SCALE FACTOR= 1.200 k c/s, OFFSET= 0.000 k c/s PASS ENERGY= 44.750 eV AT 300 W



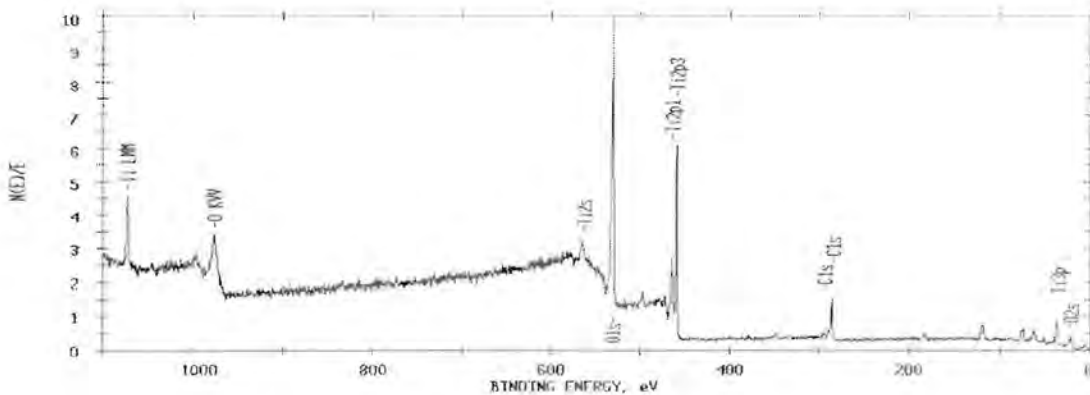
Ti6Al4V cast ES RFGDT sample

ESCA SURVEY 8/29/91 ANGLE= 65 deg ACO TIME=9.17 min
FILE: F22C1 LC - J Ti cast SI enhanced
SCALE FACTOR= 0.884 k c/s, OFFSET= 0.000 k c/s PASS ENERGY= 44.750 eV AT 300 W



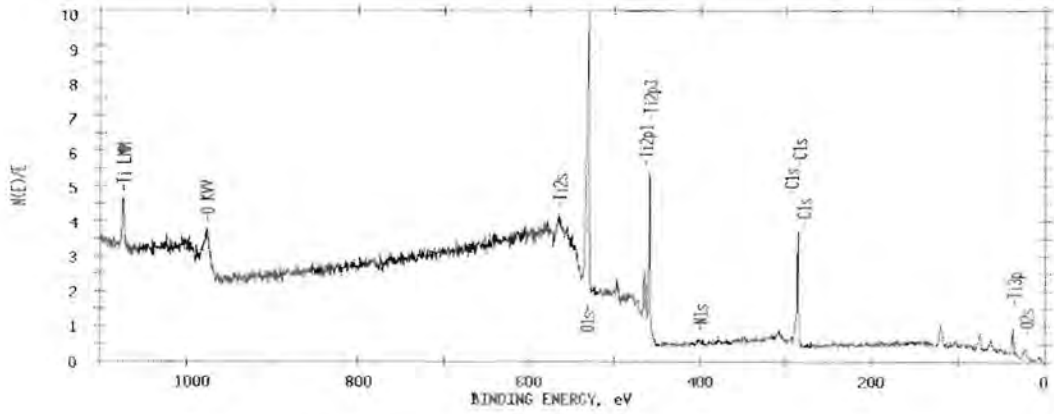
cpTi cast SI sample

ESCA SURVEY 8/29/91 ANGLE= 65 deg ACO TIME=9.17 min
FILE: F22D1 LC - JG Ti cast SI enhanced RFGD
SCALE FACTOR= 1.572 k c/s, OFFSET= 0.000 k c/s PASS ENERGY= 44.750 eV AT 300 W



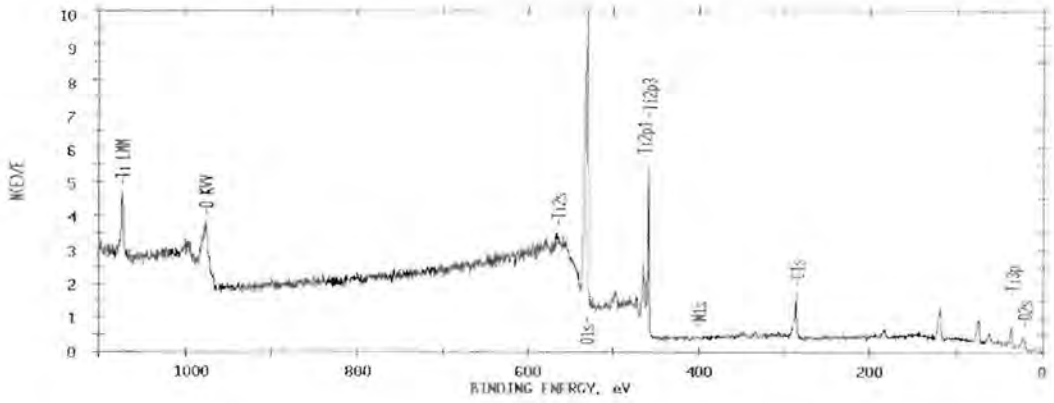
cpTi cast SI RFGDT sample

ESCA SURVEY 8/29/91 ANGLE= 65 deg ACO TIME=9.17 min
FILE: F22E1 LC - K Ti alloy cast SI enhanced
SCALE FACTOR= 1.219 k c/s. OFFSET= 0.016 k c/s PASS ENERGY= 44.750 eV A1 300 W



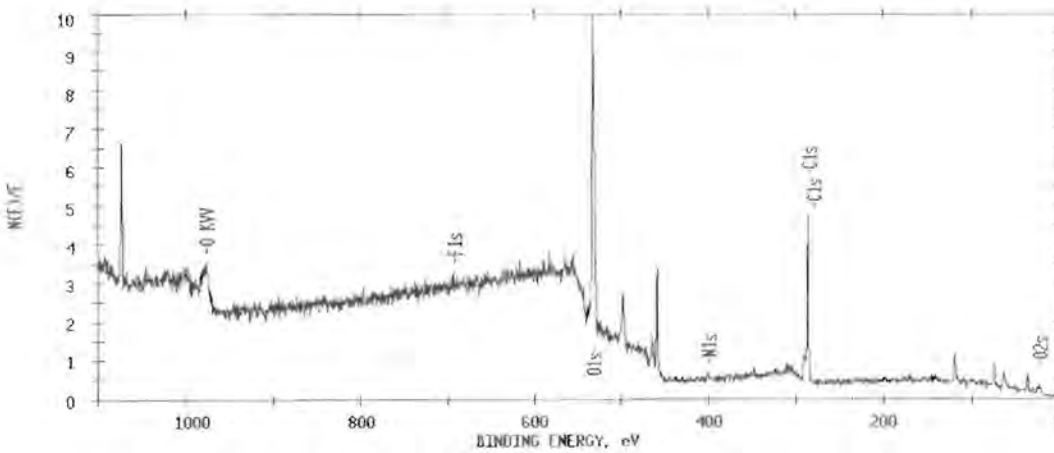
Ti6Al4V cast SI sample

ESCA SURVEY 8/29/91 ANGLE= 65 deg ACO TIME=9.17 min
FILE: F22F1 LC - K Ti alloy cast SI enhanced RFGD
SCALE FACTOR= 1.205 k c/s. OFFSET= 0.000 k c/s PASS ENERGY= 44.750 eV A1 300 W



Ti6Al4V cast SI RFGD sample

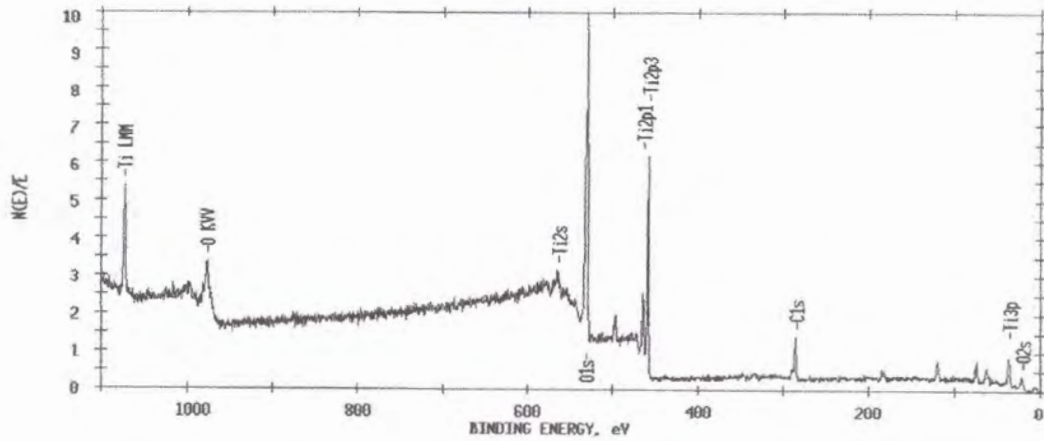
ESCA SURVEY 8/30/91 ANGLE= 65 deg ACO TIME=9.17 min
FILE: F22G1 LC - L Ti alloy machined enhanced SI
SCALE FACTOR= 0.807 k c/s. OFFSET= 0.000 k c/s PASS ENERGY= 44.750 eV A1 300 W



Ti6Al4V machined SI sample



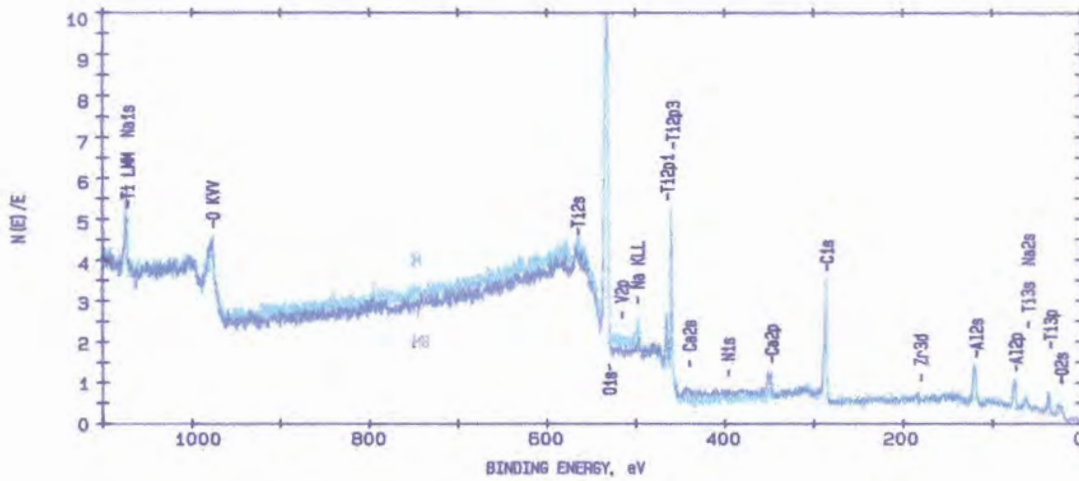
ESCA SURVEY 8/30/91 ANGLE= 65 deg ACQ TIME=9.17 min
FILE: f23a1 LC - LG Ti alloy machined enhanced SI RFGD
SCALE FACTOR= 1.303 k c/s, OFFSET= 0.000 k c/s PASS ENERGY= 44.750 eV A1 300 W



Ti6Al4V machined SI RFGDT sample

Comparison of different samples

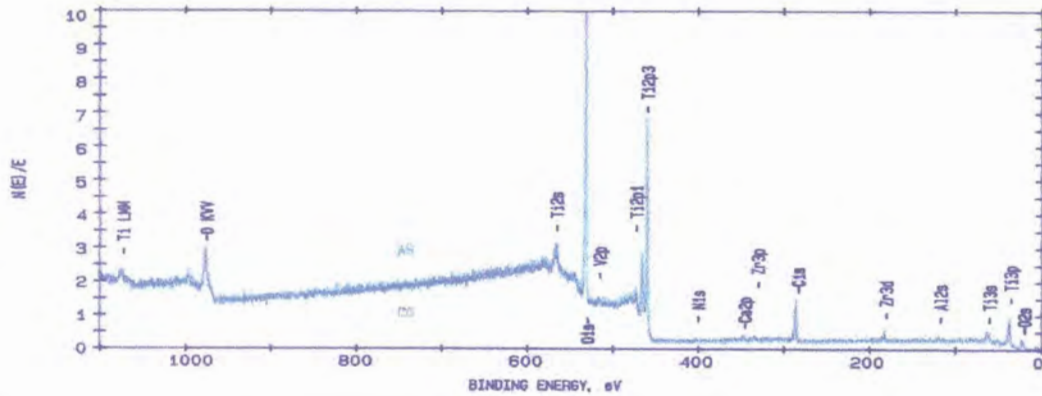
ESCA SURVEY 4/15/91 ANGLE= 65 deg ACQ TIME=14.67 min
FILE: f32c3 Carneiro - Ti alloy cast HS
SCALE FACTOR= 0.682 k c/s, OFFSET= 0.005 k c/s PASS ENERGY= 44.750 eV A1 300 W



Ti6Al4V cast control sample before and after RFGDT

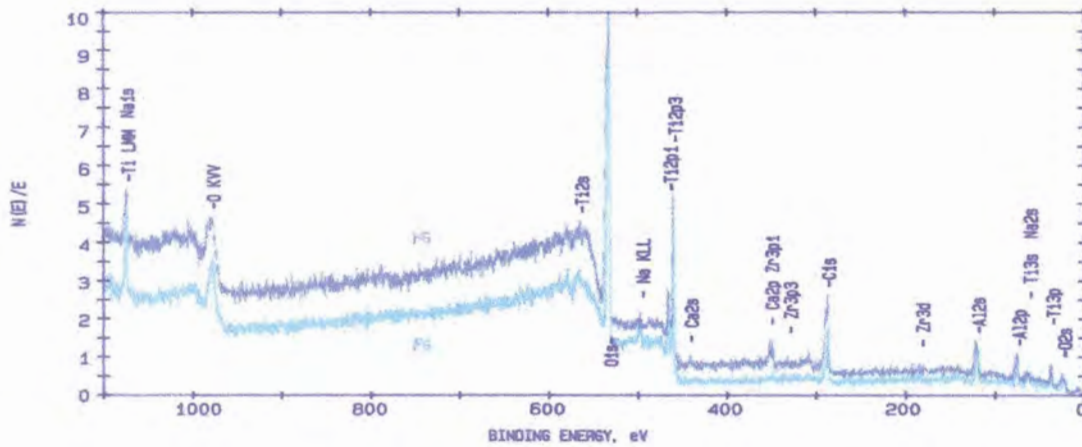


ESCA SURVEY 4/10/91 ANGLE= 65 deg ACQ TIME=9.17 min
FILE: f27A1 Carneiro - Ti Alloy machined CS
SCALE FACTOR= 1.436 k c/s, OFFSET= 0.000 k c/s PASS ENERGY= 44.750 eV Al 300 W



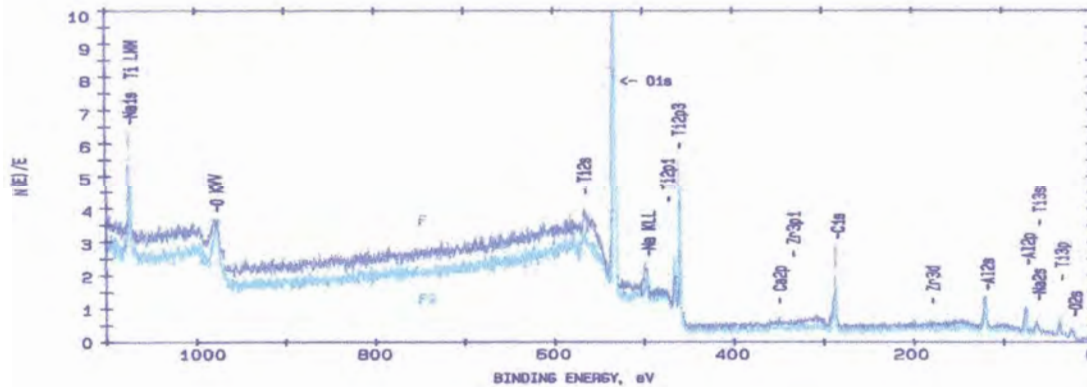
cpTi and Ti6Al4V machined control samples after RFGDT

ESCA SURVEY 4/15/91 ANGLE= 65 deg ACQ TIME=9.17 min
FILE: f32C1 Carneiro - Ti alloy cast HG
SCALE FACTOR= 0.648 k c/s, OFFSET= 0.000 k c/s PASS ENERGY= 44.750 eV Al 300 W



cpTi and Ti6Al4V cast control samples after RFGDT

ESCA SURVEY 4/10/91 ANGLE= 65 deg ACQ TIME=9.17 min
FILE: f27I1 Carneiro - Ti F
SCALE FACTOR= 0.759 k c/s, OFFSET= 0.004 k c/s PASS ENERGY= 44.750 eV Al 300 W



cpTi cast control sample before and after RFGDT

SURFACE TOPOGRAPHY OF MACHINED AND CAST TITANIUM AND TITANIUM ALLOYS USED IN DENTISTRY.

L.C. Carneiro, S.J. Botha, P.L. Kemp* and T. von Moltke**

Centre for Stomatological Research, *Department of Prosthetics, School of Dentistry and **Department of Material Science and Metallurgical Engineering, University of Petoria.

Surface roughness of prefabricated titanium implants has been reported to alter the phenotypic expression of cells. Therefore, preparation of these surfaces and cleaning procedures adopted for implants should aim at maintaining the elemental composition without modifying surface topography. With the introduction of cast titanium, an alternative method of implant fabrication was developed, but little is known of the surface characteristics of these cast metals.

This study aimed to determine and compare the surface topography of cast and machined titanium surfaces manufactured from both pure titanium and titanium alloy as well as the effect of Radio Frequency Glow Discharge (RFGD) treatment on surface topography of these materials.

Circular machined and cast discs of 6.35mm diameter and 2mm thick were fabricated in duplicate from titanium (Grade 3) and titanium alloys (Grade 5 and 23). One sample from each group was RFGD treated and the other served as control. Surface topography was determined using the Atomic Force Microscope (Topometrix TMX 2010 Discoverer). On each sample five scans were performed of range of 20µm and 5µm. Data from the different scans were compared and specific properties of the surface topography were calculated.

Results show that for both scanned areas the average R_a value for cast samples was higher compared to the machined surfaces thereby confirming that the cast samples had a larger surface area than the machined surfaces. Similarly, other results (RMS and average height) were higher for cast samples. For both scan ranges no differences were noted between results for neither the titanium and titanium alloys nor for samples that were radio frequency glow discharged treated. The averages of the line analysis of the different measurements for the different scans done also show that cast samples are rougher than machined samples. R_m values indicate a consistent surface finish for machined and cast surfaces; 237-314µm and 870-1020µm respectively. The cast surfaces had a very high R_t value as compared to machined surfaces (2000µm vs 600µm) indicating a very large difference between the highest and lowest peak for the cast samples. The low R_{pm} as compared to the high R_m indicates a plateau surface seen in both the machined and cast samples.

It can be concluded that the method of fabrication determined the surface topography. Furthermore, RFGD treatment did not significantly modify the surface topography of these materials. The surface roughness of cast samples was probably related to the method of investment removal.

Table 1: Average values of secondary surface topography obtained from a 20µm scan.

	Ti, mach	Ti, mach, RFGD	Ti-alloy, mach	Ti -alloy, mach, RFGD	Ti, cast	Ti, cast, RFGD	Ti-alloy, cast	Ti-alloy, cast, RFGD
Average of R_a (µm)	0.140	0.098	0.088	0.144	0.520	0.647	0.450	0.412
Average area of RMS (µm)	0.172	0.127	0.110	0.182	0.654	0.792	0.554	0.522
Average surface area (µm ²)	416.180	416.340	415.000	425.020	531.920	559.140	508.260	535.260
Average height (µm)	0.585	0.439	0.635	0.532	1.882	2.209	1.741	1.922

Table 2: Average values of primary surface topography obtained from a 5µm scan.

	Ti, mach	Ti, mach, RFGD	Ti-alloy, mach	Ti -alloy, mach, RFGD	Ti, cast	Ti, cast, RFGD	Ti-alloy, cast	Ti-alloy, cast, RFGD
Average of R_a (µm)	0.060	0.070	0.080	0.110	0.260	0.270	0.090	0.200
Average area of RMS (µm)	0.070	0.080	0.100	0.130	0.320	0.340	0.310	0.250
Average surface area (µm ²)	27.280	26.560	27.980	28.00	32.860	34.270	34.940	32.390
Average height (µm)	0.270	0.220	0.350	0.310	0.680	0.800	0.750	0.580

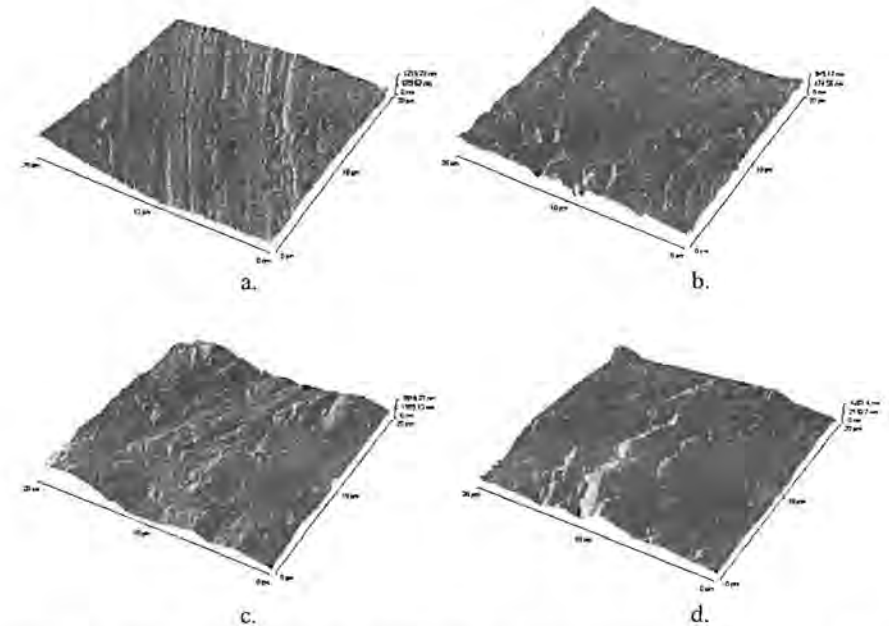


Figure 1: AFM 20µm scans of: a.) Pure Ti, machined sample; b.) Ti-alloy, machined sample; c.) Pure Ti, cast sample; d.) Ti-alloy, cast sample.

lcarneur@postillion.up.ac.za and sjbotha@medic.up.ac.za

X-RAY SPECTROSCOPY OF DIFFERENTLY CHARACTERISED MACHINED AND CAST TITANIUM AND TITANIUM ALLOYS.

L.C. Carneiro, S.J. Botha, P.L. Kemp* and T. von Moltke**

Centre for Stomatological Research, *Department of Prosthetics, School of Dentistry and **Department of Material Science and Metallurgical Engineering, University of Pretoria.

Surface contaminants are inherently related to the surface preparation procedures that are used when manufacturing implants. The outermost atomic layer of the implant surface is a key factor in bio-acceptability. Radio Frequency Glow Discharge (RFGD) treatment has been promoted as a method for cleaning, as well as sterilizing metal surfaces for biological use. The aim of this study was to analyze the chemical composition after RFGD treatment on differently characterized machined and cast Titanium (Ti) and Titanium alloy (Ti-alloy) surfaces.

Circular discs of 6.35mm diameter and 2mm thick were fabricated from Titanium (Grade 3) and Titanium alloy (Grade 5) by machining and casting. The samples were characterized by blasting with 250µm or 110µm Aluminium-Oxide particles and acid etching (enhanced). The control group was not blasted with Aluminium-Oxide or acid etched. RFGD treatment was performed on the surface of one of the samples in each group while the others were analyzed as only enhanced samples. The chemical composition was determined using a Perkin-Elmer – PHI 5400 X-ray photoelectron spectrometer.

Results of the average values of elemental chemical composition is given in Table 1. It is evident that RFGD treatment removed the impurities – Zn, Pb, N and V. Pure Ti, machined samples, that were not enhanced had no Al, but a significant concentration of Al ranging from 1-15 percent was detected on all the other machined, cast and enhanced surfaces. Machined pure Ti and Ti-alloy that were RFGD treated, showed no Ca on the surface, but Ca (0.06-1.03%) was found on all other surfaces that were analyzed. Sodium was found on all the cast samples and is probably introduced to the surface by the technical process of cast sample preparation. RFGD significantly reduced C concentrations on the surface and therefore increased the O and Ti elemental concentrations. This may be advantageous for the formation of optimal TiO or TiO₂ surfaces that promote bio-acceptability and osseo-intergration.

Although RFGD treatment can be promoted as a method of preparing metallic surfaces for biological and clinical application, especially because of the increase in elemental Ti and O on the surface, its use in the removal of Al introduced by surface characterization is apparently restricted. Furthermore, acid etching did not influence the Al content probably because the Aluminium oxide particles were embedded onto the surface. If it is found that bio-acceptability is restricted then further investigation is required to facilitate elimination of the Al surface that was introduced by Aluminium-Oxide sandblasting and the Na that was introduced by cast sample preparation techniques.

Table 1: Elemental composition in Atomic Percent of the differently prepared surfaces of pure Titanium and Titanium-alloy as determined with X-ray photoelectron spectroscopy.

Element	C	O	Ti	Zn	Pb	Na	Ca	N	V	Zr	Al
Ti, machined	37.7	45.8	11.2	2.7	0.5		0.6	1.4			
Ti, machined, RFGD	20.8	56.4	21.6					0.8		0.4	
Ti, machined, enh 110µm	41.5	43.6	7.2	0.5			0.4				5.2
Ti, machined, enh 110µm, RFGD	19.9	52.7	12.9				0.3				9.7
Ti, machined, enh 250µm	29.5	51.4	8.8	1.4			0.9				5.8
Ti, machined, enh 250µm, RFGD	15.1	55.9	14.7				0.4				7.5
Ti-alloy, machined	36.8	48.7	10.3	2.1	0.4		0.3	0.5	0.9		1.0
Ti-alloy, machined, RFGD	21.8	56.7	18.8							0.7	1.2
Ti-alloy, machined, enh 110µm	36.7	43.8	4.2			5.9	0.2	0.5			8.7
Ti-alloy, machined, enh 110µm, RFGD	14.9	55.3	12.9	0.2		6.2	0.3			0.4	9.8
Ti-alloy, machined, enh 250µm	29.2	52.2	5.5	0.7			0.8				9.5
Ti-alloy, machined, enh 250µm, RFGD	16.1	55.5	13.7				0.3				9.2
Ti, cast	23.6	53.6	5.3			4.6	0.2				12.7
Ti, cast, RFGD	15.1	57.9	9.2			4.7	0.4			0.2	12.9
Ti, cast, enh 110µm	37.3	43.9	4.3	0.2		2.2	0.5	1.1			10.5
Ti, cast, enh 110µm, RFGD	15.5	56.3	14.6			4.5	0.4			0.5	8.2
Ti, cast, enh 250µm	25.6	52.9	7.1	0.7		3.3	0.5				9.8
Ti, cast, enh 250µm, RFGD	23.1	51.3	12.9			3.0	0.5	0.9		0.3	7.9
Ti-alloy, cast	28.7	51.4	5.6			3.3	0.4	0.8	0.2		9.6
Ti-alloy, cast, RFGD	25.3	55.4	6.2			1.5	1.0			0.1	10.5
Ti-alloy, cast, enh 110µm	32.7	47.7	8.4	0.1		2.2	0.2	0.7			8.0
Ti-alloy, cast, enh 110µm, RFGD	14.9	55.5	9.9			3.5	0.1			0.4	15.1
Ti-alloy, cast, enh 250µm	28.9	52.2	4.8	0.5		2.4	0.6	0.4			10.1
Ti-alloy, cast, enh 250µm, RFGD	15.9	56.6	12.6			3.2	0.4			0.4	10.9

lcarneur@postillion.up.ac.za and sjbotha@medic.up.ac.za